

PHOTON SCIENCE 2015.

Highlights and Annual Report

Accelerators | Photon Science | Particle Physics

Deutsches Elektronen-Synchrotron
A Research Centre of the Helmholtz Association





Cover

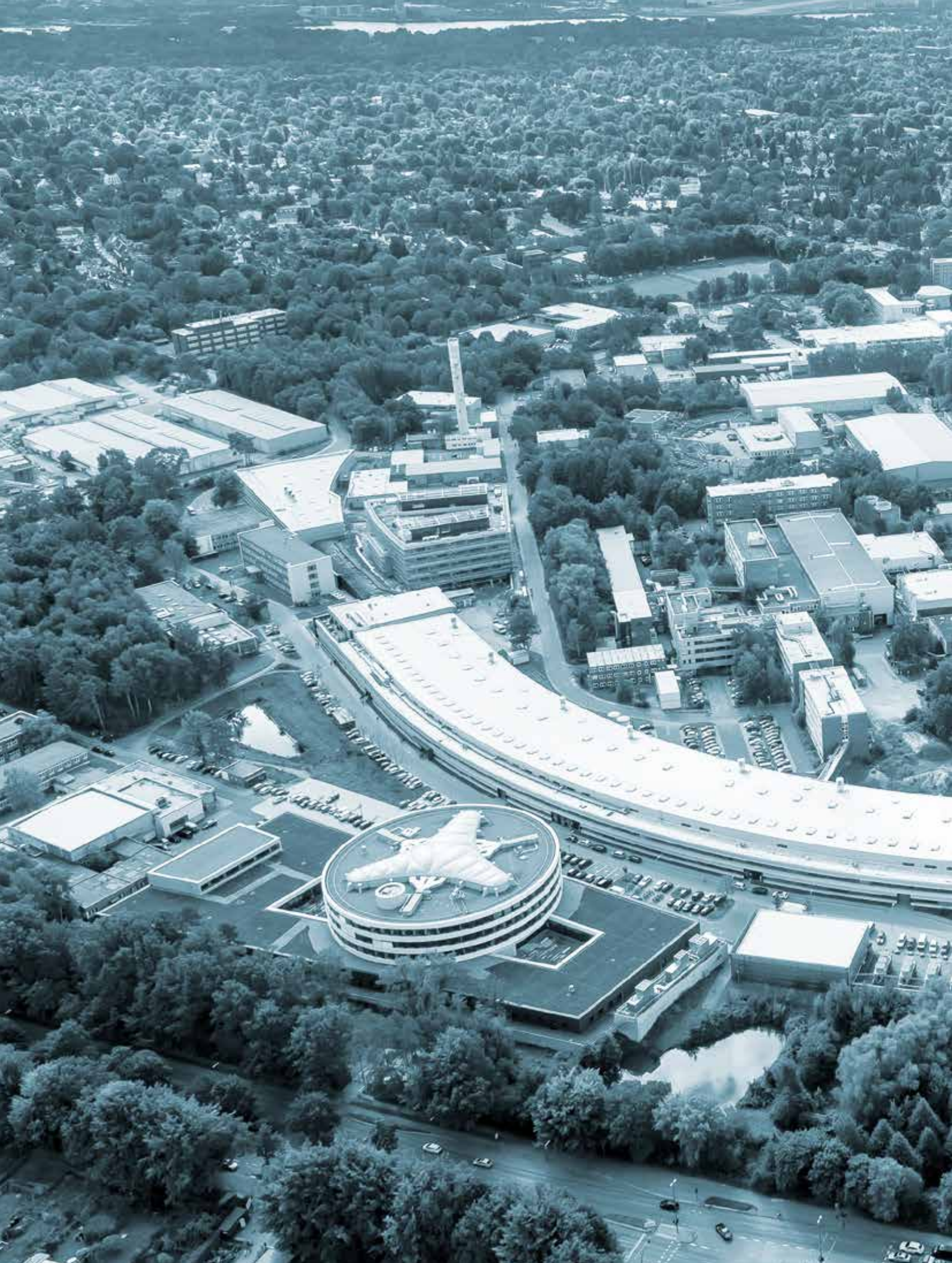
Tilt distribution of individual core-shell nanowires measured with the nanofocused X-ray beam at PETRA III beamline P06.

More information on these measurements can be found on page 58.



PHOTON SCIENCE 2015.

Highlights and Annual Report



Contents.

> Introduction	4
> News and Events	8
> Science Highlights	22
• Atomic and molecular dynamics	24
• Surfaces, thin films and interfaces	32
• Electronic and magnetic structure	42
• Structure and structural dynamics	50
• Macromolecular crystallography	62
• Science of X-ray sources	72
> Light Sources	86
> Campus and Collaborations	96
> Facts and Numbers	114

User Contributions to the Annual Report.

Publications

The list of publications based on work done at DESY Photon Science is accessible online: http://photon-science.desy.de/research/publications/list_of_publications/index_eng.html

DESY tries to keep this list as complete and as updated as possible, and relies on the support by all users, who are kindly requested to register their publications via DOOR.

The year 2015 at DESY.

Chairman's foreword

*Dear Colleagues and
Friends of DESY,*

2015, the UNESCO "International Year of Light", has been a highly dynamic year for Photon Science at DESY. Our research centre has been buzzing with activity. In case of the construction projects, the progress is obvious, and these new user facilities have come quite some steps closer to the start of their operating phase. At the same time, we have engaged in new national and international research collaborations and in developing a concept for a location of excellence for both the Hamburg and Zeuthen campus.

The construction of our largest project, the European X-ray Free-Electron Laser XFEL, is at full swing. More than two-thirds of the required 100 super-conducting accelerator modules have already been manufactured and tested successfully, many of them have been installed in the tunnel, and it is our ambition to have the first electron beam injected into the linear accelerator before the end of 2016.

The outer facades of the two PETRA III extension halls are completed. Now, the technical equipment is being put into



In a symbolic ceremony, the two FLASH experimental halls were named after Nobel laureates Albert Einstein and Kai Siegbahn by Beatrix Vierkom-Rudolph of the Federal Ministry of Research, the Swedish secretary of state Anders Lönn, DESY director Helmut Dosch, Hamburg's mayor Olaf Scholz and Hans Siegbahn, son of Kai Siegbahn (from left to right).



Accelerator tunnel of the European XFEL (April 2015).

place, and the hutches for the new beamlines are under construction. Also, the FLASH II construction project experimental hall “Kai Siegbahn” was completed this year. Commissioning of the experimental setups has started while experiments in the experimental hall “Albert Einstein” next door at FLASH are operating routinely.

Moreover, we celebrated the topping-out ceremony of the building for the new Centre for Structural Systems Biology (CSSB) that will become home for many new colleagues in 2017, who will strike new paths in infection research by following a uniquely interdisciplinary approach.

I am aware that running all those projects in parallel has been a paramount effort for everyone involved. I cannot extend a big enough thank you to all our dedicated collaborators to fully express the appreciation I have for their excellent work and their continued commitment.

Finally, I would like to mention two honours that were bestowed on DESY researchers this year: For their pioneering contributions to the development of free-electron lasers, DESY scientists Mikhail Yurkov and Evgeny Schneidmiller received the renowned international FEL prize. Henry Chapman (Center for Free-Electron Laser Science CFEL, DESY and University of Hamburg) was awarded the Gottfried Wilhelm Leibniz Prize of the Deutsche Forschungsgemeinschaft DFG for his groundbreaking work on serial femtosecond crystallography. ●

Helmut Dosch
Chairman of the DESY Board of Directors



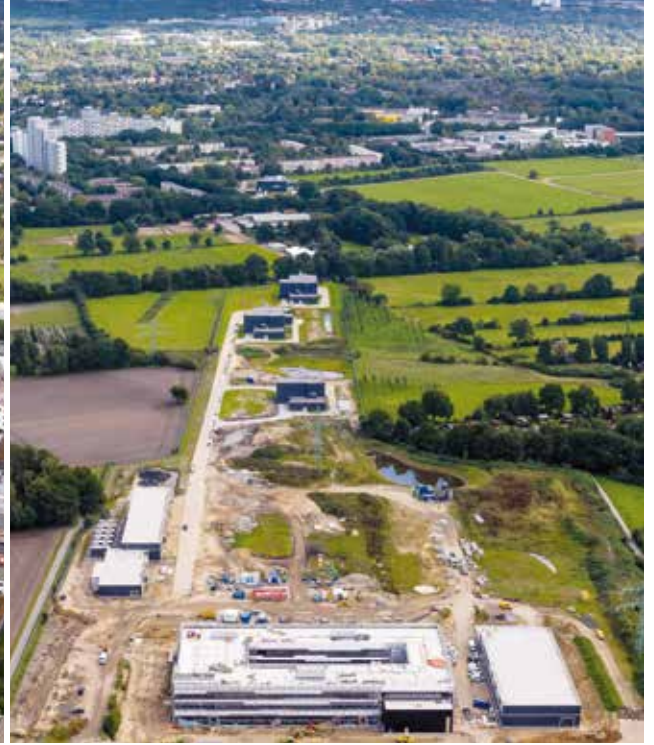
Topping-out ceremony of the CSSB building with its founding director Professor Matthias Wilmans, Dr. Karl Eugen Huthmacher from BMBF, the Minister for Social Affairs, Health, Science and Equality in Schleswig-Holstein, Kristin Alheit, Professor Helmut Dosch and the Senator for Science and Research in Hamburg, Katharina Fegebank.

Photon Science at DESY.

Introduction



The DESY site (Hamburg) with the European XFEL site in the far background (left upper corner) and the construction site of the CHyN building of the University of Hamburg (left lower corner) in September 2015.



The European XFEL site (Schenefeld) with the DESY site in the far background. The 3.4-kilometre-long European XFEL runs from DESY to the underground experimental hall in the main building (foreground).

For the DESY Photon Science facilities the year 2015 was a major step towards normal user operation after the heavy construction work during the year before.

At the free-electron laser FLASH nearly 4500 hours of user operation were offered to the user community. The FLASH II project was officially declared completed after the first beam had been delivered to the new FLASH2 experimental hall “Kai Siegbahn”. Meanwhile, the commissioning of the second free-electron laser (FEL) undulator has made great progress with parallel lasing of both FELs successfully demonstrated. The advantage of gap tuneable undulators was explored for FELs at FLASH2 allowing for a fine-tuning of the lasing process.

This resulted in new record values of the achievable single pulse intensities. At present two beamlines at FLASH2 are

under construction and first experiments are planned for spring 2016.

In spring 2015 PETRA III restarted user operation after more than a year of construction work for the extension. Although more than 160 m of the storage ring have been completely rebuilt to allow for the installation of additional insertion devices, the restart of the PETRA III storage ring and of the user operation in the experimental hall “Max von Laue” was comparatively smooth. At the same time, the construction of the first two beamlines made progress and commissioning of these experiments in the extension hall north took place by the end of the run.

Due to the need for installation of additional front end components for the extension beamlines in the ring tunnel,

the 2015/2016 and the 2016/2017 winter shutdowns will be longer than usual before PETRA III returns to normal user operation with approximately 5000 h for synchrotron radiation experiments per year. DESY investigates the possibility to develop PETRA III towards a diffraction limited light source on the long run.

DESY and its partners of the accelerator consortium for the construction of the European XFEL linear accelerator were able to significantly speed up the production, testing and installation of the superconducting accelerator modules with almost 60 % of them being installed by the end of the year 2015. Therefore, we are confident that first electron bunches will be accelerated before the end of 2016 so that first experiments can be carried out in the first half of 2017.

The science platforms on the DESY/Bahrenfeld campus made significant progress in 2015. We congratulate Henry Chapman (Center for Free-Electron Laser Science CFEL, DESY and University of Hamburg) for being awarded the Gottfried Wilhelm Leibniz Prize from the DFG for his achievements in the field of serial femtosecond crystallography. The construction of the new building for the Centre for Structural Systems Biology (CSSB) is progressing very well with the topping-out ceremony having taken place in



Henry Chapman (DESY/CFEL) received the 2015 Leibniz Prize from the DFG president Peter Strohschneider (left) on 3 March 2015 in Berlin.

September. Nearly all group leaders for the CSSB research groups of the nine participating institutes have been appointed. CSSB will come to full operation as soon as the groups will have moved into the new building, which is expected for the beginning of the year 2017.

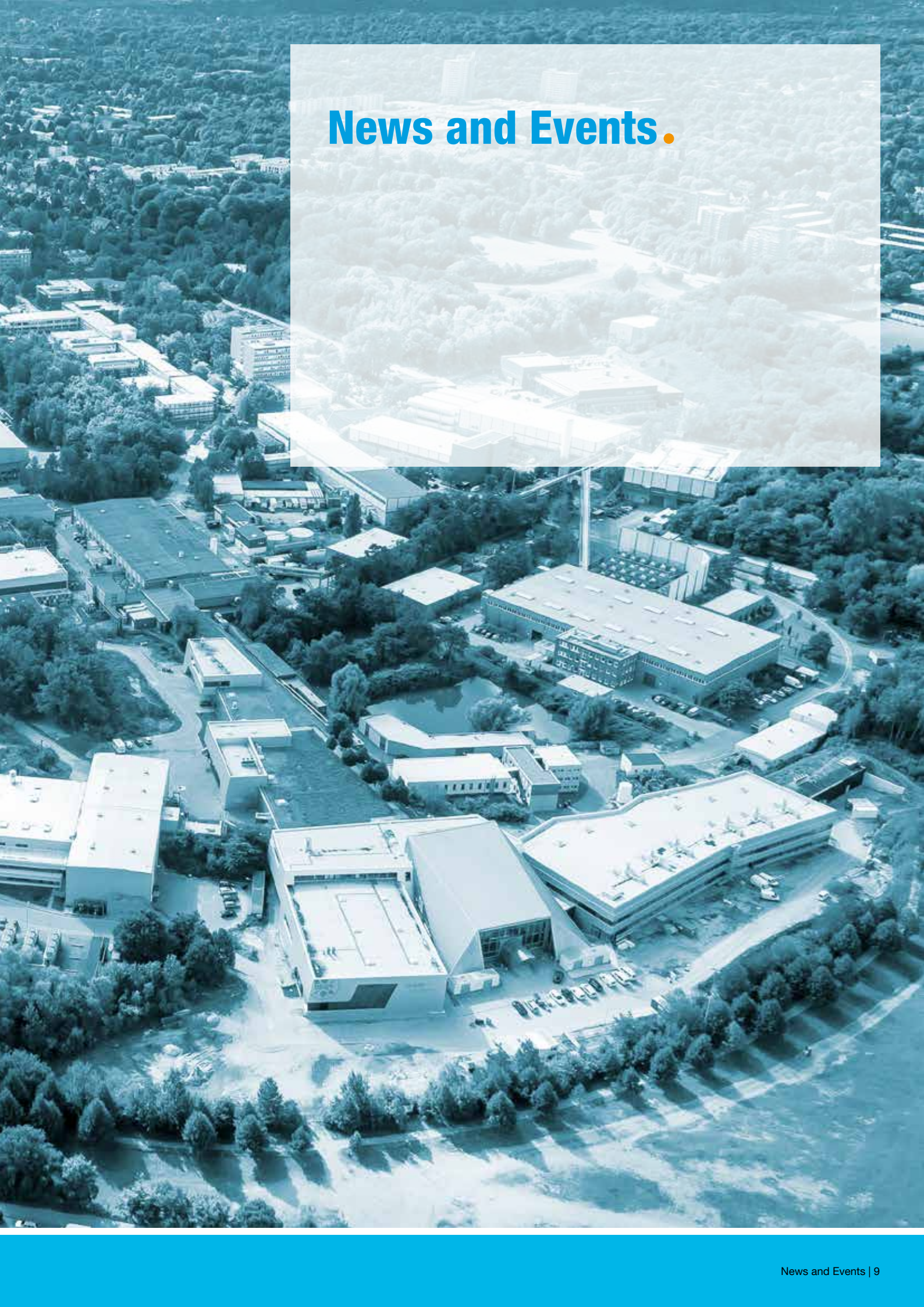
The planning for the new Photon Science building at DESY has been finalized and the start of construction is envisaged for mid-2016. This building will house the DESY NanoLab, which provides tools for user sample preparation and characterisation as well as for in-house research experiments.

In this report you will find a number of examples of science and technology developments that have been published or carried out during the year 2015 by users at our facilities PETRA III and FLASH as well as from in-house research performed at ours but also at other facilities and within CFEL. It shows that this campus with all its partners is already now a very exciting place for research using photons. However, the development of the campus is still continuing. The Max Planck Society will construct a building to house additional groups of the recently established Max Planck Institute for the Structure and Dynamics of Matter (MPSD) from mid-2016 on close to the present CFEL building and the PETRA III experimental halls. Also at the Bahrenfeld campus the new Centre for Hybrid Nanostructures (CHyN) is being established by the University of Hamburg. The topping-out ceremony has taken place mid-December 2015.

All these activities are only possible due to the dedication of all DESY staff as well as of our users and collaborators. I wholeheartedly would like to thank all of them for their continued effort and support. ●

Edgar Weckert
Director Photon Science



An aerial photograph of a university campus, showing various buildings, parking lots, and green spaces. A semi-transparent white rectangular box is overlaid on the upper portion of the image, containing the text 'News and Events.' in a bold, blue, sans-serif font. The text is positioned in the upper left quadrant of the white box. The background image shows a dense cluster of buildings, some with flat roofs and others with more complex structures, interspersed with trees and parking areas. The overall color palette is dominated by the blue of the text and the white of the box, set against the natural colors of the campus scene.

News and Events.

News and Events.

A busy year 2015

January

5 January:

Robin Santra Elected APS Fellow

Robin Santra, head of the theory group at the Center for Free-Electron Laser Science (CFEL) at DESY and professor of physics at the University of Hamburg, was elected Fellow of the American Physical Society. He has been awarded for his successful theoretical description of light-matter interactions, especially for processes involving X-ray laser light and inner-shell electrons in atoms and molecules. With the fundamental understanding of these processes it is possible to extend the areas of application at modern radiation sources like the free-electron X-ray lasers FLASH and European XFEL currently under construction.



Robin Santra.

28 – 30 January:

Record Attendance at the Joint European XFEL and DESY Photon Science Users' Meeting

The annual users' meeting of the light sources at DESY and the future X-ray laser European XFEL has again seen a record attendance: More than 900 participants registered for the three-day event, more than ever before. In over 30 presentations, the participants from 38 countries discussed new developments of the DESY facilities, the construction progress of the European XFEL, and current research.

Research highlights presented at the users' meeting included investigation and optimisation of custom made cellulose fibres, snapshots of ultrafast magnetisation processes and the first frames of a molecular movie of photosynthesis. In addition, the extension of the heavily overbooked light sources FLASH and PETRA III was discussed, as well as the planned experimental stations at the currently built European XFEL. Numerous satellite workshops on specific topics, a poster exhibition and an industry fair presenting current technological inventions completed the program.



Lively discussions during a coffee break at the Photon Science Users' Meeting.

February

18 February:

Topping-out Ceremony for the Headquarters Building of the European XFEL

The European XFEL held the topping out ceremony for its headquarters building in Schenefeld in the German federal state of Schleswig-Holstein. The event marked a milestone in the construction of the X-ray free-electron laser, which is one of Europe's largest new international research facilities. Over 350 guests, including representatives from the federal government, the states of Schleswig-Holstein and Hamburg, the consular corps, local politicians and administration, the European XFEL Council, and European XFEL employees and their colleagues from DESY, gathered on the construction site to celebrate the event.



Traditional toast raised by the foreman of the construction workers.

The headquarters building is constructed on top of the underground experiment hall. The complex is 3.4 km away from the starting point of the facility at the DESY site and is linked to it by a system of tunnels for the linear accelerator and undulators. When completed, the European XFEL will be a user facility open to scientists around the world. They will be able to study the nanocosmos using ultrashort flashes of X-ray light a billion times brighter than traditional light sources. The scientists will work in the experiment hall, which was completed in 2013, and in the headquarters' ground floor, which will be equipped with laboratories for biology, electron microscopy, and sample preparation. The three-storey building will also house the facility's offices. The facility is under construction since 2009, and work on the headquarters building, the final major aboveground structure to be erected, started in May 2014. Construction and commissioning of the facility is supported by 11 countries. European XFEL employees will move into the headquarters building next year as they prepare for the beginning of user operation in 2017.



At the topping out ceremony of the European XFEL headquarters building. From left: Rolf Fischer, Beatrix Vierkorn-Rudolph, Dorothee Stapelfeldt, Helmut Dosch, Massimo Altarelli, Martin Meedom Nielsen celebrate the headquarters building.

March

25 – 27 March: 14th DESY Research Course on X-ray Science

The 14th course of this series was entitled “New Trends in X-Ray Scattering and Spectroscopy from Magnetic Materials” and aimed to provide an introduction to the recent developments in the field of magnetic materials under X-ray light. In 15 talks special attention was paid on modern experimental techniques and scientific applications. The course series addresses master and PhD students, young research fellows, as well as interested scientists.

April

27 April: Restart of PETRA III

After a one-year shutdown, the science programme at PETRA III has finally been resumed. The shutdown had cleared the way for a substantial expansion of the number of measuring stations at this much requested X-ray source.



The large experimental hall „Max von Laue“ at PETRA III.

Every year about 2000 researchers use the X-ray light of PETRA III to get unique insights into the nanoworld. They study new drug substances, new materials or chemical processes with highly brilliant X-rays up to 5000 times finer than a human hair. Therefore, beam time at PETRA III is much sought after by scientists from around the world. The available measurement time is regularly completely overbooked, only a fraction of the experiment requests can be granted. In the future, two new experimental halls will allow more researchers to get access to beamtime. While the research program was resumed on 27 April at the 14 existing experimental stations, two new experimental halls will be gradually equipped with up to 11 additional stations which will focus on studying the properties of new materials.

For the construction of these two new halls the PETRA III storage ring tunnel had to be completely torn down in two sections of about 80 metres each. In these sections, the storage ring was rebuilt with new components after the foundations for the new experimental halls had been finished.

May

20 May: Celebrating FLASH

FLASH delivers extremely short and intense flashes of X-rays, which can be used to observe ultra-fast processes taking place in the world of molecules and atoms. Each year the facility is used by about 200 scientists from all over the world, but this is only a small fraction of the research proposals submitted. In the past three years, DESY has extended the facility spending 33 million Euros, adding a second laser line and a second experimental hall. This not only increases the number of available experimental stations to up to twelve but the quality of the X-ray flashes has also been improved by means of new technological developments. In contrast to the original laser FLASH1, the wavelength of the X-rays on the new laser line FLASH2 can be altered during operation easily.

During a ceremony, Olaf Scholz, First Mayor of Hamburg, and Anders Lönn, State Secretary to Sweden’s Minister for Higher Education and Research, named the two FLASH experimental halls after the physicists and Nobel Prize winners Albert Einstein and Kai Siegbahn.

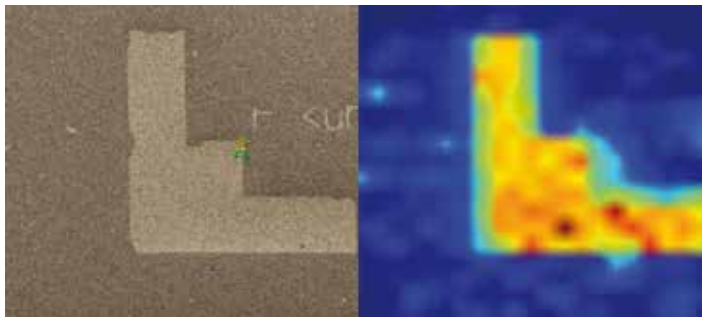
There is a special relationship between Albert Einstein, Kai Siegbahn and the research carried out at FLASH. Einstein’s explanation of the photoelectric effect forms the basis of electron spectroscopy, a method which 50 years later was introduced by the Swedish physicist Kai Siegbahn. This technique allows revealing the chemical composition of matter and has become an indispensable tool for material scientists. At FLASH this tool is actually being developed further as a way of studying ultra-fast processes. The choice of Kai Siegbahn’s name is also intended to emphasise the close and fruitful German-Swedish collaboration in research, which has been taken to a new level with the Röntgen-Ångström-Cluster, a very successful collaboration between German and Swedish research centres and partners from universities.



Hamburg's mayor Olaf Scholz making a speech at the FLASH celebration.

**27 May:
EU Approves Funding for Nanotech Research Project at DESY**

DESY is involved in a new EU project that aims to coordinate research in the field of nanoscience in Europe. In future “Nanoscience Foundries and Fine Analysis” (NFFA Europe) will more closely link the leading European facilities for research into nanomaterials with the various groups studying nanoscale phenomena and nanotechnology. The European Union gave a go-ahead for this ten-million-euro project, which beside DESY involves further 19 partners from ten European countries. The aim is to promote multidisciplinary research on the nanoscale, from synthesising and characterizing nanomaterials to the development of the underlying theory and numerical simulations using high-performance computers.



Electron beam induced marker of platinum on a site nearby a preselected nano-object, imaged with a high resolution scanning electron microscope (left) at DESY NanoLab and after re-localizing with the Pt X-ray fluorescence at the X-ray beamline P10 at PETRA III (right). Total area is 150 x 150 μm^2 .

Within the new NFFA Europe infrastructure the NanoLab at DESY offers European users means for synthesis, chemical and structural analysis, and structuring of nanomaterials. The focus is particularly on the combination of electron microscopy with synchrotron radiation based techniques at dedicated PETRA III beamlines which were funded by the Federal Ministry for Education and Research to encourage collaborative research. Beyond this, the NanoLab is in charge of developing a new procedure, known as “Advanced Nano-Object Transfer and Positioning”, together with five European partners from France, Italy and Greece as part of the NFFA Europe project. In future, this will make it easier to label individual nano-objects in the laboratory and specifically analyse them using a nanofocused X-ray beam, allowing individual nanoparticles or nanostructures to be characterised using complementary X-ray and electron based techniques.

June

**2 June:
Breakthrough in the sFLASH Seeding Experiment**

A team of researchers from DESY, the University of Hamburg and the Technical University of Dortmund has managed to demonstrate seeding by a procedure known as high gain harmonic generation (HG) at the sFLASH test facility. Free-electron lasers (FEL) produce very brief, high-intensity pulses of X-rays. Synchrotron radiation is generated by bunches of electrons close to the speed of light travelling through an undulator whereby light of a certain wavelength is spontaneously amplified by orders of magnitude to produce short X-ray laser pulses. Due to the nature of this spontaneous amplification the properties of the individual pulses vary. In order to improve the temporal and energy resolution of FEL experiments, scientists are looking for ways of triggering (“seeding”) the process of producing radiation by introducing a carefully defined pulse of laser radiation. The FLASH seeding experiment sFLASH uses its own ten metre long undulator in the accelerator tunnel, as well as a special measuring station in the FLASH tunnel, at which the pulses of photons can be studied.



The sFLASH undulators in the FLASH tunnel.

The scientists superimposed laser light of 266 nm wavelength with the electron beam from FLASH. During its passage through a special arrangement of magnets, the packet of electrons is divided into a periodic microstructure, which leads to a selective amplification of the FEL radiation. This does not only happen at the seeding laser wavelength, but also at far shorter lengths represented by higher harmonics of the seeding laser radiation. With the seventh harmonic at 38.1 nm the researchers managed to produce high-intensity flashes of FEL light with more than ten micro joules of energy in the sFLASH undulator. This result marks a crucial step towards studying an as yet unknown area of FEL seeding technology.

**7 – 13 June:
International Summer School of Crystallography 2015**

The Center for Free-Electron Laser Science (CFEL) for the second time hosted the International Summer School of Crystallography which was instigated by Cornelius Gati in 2014 on the occasion of the UNESCO International Year of Crystallography. Following the success of the first Summer School in 2014, this year 31 participants of 17 different nationalities spent an intense week learning the fundamentals of crystallography. Again the organizers could win Carmelo Giacovazzo from the University of Bari as tutor, who guided the attendants, mainly PhD students working in this field, through the week with lessons about history, theory, and the mathematical background of crystallography. He was supported by scientists from DESY, CFEL, University of Hamburg, European XFEL, and EMBL who gave additional lectures on specific topics. Financial and organisational support for the school came from the EU project BioStruct-X, the PIER Helmholtz Graduate School, the Hamburg Centre for Ultrafast Imaging (CUI), CFEL, the International Max Planck Research School (IMPRS) for Ultrafast Imaging and Structural Dynamics, the European XFEL GmbH, and DESY.



Participants of the International Summer School of Crystallography.

**16 June:
Support for DESY Spin-Offs**

The Helmholtz Association is providing support to two companies that have recently been set up to bring DESY research results to the market. In this context the start-up “Suna-Precision GmbH” received 100 000 Euros from the Helmholtz Enterprise programme, while the company “Cycle GmbH” obtained 130 000 Euros. This financial support was doubled by DESY.

Suna-Precision GmbH founded in 2014 will provide nano positioning systems for the scientific market and more particularly for synchrotron radiation sources worldwide. The company will exploit technological achievements obtained at the PETRA III beamline P11. The founders intend to make use of their technological lead and focus on putting together a commercial portfolio in the course of a one-year project “Synchrotron Nanopositioning”.

The second company, Cycle GmbH, was started in 2015 as a spin-off of the Ultrafast Optics and X-rays Group at the Center for Free-Electron Laser Science CFEL and supplies innovative products that use ultrafast laser technology for scientific and industrial applications, such as synchronisation units with femtosecond precision. The company will use the funds to turn an already patented ultrashort pulse laser (USP laser) into a finished product.

Already in June X-Spectrum GmbH, another DESY spin-off enterprise which was assigned funding from the Helmholtz Enterprise support programme last year received the Hamburg Innovation Award in the category “Start” for its innovative high-speed X-ray camera. The prize is presented annually in the categories “Idea”, “Start”, and “Growth”.



The X-Spectrum team receives the Hamburg Innovation Award.

**22 – 25 June:
Ultrafast X-ray Summer School**



The attendees of UXSS 2015 gathering in the foyer of the CFEL building.

More than 100 participants from 19 countries attended this year's Ultrafast X-ray Summer School UXSS 2015 at the Center for Free-Electron Laser Science CFEL. During four days the course aimed for giving doctoral students and postdoctoral researchers the opportunity to learn about the latest developments and opportunities in ultrafast X-ray science.

The topics in the highly interdisciplinary program ranged from accelerator physics to molecular biology. In lectures given by nine internationally renowned experts, the participants could learn about the impact of the fast developing ultrafast X-ray techniques on fields like structural biology, plasma physics, and chemistry. The lecture program was complemented by practical group work, where participants wrote mock proposals for experiments at Europe's future X-ray laser European XFEL that is currently being built. In a poster session the best proposal was awarded.

UXSS 2015 was jointly organized by CFEL and the PULSE institute at SLAC National Accelerator Laboratory in the U.S., and financially supported by the VolkswagenStiftung. The UXSS is alternately held at CFEL and PULSE every other year.

**28 June – 2 July:
17th International Workshop on Radiation Imaging Detectors
"iWoRiD 2015"**

The International Workshops on Radiation Imaging Detectors are held yearly and provide an international forum for discussing current research and developments in the area of position sensitive detectors for radiation imaging, including semiconductor detectors, gas and scintillator-based detectors.

Topics include processing and characterization of detector materials, hybridization and interconnect technologies, design of counting or integrating electronics, readout and data acquisition systems, and applications in various scientific and industrial fields. This year the workshop was organized by DESY with focus on high-intensity X-ray Photon sources and could welcome almost 200 participants. The workshop with an exceptionally high level of talks was complemented by a lively poster session and an industrial exhibition.



Attendees of the iWoRiD 2015 listening to a talk in the DESY auditorium.

July

12 – 17 July: 12th International Conference on Femtochemistry

Femtochemistry deals with the ultrafast chemical interactions between molecules and atoms and is of fundamental importance for a broad spectrum of questions in many disciplines, from basic chemistry to physics, biology, medicine, and materials sciences. World leading experts in this field gathered at DESY on the occasion of the 12th International Conference on Femtochemistry "FEMTO12". 250 participants from all over the world discussed the latest developments and advances. The conference was opened by Hamburg's Second Mayor and Senator for Science, Katharina Fegebank, the Vice President of the University of Hamburg, Claudia Leopold, and the Chair of DESY's board of directors, Helmut Dosch. Femtochemistry pioneer and Nobel laureate Prof. Ahmed Zewail from the California Institute of Technology (Caltech) held a public scientific lecture entitled "Light and Enlightenment".

This year's edition of the biennial conference was hosted by the Hamburg Centre for Ultrafast Imaging (CUI), DESY, and the Center for Free-Electron Laser Science (CFEL). It took place within the framework of UNESCO's International Year of Light and was organized and chaired by Jochen Küpper, who works at CFEL and CUI and is a professor of physics at the University of Hamburg. Presented highlights include the recording of molecular movies of chemistry in action, laser-controlled molecular dynamics, electron and energy transport for solar energy harvesting, and ultrafast processes in biochemical and biological systems. Such chemical processes typically take place on the time scale of femtoseconds.

Femtochemistry uses different tools that are mostly based on light. With its soft X-ray laser FLASH, DESY operates a super slow-motion camera for the nanocosmos. Scientists at DESY also develop next generation laser light sources for ultra-short pulses in the even shorter attosecond regime, and starting 2017, the European XFEL will open previously inaccessible views into the ultrafast dynamics of molecules and atoms.



Ahmed Zewail giving a public scientific lecture at the Femto12.

21 July: DESY Summer Student Program 2015

A total number of 519 students applied for the summer student program 2015. This year DESY could again welcome 115 of these students at both its locations in Hamburg and Zeuthen. During the following eight weeks, the junior researchers from 28 nations got a practical insight into research at DESY. 19 female and 19 male students were selected for the part of the program dedicated to photon science.

These 38 students came from Germany, China, Colombia, Czech Republic, Great Britain, Hong Kong, Indonesia, Italy, Kazakhstan, Norway, Poland, Russia, Slovakia, Thailand, Turkey, and Ukraine. They attended a special lecture series on research with photons at DESY and worked on small projects within research groups at PETRA III, FLASH, CFEL, European XFEL and University of Hamburg. The summer student program is a significant part of DESY's educational activities.

During their stay the students live on the DESY campus and it is a great and valuable experience to work in the international ambience of a large scale facility and to meet other students from all over the world. Each year a number of students from previous years return to DESY to pursue their academic training.



Summer students 2015 working in the field of photon science with Rainer Gehrke (right), coordinator of the photon science part of the DESY summer student program.

August

24 August:

Free-Electron Laser Prize Awarded to DESY Pioneers

At the 37th International Free Electron Laser Conference FEL 2015 in Daejeon, South Korea this year's FEL Prize was awarded to the DESY scientists Mikhail Yurkov and Evgeny Schneidmiller for their pioneering work in developing and improving free-electron lasers. The award recognises outstanding contributions to the study and development of this key future-oriented technology.

Right from the start, Yurkov and Schneidmiller participated in designing the free-electron laser at DESY's TESLA Test Facility, which gave rise to FLASH in 2005. They also made key contributions towards improving the performance of FLASH. At the European XFEL, where Mikhail Yurkov is leading the work package on FEL concepts, they are very strongly involved in calculating and optimising the FEL processes. Reinhard Brinkmann, the director of DESY's accelerator division, presented the award to the prize winners. This was already the second time that the award went to Hamburg: in 2006, the FEL Prize was awarded to Jörg Roßbach from University of Hamburg and Evgeny Saldin from DESY.



First row, from right to left: Mikhail Yurkov and Evgeny Schneidmiller with the Director of DESY's Accelerator Division, Reinhard Brinkmann, and the Chairman of the DESY Board of Directors, Helmut Dosch.

22 – 29 August:

Third Summer School of the Röntgen-Ångström-Cluster and the Ioffe Röntgen Institute

About 70 participants attended the third RACIRI summer school jointly held by the Röntgen-Ångström Cluster (RAC) and the Ioffe Röntgen Institute (IRI). The RACIRI Summer School is a joint initiative by Germany, Russia and Sweden in the field of material and nanoscience with a regional focus on major facilities in the Baltic region. The Röntgen-Ångström-Cluster is collaboration between German and Swedish research centres; the Ioffe Röntgen Institute is a German-Russian research cooperation aiming to promote collaboration between large research facilities. This year the event was organized for the first time by DESY in Germany. It took place on the island of Rügen and focused on the investigation of dynamic processes such as photosynthesis using time-resolved measurements with X-rays and neutrons.

One of the highlights of the event was the keynote address held by the Israeli structural biologist Ada Yonath, who was awarded the Nobel Prize in 2009 for her examination of the ribosome. She had used modern methods of X-ray crystallography to determine the precise structure of these protein factories that operate inside biological cells. Some of her ground breaking work took place at DESY. On the occasion of her presence at the RACIRI Summer School, the mayor of Remscheid, Burkhard Mast-Weisz, presented the city's renowned Röntgen Medal for the year 2014 to Ada Yonath, in recognition of her achievements.



Ada Yonath (middle) with students of the RACIRI summer school.

September

3 September: Series of Short Workshops on Future Science Perspectives at FLASH

In order to start an exchange of ideas between the FLASH team and current and potential users of FLASH about which direction the facility should take over the next few years, DESY hosted a series of one-day workshops in 2014 and 2015 covering various science areas at FLASH. The immediate scope concerned short and medium term developments at FLASH1 and FLASH2, seeding options, etc. Longer-term upgrades were also discussed but were not at the centre of these workshops. Some of the discussed questions were: What will be burning questions in the respective field in the next few years and which direction will it be moving into? What can FLASH do to help tackle these questions, what parameters does it have to provide and how does the facility have to be developed to stay competitive with other sources? The various workshops covered the topics atomic, molecular and optical physics (AMO) science at FLASH, condensed matter science, gas phase and surface chemistry, ion spectroscopy at FLASH, and THz driven science.

In summary, it was concluded that FLASH is unique with respect to THz-XUV pump-probe as well as XUV pump-XUV probe facilities, with three split-and-delay stages at FLASH1 and two planned for FLASH2. An important feature is the high repetition rate which facilitates experiments that require high statistics due to low signal intensity. For some experiments, the pointing and energy stability of SASE is presently the limiting factor; seeding would help here. Other issues were even shorter pulses and better synchronization than presently achievable. Here, many technical developments, in particular with respect to optical lasers and further timing stabilization are in progress at FLASH.



Experiments at FLASH.

9 September: CSSB Topping-Out Ceremony

The Centre for Structural Systems Biology (CSSB) celebrated its topping-out ceremony on the DESY Campus. Hamburg's Second Mayor and Senator for Science, Katharina Fegebank, Karl Eugen Huthmacher from the German federal government, Schleswig-Holstein's Science Minister, Kristin Alheit and DESY Director Helmut Dosch and other representatives of CSSB's nine partners joined CSSB Scientific Director, Matthias Wilmanns, in celebrating this important milestone. From 2017 the CSSB will conduct research on the mechanisms of bacterial and viral infections using a unique and interdisciplinary approach in a joint initiative of nine Northern German research institutes. The novel light sources at DESY and the cryo-electron microscopes in the future CSSB building will be used for this purpose. This combines the excellent possibilities of the DESY light sources with additional powerful methods in order to promote the understanding of the molecular processes of infections and disease patterns. This is the foundation for the development of customized drug treatments which will ultimately result in more effective control of infections.

In their welcome addresses, Hamburg's Senator, Katharina Fegebank, and Schleswig-Holstein's Minister, Kristin Alheit, highlighted the important role which CSSB plays in fostering interdisciplinary scientific cooperation in Northern Germany.



The foreman of the construction workers, Ingo Ehbrecht (Company Wayss & Freytag), during the traditional topping-out ceremony for the CSSB building.

**13 – 18 September:
International Conference on the Applications of the
Mössbauer Effect**

A large part of the research community working in the field of Mössbauer spectroscopy attended the “International Conference on the Applications of the Mössbauer Effect” (ICAME 2015) in Hamburg. The conference has been staged biennially for almost 50 years now, at changing global venues, regularly attracting 200 to 300 participants from over 40 different countries. It is dedicated to scientific applications of the Mössbauer effect, which has become an indispensable tool both in fundamental research and in modern materials science.

The Mössbauer effect can provide unique insights into the internal structure and dynamics of solids. It can be used, for example, to build an extremely sensitive “speed trap” to measure the velocity of atoms moving within matter. Or it can be used to realise a microscope to examine on the atomic level the magnetic structure of new materials for the next generation of data storage devices. This potential was also recognised by Erich Gerdau, who observed the Mössbauer effect using synchrotron radiation at DESY in 1985 for the first time, opening up a new field of research with entirely new applications. After the first experiments in Hamburg, the field of synchrotron Mössbauer spectroscopy rapidly spread throughout the world, and it will continue to produce brilliant insights in all fields of the natural sciences, particularly by using the high-brilliance X-rays available at PETRA III and the future European XFEL.

The year 2015 marks the 30th anniversary of Mössbauer spectroscopy using synchrotron radiation, the fifth anniversary of the method being applied for the first time at PETRA III, and – last, but by no means least – the 80th birthday of the man who pioneered this technique, Erich Gerdau, who was professor of experimental physics at Hamburg University until his retirement in 2000.



Participants of the ICAME 2015 in front of the main building of the University of Hamburg where the conference took place.



Edgar Weckert (Director Photon Science) presents Erich Gerdau (right) with the DESY Silver Badge of Honour at the ICAME2015.

This year's DESY events related to photon science were in perfect accord with the UNESCO International Year of Light 2015.

The goal of International Year of Light 2015 was to highlight to the citizens of the world the importance of light and optical technologies in their lives, for their futures and for the development of society.



**INTERNATIONAL
YEAR OF LIGHT
2015**

October

7 October: DESY Again Hosted the Russian-German “Travelling Seminar”

The “travelling seminar” is an initiative started a few years ago by the University of Erlangen-Nürnberg and funded by the German Ministry of Education and Research (BMBF) in the framework of the German-Russian Cooperation. Every year, alternatively in Germany and Russia, a group of Russian and German PhD students and young scientists, selected by a bilateral commission, participate in a two-week summer school in photon science, of which one week is dedicated to visiting synchrotron radiation and FEL facilities in the hosting country. In 2015, the travelling seminar took place in Germany, and comprised a visit of DESY.

The group of about 25 students, accompanied by four faculty members from Erlangen, attended talks held by DESY scientists illustrating the DESY photon sources and especially addressing nanosciences.



The participants of the Russian-German “Travelling Seminar” on their visit at DESY.

November

7 November: DESY Day

More than 18000 visitors were counted when DESY opened its doors to the public at the DESY Day. From 12:00 a.m. until midnight more than 1200 colleagues from DESY and its partner institutes presented our activities to curious people of all ages, answered questions and performed demonstration and hands-on experiments. They showed that research at DESY is not only about fascinating machines but also about engaged and excited people. About 120 attractions, lectures, and join-in activities made the DESY Day a great experience for our guests.

The DESY Day was part of the Hamburg “Night of Knowledge”. About 1000 program points all over the city attracted more than 30000 citizens to gain insight into the research activities in Hamburg. This was a record attendance.



At the DESY Day: Curious visitors in the PETRA III experimental hall “Max von Laue”.



Colorfully illuminated PETRA III hall.

December

14 December

PhD Thesis Prize for Denise Erb and Timon Mehrling

The PhD thesis award of the Association of the Friends and Sponsors of DESY is presented annually for one or two outstanding PhD theses. In 2015 this prize is shared by Denise Erb and Timon Mehrling.

Denise Erb was born in Essen and studied physics at the Ruhr University in Bochum. In 2010 she joined the group of Ralf Röhlsberger at DESY to start her PhD work entitled “Highly-Ordered Magnetic Nanostructures on Self-Assembled $\alpha\text{-Al}_2\text{O}_3$ and Diblock Copolymer Templates”. It addresses the preparation of large areas of uniform periodic metal nanostructures on surfaces by means of self-assembly and their characterization with atomic force microscopy, grazing incidence small angle scattering, and nuclear resonant scattering. Starting from a nanostructured surface, pattern formation in subsequently deposited layers of various materials is guided by the previous layer. This “bottom-up” approach finally leads to a variety of morphologies like nanodots or -wires with defect densities comparable to those of “top-down” nanofabrication techniques. The method offers the potential to be a much faster alternative to these techniques. More detailed information can be found in this report under the contribution “Metal Nanopatterning in Three Easy Steps”.

Timon Mehrling was born in Interlaken-Untersen in Switzerland and studied physics in Freiburg, Trondheim, and Munich before he came to DESY to start his PhD work in the group of Jens Osterhoff. In his work entitled “Theoretical and Numerical Studies on the Transport of Transverse Beam Quality in Plasma-Based Accelerators” Timon Mehrling developed a new 3D Particle-In-Cell code for modelling the behaviour of this new type of particle accelerators. The results of his studies lead to a better understanding of the effects which influence the transverse beam quality and open new possibilities to improve this quality.



At one of the numerous demonstration experiments during the DESY Day: Gummy bears in a stretching bank.



Attentive audience in the FLASH seminar room.



The winners of the PhD thesis award, Denise Erb and Timon Mehrling, with Helmut Dosch (left) and Friedrich-Wilhelm Büber (right), chairman of the “Association of the Friends and Sponsors of DESY”.



Science Highlights

Atomic and molecular dynamics

- > Nonlinear photoionization reveals hidden substructure 24
- > A new phase for X-ray quantum optics 26
- > Making a four-body Auger process happen 28
- > Synchronised molecular rotations for novel investigations 30

Surfaces, thin films and interfaces

- > Metal nanopatterning in three easy steps 32
- > Nanoparticles increase efficiency of organic solar cells 34
- > Watching layers of C₆₀ molecules grow 36
- > Elucidating the formation mechanism of layered thermoelectric oxides 38
- > Crystal meets amorphicity 40

Electronic and magnetic structure

- > Ultrafast tracking of electron spins 42
- > Enabling a new class of electronic devices 44
- > Fading of Van Gogh's red lead pigment 46
- > Superconductivity in new geometries of matter 48

Structure and structural dynamics

- > Platonic beauties caught in flight 50
- > Heavy metal at ultra-high static pressures 52
- > New insight in materials synthesis 54
- > Visualising aging in Li ion battery electrodes 56
- > Fast strain mapping of nanowire LEDs using X-ray nanobeams 58
- > Real-time imaging of grain dynamics 60

Macromolecular crystallography

- > Nature's tiny solar panels 62
- > Looking into the mirror 64
- > Insights into bi-specificity of A domains 66
- > Uncovering protein secrets using X-FEL pulses 68

Science of X-ray sources

- > How to assess data misfits if experimental errors are unknown 72
- > Towards miniaturized particle accelerators 74
- > FLASH2 undulators 76
- > The right time, in the right spots 78
- > X-ray focusing down to below 10 nm 80
- > Simple and advanced X-ray 3D imaging 82
- > A new sample holder for thousands of micro-crystals 84

Nonlinear photoionization reveals hidden substructure.

The xenon giant dipole resonance revisited

Photoionization of atoms is a powerful tool for the investigation of atomic structure and intra-atomic electron dynamics. In combination with photoelectron spectroscopy it provides insight into many-body interactions within the atomic shells. Using atomic xenon as a prime example, we have demonstrated for the first time how nonlinear XUV spectroscopy can probe electron correlations within a many-body system and how features in the atomic response, normally hidden in linear spectra, thus can be uncovered. Excellent agreement between theory and experiment supports the prediction that two distinct quantum resonance states underlie the 4d giant dipole resonance in xenon.

In the early 60s, measurements of absorption characteristics of inner shell electrons with high angular momentum in the extreme ultraviolet (XUV) photon energy range revealed a huge and broad resonance in the photoabsorption cross section of the 4d electrons in xenon (nuclear charge $Z = 54$) [1]. Since then, this giant dipole resonance, which corresponds to a one-photon excitation of one electron from the 4d shell into a temporarily trapped state in the continuum (shape resonance), was the topic of numerous theoretical and experimental studies. The process cannot be described correctly in the independent-electron picture and, hence, it is an illustrative example of a collective excitation. Xenon's resonating character under XUV radiation is interpreted as the collective response of all ten 4d electrons to an external weak-field perturbation, analogously to phenomenology observed in condensed-matter or nuclear physics [2]. Only when electron correlation effects within the 4d shell are included, quantitative agreement with experimental data is achieved. Figure 1 shows a graphical representation of a $4d_0$ orbital in xenon. So far, observations have been compatible with the assumption that the 4d giant dipole resonance is a single broad resonance, which means that it is associated with only a single quantum resonance state.

Free-electron lasers (FELs) with their high brilliance enable the investigation of collective response mechanisms of many-body systems in the nonlinear regime. To study the 4d ionization of xenon beyond the linear response we recently combined photoelectron spectroscopy with first-principles calculations. This joint work demonstrates that XUV two-photon spectroscopy can reveal the existence of substructures in the absorption profile, which remain unresolved in one-photon spectroscopy.

The experiment was performed at the BL2 beamline of FLASH. FEL pulses at photon energies of 105 and 140 eV, i.e., in the

range of the xenon 4d giant dipole resonance, were focused to a few microns. A magnetic bottle electron spectrometer served for measuring the kinetic energy of the electrons produced by one- and two-photon absorption. The 4d two-photon emission lines appear in the photoelectron spectrum at high kinetic energies, separated from the one-photon lines by the energy of one photon. The electron yields for one- and two-photon absorption are obtained by integrating over the corresponding photoelectron peaks. They are represented as a function of the FEL intensity in Fig. 2 (top panel) to extract the two-photon ionization cross section.

The theoretical model captures many-body processes also in the nonlinear response regime and allows for the selective inclusion of those correlation effects that are responsible for collectiveness [3]. The cross sections for one- and two-photon ionization are calculated both including correlations and switching them off (Fig. 2b and 2a), in order to relate the effect to the collective response of the system. Employing a rate equation scheme the electron yields are calculated for the intensities used in the experiment.



Figure 1

Graphical representation of a $4d_0$ electron orbital in atomic xenon. In order to describe the 4d giant dipole resonance correctly all 4d orbitals have to be taken into account.

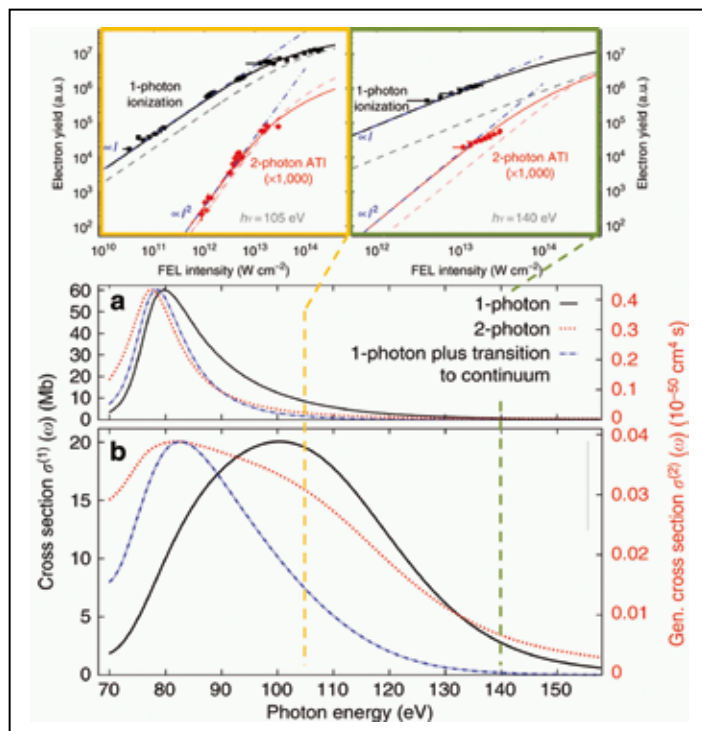


Figure 2

Top panel: Electron yields as a function of intensity at 105 and 140 eV. Experiment and theory are compared. The solid lines represent the case including electron correlation effects and match nicely the experimental data depicted with full points. Panel a) shows the model without correlation effects, while panel b) shows the model with correlation effects. The blue curves, which fail to describe the experimental data, assume a single intermediate resonance state. The red curve in panel b) is the two-photon cross section including correlation effects, which can describe the experimental results at both photon energies. It is broader than the one-photon cross section (black curve) and exhibits a knee-type structure hinting at the second resonance state underlying the 4d giant dipole resonance.

Comparison to the experiment shows excellent agreement at both photon energies when including the Coulomb coupling between all possible electron-hole states, which is responsible for the collective electronic response. In contrast, the single-particle model fails to describe the experiment. The agreement is evident in the ratio between the one- and two-photon yields, the slopes and the onset of saturation.

Having validated our theoretical model by this comparison, we analysed the two-photon cross section over the whole photon-energy range of the giant dipole resonance (70–150 eV). Surprisingly, the two-photon cross section is even broader than the one-photon curve and exhibits a knee-type structure. Assuming one single intermediate resonance state (blue curves in Fig. 2) this shape and broadening of the curve cannot be explained. For a single resonance state the cross section could be described as the product of two one-photon cross sections: one for exciting the resonance and one for the continuum-continuum transition, which decreases monotonically with increasing energy. Therefore, the two-photon process is expected to result in a

narrower profile. On the other hand, if a second intermediate resonance state is accounted for, the two-photon cross section is characterized by the occurrence of interference terms between the two intermediate states, resulting in the broadening and the knee-type structure of the cross section (red curves in Fig. 2a, b).

For the first time, the agreement of experiment and theory beyond the linear response regime legitimizes the prediction of two quantum resonance states underlying the 4d giant dipole resonance in xenon. Nonlinear XUV spectroscopy provides significant sensitivity to unresolved substructures in the collective excitation of many-body systems. Nonlinear spectroscopic techniques enabled by modern short-wavelength light sources might lead to a deeper understanding of collective behaviour in quantum systems.

Contact: Michael Meyer, michael.meyer@xfel.eu, Robin Santra, robin.santra@cfel.de

Authors

Tommaso Mazza¹, Antonia Karamatskou^{2,3}, Markus Ilchen^{1,4}, Sadegh Bakhtiarzadeh^{1,3}, Amir Jones Rafipoor^{1,3}, Patrick O’Keeffe⁵, Mossy Kelly⁶, Nichola Walsh⁶, John T. Costello⁶, Michael Meyer¹, and Robin Santra^{1,3}

1. European XFEL GmbH, Albert-Einstein-Ring 19, 22761 Hamburg, Germany
2. Center for Free-Electron Laser Science, DESY, Notkestrasse 85, 22607 Hamburg, Germany
3. Department of Physics, University of Hamburg, Jungiusstrasse 9, 20355 Hamburg, Germany
4. Stanford PULSE Institute, SLAC National Accelerator Laboratory, Menlo Park, 2575 Sand Hill Road, CA 94025, USA
5. CNR Istituto di Struttura della Materia, CP10, I-00016 Monterotondo Scalo, Italy
6. School of Physical Sciences and NCPST, Dublin City University, Dublin 9, Ireland

*These authors contributed equally to this work.

Original publication

“Sensitivity of nonlinear photoionization to resonance substructure in collective excitation”, *Nature Communications* 6, 6799 (2015). DOI: 10.1038/ncomms7799

References

1. D.L. Ederer, “Photoionization of the 4d Electrons in Xenon”, *Phys. Rev. Lett.* 13, 760-762 (1964); A.P. Lukirskii, I.A. Brytov and T.M. Zimkina, “Photoionization absorption of He, Kr, Xe, CH₄, and Methylal in the 23.6-250 Å region”, *Opt. Spectrosc. (USSR)* 17, 234-237 (1964).
2. M. Ya. Amusia and J.-P. Connerade, “The theory of collective motion probed by light”, *Rep. Prog. Phys.* 63, 41-70 (2000).
3. L. Greenman et al., “Implementation of the time-dependent configuration interaction singles method for atomic strong-field processes”. *Phys. Rev. A* 82, 023406 (2010).

A new phase for X-ray quantum optics.

Towards X-ray quantum-state tomography

X-rays encode information in intensity and phase, whereas detectors register only the intensity. This phase problem is well-known in crystallography and coherent imaging, but also impedes the exploration of quantum optics at X-ray energies. We demonstrate phase-sensitive measurements characterizing the quantum state of a nuclear two-level system at hard X-ray energies. The nuclei are initially prepared in a superposition state. Subsequently, the relative phase of this superposition is interferometrically reconstructed from the emitted X-rays. Our measurement forms an important step towards X-ray quantum-state tomography, and opens a number of promising research directions.

Fundamental research and applications across all the natural sciences are fueled by the control of matter using light. At microwave to optical frequencies, the control capabilities have progressed to the quantum level. Modern synchrotron light sources and X-ray free-electron lasers strive to continue this success story at hard X-ray energies, and first steps have already been taken in X-ray quantum optics with nuclei [1-5]. A basic requirement for further progress is the capability to determine the quantum state of a given system. But unlike in the classical case, a single measurement reveals little, since it merely projects the system into an eigenstate with a certain probability according to the system's wave function. As an example, consider a wave function of the form $|\Psi\rangle = \sin(\alpha) |g\rangle + e^{i\varphi} \cos(\alpha) |e\rangle$, characterizing a two-level system with states $|g\rangle$ and $|e\rangle$. Multiple measurements are necessary already to determine the state probabilities $\sin^2(\alpha)$ and $\cos^2(\alpha)$. However the equally important phase φ poses a particular challenge, since standard detectors are sensitive to intensities only, but not to phases.

We demonstrate such phase-sensitive measurements on an archetype quantum-mechanical two-level system at hard X-ray energies. The two-level system is realized using an ensemble of ^{57}Fe nuclei embedded in a nanoscale planar cavity. We operated the system in such a way that the incident X-rays couple the nuclear ground state to a single-photon collectively excited state of the large ensemble of nuclei, effectively forming a two-level system. The incident X-ray pulses of about 50 ps duration were nearly instantaneous on the 141 ns nuclear life time scale and prepared the two-level system in a state $|\Psi\rangle$ as considered above. We then measured the phase of the light emitted by the two-level system, which enabled us to characterize the initial state prepared by the X-ray pulse.

We achieve phase sensitive measurements by interpreting our cavity as an X-ray interferometer. The first arm of the interferometer is formed by all possible X-ray pathways through the cavity which do not involve interactions with the

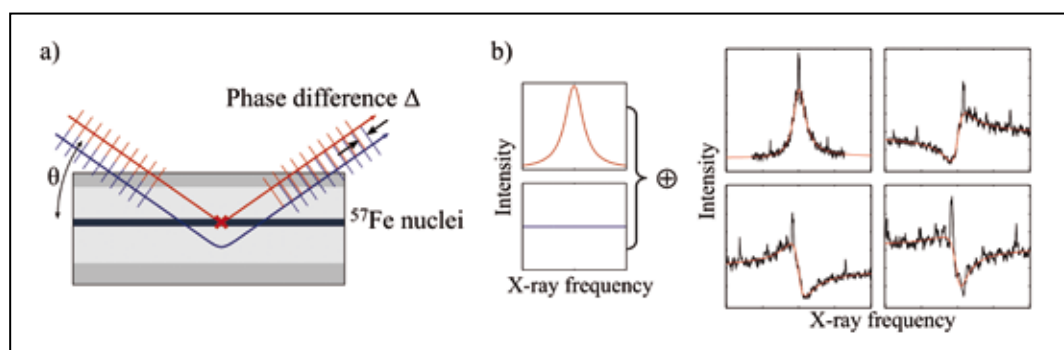


Figure 1 Panel (a) shows the cavity with X-rays impinging from the left at grazing incidence angle θ . The interferometer is formed by the two arms indicated in red and blue. The red arm comprises scattering processes involving at least one interaction with the nuclei. The blue arm is formed by all other scattering contributions. Varying the phase of this blue arm enables determination of the phase of the response of the nuclei in the red arm via the total intensity measured in reflection. (b) The spectrally narrow response of the nuclei in the red arm interferes with the spectrally broad cavity response of the blue arm, resulting in a Fano line shape. Varying the relative phase between the two arms enables controlled modification of this Fano line shape, as shown for four different incidence angles (black: experimental data, red: theory curve).

nuclei. The second arm comprises all other contributions with one or more interactions with the nuclei. The phase of the light emitted by the nuclei then becomes accessible via monitoring the intensity of the reflected X-rays as function of phase shifts Δ in the first interferometer arm. Using a recently established framework for nuclei in X-ray waveguides [6], we could show that Δ can be geometrically controlled by varying the incidence angle θ of the X-ray beam.

In the experiment at the PETRA III Dynamics Beamline P01, we employed nuclear resonant scattering to probe the Mössbauer transition of the embedded ^{57}Fe at 14.4 keV, as illustrated in Fig. 1a. The cavity is formed by a Pd(4 nm)/C(36 nm)/Pd(14 nm) layer system with the Pd layers acting as the mirrors and the C as guiding layer. The nuclei are placed as a 1.2 nm thick layer in the centre of the carbon layer. X-ray light impinges on the cavity in grazing incidence at different angles θ , and we recorded the spectrum of the reflected light to eliminate which-way information encoded in the different temporal evolution of the two interferometer arms.

Some of the recorded spectra are shown in Fig. 1b. Our theoretical analysis revealed that the control of the phase enabled a conversion of the original Lorentzian resonance line shape into Fano line profiles [7]. These Fano line shapes arise from the interference of a spectrally narrow nuclear response governing the second interferometer arm with a spectrally broad cavity response of the other arm.

In the presence of loss channels, quantum states are potentially mixed, and have to be characterized by the corresponding density matrix. The desired phase φ between the ground state and the excited state is contained in the off-diagonal density matrix element of the two-level system. We could show that this density matrix element is directly proportional to the emitted light amplitude. Hence, the phase of the emitted light gives access to φ . Using multiple spectra recorded at different phase shifts Δ we could then reconstruct the desired nuclear phase φ . Results of our analysis are shown in Fig. 2, clearly reproducing the theoretically predicted result. Our phase recovery does not make use of the theoretically known line shape of the two-level system. Thus, we expect the

method to work also for more complex systems. Combined with a measurement of the state probabilities, a complete quantum-state tomography at X-ray energies could be developed. Beyond that, the capability to detect tiny phase changes with high precision, assisted by a precise theoretical model for the different observed line shapes, invites for applications in precision spectroscopy and metrology. Finally, the phase-sensitive measurements provide access to the complex optical susceptibility of the nuclear ensemble, rather than only its imaginary part determining the absorption. By controlling the nuclear dispersion given by the real part of the susceptibility, we could recently slow down X-ray light pulses in a nuclear medium, inducing a variable delay of up to 35 ns [5]. An interferometric measurement of the dispersion could also be used to detect nonlinear light-matter interactions in future free-electron-laser experiments.

Contact: Jörg Evers, joerg.evers@mpi-hd.mpg.de

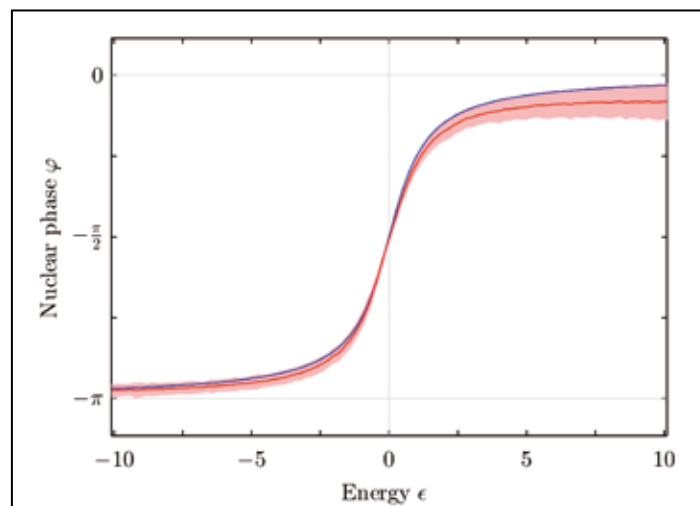


Figure 2

Our interferometric detection method enables the reconstruction of the nuclear phase from the scattered X-ray light. The red line shows the experimentally retrieved phase as a function of a dimensionless scaled energy ϵ relative to the nuclear resonance energy. Error ranges are depicted in light red shading. The theoretically expected phase of the Lorentzian typical for a two-level system and reminiscent of a simple harmonic oscillator is shown in blue.

Authors

Kilian P. Heeg¹, Christian Ott¹, Daniel Schumacher², Hans-Christian Wille², Ralf Röhlsberger², Thomas Pfeifer¹, and Jörg Evers¹

1. Max-Planck-Institut für Kernphysik, Saupfercheckweg 1, 69117 Heidelberg, Germany
2. Deutsches Elektronen-Synchrotron DESY, Notkestraße 85, 22607 Hamburg, Germany

Original publication

“Interferometric phase detection at x-ray energies via Fano resonance control”, *Phys. Rev. Lett.* 114, 207401 (2015). DOI: 10.1103/PhysRevLett.114.207401

References

1. R. Röhlsberger, K. Schlage, B. Sahoo, S. Couet, and R. Ruffer, “Collective Lamb Shift in Single-Photon Superradiance”, *Science* 328, 1248 (2010).
2. R. Röhlsberger, H.-C. Wille, K. Schlage, and B. Sahoo, “Electromagnetically induced transparency with resonant nuclei in a cavity”, *Nature* 482, 199 (2012).

3. K. P. Heeg, H.-C. Wille, K. Schlage, T. Guryeva, D. Schumacher, I. Uschmann, K. S. Schulze, B. Marx, T. Kämpfer, G. G. Paulus, R. Röhlsberger, and J. Evers, “Vacuum-assisted generation and control of atomic coherences at x-ray energies”, *Phys. Rev. Lett.* 111, 073601 (2013).
4. F. Vagizov, V. Antonov, Y. V. Radeonychev, R. N. Shakhmuratov, and O. Kocharovskaya, “Coherent control of the waveforms of recoilless γ -ray photons”, *Nature (London)* 508, 80 (2014).
5. K. P. Heeg, J. Haber, D. Schumacher, L. Bocklage, H.-C. Wille, K. S. Schulze, R. Loetzsch, I. Uschmann, G. G. Paulus, R. Ruffer, R. Röhlsberger, and J. Evers, “Tunable Subluminal Propagation of Narrow-band X-Ray Pulses”, *Phys. Rev. Lett.* 114, 203601 (2015).
6. K. P. Heeg and J. Evers, “X-ray quantum optics with Mössbauer nuclei embedded in thin film cavities”, *Phys. Rev. A* 88, 043828 (2013).
7. C. Ott, A. Kaldun, P. Raith, K. Meyer, M. Laux, J. Evers, C. H. Keitel, C. H. Greene, and T. Pfeifer, “Lorentz meets Fano in spectral line shapes: A universal phase and its laser control”, *Science* 340, 716 (2013).

Making a four-body Auger process happen.

Unambiguous observation of an exotic new atomic decay mechanism

Plain Auger decay is the emission of an electron from a highly excited atom. At sufficiently high excitation energies, the emission of three electrons becomes possible. By selective inner-shell photoexcitation of carbon ions with a carefully chosen charge state of $q = 1$ and by observing the subsequent occurrence of $q = 4$ products, unambiguous proof could be provided for the triple-Auger decay mechanism which involves simultaneous emission of three electrons while a fourth electron drops into the initially produced inner-shell vacancy.

During the 19th century, scientists learned that chemical elements emit light with characteristic wavelengths when exposed to flames. With increasing understanding of the structure of matter, it was realized that atoms in hot surroundings can be excited to discrete states with characteristic energy levels. The decay of excited states produces photons with discrete wavelengths.

An alternative decay mechanism for a highly excited atom was discovered about 90 years ago by P. Auger [1]. In a sufficiently hot environment, atoms can be so highly excited that their energy exceeds the threshold for the release of an electron from the atom. A possible de-excitation mechanism is then the emission of an electron rather than a photon. This new atomic decay was termed 'Auger process'. It produces a singly charged ion and a free electron with a discrete characteristic energy. A possible scenario for this process is the removal of an electron from the innermost electron shell with principal quantum number $n = 1$, the K shell, by an incident energetic charged particle and subsequent filling of the K-shell vacancy by an L-shell electron ($n = 2$) and ejection of a second electron, e.g., also from the L shell.

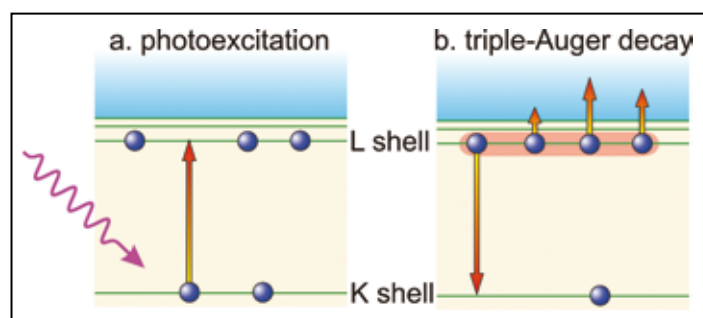


Figure 1

Schematic energy level diagram showing the preparation of an inner-shell excited state and the subsequent triple-Auger decay in which four outer-shell electrons interact with one another so that one of them falls into the initially produced inner shell vacancy while three remaining electrons are simultaneously ejected in a single event.

Several decades later a more exotic, higher-order Auger decay mechanism, the double-Auger process, was discovered [2] in which two electrons are simultaneously ejected from a highly excited atom or ion. In this case, the interaction of three electrons above an inner-shell vacancy causes one of the three electrons to jump into the inner-shell vacancy while the excess energy becoming available by that transition is distributed among the remaining two electrons which both become unbound and leave the atom. Since the ejected electrons share a discrete transition energy their spectra are continuous which makes identification of the process a difficult task. Clearly, identifying the next-order process in the sequence,

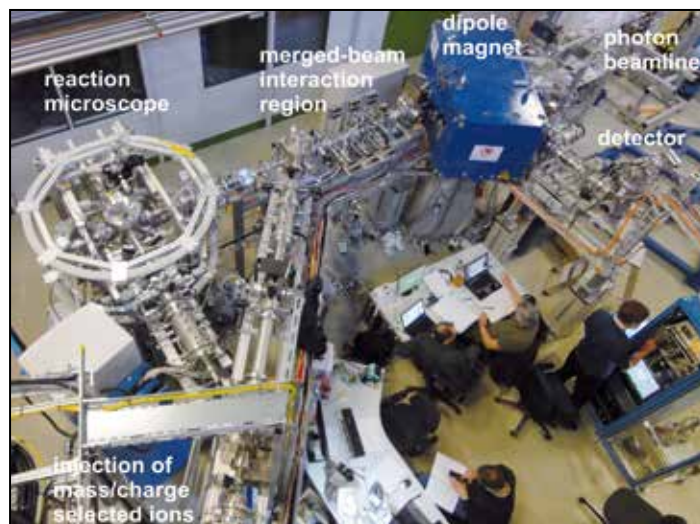


Figure 2

Experimenting at the PIPE (Photon-Ion Spectrometer at PETRA III) endstation of beamline P04. The core part of the apparatus can be seen. In the present experiments photons from the P04 monochromator interact with a counter-propagating ion beam inside the merged-beam interaction region. A separate small accelerator unit (not shown) provides isotopically clean beams of ions. The ion beam can be deflected and sent to a reaction microscope or directed to a deflector which bends the ion beam onto the axis of the photon beam. Product ions arising from photon-ion interactions are separated from the parent ion beam by a dipole magnet and counted by a suitable detector unit.

the triple-Auger decay (see Fig. 1) which requires simultaneous ejection of three electrons in combination with a transition of a fourth electron into a core vacancy, constitutes a substantial challenge. As a consequence and although long sought for, the process was unambiguously observed only recently by the present collaboration.

Rather than trying to identify three ejected electrons arising from one single electronic transition, a totally new approach was chosen to observe triple-Auger decay. The new endstation “PIPE” (Photon-Ion Spectrometer at PETRA III, see Fig. 2) of beamline P04 was employed, which facilitates studies of photon interactions with ion beams [3]. PIPE has been designed and built within a collaborative effort of different BMBF-funded university groups with leading contributions by the Gießen team. By exploiting the narrow bandwidth of the monochromatized undulator radiation, C^+ ions in their electronic $1s^2 2s^2 2p^2 P$ ground term were selectively excited by resonant photoabsorption to either the $1s 2s^2 2p^2 \ ^2D$ or the $1s 2s^2 2p^2 \ ^2P$ terms. The excited states could then decay by emission of photons or electrons. Flight times of the ions before the analysis of their charge state were of the order of two microseconds, i.e., many orders of magnitude longer than the decay times for radiative or Auger transitions. Thus, all ions initially produced in K-shell excited states decayed on their way to the analyzer magnet and their final charge states could be measured by detecting all products that had lost one, two or three electrons.

The observation of carbon ions in this experiment that have lost three electrons is unambiguous evidence for the occurrence of the triple-Auger process (Fig. 1). With only four electrons in the L shell the only mechanism for the initially K-shell excited C^+ ions to lose three electrons is the simultaneous ejection of three of the L-shell electrons while the fourth falls into the K vacancy. Cascade processes cannot produce a final C^{4+} ion. PIPE facilitates the measurement of absolute cross sections for photoionisation of ions. The results for single, double and triple ionisation as a consequence of the selected excitations of C^+ are displayed in Fig. 3. From the cross section ratios the probabilities for the different Auger decays were determined with the triple-Auger processes occurring in 128 and 129 out

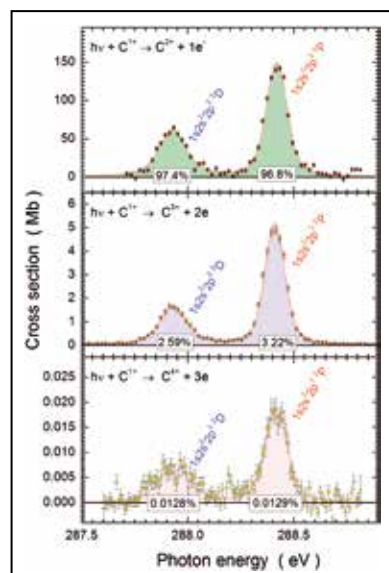


Figure 3

Experimental cross sections for single, double and triple ionisation of $C^+(1s^2 2s^2 2p^2 P)$ ions measured as a function of photon energy. The resonances are associated with photoexcitation from the ground term to the two excited terms indicated in each panel of the figure. Probabilities of single-, double- and triple-Auger decays resulting from this measurement are indicated by the given percentages for the two excited terms investigated.

of a million decays, respectively. Measurements with a resolution of 16 meV made it possible to determine the natural widths of the K-shell excited levels from which the lifetime of the associated states could be deduced. From the absolute cross sections the absorption oscillator strengths [4] were derived and hence the transition probabilities [4] and lifetimes could be inferred. Bringing all this information together results in triple-Auger decay rates of $1.9 \times 10^{10} \text{ s}^{-1}$ for the $C^+(1s 2s^2 2p^2 \ ^2D)$ and $9.7 \times 10^9 \text{ s}^{-1}$ for the $C^+(1s 2s^2 2p^2 \ ^2P)$ intermediate resonantly-excited terms investigated in this study.

In summary, a fundamental atomic decay mechanism involving four-electron interactions has been identified and the associated transition rates were experimentally determined for specific excited states. The results of this work are relevant to numerous multi-electron processes in physics and could help, for example, to improve our understanding of the multiple excitations observed in experiments using X-ray lasers or to rationalize the presence of multiply charged ions in the interstellar medium.

Contact:

Alfred Müller, Alfred.Mueller@iamp.physik.uni-giessen.de

Authors

A. Müller¹, A. Borovik, Jr.¹, T. Buhr^{1,3}, J. Hellhund¹, K. Holste^{1,2}, A. L. D. Kilcoyne⁴, S. Klumpp⁵, M. Martins⁵, S. Ricz^{1,6}, J. Viehhaus⁷, and S. Schippers^{1,2}

- Institut für Atom- und Molekülphysik, Justus-Liebig-Universität Gießen, 35392 Gießen, Germany
- I. Physikalisches Institut, Justus-Liebig-Universität Gießen, 35392 Gießen, Germany
- Physikalisch-Technische Bundesanstalt, 38116 Braunschweig, Germany
- Advanced Light Source, Lawrence Berkeley National Laboratory, Berkeley, California 94720-8225, USA
- Institut für Experimentalphysik, Universität Hamburg, 22761 Hamburg, Germany
- Institute for Nuclear Research, Hungarian Academy of Sciences, 4001 Debrecen, Hungary
- Deutsches Elektronen-Synchrotron DESY, 22607 Hamburg, Germany

Original publication

“Observation of a Four-Electron Auger Process in Near-K-Edge Photoionization of Singly

Charged Carbon Ions”, *Physical Review Letters* 114, 013002 (2015).

DOI: 10.1103/PhysRevLett.114.013002

References

- P. Auger, “Sur les rayons β secondaires produits dans un gaz par des rayons X”, *Comptes Rendus* 180, 65-68 (1925).
- T. A. Carlson and M. O. Krause, “Experimental evidence for double electron emission in an Auger process”, *Phys. Rev. Lett.* 14, 390-392 (1965).
- S. Schippers, S. Ricz, T. Buhr, A. Borovik Jr., J. Hellhund, K. Holste, K. Huber, H.-J. Schäfer, D. Schury, S. Klumpp, K. Mertens, M. Martins, R. Flesch, G. Ulrich, E. Rühl, T. Jahnke, J. Lower, D. Metz, L. P. H. Schmidt, M. Schöffler, J. B. Williams, L. Glaser, F. Scholz, J. Seltmann, J. Viehhaus, A. Dorn, A. Wolf, J. Ullrich, and A. Müller, “Absolute cross sections for photoionization of Xe^{q+} ions ($1 \leq q \leq 5$) at the 3d ionization threshold”, *J. Phys. B* 47, 115602 (2014).
- A. Müller, “Precision studies of deep-inner-shell photoabsorption by atomic ions”, *Phys. Scr.* 90, 054004 (2015).

Synchronised molecular rotations for novel investigations.

Controlling the collective quantum motion of molecules

We demonstrate strong laser-field-free orientation of ground-state-selected carbonyl sulphide molecules *via* coherent superposition of its two lowest rotational states. The states were coupled by the combined action of a 485-ps-long non-resonant laser pulse and a weak static electric field. The observed wave packet motion exhibits strong transient molecular orientation after the control laser pulse has been switched off. The experimentally attained degree of orientation $\langle \cos \theta \rangle \approx 0.6$ corresponds to the theoretical maximum for mixing of the two states. Simulations show that switching off the static field would provide the same orientation completely field free.

Alignment and orientation of small molecules in the gas phase opens up new opportunities for molecular imaging and for studies of chemical dynamics. Applications range from stereo-chemistry [1] over imaging of molecular orbitals via measurements of photoelectron angular distributions in the molecular frame [2] or high-order harmonic generation [3] to electron [4] and X-ray diffraction [5]. Individual molecules do not produce strong enough diffraction signals when exposed to intense X-ray flashes from, e.g., free-electron

lasers — in contrast to molecules in crystals. It is, therefore, highly desirable to control the spatial orientation of isolated molecules in the gas phase, which allows for adding up signals from many individual samples. Furthermore, controlling the spatial orientation of the molecules leads to an enhancement of the information that can be retrieved from a diffraction pattern, such as bond angles. However, molecular-frame photoelectron-angular-distribution imaging of adiabatically oriented molecules can show unwanted streaking features due to the presence of the alignment-laser field.

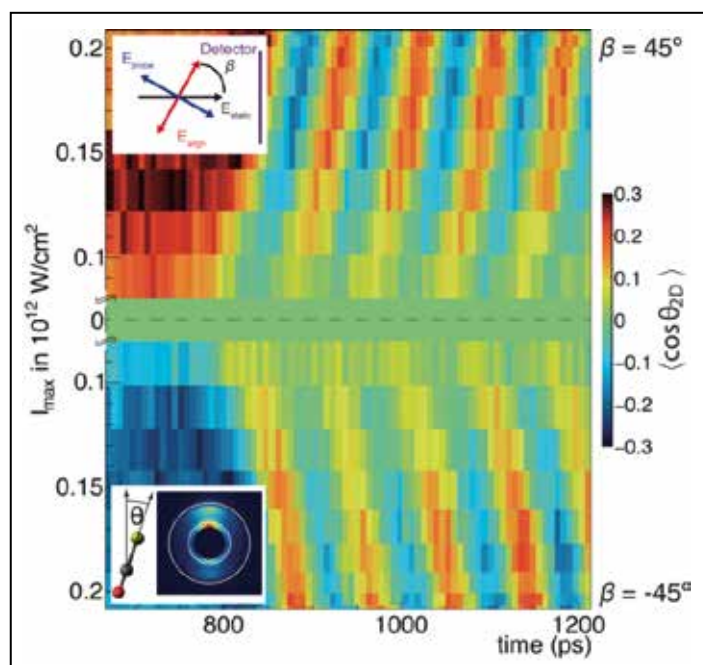


Figure 1

Experimental evolution of the degree of orientation as a function of the relative timing between the orientation laser pulse and the probe pulse and the peak intensity of the orientation laser for $\beta = 45^\circ$ (upper half) and $\beta = -45^\circ$ (lower half). β is defined as the angle between the DC static electric field and the polarisation axis of the orientation laser. θ is defined as the angle between the projected bond axis of the molecule and the vertical axis of the integrated detector image.

In our experiment, a pulsed molecular beam was provided by expanding 500 ppm of carbonyl sulphide (OCS) seeded in 6 bar of neon through a cantilever piezo valve, resulting in a rotational temperature of about one Kelvin. Using the electric deflector the molecules were dispersed in space according to their quantum state [6], and a pure sample of ground-state OCS was selected. These molecules were oriented by the combined action of a moderately intense, 485-ps-long, linearly polarised laser pulse ($I_{\text{control}} \approx 0.215 \text{ TW/cm}^2$) and a weak DC electric field ($E_{\text{stat}} = 840 \text{ V/cm}$) inside a velocity map imaging (VMI) spectrometer. The polarisation of the control laser was set to an angle of $\beta = \pm 45^\circ$ with respect to the static electric field. The spatial distribution of the molecules was probed using Coulomb explosion imaging following multiple-ionisation with a 30 fs laser pulse. The detected S^+ ion velocity distribution was highly directional and provided direct information on the orientation of the OCS molecules at the time of ionisation.

The coupling between the two rotor states is induced by the interaction with the mixed DC and AC electric field. As the control laser field is switched on, the almost free molecular rotor transforms into so-called pendular states, eigenstates of the complete Hamiltonian of the molecule in the field, which librate about the polarisation axis of the control laser. The mixing of the two lowest pendular states is provided *via* a

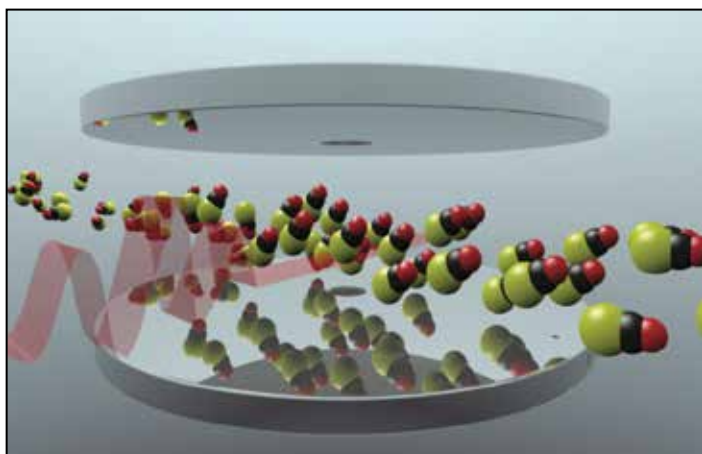


Figure 2

Artistic view of the collective orientation. A near-infrared laser (red) makes the originally disordered molecules perform synchronised cartwheels so that all the molecules at a particular position along the beam are oriented in the same direction.

non-adiabatic coupling by the fast rising and falling edges of the applied laser field. After the laser pulse, the resulting coherent superposition of the *s*- and *p*-rotor states propagates in time. This leads to an up-down-inverting oscillation of the dipole moment and the atoms of the molecule.

Figure 1 shows the experimental temporal evolution of the degree of orientation, in colour code, during and after the laser pulse. This is plotted, in the upper half of Fig. 1 for $\beta = 45^\circ$ and in the lower half of Fig. 1 for $\beta = -45^\circ$, as a function of the relative timing between the orientation and the probe laser pulses and of the peak intensity of the orientation pulse. After the former has been switched off a strong oscillatory behaviour was observed due to the coherent superposition of the field free *s* and *p* rotational states. A phase shift of π is observed when the polarisation of the laser field is rotated from $\beta = 45^\circ$ to $\beta = -45^\circ$ with respect to the static electric field.

Figure 2 shows an artistic view of the collective orientation. A near-infrared laser (red) makes the originally disordered molecules perform synchronised cartwheels so that all the

molecules at a particular position along the beam are oriented in the same direction — and this is repeated regularly, *virtually* forever.

The maximum orientation of the post pulse dynamics can be controlled, i.e., enhanced or suppressed, by the exact timing of the switching off and the intensity of the control pulse. This includes a complete population transfer into one of the involved states — effectively switching off all dynamics. To efficiently transfer the population back to the ground state, in our field configuration the falling edge of the laser pulse should start after a few nanoseconds, due to the slow dynamics of the field-dressed near-degenerate pendular states in the strong laser field. A complete transfer to the excited state, corresponding to a π -pulse, is obtained at exactly half of this time.

In summary, the preparation of molecules in a coherent superposition of free-rotor states of opposite parity results in strong, laser-field-free oriented samples. The mixing of the two states can be completely controlled by the combination of strong picosecond laser pulses and weak DC electric fields. Furthermore, simulations show that rapidly turning off the DC electric field, down to $\tau = 100$ ps, would not alter the wave packet dynamics and result in strong fully field-free orientation. The preparation of such ideal samples paves the way for novel experiments, such as electron and X-ray diffraction of small controlled molecules in the gas phase. In combination with molecular frame photoelectron angular distributions, complete molecular movies could be observed by simultaneous mapping of the molecular orbitals and the positions of the individual atoms during a chemical reaction.

Contact: Jochen Küpper, jochen.kuepper@desy.de

Authors

Sebastian Trippel^{1,2}, Terry Mullins¹, Nele L. M. Müller¹, Jens S. Kienitz^{1,2}, Rosario González-Férez^{2,3}, and Jochen Küpper^{1,2,4}

- Center for Free-Electron Laser Science CFEEL, DESY, 22607 Hamburg, Germany
- The Hamburg Centre for Ultrafast Imaging CUI, University of Hamburg, 22761 Hamburg, Germany
- Instituto Carlos I de Física Teórica y Computacional and Departamento de Física Atómica, Molecular y Nuclear, Universidad de Granada, 18071 Granada, Spain
- Department of Physics, University of Hamburg, 22761 Hamburg, Germany

Original publication

“Two-State Wave Packet for Strong Field-Free Molecular Orientation”, *Phys. Rev. Lett.* **114**, 103003 (2015). DOI: 10.1103/PhysRevLett.114.103003

References

- P. R. Brooks, “Reactions of Oriented Molecules”, *Science* **193**, 11 (1976).
- L. Holmegaard, J. L. Hansen, L. Kalthøj, S. L. Kragh, H. Stapelfeldt, F. Filsinger, J. Küpper, G. Meijer, D. Dimitrovski, M. Abusamha, C. P. J. Martiny, and L. B. Madsen, “Photoelectron angular distributions from strong-field ionization of oriented molecules”, *Nat. Phys.* **6**, 428 (2010).
- P. M. Kraus, B. Mignolet, D. Baykusheva, A. Rupenyan, L. Horny, E. F. Penka et al., “Measurement and laser control of attosecond charge migration in ionized iodoacetylene”, *Science*, 790-795 (2015).
- C. J. Hensley, J. Yang, and M. Centurion, “Imaging of Isolated Molecules with Ultrafast Electron Pulses”, *Phys. Rev. Lett.* **109**, 133202 (2012).
- J. Küpper et al., “X-Ray Diffraction from Isolated and Strongly Aligned Gas-Phase Molecules with a Free-Electron Laser”, *Phys. Rev. Lett.* **112**, 083002 (2014).
- Y.-P. Chang, D. A. Horke, S. Trippel, and J. Küpper, “Spatially-controlled complex molecules and their applications”, *Int. Rev. Phys. Chem.* **34**, 557 (2015).

Metal nanopatterning in three easy steps.

Large areas of scalable, monodisperse metal nanostructures produced by hierarchical self-assembly

Nanoscale materials have become essential to science and technology. Progress in nanoscience often depends on finding ways to decrease the size of nanostructures while increasing their uniformity and the patterned area. Success in industrial production of nanomaterials, on the other hand, means to reduce costs and save time. For both fundamental research and product development, it can be a decisive advantage to be able to observe nanostructure formation while it takes place. We present a procedure for metal nanostructure fabrication that employs exclusively self-assembly processes and produces outstandingly uniform metal nanostructures in highly regular arrays covering large areas. The sample material, the nanostructure size, and the pattern morphology are variable and *in situ* characterization during the growth of the nanostructure is feasible.

Self-assembly is the spontaneous formation of a globally ordered structure in a system of components with merely local interactions. In nanoscience, self-assembly processes are increasingly used as alternative to top-down nanofabrication techniques. In these “parallel” ordering processes the structure formation occurs simultaneously throughout the entire system – making nanostructuring enormously rapid in comparison to “sequential” top-down methods. By providing guiding restraints, the intrinsically high defect density in self-assembled patterns can be reduced to be competitive with defect densities achieved by conventional top-down techniques [1]. Intriguingly, self-assembling systems can be combined in a hierarchical manner. The pattern established in the preceding system guiding the pattern formation in the subsequent one.

We present a hierarchical approach with three self-assembling systems to form regular arrays of uniform metal nanostructures (see Fig. 1). The surface reconstruction of $\alpha\text{-Al}_2\text{O}_3$ guides the microphase separation of diblock copolymers which then directs the surface diffusion of metal atoms into the growth of nanodots and wires. First, a $\alpha\text{-Al}_2\text{O}_3$ substrate is nanofaceted by high-temperature annealing. In the next step, a diblock copolymer thin film is spin coated onto the $\alpha\text{-Al}_2\text{O}_3$ substrate. Upon exposure to solvent vapor, the copolymer film undergoes microphase separation into uniformly shaped and evenly spaced domains of nanoscale size, consisting exclusively of one of the two copolymer components (“blocks”). Here, the faceted substrate surface defines a preferential direction, inducing long-range order in the lateral positioning of the chemical domains within the copolymer film [2]. Thus, the copolymer film presents a topographically almost flat but distinctly chemically structured surface of high regularity. This can be used as a template to grow a metal nanostructure pattern of the same morphology by sputter deposition: Given

different interaction strengths between the metal atoms and the two distinct copolymer blocks, metal atoms will agglomerate on only one of the copolymer blocks via surface diffusion (“selective wetting”) [2]. Thereby the well-ordered two-dimensional chemical structuring of the template surface is transferred into a regular pattern of uniform metal nanostructures.

The sizes and shapes of the metal nanostructures are determined by selecting the appropriate chemical composition

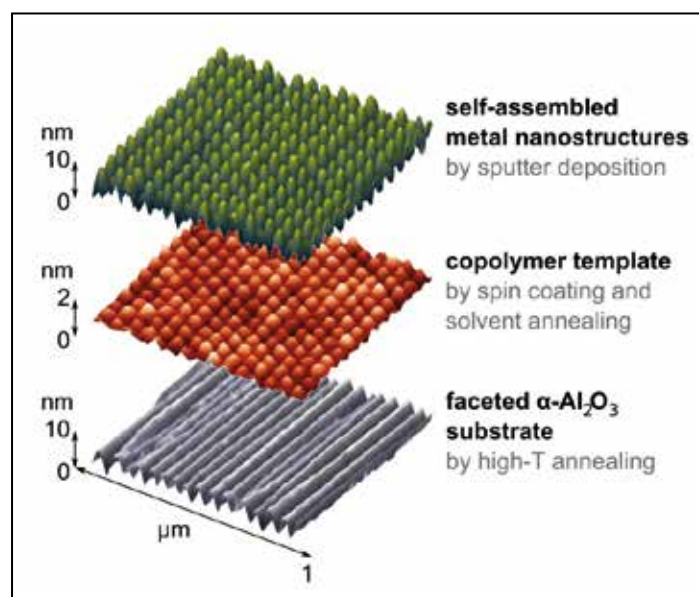


Figure 1

The new bottom-up approach allows producing large arrays of uniform metal nanostructures with scalable lateral dimensions. Various nanostructure morphologies including dots, antidots, and wires can be realized. This routine opens up intriguing new possibilities for nanostructure fabrication and characterization in science and technology.

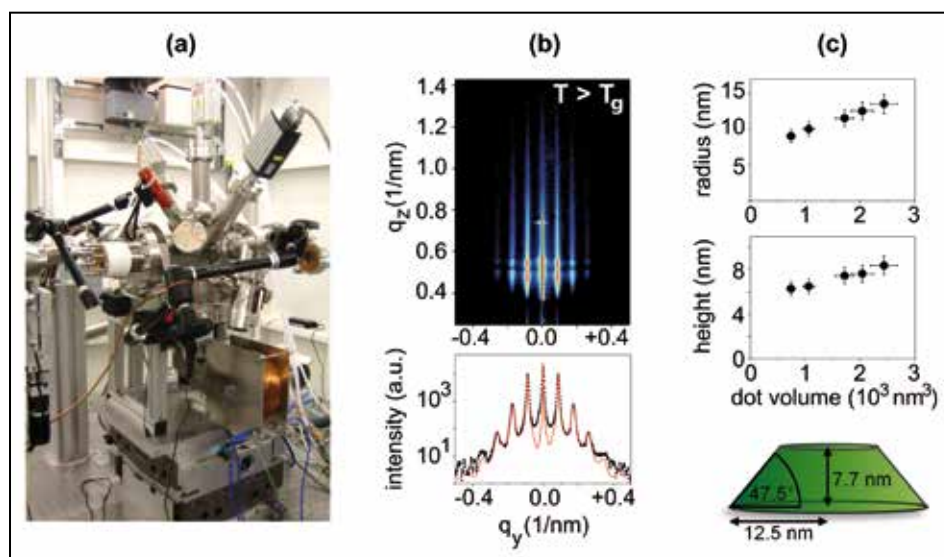


Figure 2

(a) Custom-made UHV device for sputter formation, manipulation, and *in situ* characterization of magnetic nanostructures, mounted at the beamline P01 at PETRA III.

(b) GISAXS pattern recorded *in situ* during Fe nanodot growth. Below: horizontal section through the Yoneda region (black symbols) with simulated data (red curve).

(c) The development of some geometrical parameters as obtained from sequences of GISAXS patterns recorded during Fe deposition. Model of a nanodot showing its radius, height, and base angle.

and molecular weight for the diblock copolymer. Feature sizes can be varied from less than 5 nm to a few hundred nanometers. Possible pattern morphologies comprise for instance hexagonally packed dots, antidots, or rings, parallel wires, dots aligned along wires, square or honeycomb lattices [3].

The self-assembly approach allows for *in situ* x-ray scattering studies of the nanostructure formation. At beamline P01 at PETRA III we have observed the growth of Fe nanodots on diblock copolymer templates at different growth conditions using a custom-made *in situ* UHV device (see Fig. 2a). Typical results of the morphological characterization by GISAXS are shown in Fig. 2b,c. Geometrical parameters describing the arrangement, shape, size, and proportions of the nanodots can be obtained from simulations of the GISAXS patterns [4] and can be tracked over the course of the deposition process. A very good agreement between simulations and experimental data was achieved without using any distributions of the geometrical parameters for the simulations. This demonstrates the high shape uniformity and pattern regularity achieved by hierarchical self-assembly. Both the lateral arrangement of the nanodots in a hexagonal lattice (lattice parameter: 83 nm) and their general truncated cone shape are only defined by the chemical surface patterning

of the template. However, the nanodot proportions, appear to depend on the template temperature via its influence on the mobility of Fe atoms on the template surface. A surface area minimization is impeded by low mobility at lower temperatures, resulting in the growth of wide and flat nanostructures. In contrast, the increased mobility of Fe atoms and clusters at elevated temperatures allows for the formation of compact nanostructures with low surface/volume ratio. This finding indicates a possible approach to sculpt self-assembling nanostructures via external process conditions.

Hierarchical self-assembly can eliminate the need for complex and slow lithography devices and allows for *in situ* monitoring of the sample properties during structure formation. Structure uniformity, pattern regularity as well as variability in morphology and material make our method an attractive option for fast, facile, versatile, and economic nanostructure fabrication. This new bottom-up technique may enable a faster and simpler production of high-density magnetic recording media, surface plasmon resonance sensors, or high-performance catalytic materials.

Contact: Denise Erb, denise.erb@desy.de

Authors

Denise Erb^{1,2}, Kai Schlage¹, and Ralf Röhlsberger^{1,2}

1. Deutsches Elektronen-Synchrotron DESY, 22607 Hamburg, Germany

2. Universität Hamburg, The Hamburg Centre for Ultrafast Imaging, 22761 Hamburg, Germany

Original publication

"Uniform metal nanostructures with long-range order via 3-step hierarchical self-assembly", *Science Advances* Vol. 1, No. 10, e1500751
DOI: 10.1126/sciadv.1500751

References

1. S. Park, D.H. Lee, J. Xu, B. Kim, S.W. Hong, U. Jeong, T. Xu, and T.P. Russell, "Macroscopic 10-terabit-per-square-inch arrays from block copolymers with lateral order", *Nature* 323, 1030 (2009).
2. W. A. Lopes and H.M. Jaeger, "Hierarchical self-assembly of metal nanostructures on diblock copolymer scaffolds", *Nature* 414, 735-738 (2001).
3. Y. Matsushita, K. Hayashida, T. Dotera, and A. Takano, "Kaleidoscopic morphologies from ABC star-shaped terpolymers", *J. Phys.: Condens. Matter* 23, 284111 (2011).
4. R. Lazzari, "IsGISAXS: a program for grazing-incidence small-angle X-ray scattering analysis of supported islands" *J. Appl. Cryst.* 35, 406 (2002).

Nanoparticles increase efficiency of organic solar cells.

A matter of spin

The further increase in performance of organic photovoltaic devices requires fine tuning of the morphology of the different materials present in them, and the difficulty of morphology tailoring at the nanoscale progressively demands more creative approaches. One of the most innovative ones consists of the extension of the exciton lifetime taking advantage of diverse physical phenomena, such as spin rephasing. To achieve this aim, we dope P3HT:PCBM organic solar cells with Fe_3O_4 nanoparticles, thereby obtaining very promising results for the exciton diffusion length and increasing the efficiency of solar devices by 11 %. In the process of parametrizing this improvement, advanced grazing incidence X-ray scattering techniques were of vital importance in tracking potential changes in the system's morphology.

One approach that dramatically stimulated the field of organic photovoltaics is the introduction of the concept of the bulk heterojunction (BHJ), in which the photoactive layer is composed of two organic materials blended together (referred as donor and acceptor). These exhibit an offset between their optical bandgaps, creating at the donor/acceptor interface an internal electric field that aids the splitting of the photogenerated excitons (see Fig. 1b) [1]. Given that the exciton diffusion length is limited to few nanometres, the importance of the morphological arrangement between the two phases becomes clear, since it will mainly determine the rate of excitons that successfully get split into usable charge carriers [2].

Due to the difficulties in tuning the donor-acceptor morphology at the nanoscale via dedicated physical and chemical processes, one innovative approach consists of increasing the diffusion length of the excitons [3]. This has been achieved by embedding metal-oxide nanoparticles (NPs) in the active layers of the organic solar cells. These actively contribute to increase the

efficiency of the intersystem crossing (ISC) mechanism in organic molecules. The ISC is the process that describes the probability for the photogenerated excitons to migrate from the singlet to the triplet spin manifold (see Fig. 2a). Triplet excitons are, according to quantum selection rules, not allowed to decay to the singlet ground state. Thus, the probability for radiative recombination is reduced, the average exciton lifetime and, therefore, its diffusion length is increased. This enhances the probability for the excitons to reach the donor-acceptor interface and, thereby, the performance of the solar device. This effect has been observed in poly(3-hexylthiophene-2,5-diyl):phenyl C_{60} butyric acid methyl ester (P3HT:PCBM) solar cells doped with Fe_3O_4 NPs. At low doping concentrations (below 1 wt.%) the solar devices improved their performance up to 11 % compared to the non-doped control devices. The evolution of the power conversion efficiency (PCE) with increasing concentration of Fe_3O_4 is strongly determined by the fill factor (Fig. 2b). The fill factor is the main parameter that characterizes the recombination in the solar cell in conditions

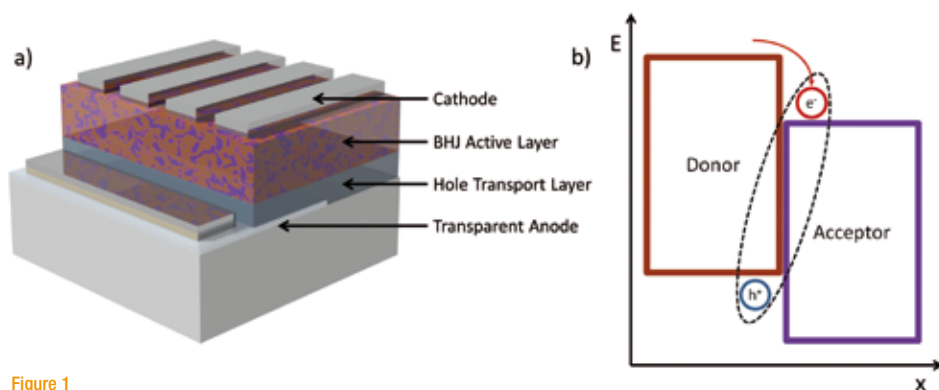


Figure 1
a) Schematic depiction of a standard bulk heterojunction (BHJ) organic solar cell. The central layer depicts the photoactive layer, in which the donor and acceptor materials are blended together, presenting brown and violet domains, respectively. b) Energy vs. space diagram and depiction of the exciton splitting mechanism in organic solar cells. The exciton, composed of a negative (indicated as e^-) and positive (h^+) charge carrier, diffuses to a donor/acceptor interface. There, the negative charge carrier is transferred to the acceptor phase and the local electric field arising from the difference in potential in the two phases aids to overcome the Coulombic barrier between the two charges arising from their different charge signs. This Coulombic binding is indicated by the black dotted line.

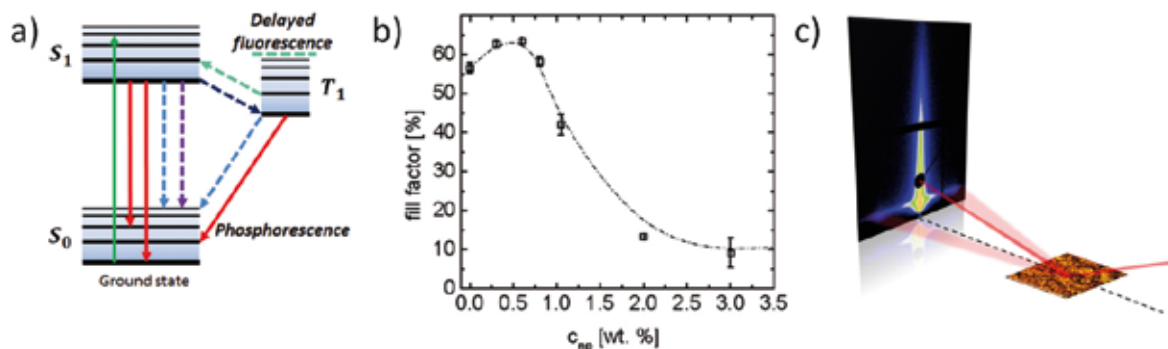


Figure 2

a) Schematic depiction of the mechanism of intersystem crossing (ISC). The ground state S_0 presents a singlet spin state, whereas in the first excited state already two spin configurations are possible: a singlet S_1 and a triplet T_1 . The presence of nanoparticles aids the transition between the two states, extending the exciton average lifetime. This effect can be detected as increased delayed fluorescence. Solid arrows represent radiative transitions, like absorption (green), fluorescence (red, S_1) or phosphorescence (red, T_1). Dashed arrows represent non-radiative transitions like non-radiative relaxation (light blue), quenching (violet), intersystem crossing (dark blue) and delayed fluorescence (turquoise blue). b) Fill factors measured for different P3HT:PCBM solar cells doped with different amounts of Fe_3O_4 nanoparticles. The dashed line is a guide to the eye. c) Schematic depiction of the GISAXS set-up. The X-ray impinges on the sample under a shallow angle. The scattered and the reflected X-ray signals are recorded on a 2D detector.

of charge carrier diffusion. The fill factor is related to the shape of the current-voltage curve and, thus, reflects the ideality of the solar diode.

One of the main aspects that needed to be controlled upon the addition of the NPs is that their presence does not alter the intermixing between the donor and the acceptor phases, so that an improved morphology can be ruled out as reason for the solar cell improvement. With the help of grazing incidence X-ray scattering (GIXS) measurements the morphology was probed. The non-destructive nature of the method, as well as the grazing incidence configuration, which substantially increases the sample volume that interacts with the incoming X-ray beam, makes it an optimal tool for characterizing thin films (see Fig. 2c). Experiments were carried out at the Micro- and Nanofocus X-ray Scattering beamline P03 at PETRA III (MiNaXS) [4]. Grazing incidence small angle X-ray scattering (GISAXS) investigations regarding domain arrangement and morphology rapidly discarded structural changes as origin of the device improvement. All the organic regions and domains with sizes in the range of the exciton diffusion length for the materials employed remained virtually unchanged upon addition of NPs. Moreover, grazing incidence wide angle X-ray scattering (GIWAXS) investigations proved no increase or major change in sample crystallinity in the doping region of device improvement.

Subsequent optoelectronic characterization based on photoluminescence measurements allowed tracking a higher exciton quenching at low doping regime, i.e. a reduced recombination. Moreover, comparison of the delayed fluorescence to the prompt fluorescence signals allowed tracking an increased delayed-to-prompt fluorescence ratio, reinforcing the hypothesis of increased ratio of intersystem crossing.

Finally, time-resolved delayed fluorescence investigations allowed estimating the average exciton lifetime, which also showed an increase in the region of best solar cell PCE.

In this investigation, the use of advanced scattering techniques was crucial from the beginning to dismiss any morphological effect on the sample that could mimic the pursued triplet exciton effect. Moreover, GIWAXS investigations on the crystal structure of P3HT showed excellent agreement between the evolution with Fe_3O_4 concentration of the sample's active layer crystallinity and the current extracted from the device in short-circuit conditions, reinforcing the importance of film crystallinity for an efficient charge carrier transport [5].

In summary, our findings open a new door for investigation of the possibilities for further increasing the performance of organic photovoltaic devices exploiting fundamental physical properties.

Contact: Peter Müller-Buschbaum, muellerb@ph.tum.de

Authors

Daniel Moseguí González¹, Volker Körstgens¹, Yuan Yao¹, Lin Song¹, Gonzalo Santoro², Stephan V. Roth², and Peter Müller-Buschbaum¹

¹ Chair for Functional Materials, Physics Department, Technical University of Munich (TUM), 85748 Garching, Germany

² Deutsches Elektronen-Synchrotron DESY, 22607 Hamburg, Germany

Original publication

"Improved Power Conversion Efficiency of P3HT:PCBM Organic Solar Cells by Strong Spin-Orbit Coupling-Induced Delayed Fluorescence", *Adv. Energy Mater.* 5(8), 1401770 (2015). DOI: 10.1002/aenm.201401770

References

- C. J. Brabec et al., "Polymer-Fullerene Bulk-Heterojunction Solar Cells", *Adv. Mater.* 22, 3839-3856 (2010).
- M. A. Ruderer et al., "Solvent-Induced Morphology in Polymer-Based Systems for Organic Photovoltaics", *Adv. Func. Mater.* 21, 3382-3391 (2011).
- C.-M. Yang et al., "Enhanced photovoltaic response of organic solar cell by singlet-to-triplet exciton conversion", *Appl. Phys. Lett.* 90, 133509 (2007).
- A. Buffet et al., "P03, the microfocus and nanofocus X-ray scattering (MiNaXS) beamline of the PETRA III storage ring: the microfocus endstation", *J. Synchrotron Radiat.* 19, 647-653 (2012).
- J. D. Zimmerman et al., "Independent control of bulk and interfacial morphologies of small molecular weight organic heterojunction solar cells", *Nano Lett.* 12, 4366-4371 (2012).

Watching layers of C_{60} molecules grow.

Towards understanding growth on the molecular scale

Assembly of molecular building blocks into functional nanomaterials is increasingly used in devices, but the understanding of molecular film growth on a nanoscopic, molecular level is still in its infancy. We use real-time and *in situ* specular as well as diffuse X-ray scattering in combination with kinetic Monte-Carlo (KMC) simulations to unravel the multilayer growth of the fullerene C_{60} in terms of microscopic processes such as surface diffusion, nucleation and step-edge crossing. Particle-resolved dynamics show a lateral diffusion behaviour similar to colloids, but are characterized by an atom-like Ehrlich-Schwoebel barrier. Our results contribute to a fundamental understanding of molecular growth processes for a system which forms an important intermediate case between atoms and colloids.

Understanding the growth of molecular materials, such as the prototypical molecular semiconductor C_{60} , is an indispensable prerequisite for the rational design of complex nanomaterials from molecular building blocks. To achieve a molecular scale understanding of nucleation and multilayer growth the three major surface processes during growth have to be considered: (1) surface diffusion of a single molecule, (2) lateral binding of molecules and (3) the step-edge crossing of molecules across island edges.

To address this question, we employ a combination of specular X-ray growth oscillations with real-time diffuse X-ray scattering (see Fig. 1) to simultaneously follow the vertical and lateral morphology during the growth of the fullerene C_{60} on the muscovite mica. These challenging experiments are made possible through the high X-ray brilliance, high resolution and advanced detectors with high dynamic range at the MiNaXS beamline P03 at PETRA III.

The time-dependent specular X-ray reflectivity as a function of molecular exposure is shown in Fig. 1a for a substrate temperature of 60 °C and a deposition rate of 0.1 ML min^{-1} . The scattered intensity at the so-called anti-Bragg point, which lies at half of the Bragg angle, oscillates with a period of two monolayers (ML), as the X-rays are reflected from consecutive C_{60} layers and alternately interfere destructively and constructively. The X-ray growth oscillations provide information about the vertical layer filling during growth and are indicative of layer-by-layer growth. While the diffuse scattering is weak, it nevertheless contains important lateral information. Figure 1b shows a map of the diffusely scattered intensity as a function of q_{\parallel} and molecular exposure. For each C_{60} layer, the diffusely scattered intensity has two maxima along q_{\parallel} , because the characteristic average island distance D causes an increase in the diffusely scattered intensity at $\Delta q_{\parallel} = \pm 2\pi/D$. The peak positions enable us to quantitatively describe the nanostructure

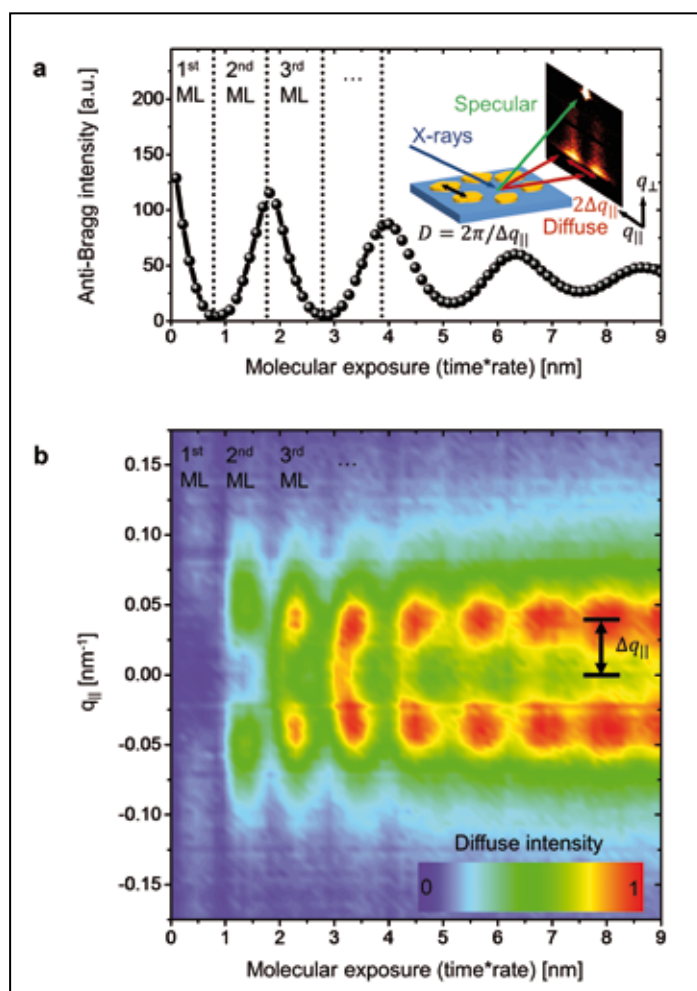


Figure 1

(a) Specular X-ray growth oscillations during the growth of the fullerene C_{60} (inset: X-ray scattering geometry). The distinct growth oscillations are indicative for layer-by-layer growth. (b) Diffuse X-ray scattering (GISAXS) during the growth of the fullerene C_{60} . For each C_{60} layer, the diffusely scattered intensity has two maxima along q_{\parallel} , because the characteristic average island distance D causes an increase in the diffuse scattered intensity at $\Delta q_{\parallel} = \pm 2\pi/D$.

through the island density $N \propto 1/D^2$ [2, 3]. To understand the morphological evolution on a molecular level the experimental data have been evaluated using kinetic Monte-Carlo (KMC) simulations [1]. From simulated growth morphologies, the vertical and lateral structure during growth is deduced. In

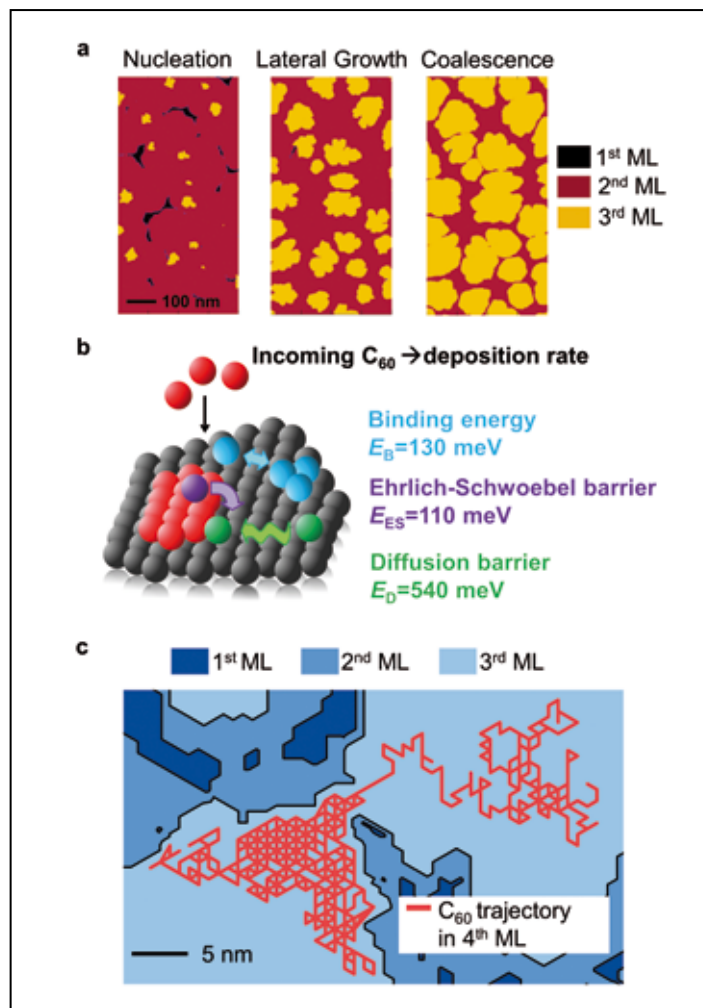


Figure 2

(a) Kinetic Monte-Carlo (KMC) simulated film morphologies: Three different growth stages are observed: (1) nucleation, (2) lateral island growth and (3) coalescence. (b) Surface processes in C_{60} growth. The diffusion barrier E_D , binding energy E_B and Ehrlich-Schwoebel barrier E_{ES} determine island nucleation and interlayer transport in multilayer growth. Included are numerical values determined by fitting the experiment using KMC simulations. (c) Trajectory of a single C_{60} -molecule.

Fig. 2a three different simulated growth stages, (1) nucleation, (2) lateral island growth and (3) coalescence, are shown.

By comparing the experimentally observed vertical and lateral structure information with KMC simulations we determine a complete set of energy parameters describing the intra- and interlayer diffusion processes of C_{60} . This comparison yields an effective step-edge crossing, so-called Ehrlich-Schwoebel barrier of $E_{ES} = 110$ meV, a surface diffusion barrier of $E_D = 540$ meV and a binding energy of $E_B = 130$ meV (see Fig. 2b). The high value of the surface diffusion barrier arises due to a simplified triangular lattice used in the simulation which means a diffusion step goes across two sites of the real hexagonal lattice.

Beyond an explanation of the experimental data, the KMC simulations allow us to study particle-resolved dynamics (see Fig. 2c for a trajectory of a single C_{60} molecule), which reveal similarities and differences between atomic, molecular and colloidal systems during growth. When comparing the average surface free diffusion times, C_{60} is able to diffuse much longer than an atomic species before immobilization on the surface, which we attribute to the colloid-like short range of C_{60} -interactions. Both C_{60} and soft-matter colloids can form bonds only with the immediate vicinity due to the short interaction range of C_{60} van der Waals forces and colloidal interactions. Nevertheless, we find that the step-edge crossing process for C_{60} differs from colloidal systems. In contrast to C_{60} , for which we find a truly energetic Ehrlich-Schwoebel barrier, colloidal epitaxy exhibits a flat energy landscape at the step-edge.

Since C_{60} features aspects of both atomic and colloidal systems, our findings will help to gain insight into island nucleation and surface growth processes for molecules between the length scales of atomic and colloidal systems. This quantitative, scale-bridging understanding enables predictive simulations and a rational choice of growth conditions, which, together with molecular design and synthesis, ultimately leads to a systematic understanding of growth of molecular and soft materials. For more details see the original publication.

Contact: Sebastian Bommel, sebastian.bommel@desy.de, Stefan Kowarik, stefan.kowarik@physik.hu-berlin.de

Authors

S. Bommel^{1,2}, N. Kleppmann³, C. Weber¹, H. Spranger¹, P. Schäfer¹, J. Novak⁴, S. V. Roth², F. Schreiber⁴, S. H. L. Klapp³, and S. Kowarik¹

1. Institut für Physik, Humboldt-Universität zu Berlin, Newtonstr. 15, 12489 Berlin, Germany
2. Deutsches Elektronen-Synchrotron (DESY), Notkestr. 85, 22607 Hamburg, Germany
3. Institut für Theoretische Physik, Technische Universität Berlin, Hardenbergstr. 36, 10623 Berlin, Germany
4. Institut für Angewandte Physik, Universität Tübingen, Auf der Morgenstelle 10, 72076 Tübingen, Germany

Original publication

„Unravelling the multilayer growth of the fullerene C_{60} in real-time“, *Nature Communications* 5, 5388 (2014), doi: 10.1038/ncomms6388

References

1. N. Kleppmann and S.H.L. Klapp, "Particle-resolved dynamics during multilayer growth of C_{60} ", *Phys. Rev. B* 91, 045436 (2015).
2. M. Schwartzkopf, A. Buffet, V. Köstgens, E. Metwalli, K. Schlage, G. Benecke, J. Perlich, M. Rawolle, A. Rothkirch, B. Heidmann, G. Herzog P. Müller-Buschbaum, R. Röhlberger, R. Gehrke, N. Stribeck, and S. V. Roth, "From atoms to layers: in situ gold cluster growth kinetics during sputter deposition", *Nanoscale* 5, 5053 (2013).
3. C. Frank, J. Novak, R. Banerjee, A. Gerlach, F. Schreiber, A. Vorobiev, and S. Kowarik, "Island size evolution and molecular diffusion during growth of organic thin films followed by time-resolved specular and off-specular scattering", *Phys. Rev. B* 90, 045410 (2014).

Elucidating the formation mechanism of layered thermoelectric oxides.

In situ real-time characterization of $\text{Ca}_3\text{Co}_4\text{O}_9$

The layered cobaltate $\text{Ca}_3\text{Co}_4\text{O}_9$ is of interest for energy-harvesting and heat-conversion applications because of its good thermoelectric properties and the fact that the raw materials Ca and Co are nontoxic, abundantly available, and inexpensive. While single-crystalline $\text{Ca}_3\text{Co}_4\text{O}_9$ exhibits high Seebeck coefficient and low resistivity, its widespread use is hampered by the fact that single crystals are too small and expensive. A promising alternative approach is the growth of highly textured and/or epitaxial $\text{Ca}_3\text{Co}_4\text{O}_9$ thin films with correspondingly anisotropic properties. We have developed a two-step sputtering/annealing method for synthesis of $\text{Ca}_3\text{Co}_4\text{O}_9$ with compositional control by tuning the initial proportions of CaO and CoO phases. The thermally induced phase transformation mechanism was investigated by *in situ* time-resolved annealing experiments using synchrotron-based 2D X-ray diffraction as well as *ex situ* annealing experiments and standard lab-based X-ray diffraction.

Thermoelectrics have the potential to play an important role for thermal management and conversion of waste heat into electricity in environmentally friendly energy systems. Their general applicability is impeded by the profound interrelations between the key materials parameters determining their efficiency; the Seebeck coefficient, the electrical resistivity, and the thermal conductivity. High power generation efficiencies thus require high-Seebeck materials that readily scatter phonons (low thermal conductivity) without impeding the transport of charge carriers (low electrical resistivity). Such an ideal thermoelectric material is often referred to as a 'phonon-glass-electron-crystal'.

Materials systems with layered structures are one approach towards realizing a 'phonon-glass-electron-crystal'. Alternating layers act as scattering layers for phonons and conducting layers for charge carriers. One class of layered thermoelectric materials are the misfit-layered cobalt oxides, which comprise alternately stacked layers of rocksalt-type layers, acting as phonon blocking layers, and CoO_2 layers, acting as charge carrier conducting channels. This class of materials exhibits good thermoelectric properties, they are non-toxic, and the raw materials are abundant and inexpensive.

The most important misfit-layered cobalt oxide is the archetype $\text{Ca}_3\text{Co}_4\text{O}_9$, which exhibits a high Seebeck coefficient and low electrical resistivity. The physical properties of $\text{Ca}_3\text{Co}_4\text{O}_9$ are anisotropic due to its inherently nanolaminated structure. Technical challenges and high cost associated with the growth of larger size $\text{Ca}_3\text{Co}_4\text{O}_9$ single crystals make them difficult to apply in practice. A more promising approach to exploit these anisotropic properties is the growth of textured and/or epitaxial thin films, whose thermoelectric properties may be comparable to that of single crystalline $\text{Ca}_3\text{Co}_4\text{O}_9$.

Synthesis of $\text{Ca}_3\text{Co}_4\text{O}_9$ thin films has been demonstrated by both physical vapor deposition (PVD) and chemical techniques such as chemical vapor deposition (CVD). PVD has broad advantages compared to chemical methods since PVD operates far from thermodynamic equilibrium and offers atomistic control of the deposition flux.

We have reported a method for the growth of $\text{Ca}_3\text{Co}_4\text{O}_9$ thin films by a two-step sputtering/annealing method. CaO-CoO films are first deposited by reactive magnetron co-sputtering from Ca and Co targets followed by annealing in an oxygen atmosphere to form $\text{Ca}_3\text{Co}_4\text{O}_9$. The phase transformation mechanism was investigated by *in situ* time-resolved annealing experiments using synchrotron-based X-ray diffraction (XRD) with a 2D-detector as well as *ex situ* annealing experiments

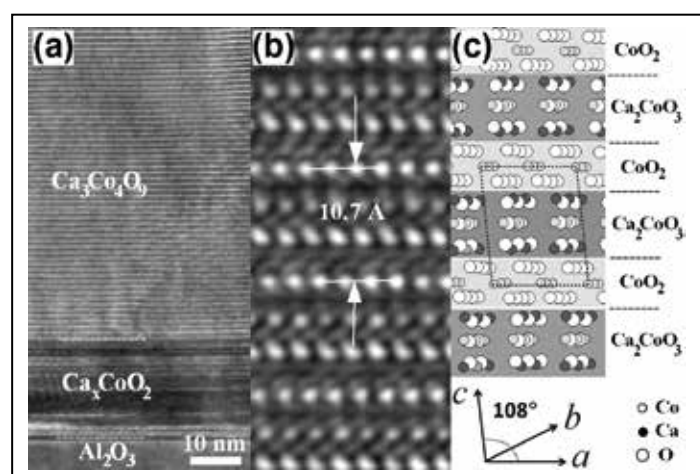
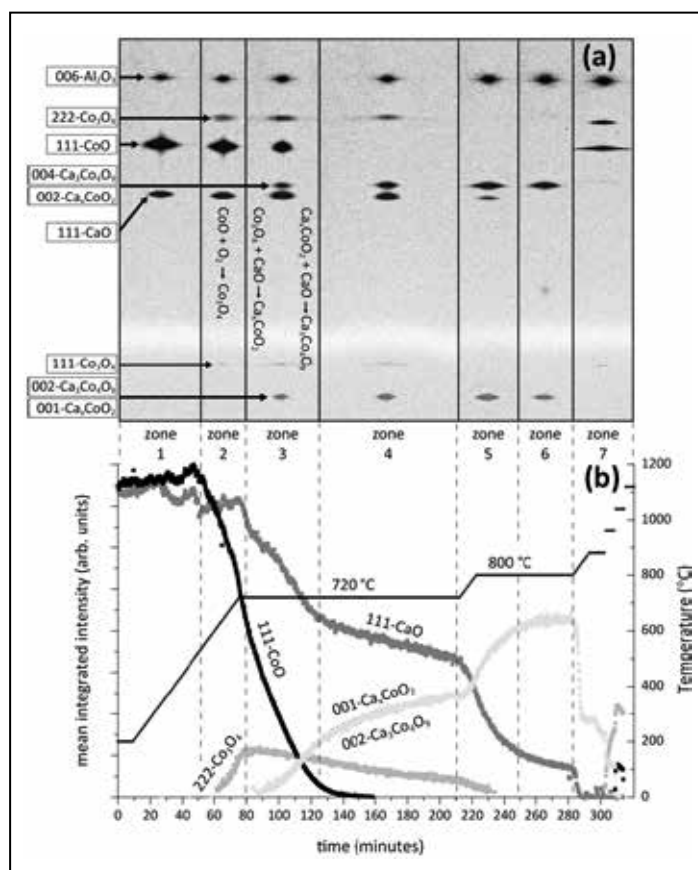


Figure 1

a) TEM image of Ca-Co-O thin film showing the layered $\text{Ca}_3\text{Co}_4\text{O}_9$ structure with a 17 nm region from the interface comprised of Ca_2CoO_3 . b) Lattice-resolved TEM image and c) schematic of the atomic arrangement of the layers.

Figure 2

- a) 2D X-ray diffraction-based images for seven different zones of *in situ* annealing experiments using time-resolved synchrotron-based 2D X-ray diffraction.
- b) Integrated XRD peak intensities of different phases as a function of annealing time and temperature.



and standard lab-based XRD. Figure 1 displays overview and lattice-resolved TEM images of the resulting Ca-Co-O thin films showing the layered $\text{Ca}_3\text{Co}_4\text{O}_9$ structure with a 17 nm interface region comprised of Ca_xCoO_2 .

Figure 2 shows 2D X-ray diffraction-based images for different zones of *in situ* annealing experiments using time-resolved synchrotron-based 2D X-ray diffraction. Here, it is seen that CaO, CoO, Co_3O_4 , Ca_xCoO_2 and $\text{Ca}_3\text{Co}_4\text{O}_9$ are present at various stages of the annealing process (a time-resolved video is also available as Supporting Information for the original paper). The diffraction images show that CoO first oxidizes to the intermediate Co_3O_4 phase, which then reacts with CaO to form Ca_xCoO_2 . Ca_xCoO_2 subsequently reacts with CaO to form the $\text{Ca}_3\text{Co}_4\text{O}_9$ phase. As the 00l diffraction spots of Ca_xCoO_2 coincide with those of $\text{Ca}_3\text{Co}_4\text{O}_9$, they are indistinguishable in the 2D diffraction images. The formation of Ca_xCoO_2 as an intermediate phase via the reaction of Co_3O_4 with CaO was verified by *ex situ* annealing and XRD experiments. It is apparent that those 2D diffraction spots will initially be from the (001) and (002) planes of Ca_xCoO_2 and at the end from the (002) and (004) planes of $\text{Ca}_3\text{Co}_4\text{O}_9$. Annealing temperatures above 880 °C led to the loss of calcium from $\text{Ca}_3\text{Co}_4\text{O}_9$ and the formation of CoO and Co_3O_4 cobalt oxide phases.

The method carries important advantages in that by tuning the proportion of initial CaO and CoO phases during film deposition, the method enables synthesis of thin films of the related phase Ca_xCoO_2 thin films as well as $\text{Ca}_3\text{Co}_4\text{O}_9$. Further advantages include the high deposition rate (compared to deposition from oxide sources) associated with reactive sputter-deposition and the abundant availability of metallic Ca and Co targets.

The *in situ* experiments were performed at the P07 beamline “High Energy Materials Science” (HEMS) and made possible through the Röntgen-Ångström Cluster project «X-Cut» which is a collaboration between Linköping University and Helmholtz-Zentrum Geesthacht.

Contact: Biplab Paul, bippa@ifm.liu.se, Per Eklund, perek@ifm.liu.se

Authors

Biplab Paul¹, Jeremy L. Schroeder¹, Sit Kerdsonpanya¹, Ngo Van Nong², Norbert Schell³, Daniel Ostach³, Jun Lu¹, Jens Birch¹, and Per Eklund¹

¹. Thin Film Physics Division, Department of Physics, Chemistry, and Biology (IFM), Linköping University, SE-581 83 Linköping, Sweden

². Dept. of Energy Conversion and Storage, Technical University of Denmark, Risø Campus, Frederiksborgvej 399, Building 779, 4000 Roskilde, Denmark

³. Helmholtz-Zentrum Geesthacht, Centre for Materials and Coastal Research, Institute for Materials Research, Max-Planck-Straße 1, 21502 Geesthacht, Germany

Original publication

“Mechanism of Formation of the Thermoelectric Layered Cobaltate $\text{Ca}_3\text{Co}_4\text{O}_9$ by Annealing of CaO-CoO Thin Films”, *Advanced Electronic Materials* 1, 1400022 (2015)
DOI: 10.1002/aem.201400022.

Crystal meets amorphicity.

Interfacing silicon with its native oxide

The surface of crystalline silicon is passivated by a layer of its own amorphous oxide. The structure of the interface between the two has not been hitherto resolved on an atomic scale. This has severely limited the accuracy in X-ray reflectivity (XRR) characterization of the nanoscale structure of adlayers and self-assembled monolayers on silicon substrates, widely used in nano-science and -technology. Our XRR measurements reveal a low-density layer at the junction between the crystalline silicon and its native oxide. Accounting for this low density region significantly enhances the accuracy achievable in studies of silicon-supported nanometre-thick films.

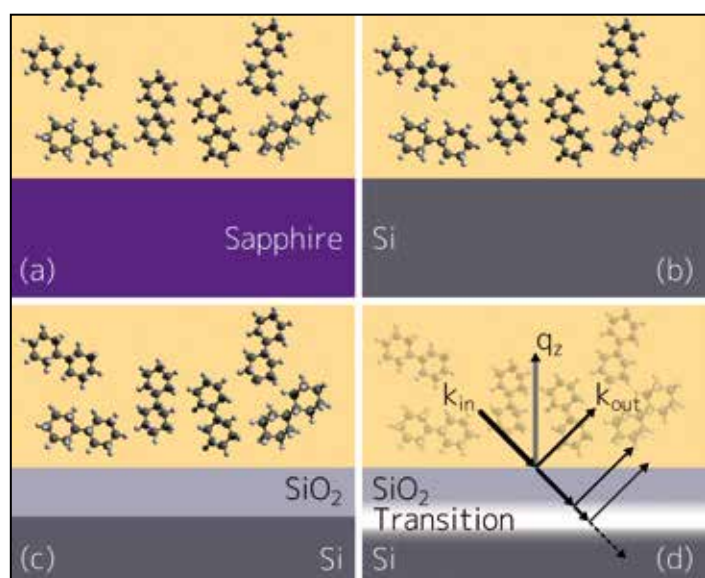


Figure 1
Models of the interfaces studied. The corresponding X-ray reflectivities are shown in Figure 2. The arrows in (d) represent the reflected and refracted beam at each interface.

Polished silicon wafers, developed for use in the semiconductor industry, are by far the most widely used substrates for studying deposited and self-assembled organic thin films due to their low cost and Ångstrom-scale smoothness. Their surface is invariably terminated by a few nanometre-thick amorphous native SiO_2 layer. However, the transition region between the silicon and its oxide was hitherto neither well characterized nor well understood [1].

To resolve this issue, we have performed a high-resolution XRR study of native-oxide-terminated (001)-oriented silicon substrates in contact with an organic liquid (bicyclohexyl, BCH) at beamline P08, PETRA III. For comparison, a sapphire (0001) substrate in contact with BCH was investigated. We have also measured XRR of Si-substrates covered by monolayers of

octadecyltrichlorosilane, and alcohol. Fig. 1 illustrates the sapphire/BCH and Si/BCH interfaces for the different models discussed below. The immersion in bulk BCH keeps the substrate's surface clean during the XRR measurements without having to resort to UHV conditions.

Fig. 2a (symbols 2.1) shows the measured Fresnel-normalized XRR (R/R_F) of a simple, unstructured, sapphire/BCH solid/liquid interface (illustrated in Fig. 1a). Sapphire, single-crystal Al_2O_3 , has no surface oxide layer. Therefore, a model consisting of just a single interface, between the sapphire and the liquid bulk, provides a good fit to the data (solid line). The finite-width transition between the two bulks in the corresponding electron density profile, $\rho(z)$, in Fig. 2b is due to the interfacial roughness of ~ 1.7 Å.

In contrast to the monotonically decreasing R/R_F of the sapphire/BCH interface, the silicon/BCH interface's R/R_F (symbols 2.2-2.4) is non-monotonic, exhibiting a pronounced dip at $q_z \approx 0.7$ Å⁻¹ and a broad, shallow peak centred at $q_z \approx 0.5$ Å⁻¹. Consequently, a simple single-interface model, which reproduced well the former data (line, 2.1), is inadequate for the later, as demonstrated in 2.2 (line). Moreover, obtaining a dip in an R/R_F curve requires the presence of at least two interfaces from which waves are reflected and interfere, in this case destructively, in the far field due to their different optical path lengths. The presence of such a dip in 2.2-2.4 reveals, therefore, the existence of at least one additional interface. An earlier model [2] introduced a second interface by adding between the bulks of the silicon and the BCH an oxide slab of a density slightly lower than that of the silicon. While the best fit of this model (line, 2.3 in Fig. 2a, and corresponding $\rho(z)$ in Fig. 2b) does produce the required dip at $q_z \approx 0.7$ Å⁻¹, in order to yield sufficient depth, the fit drives the Si/SiO₂ interfacial roughness to zero, an unphysical value. Moreover, the shallow peak at $q_z \approx 0.5$ Å⁻¹ and the post-dip rise in R/R_F are not well reproduced by this model (see 2.3 in Fig. 2a).

Following extensive tests with numerous different models, we found that the discrepancy between model and experiment could be fully eliminated by including an electron depletion layer at the Si/SiO₂ interface, as illustrated in Fig. 1d. The corresponding fit (line, 2.4 in Fig. 2a and corresponding $\rho(z)$ in Fig. 2b) gives $d = 1.5 \text{ \AA}$, $\rho = 0.51 \text{ e}^-/\text{\AA}^3$, $\sigma = 1.5 \text{ \AA}$, and $d_{\text{oxide}} = 10.7 \text{ \AA}$, for the depletion layer's width, electron density and roughness, and the oxide layer's thickness, respectively, along with a physically acceptable oxide roughness of 2.1 \AA .

The presence of the depletion layer is also responsible for a more subtle effect. The close-spaced interfaces of this layer give rise to a long-period modulation of the R/R_F curve. This results in a rising-intensity envelope at low q_z , which is responsible for the enhancement of the shallow peak at $q_z \approx 0.5 \text{ \AA}^{-1}$ and the post-dip R/R_F rise in curve 2.4, as compared to 2.3. The measured R/R_F is now well reproduced by this model over the entire q_z range (2.4 in Fig. 2b). Recent measurements show that this novel Si/SiO₂ interface model is crucial for faithfully reproducing R/R_F of silicon-supported silane [3] and alcohol [4] self-assembled monolayers (SAMs). For example, Fig. 2(c) shows the R/R_F (symbols) of a C₁₈OH SAM at 63 °C, together with fits including (blue line) and excluding (dashed green line) the Si/SiO₂ interface depletion layer. The electron density profile corresponding to the superior

depletion-including fit is shown in Fig. 2(d). We note that a distinction between the two model fits is only possible when utilizing modern synchrotrons like PETRA III, which provide intensities that enable measurements over extended q_z -ranges.

The inclusion of a depletion layer at the Si/SiO₂ interface in the model is also motivated by experimental studies showing the presence of various oxidation states of silicon at the Si/SiO₂ interface, in part due to dangling bonds and hydrogen, resulting from the mismatch in bond density between Si and SiO₂ [5]. Furthermore, theoretical studies also predict an interfacial layer with reduced density [6,7]. The depletion found in our study is equivalent to $\sim 6 - 8$ missing electrons in the electron density profile per unit Si cell area ($5.43 \times 5.43 \text{ \AA}^2$). This is equivalent to one missing oxygen atom whose bonds remain hydrogen passivated.

Our findings provide significant increase in the accuracy of XRR characterization of the surface normal structure of nanometre-thick layers on silicon. As such layers play an important role in both basic science and technology of a broad range of nanoscale devices and constructs, this study should benefit many disciplines.

Contact: Hans-Georg Steinrück, hgs@slac.stanford.edu

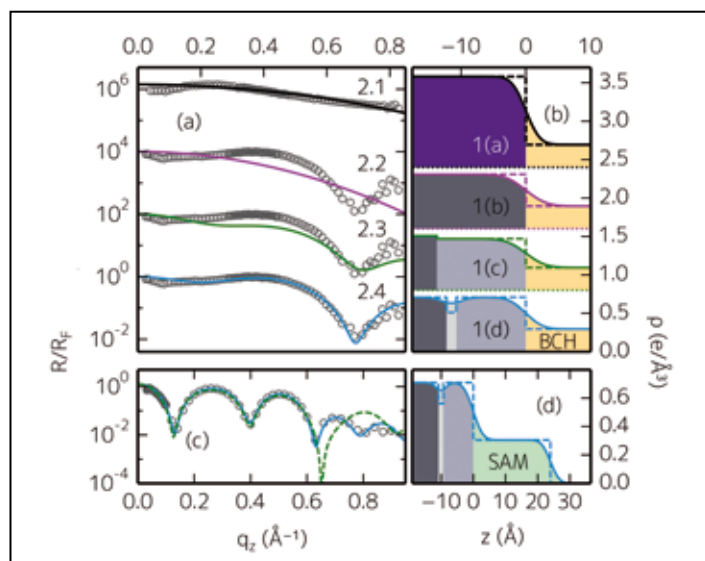


Figure 2

(a) Measured Fresnel-normalized X-ray reflectivity (symbols) from a sapphire/bicyclohexyl (BCH) (2.1) and silicon/BCH (2.2-2.4) solid/liquid interface, measured at beamline P08, PETRA III, with $\lambda = 0.689 \text{ \AA}$. Lines show fits to a simple model of two semi-infinite, uniform density slabs (2.1 and 2.2) and to a model with a distinct oxide layer, excluding (2.3) and including (2.4) a depletion layer at the SiO₂/silicon interface. The corresponding molecular models are illustrated in Fig. 1. (b) Surface-normal electron density profiles corresponding to the fits in (a) with (solid lines) and without (dashed lines) interfacial roughness. (c) Measured Fresnel-normalized X-ray reflectivity (symbols) from a C₁₈OH self-assembled monolayer (SAM) on silicon, together with fits including (blue line) and excluding (dashed green line) the Si/SiO₂ interface depletion layer (Data measured at P08/LISA, PETRA III, with $\lambda = 0.496 \text{ \AA}$). (d) Surface-normal density profiles corresponding to the blue fit in (c). Area colours in the electron density profiles correspond to Fig. 1. All curves are vertically spaced for clarity. Note the different x-axis ranges in (d) and (b).

Authors

Hans-Georg Steinrück^{1,2}, Andreas Schiener¹, Torben Schindler¹, Johannes Will¹, Andreas Magerl¹, Oleg Kononov³, Giovanni Li Destri³, Oliver H. Seeck⁴, Markus Mezger⁵, Julia Haddad⁶, Moshe Deutsch⁶, Antonio Checco⁷, and Benjamin M. Ocko⁷

1. Crystallography and Structural Physics, University of Erlangen-Nürnberg, 91058 Erlangen, Germany
2. SLAC National Accelerator Laboratory, Menlo Park, California 94025, United States
3. ESRF, 6 Rue Jules Horowitz, B.P. 220, 38043 Grenoble Cedex, France
4. Deutsches Elektronen-Synchrotron DESY, Notkestrasse 85, 22607 Hamburg, Germany
5. Max Planck Institute for Polymer Research, Ackermannweg 10, 55128 Mainz, Germany
6. Physics Department, and Institute of Nanotechnology and Advanced Materials, Bar-Ilan University, Ramat-Gan 52900, Israel
7. Condensed Matter Physics & Materials Science Department, Brookhaven National Laboratory, Upton, New York 11973, United States

Original publication

"Nanoscale Structure of Si/SiO₂/Organics Interfaces", ACS Nano 8, 12676–12681 (2014). DOI: 10.1021/nn5056223

References

1. S. Shaikhutdinov, H.-J. Freund, "Ultrathin Silica Films on Metals: The Long and Winding Road to Understanding the Atomic Structure", Adv. Mat 25, 49–67 (2013).
2. I. M. Tidswell et al., "X-ray specular reflection studies of silicon coated by organic monolayers (alkylsiloxanes)", Phys. Rev. B 41, 1111 (1990).
3. H.-G. Steinrück, J. Will, A. Magerl, and B. M. Ocko, "Structure of n-alkyltrichlorosilane monolayers on Si(100)/SiO₂", Langmuir 31, 11774-11780 (2015).
4. J. Haddad et al., "Order and Melting in Self-Assembled Alkanol Monolayers on Amorphous SiO₂", J. Phys. Chem. C, 119, 17648-17654 (2015).
5. F. J. Himpsel et al., Phys. Rev. B 38, 6084 (1988).
6. Y. Tu and J. Tersoff, "Structure and energetics of the Si-SiO₂ interface", Phys. Rev. Lett. 84, 4393 (2000).
7. A. Bongiorno, A. Pasquarello, M. S. Hybertsen, and L. C. Feldman, "Transition Structure at the Si(100)-SiO₂ Interface", Phys. Rev. Lett. 90, 186101 (2003).

Ultrafast tracking of electron spins.

A nuclear sensor for high frequency magnetics

Spin waves, collective excitations of the magnetization, resonate at a few Gigahertz when stimulated by a magnetic field of that frequency. Many properties like the resonance frequency and dispersion relation of the spin waves can be probed by established methods like Raman scattering, Brillouin light scattering, or inelastic neutron scattering. However, the precession orbit of the spins in the magnetic material is not easily accessible, although many effects, that might bring the spin waves into real applications, crucially depend on this property. By utilizing a nuclear sensor we could determine the spin precession in a magnetic thin film system.

Our present digital information and storage technologies are based on two properties of the electron. The first is its charge, which is used in electronic circuits to process information. The second is its spin, which represents the information stored on a magnetic hard disk. Recent research attempts to make use of the charge and the spin of the electron simultaneously. This approach could enhance functionality, capacitance, energy consumption, and speed of today's information technology.

In the present work the spin precession of a spin wave could be tracked at high frequencies that are of technological importance. Spin waves are collective excitations of the magnetization that resonate typically at GHz frequencies. They play a crucial role for new concepts of logical operations, spin-torque oscillators, or signal processing, and constitute a

basis of the emerging fields of spintronics and magnonics [1]. The spin precession is characterized by the opening angle of the precession cone that determines spin related effects that are currently explored and proposed for new functional devices.

Spin waves are often probed by inelastic scattering techniques that rely on analysis of the energy transfer to the scattered photons. We have used a different approach by enriching a 13 nm thick magnetic permalloy ($\text{Ni}_{80}\text{Fe}_{20}$) film with the Mössbauer isotope ^{57}Fe . At its nuclear transition energy it absorbs X-rays with an energy of 14.4125 keV and reemits them after a few nanoseconds on the timescale of its natural lifetime of 141 ns. The technique is called nuclear resonant scattering (NRS) [2] and in contrast to inelastic scattering techniques, it utilizes a coherent and elastic scattering process. The precessing spins leave a fingerprint in the time dependence of the emitted photons giving access to the orbit of the spins.

In the experiment performed at the Dynamics Beamline P01 at PETRA III, the sample was excited with an external magnetic high-frequency field that initiates a precession of the spins at the ferromagnetic resonance. To apply the stimulus, a microwave stripline was prepared which consists of a 10 μm wide signal line nested by two large ground lines as visible in Fig. 1. The ferromagnetic film was placed on top. A high-frequency electrical current applied to the strip is accompanied by a magnetic field that excites the film above the signal line. On this part of the sample the X-rays are exactly focused onto by a Kirkpatrick-Baez multilayer mirror that has a spot size of $10 \times 10 \mu\text{m}^2$, whereby it is illuminated under grazing incidence at 0.25° .

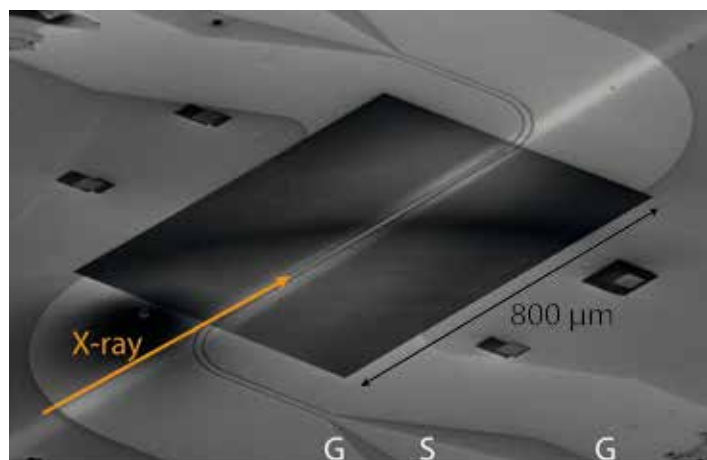


Figure 1

The scanning electron micrograph of the sample shows the electrical stripline (S) with its ground lines (G) and the magnetic film on top (dark). The X-rays are impinging in grazing incidence at 0.25° .

The nuclear transition is Zeeman split due to the presence of a strong intrinsic magnetic hyperfine field of 27.6 T acting on

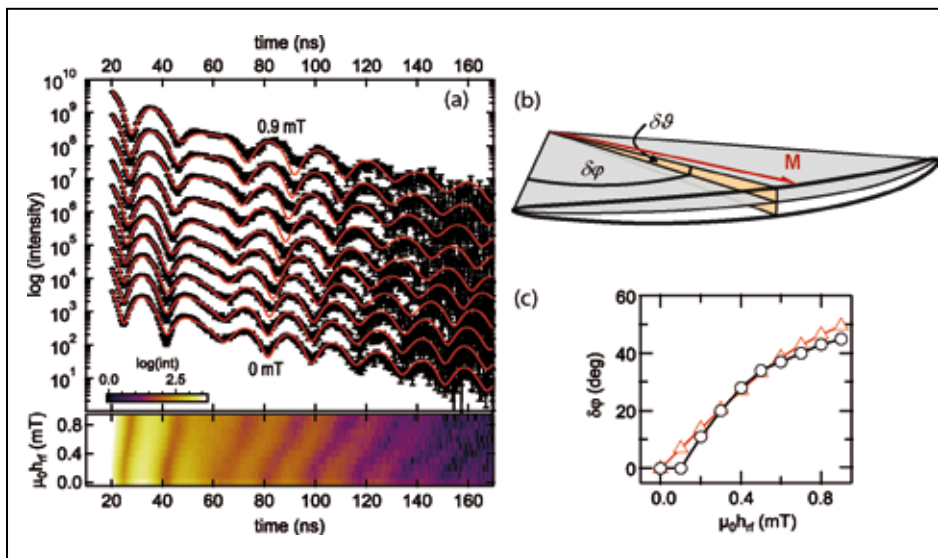


Figure 2

a) Nuclear resonance scattering time spectra (black) at different excitation field amplitudes ranging from 0 to 0.9 mT together with fits using the stochastic relaxation model (red). The lower panel shows a colour plot of the data for increasing excitation amplitude. (b) Deduced precession cone of the magnetization. The in-plane opening angle of the precession ($\delta\varphi$) is a factor of 13 larger than the out-of-plane one ($\delta\theta$). (c) Amplitude of the in-plane opening angle with increasing excitation amplitude at resonance. Measured values (black) are compared to micromagnetic simulations (red).

the nucleus. The nuclei are excited by the synchrotron pulse that excites all six dipole-allowed nuclear transitions simultaneously. Their frequency differences manifest as quantum beats in the temporal evolution of the nuclear decay. This is visible in the recorded NRS time spectra shown in Fig. 2a which show the intensity of the reemitted photons from the excited nucleus after excitation at time zero. The time spectra contain all information about the magnetic environment at the nucleus.

Time spectra at different high-frequency magnetic field amplitudes are shown whereby the film was driven at its ferromagnetic resonance of 1.93 GHz. As observed the overall shape of the time spectra changes with increasing excitation field amplitudes. A shift of the extrema to later times with increasing dynamic field is best visible in the colour plot. The observed shift of the extrema originates from the excited spin wave.

For a quantitative evaluation of the influence of the spin wave on the time spectra, calculations within a stochastic relaxation

model are performed to model the decay of the excited nuclear state [3]. This model was adapted to a ferromagnetic resonance theory which employs the free energy of the magnetic system to derive dynamic properties of the magnetization [4]. The data were fitted using the program package CONUSS [5] as shown by the red lines. The outcome is that the spins precess on a highly elliptical rather than on a circular orbit (see Fig. 2b). The experimental results confirm theoretical calculations on the shape of the spin precession. Moreover the absolute amplitude can be determined with high precision even in the non-linear regime (Fig. 2c).

The elliptical motion of the spins in the thin film has many implications for the research fields of spintronics and magnonics. With the given nuclear scattering technique and the findings on the spin motion, systems can be tuned to optimize the orbit of the spin and with it the functionality of future spin-based devices.

Contact: Lars Bocklage, lars.bocklage@desy.de

Authors

Lars Bocklage^{1,2}, Christian Swoboda^{3,2}, Kai Schlage¹, Hans-Christian Wille¹, Liudmila Dzemiantsova^{1,2}, Saša Bajt¹, Guido Meier^{4,3,2}, and Ralf Röhlsberger^{1,2}

1. Deutsches Elektronen-Synchrotron DESY, Notkestraße 85, 22607 Hamburg, Germany
2. The Hamburg Centre for Ultrafast Imaging, Luruper Chaussee 149, 22761 Hamburg, Germany
3. Institut für Nanostruktur und Festkörperphysik, Universität Hamburg, Jungiusstrasse 11, 20355 Hamburg, Germany
4. Max-Planck Institute for the Structure and Dynamics of Matter, Luruper Chaussee 149, 22761 Hamburg, Germany

Original publication

“Spin Precession Mapping at Ferromagnetic Resonance via Nuclear Resonant Scattering of Synchrotron Radiation”, *Physical Review Letters* 114, 147601 (2015).

DOI: 10.1103/PhysRevLett.114.147601

References

1. V. V. Kruglyak, S. O. Demokritov, and D. Grundler, “Magnonics”, *J. Phys. D* 43, 264001 (2010).
2. R. Röhlsberger, “Nuclear Condensed Matter Physics with Synchrotron Radiation”, *Springer Tracts in Modern Physics*, Vol. 208 (Springer, Berlin, 2005).
3. M. Blume, “Stochastic Theory of Line Shape: Generalization of the Kubo-Anderson Model”, *Phys. Rev.* 174, 351 (1968).
4. J. Smit and H. G. Beljers, “Ferromagnetic resonance absorption in BaFe₁₂O₁₉, a highly anisotropic crystal”, *Philips Res. Rep.* 10, 113 (1955).
5. W. Sturhahn, “CONUSS and PHOENIX: Evaluation of nuclear resonant scattering data”, *Hyperfine Interact.* 125, 149 (2000).

Enabling a new class of electronic devices.

Using self-aligned nanodomain boundaries to open a charge transport gap in trilayer graphene

Trilayer graphene reveals unique electronic properties appealing for fundamental science and electronic technologies. We propose a simple method to open a charge transport gap and achieve a high on-off current ratio in Bernal-stacked trilayer graphene synthesized on vicinal (stepped) SiC(001)/Si(001) wafer. Low-temperature measurements show that self-aligned, periodic nanodomain boundaries induce a huge charge transport gap of more than 1.3 eV at 10 K and 0.4 eV at 100 K. Our studies indicate the feasibility of creating electronic nanostructures using graphene on cubic-SiC/Si wafers.

Graphene is a single-atom-thick carbon sheet with properties unrivalled by any other known material. It will likely lead to a revolution in many areas of technology, but there are still some open questions. Ideally, graphene-based electronics would consist of just one or a few layers of graphene. The absence of an energy band gap like that of a semiconductor hampers the design of graphene-based device architectures. No gap opening in trilayer graphene with ABA (Bernal) stacking, i.e. the top sheet is exactly on top of the lowest sheet, has been shown until now.

Recent theoretical works [1] show that nanodomain boundaries (NBs) in the graphene lattice that exhibit a periodic atomic structure along their length can perfectly reflect charge carriers over a large range of energies. Harnessing this would provide a new way to control the charge carriers without the need to introduce an energy band gap. The main challenge is to produce self-aligned nanodomains with periodic boundaries on a semiconducting substrate compatible with existing processes. We present a simple method to synthesize such a system with self-aligned periodic NBs.

In 2015 the new dynamic-XPS end-station, based on the Argus spectrometer, was finally installed on the high-brilliance soft X-ray P04 beamline at PETRA III. Users can now observe fast processes by following the evolution of photoemission core-level spectra (~ 0.1 sec/spectrum). The setup allows X-ray photoelectron spectroscopy (XPS) users to observe surface modifications in real time. One can follow the relative contribution of different components during overlayer growth or interface formation by measuring core-level XPS spectra in scanning and snapshot modes in a loop. This opens a way to study dynamic processes at surfaces and interfaces and control the surface composition in real time.

By acquiring XPS spectra of the C 1s and Si 2p transitions during graphene growth on the cubic-SiC/Si wafer, we could stop the process as soon as the desired number of graphene layers was reached. To our knowledge no other beamline-endstation allows such control over layer-by-layer graphene growth. In terms of spectrum acquisition speed, photon flux, photon energy range, and photon energy resolution, for this

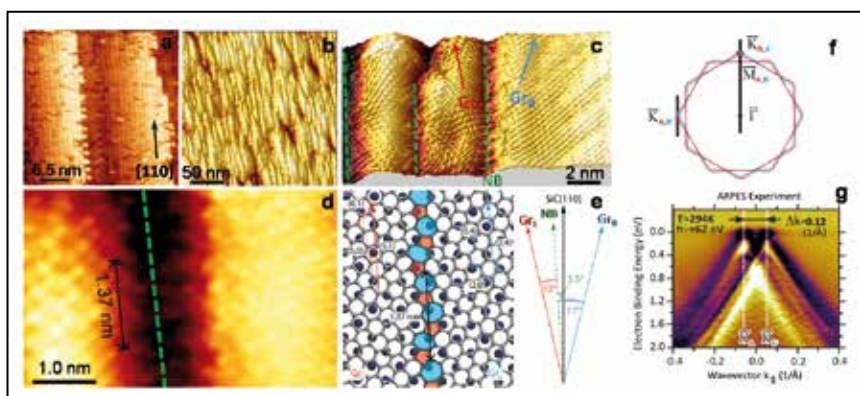


Figure 1

(a) STM image of the vicinal SiC(001) surface. The step direction is close to the [110] direction of the SiC crystal lattice. (b) Large-area STM image of graphene nanoribbons synthesized on the vicinal SiC(001). (c) and (d) Atomically resolved STM images of the graphene surface. The system of domains is rotated 17° clockwise (Gr_{17}) and 10° anticlockwise (Gr_{10}) relative to the NB. The NB is itself rotated 3.5° anticlockwise from the [110] direction. (e) Schematic model of the NB for the asymmetrically rotated nanodomains in panels (c) and (d). For the angles shown a periodic structure of distorted pentagons and heptagons is formed. (f) Effective surface Brillouin zone corresponding to four rotated graphene domain variants. (g) Dispersion of the π -band in the graphene along the K_x - K_y direction indicated in panel (f). The electronic structure is typical of Bernal-stacked trilayer graphene.

use the dynamic-XPS is unrivalled. The developed setup helped us to optimize the synthesis of few-layer graphene samples [2].

The fabrication method uses Si-atom sublimation followed by high-temperature surface graphitization in ultra-high vacuum [3–6]. The steps of the vicinal (2° miscut) SiC(001)/Si(001) wafers impart a preferential NB direction to the trilayer graphene. The step direction was close to $[110]$, as Fig. 1a illustrates. Scanning tunnelling microscopy (STM) studies reveal that the graphene contains nm-scale domains with boundaries elongated in one direction (Fig. 1b), which is close to the step direction of the vicinal SiC(001) substrate (Fig. 1a). Figure 1c shows an atomically resolved STM image containing several nm-scale domains connected to each other by the NBs.

Detailed analysis of the STM images measured near the NBs shows that, in most cases, NBs on the vicinal sample (Fig. 1c) are rotated by 3.5° relative to one of the family $\langle 110 \rangle$ crystallographic directions. As Fig. 1e illustrates, the asymmetric rotation of the graphene lattices relative to the NBs leads to the formation of a periodic structure along the boundaries, with a period of 1.37 nm. The periodic structure consists of distorted heptagons and pentagons (Fig. 1e), which produce modulations in the atomically resolved STM image measured at the NB (Fig. 1d).

Angle-resolved photoemission spectroscopy measurements (Figs. 1f–g) allow us to extract information about the stacking order of the graphene. The fine structure indicates Bernal stacking, and the Dirac points, where the conduction and valence bands meet, are close to the Fermi level (Fig. 1g). This is in full agreement with theoretical simulations for ideal trilayer graphene.

Figure 2a shows a schematic drawing of the nano-gap device. Devices with sub-30 nm gap contacts were fabricated using electron-beam lithography. Figures 2b and 2c show the current-voltage (I–V) curves measured at different temperatures. The transport gap is clearly observed below 100 K but disappears at temperatures above 150 K at voltages below ± 0.8 V due to the vanishing current. To obtain the exact value of the transport gap, we plotted the corresponding differential dI/dV curves in Fig. 2d for temperatures below 150 K. Remarkably, the transport gap is approximately the same at 50 K and 10 K but substantially lower (0.4 eV) at 100 K.

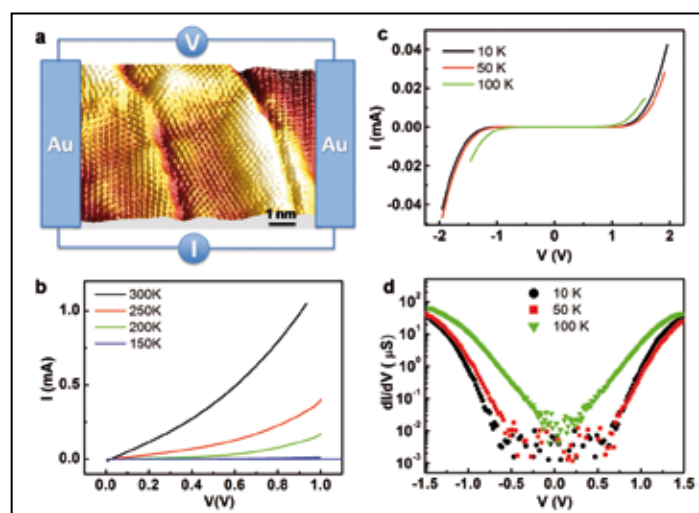


Figure 2

a) Scheme of the nano-gap device. (b) I–V curves measured at 150 K, 200 K, 250 K, and 300 K. (c) I–V curves measured at 10 K, 50 K, and 100 K. (b) and (c) are measured with the current directed across the self-aligned NBs. (d) Corresponding dI/dV curves for temperatures below 150 K.

We also measured I–V characteristics at 10 K with the current applied along the NBs. No transport gap was observed in this case and the I–V curve displayed nonlinear behaviour. This indicates that the charge transport gap observed for current across the NBs is mainly due to the reflection of charge carriers from the NBs.

We have proposed a new method to synthesize graphene with self-aligned periodic NBs. The vicinal SiC(001) substrates used are compatible with silicon processes. Electrical measurements show the opening of a transport gap in the graphene synthesized on this stepped surface. This development may lead to new tuneable electronic nanostructures made from graphene on cubic- SiC, opening up opportunities for a wide range of new applications.

Contact: Victor Aristov, victor.aristov@desy.de
 Olga Molodtsova, olga.molodtsova@desy.de
 Han-Chun Wu, wuhc@bit.edu.cn
 Alexander Chaika, chaika@issp.ac.ru

Authors

Han-Chun Wu, Alexander N. Chaika, Tsung-Wei Huang, Askar Syrtybekov, Mourad Abid, Victor Yu. Aristov, Olga V. Molodtsova, Sergey V. Babenkov, D. Marchenko, Jaime Sánchez-Barriga, Partha Sarathi Mandal, Andrei Yu. Varykhalov, Yuran Niu, Barry E. Murphy, Sergey A. Krasnikov, Olaf Lübber, Jing Jing Wang, Huajun Liu, Li Yang, Hongzhou Zhang, Mohamed Abid, Yahya T. Janabi, Sergei N. Molotkov, Ching-Ray Chang, and Igor Shvets

Affiliation details at

<http://pubs.acs.org/doi/abs/10.1021/acsnano.5b02877>

Original publication

“Transport Gap Opening and High On-Off Current Ratio in Trilayer Graphene with Self-Aligned Nanodomain Boundaries”, *ACS Nano* 9, 8967–8975 (2015). DOI: 10.1021/acsnano.5b02877

References

- O. V. Yazev and S. G. Louie, “Electronic Transport in Polycrystalline Graphene”, *Nat. Mater.* 9, 806 (2010).
- S. V. Babenkov et al., “A new dynamic-XPS end-station for beamline P04 at PETRA III/DESY”, *NIM in Physics Research A* 777, 189 (2015).
- V. Yu. Aristov et al., “Graphene synthesis on Cubic SiC/Si wafers. Perspectives for mass production of graphene-based electronic devices”, *Nano Letters* 10, 992 (2010).
- A. N. Chaika et al., “Continuous wafer-scale graphene on cubic-SiC(001)”, *Nano Research* 6, 562 (2013).
- A. N. Chaika et al., “Rotated domain network in graphene on cubic-SiC(001)”, *Nanotechnology* 25, 135605 (2014).
- A. N. Chaika et al., “Fabrication of [001]-oriented tungsten tips for high resolution scanning tunnelling microscopy”, *Scientific Reports* 4, 3742 (2014).

Fading of Van Gogh's red lead pigment.

X-ray diffraction tomography reveals presence of a rare lead mineral

Red lead, a semiconductor pigment used by artists since Antiquity, is known to undergo several discolouration phenomena. These transformations are either described as darkening of the pigment caused by the formation of plattnerite or galena or as whitening by which red lead is converted into anglesite or (hydro)cerussite. In this work the internal distribution of the different crystalline compounds in a paint sample from a Van Gogh painting was investigated using microscopic X-ray powder diffraction tomography. This revealed the presence of a very rare lead mineral, plumbonacrite ($3\text{PbCO}_3 \cdot \text{Pb}(\text{OH})_2 \cdot \text{PbO}$), which forms the missing link between on the one hand the photoinduced reduction of red lead and on the other hand (hydro)cerussite. These findings shed new light on the whitening of red lead.

Red lead, most commonly referred to as *minium*, is a semiconductor pigment used by artists since ancient times and is thought to be one of the first artificially prepared pigments. Minium corresponds to the lead (II,IV) oxide mineral of composition Pb_3O_4 and can often be found on artworks in association with lead monoxide, either litharge (*t*-PbO) or massicot (*o*-PbO).

The red lead pigment is known to be unstable with time. On the one hand, it is thought to play a role in the formation of lead soap protrusions where lead carbonate and lead soaps are formed through the reaction of red lead with the fatty acids present in the oil medium of the paint. This causes the underlying material to push the upper paint layers outwards, forming a pustular mass on the surface of the painting. On the other hand, minium found in and around lead soap protrusions is believed to have formed via remineralisation usually together with lead carbonate [1].

Besides protrusion formation, red lead can undergo severe discolouration [2]. The most frequently encountered colour

change is specified as blackening of the pigment caused by the formation of either galena (PbS) or plattnerite ($\beta\text{-PbO}_2$). A second, less documented discolouration, visible as whitening or bleaching of the pigment has also been described [3]. In this case the alteration products are either lead carbonate (hydrocerussite ($2\text{PbCO}_3 \cdot \text{Pb}(\text{OH})_2$) and/or cerussite (PbCO_3)) or lead sulphate (PbSO_4).

In the past 10 years, microscopic X-ray powder diffraction (μXRPD) mapping experiments performed on samples extracted from works of art have provided useful information for the study of degradation processes that are ongoing on paintings [4]. XRPD mapping can be used to identify, visualize and to a certain extent quantify the different crystalline components that are present in these complex heterogeneous paint systems. At state-of-the-art synchrotron radiation facilities these measurements can be done on the (sub) micrometre scale. However, an intrinsic limitation of 2D mapping remains the loss of depth information as projection images are obtained. Therefore, in order to investigate the

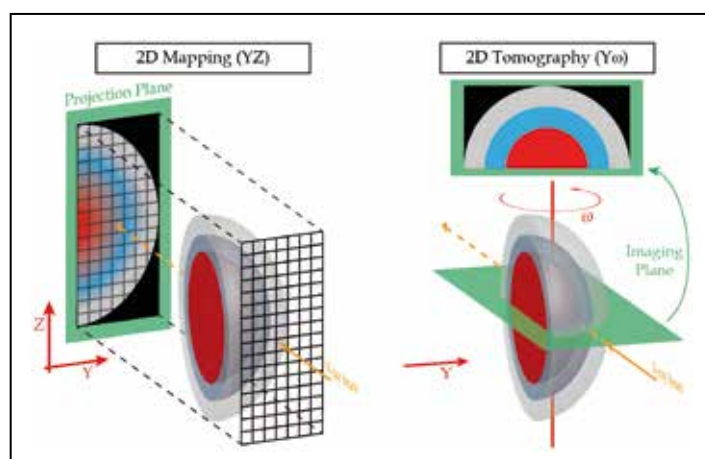


Figure 1
Schematic illustration of a (left) 2D mapping and (right) 2D tomography experiment.



Figure 2
(Left) Photograph of "Wheat stack under a cloudy sky" by Van Gogh (October 1889, oil on canvas, Kröller-Müller Museum, NL). The sampled area is indicated by the white circle. (Right) Detailed images of the microscopic paint sample.

stratigraphy of a paint system, typically a cross-section of a paint sample needs to be prepared, consuming to a lesser or greater extent part of the often unique or very rare sample. Whereas with μ XRPD tomography the inner distribution of the crystalline components present in such samples can be visualized without physically cross-sectioning the sample (Fig. 1) [5].

In this work we employed μ XRPD tomography on a microscopic sample obtained from the painting *Wheat stack under a cloudy sky* by Van Gogh (October 1889, oil on canvas, Kröller-Müller Museum, Netherlands). These experiments were carried out at the micro-probe endstation of the P06 beamline at PETRA III. The sample is a severed pustular mass which reveals a bright orange-red minium core (about 100 μ m in diameter). This core is surrounded by a light blue tinted layer containing the cobalt blue pigment mixed with lead white (a mixture of hydrocerussite and cerussite). A gray outer layer containing a finely grained mixture of zincite and hydrocerussite partially covers the pustular mass (Fig. 2).

The μ XRPD tomograms reveal a “vacant space” between the minium core and the blue-tinted lead white layer (Fig. 3). In fact a fourth lead-containing compound, plumbonacrite ($3\text{PbCO}_3 \cdot \text{Pb}(\text{OH})_2 \cdot \text{PbO}$), is found to be present in the sample and is largely situated in this “void”. To some extent an overlap between the lead white layer and plumbonacrite is visible.

Although plumbonacrite was made synthetically from the mid 20th century, to the best of our knowledge, this phase was never detected on paintings before this date, either as part of lead white mixtures or as a pure compound. In our case, the presence of this carbonate-poor lead compound in between the red lead and the carbonate-rich lead white layer strongly suggests that plumbonacrite is present as an intermediate degradation product formed during the whitening of minium. Since PbO , a remnant of the red lead production process, is more reactive than Pb_3O_4 , it may have initiated the degradation process and has been used up. Alternatively, minium itself can be photoactivated (Scheme 1).

Based on this new insight, we propose an additional step in the photochemical reaction of red lead [6]. Electron hole pairs formed upon exposure of minium with visible light (wavelength < 580 nm) [4] on the one hand can generate CO_2 *in situ* via oxidative decarboxylation of the free fatty acids. On the other hand Pb^{IV} is reduced to Pb^{II} which in turn reacts with CO_2 . This forms plumbonacrite as an intermediate that is converted to hydrocerussite and then to cerussite upon further absorption of CO_2 . By gaining new insights into the chemical processes that are ongoing in paintings, the environmental conditions (air quality, lighting, ...) used to store and exhibit these precious works to the public can be adapted to better preserve the paintings for future generations to admire.

Contact: Koen Janssens, koen.janssens@uantwerpen.be

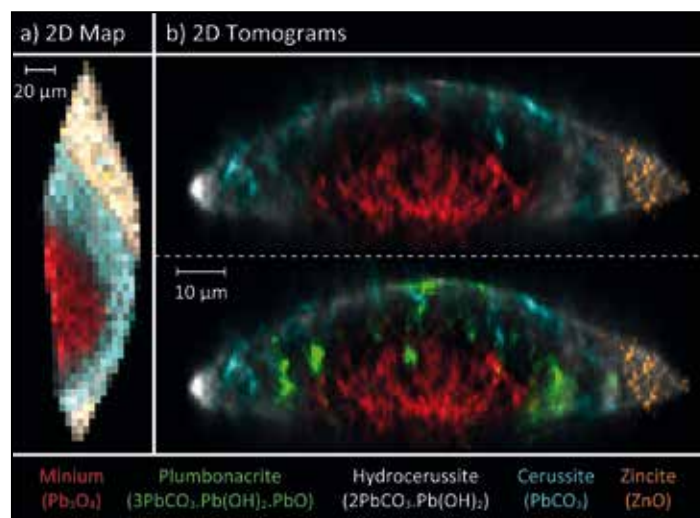
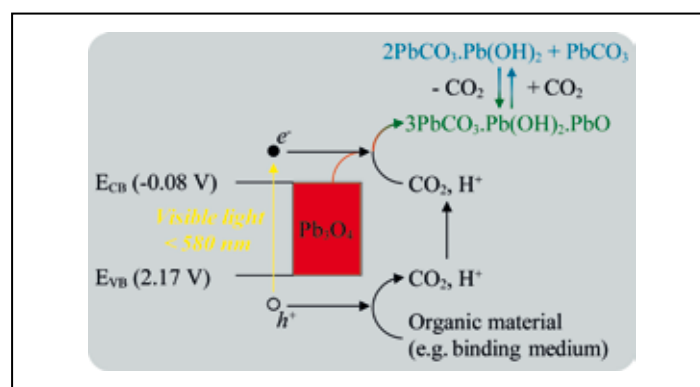


Figure 3

Colour reconstructions of the a) projected and of the b) inner crystalline distribution of the paint sample. Pixel size: a) $4 \times 5 \mu\text{m}^2$, b) $1 \times 1 \mu\text{m}^2$.



Scheme 1

Proposed pathway for the photochemical degradation of Pb_3O_4 under visible light irradiation. Conduction and valence band potentials, respectively E_{CB} and E_{VB} , are given relative to the normal hydrogen electrode (NHE) [6].

Authors

Frederik Vanmeert¹, Geert Van der Snickt¹, and Koen Janssens¹

¹. AXES, Department of Chemistry, University of Antwerp, 2020 Antwerp, Belgium

Original publication

“Plumbonacrite Identified by X-ray Powder Diffraction Tomography as a Missing Link during Degradation of Red Lead in a Van Gogh Painting”, *Angew. Chem.* 127, 3678–3681 (2015). DOI: 10.1002/ange.201411691

References

1. K. Keune and J. J. Boon, “Analytical imaging studies of cross-sections of paintings affected by lead soap aggregate formation”, *Stud. Conserv.* 52, 161–176 (2007).
2. S. Aze, J. M. Vallet, V. Detalle, O. Grauby, and A. Baronnet, “Chromatic alterations of red lead pigments in artworks: a review”, *Phase Transitions* 81, 145–154 (2008).
3. D. Saunders, M. Spring, and C. Higgitt, in 13th Triennial Meeting Rio de Janeiro Preprints, Vol. I, 455–463 (2002).
4. G. Van der Snickt, K. Janssens, J. Dik, W. De Nolf, F. Vanmeert, J. Jaroszewicz, M. Cotte, G. Falkenberg, and L. Van der Loeff, “Combined use of synchrotron radiation based micro-X-ray fluorescence, micro-X-ray diffraction, micro-X-ray absorption near-edge, and micro-fourier transform infrared spectroscopies for revealing an alternative degradation pathway of the pigment cadmium yellow in a painting by Van Gogh”, *Anal. Chem.* 84, 10221–10228 (2012).
5. W. De Nolf and K. Janssens, “Micro X-ray diffraction and fluorescence tomography for the study of multilayered automotive paints”, *Surf. Interface Anal.* 42, 411–418 (2010).
6. Y. G. Zhou, H. X. Lin, Q. Gu, J. L. Long, and X. X. Wang, “Visible light-induced highly efficient organic pollutant degradation and concomitant CO_2 fixation using red lead”, *RSC Advances* 2, 12624–12627 (2012).

Superconductivity in new geometries of matter.

Micro X-ray diffraction studies reveal a complex mesoscopic landscape needed for high temperature superconductivity

High Temperature Superconductivity competes with Incommensurate Charge Density Wave (CDW) order in presence of quenched disorder (QD) due to defects. This competition gives rise to an emerging complex scenario with phase separation at mesoscale. Using a combination of standard and scanning micro X-ray diffraction we provided direct imaging of the CDW puddles and oxygen interstitial (O-i) organization in a cuprate superconductor with a superconducting critical temperature of $T_c = 95$ K. The results show that O-i rich regions are spatially anti-correlated with CDW puddles that form a confined non-euclidean landscape where superconductivity can arise in the interstitial space.

The cause of the striking diversity of the states of matter is subject of the oldest philosophical investigation. In the last century, major studies have shown a new intriguing state of matter. In this state, some systems develop macroscopic quantum order that gives rise to superfluidity and superconductivity. Superconducting materials show zero resistance to the passage of electric current below a specific low temperature and they expel the magnetic fields present within them. Unfortunately, superconductors must be cooled down to temperatures close to the absolute zero to operate. This dramatically limits their application to particular few cases. However, a couple of decades ago it was discovered that ceramic materials can become superconductors at

higher temperatures; for example some copper oxides (cuprates) show superconductivity at -170 °C. But nowadays there is not yet a recognized microscopic theory able to describe what happens in this fourth state of matter, explaining the mechanism of this quantum phenomenon at the macroscopic scale.

A key role in this mechanism is played by the interplay of the superconducting state with other orders that compete with it like Charge Density Wave (CDW) [1,2] or Spin Density Wave (SDW) order and quenched disorder (QD). To shed light on this problem many different experimental approaches have been used so far, but no direct evidence of this competition was reported yet.

This work was conducted by an international research team coordinated by Alessandro Ricci of Deutsches Elektronen-Synchrotron DESY in Hamburg, with Gaetano Campi of Italian National Research Council (CNR) and Antonio Bianconi of Rome International Centre of Material Science. Here we studied a cuprate material containing mercury and doped by oxygen interstitials that shows superconductivity below 95 K. In this material defects are mobile and we have already demonstrated that they can get organized and forming clusters [3-5]. Similarly, in this particular compound, the electrons form crystals, called CDW, at temperatures lower than 240 K. For investigating this special order and its spatial organization we made use of a combination of multiple experimental techniques. Hard X-ray diffraction measurements have been performed at BW5 beamline of DESY and at XRD1 beamline of ELETTRA (Trieste) and the results are summarized in Fig. 1.

Figure 1a shows the behaviour of the average intensity of the CDW peak as a function of temperature with a maximum close to the superconducting critical temperature T_c , indicating its competition with the superconducting state. Figure 1b shows the short-range nature of the CDW order, indeed it forms puddles with a size of a few nanometres.

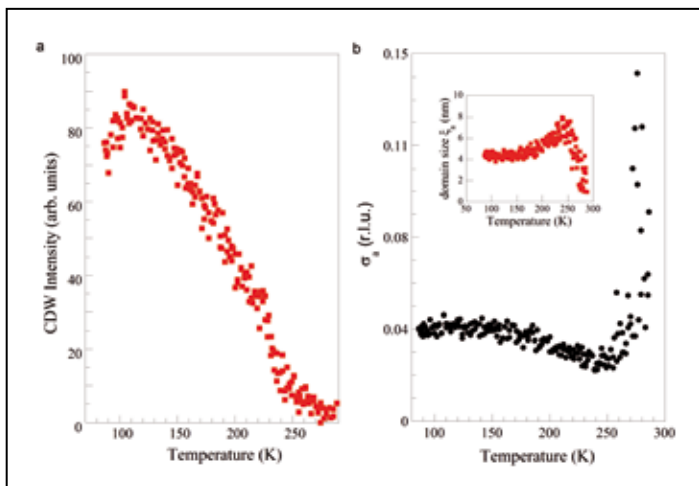


Figure 1

- a) Average intensity of the CDW peak as a function of temperature. The CDW order has a maximum close to the superconducting critical temperature T_c showing a clear competition with the superconducting state. The order-disorder transition is very broad indicating the role of a quenched disorder due to the presence of defects.
- b) Temperature dependence of the in-plane-full-width half-maximum of the CDW peak. In the inset the behaviour of the CDW domain size, along the a-direction, is shown.

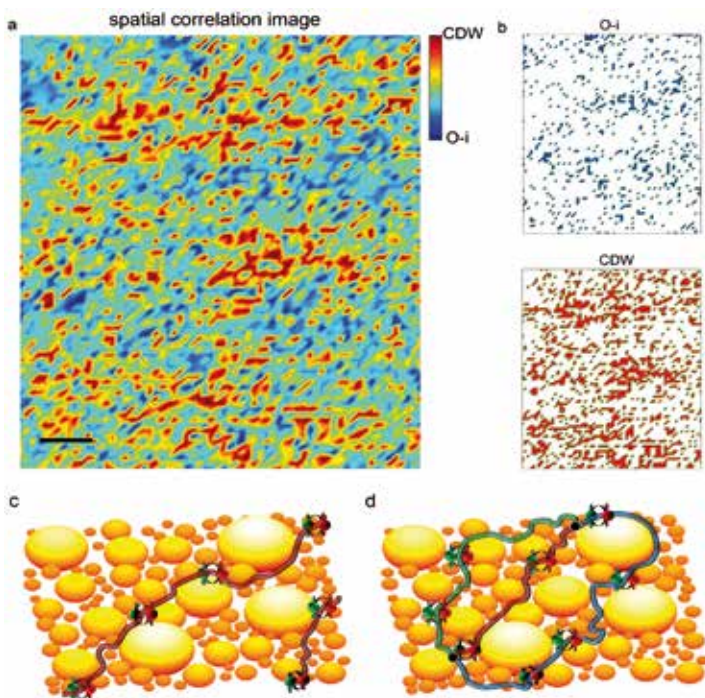


Figure 2

- a) Difference map between the Charge Density Waves (CDW) and interstitial oxygen (O-i) distribution. The map shows the spatial-anticorrelation between the CDW (in red) and the quenched disorder (in blue). The black bar corresponds to about 5 micrometres.
- b) The upper and the lower panels show the distribution of O-i and CDW respectively.
- c) The inhomogeneous landscape formed by the CDW puddles reduces the available space and confine superconductivity in the interstitial space.
- d) The new landscape formed defines non-equivalent paths for Fermi particles, running in the non-euclidean interstitial space between CDW puddles, connecting a point A to point B.

For understanding how these puddles get spatially organized in the materials and how they are correlated with the quenched disorder and the superconducting state, we performed a scanning micro X-ray diffraction experiment at the beamline ID13 of the European Synchrotron Research Facility (ESRF) in Grenoble. Firstly, a CDW peak was identified. Following, the spatial distribution of the intensity of this CDW peak was reconstructed by scanning the sample with a focused beam with size of about $1 \mu\text{m}^2$, like it was already done for studying cobaltite materials [6]. The results demonstrate that the CDW order forms an inhomogeneous pattern spatially anticorrelated with the interstitial oxygen defects order, as shown in Figs. 2a and b. The free electrons, which do not crystallize in CDW puddles, form superconducting Cooper-pairs flowing in the interstitial space outside the CDW puddles at low temperatures, as is schematized by Fig. 2c.

The short-range CDW puddles introduce a significant topological change in the available space for the free electrons. Indeed, to go from a hypothetical point A to a point B, electrons can take different paths that cannot be topologically deformed one into the other as is shown in Fig. 2d. Here different possible paths, taken by electrons at the Fermi level, run in the interstitial space out of the CDW puddles. These paths go around the CDW puddles in different ways. These different paths can create non-trivial interference effect for electrons, favouring the emergence of the superconducting state. This complex landscape is a non-euclidean space. This unexpected result opens completely new routes for both the understanding and interpretation of the mechanism that governs high temperature superconductivity and more in general for the design of new functional metamaterials.

Contact: Alessandro Ricci, alessandro.ricci@desy.de

Authors

G. Campi^{1,2}, A. Bianconi^{2,1}, N. Poccia^{3,2}, G. Bianconi⁴, L. Barba⁵, G. Arrighetti⁵, D. Innocenti^{6,2}, J. Karpinski^{6,7}, N. D. Zhigadlo⁷, S. M. Kazakov^{7,8}, M. Burghammer^{9,10}, M. v. Zimmermann¹¹, M. Sprung¹¹, and A. Ricci^{11,2}

1. Institute of Crystallography, CNR, via Salaria Km 29.300, Monterotondo Roma, I-00015, Italy
2. Rome International Center for Materials Science, Superstripes, RICMASS, via dei Sabelli 119A, I-00185 Roma, Italy
3. MESA+ Institute for Nanotechnology, University of Twente, PO Box 217, 7500AE Enschede, Netherlands
4. School of Mathematics, Queen Mary University of London, London E1, 4SN, UK
5. Institute of Crystallography, Sincrotrone Elettra UOS Trieste, Strada Statale 14 - Km 163,5 Area Science Park, 34149 Basovizza, Trieste, Italy
6. EPFL, Institute of Condensed Matter Physics, Lausanne CH-1015, Switzerland
7. ETH, Swiss Federal Institute of Technology Zurich Laboratory for Solid state Physics CH-8093 Zurich CH
8. Department of Chemistry, M.V. Lomonosov Moscow State University, Moscow 119991, Russia
9. European Synchrotron Radiation Facility, B. P. 220, F-38043 Grenoble Cedex, France
10. Department of Analytical Chemistry, Ghent University, Krijgslaan 281, S12 B-9000 Ghent, Belgium
11. Deutsches Elektronen-Synchrotron DESY, Notkestraße 85, D-22607 Hamburg, Germany

Original publication

"Inhomogeneity of charge density wave order and quenched disorder in a high T_c superconductor", *Nature* 525, 359 (2015). DOI: 10.1038/nature14987

References

1. J. Chang, E. Blackburn, A. T. Holmes, N. B. Christensen, J. Larsen, J. Mesot, Ruixing Liang, D. A. Bonn, W. N. Hardy, A. Watenphul, M. v. Zimmermann, E. M. Forgan, and S. M. Hayden, "Direct observation of competition between superconductivity and charge density wave order in $\text{YBa}_2\text{Cu}_3\text{O}_{6.67}$ ", *Nature Physics* 8, 871-876 (2012).
2. B. Phillabaum, E. W. Carlson, and K. A. Dahmen, "Spatial complexity due to bulk electronic nematicity in a superconducting underdoped cuprate", *Nature Communications* 3, 915-918 (2012).
3. M. Fratini, N. Poccia, A. Ricci, G. Campi, M. Burghammer, G. Aeppli, and A. Bianconi, "Scale-free structural organization of oxygen interstitials in $\text{La}_2\text{CuO}_{4+y}$ ", *Nature* 466, 841-844 (2010).
4. A. Ricci, N. Poccia, G. Campi, F. Coneri, L. Barba, G. Arrighetti, M. Polentarutti, M. Burghammer, M. Sprung, et al., "Networks of superconducting nano-puddles in 1/8 doped $\text{YBa}_2\text{Cu}_3\text{O}_{6.5+y}$ controlled by thermal manipulation", *New Journal of Physics* 16, 053030 (2014).
5. A. Ricci, N. Poccia, G. Campi, F. Coneri, A. S. Caporale, D. Innocenti, M. Burghammer, M. v. Zimmermann, and A. Bianconi, "Multiscale distribution of oxygen puddles in 1/8 doped $\text{YBa}_2\text{Cu}_3\text{O}_{6.67}$ ", *Scientific Reports* 3, 2383 (2013)
6. Y. Drees, Z. W. Li, A. Ricci, M. Rotter, W. Schmidt, D. Lamago, O. Sobolev, U. Rütt, O. Gutowski, M. Sprung, et al., "Hour-glass magnetic excitations induced by nanoscopic phase separation in cobalt oxides", *Nature Communications* 5, 5731 (2014).

Platonic beauties caught in flight.

Single-shot X-ray scattering of individual silver nanoparticles reveals their 3D shape

Determining the three-dimensional shape and orientation of individual nanoparticles in free space is a challenging task. In contrast to deposited or embedded nanoparticles, which can be imaged with electron microscopy or multi-shot tomographic approaches, free gas-phase clusters elude a 3D characterization with established methods. Their immobilization, however, inevitably introduces spurious interactions with the environment. Here we show that wide-angle soft X-ray scattering can be utilized to obtain the full 3D morphology of free individual silver nanoparticles in a single shot. Surprising metastable geometries such as icosahedra and extremely flat particles are revealed in a so far unexplored size regime.

The preferred shape of metal particles formed by condensation essentially depends on the influence of two competing principles: on the one hand, surface energy minimization results in the formation of crystal facets with particular orientations, leading to well-known polyhedral shapes in thermodynamic equilibrium [1]. On the other hand, each nano-object has an individual history with various intermediate configurations emerging during growth. This process leads to transient, metastable structures that might survive for extended periods of time before relaxation [2]. In order to follow the undistorted shape evolution resulting from this fundamental competition with microscopic imaging methods, any interaction of the particles with an environment, such as a substrate, must be eliminated. In this work we used single-shot X-ray scattering at beamline BL3 of the free-electron laser (FEL) FLASH for imaging metal particles while they are propagating freely in space.

Previous in-flight studies of nanoscale objects at FELs revealed the two-dimensional projection of the scattering object at the moment of light exposure [3,4]. As a result of the commonly employed small-angle scattering geometry, true 3D shape

information remains inaccessible. By using wide-angle scattering, we could show that the full 3D geometry and orientation can be identified. In a sense, wide-angle scattering turns out to enable single-shot tomography (Fig. 1). The key to extracting 3D information is that the signal in a single large-angle scattering image contains contributions from several projections of the particle, without the need to rotate and expose the object multiple times. The resulting scattering patterns may show broken point symmetry – in contrast to conventional small-angle scattering which can be essentially described by a 2D Fourier transform of the projected density.

The experiments are performed using FEL pulses with 13.5 nm wavelength and approx. 100 fs duration which are focussed onto a beam of silver particles produced in a magnetron sputtering source (Fig. 2). Scattered light is detected up to large angles of $\approx \pm 40^\circ$ in two perpendicular directions to the laser beam. The particle density is low enough to ensure that only a single cluster is imaged at a time. We employed a forward-fitting scheme for the shape identification, where the scattering images of test geometries are simulated and optimized to match the experimental data. Calculations are performed using two different methods: a multi-slice Fourier transform (MSFT) technique for fast and efficient shape identification and finite-difference time domain (FDTD) calculations for a fully-fledged solution of Maxwell's equations including static material properties. Both methods account for the full 3D shape and are beyond Born's approximation, i.e. multi-scattering effects are taken into account. This is an essential ingredient because of the high absorption of silver in the photon energy range considered.

Typical scattering images along with MSFT simulations are compiled in Fig. 3. The highly symmetric scattering distributions (left column in a-d) with two- to sixfold symmetries immediately suggest the occurrence of regular shapes. This is confirmed by the simulations (right column in a-d) revealing various polyhedral

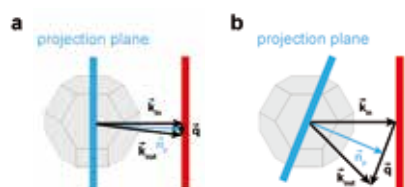


Figure 1

Small- vs. wide-angle scattering from a single nanoparticle. (a) For small-angle scattering, the transfer momentum \mathbf{q} is essentially perpendicular to the beam axis and the scattering reflects a 2D projection of the density onto a plane perpendicular to the incident beam (blue bar). (b) In the wide-angle regime, the orientation of the projection plane changes within a single scattering image. Here \mathbf{k}_{in} and \mathbf{k}_{out} indicate the incident/outgoing wave vectors and \mathbf{n}_p is the normal vector of the projection plane. The indicated projections result from a treatment of the scattering problem within the first Born approximation (from original publication).

Figure 3
Experimental (left columns in a-d and e-h, respectively) and simulated (right columns) scattering images of individual Ag particles. The identified shapes and orientations as seen from the direction of the incident FEL beam are illustrated in the centre column with the respective particle radius indicated below the polygons. In e-h the same shapes as in a-d are found, respectively, but at a different orientation giving rise to substantially altered scattering images (from original publication).

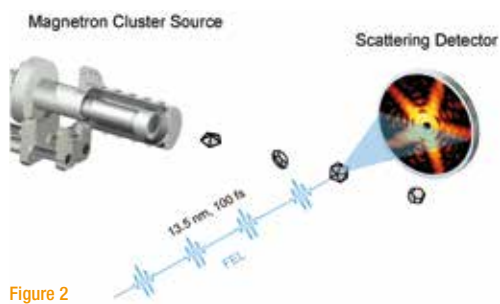
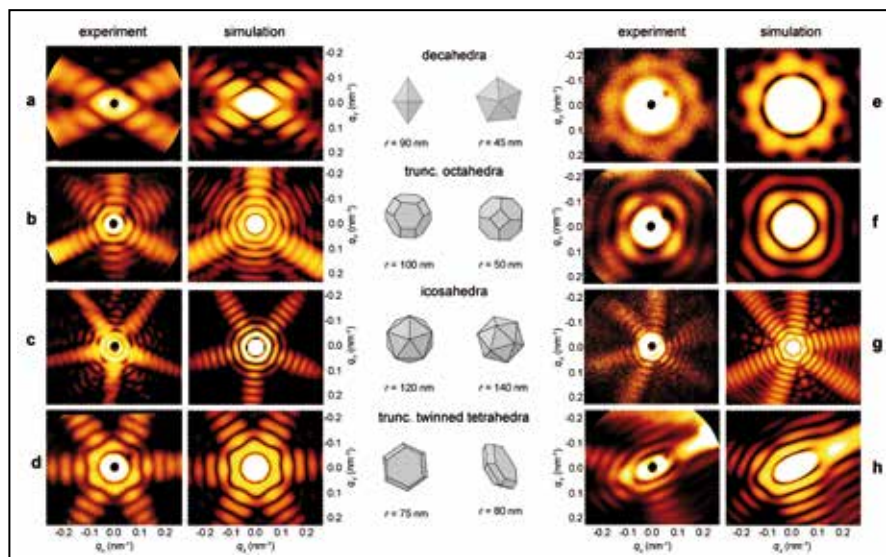


Figure 2
Schematic setup of the scattering experiment. Single clusters produced by magnetron sputtering are intercepted by intense 100 fs X-ray pulses. Scattering is recorded by a wide-angle detector (from original publication).

geometries including common Archimedean and Platonic shapes. Since the particles are captured at the moment of light exposure, their orientation in space is random. Hence, different orientations of the same shapes are expected in the data set which indeed can be identified as shown on the right hand side of Fig. 3. Clearly the scattering images are vastly altered upon rotation, underlining the importance of capturing the 3D shape, including the orientation.

The presence of true 3D information is identified immediately in the raw data if the scattering image shows broken point

symmetry (Fig. 3b,c). Among these cases is the shape of an icosahedron resulting in a five-fold scattering symmetry (Fig. 3c). Its occurrence is surprising, because, according to calculations, such shapes are energetically unfavourable for Ag particles with more than a few hundred atoms [5]. Here, we face particles with roughly a billion atoms which – when reaching equilibrium – are supposed to exhibit native face-centred cubic shapes such as the truncated octahedron (Fig. 3b). Another striking observation is the presence of highly anisotropic, plate-like shapes (Fig. 3d). All of these shapes cannot be explained by thermodynamically stable, energy-minimized geometries. Instead, their existence proves that the particles retain a memory of intermediate stages during growth, even in this so far unexplored size range.

The ability to determine the 3D shape of individual free particles opens fascinating new research opportunities, including the analysis of particle shape evolutions, non-equilibrium melting phenomena, and ultrafast changes of optical and electronic properties after pulsed laser excitation [6].

Contact: Ingo Barke, ingo.barke@uni-rostock.de
Daniela Rupp, daniela.rupp@physik.tu-berlin.de
Thomas Fennel, thomas.fennel@uni-rostock.de

Authors

Ingo Barke¹, Hannes Hartmann¹, Daniela Rupp², Leonie Flückiger², Mario Sauppe², Marcus Adolph², Sebastian Schorb^{3,2}, Christoph Bostedt^{3,5}, Rolf Treusch⁴, Christian Peltz¹, Stephan Bartling¹, Thomas Fennel¹, Karl-Heinz Meiwes-Broer¹, and Thomas Möller²

1. Institute of Physics, University of Rostock, Albert-Einstein-Str. 23, 18059 Rostock, Germany
2. IOAP, Technische Universität Berlin, Hardenbergstraße 36, 10623 Berlin, Germany
3. Linac Coherent Light Source, SLAC National Accelerator Laboratory, 2575 Sand Hill Road, Menlo Park, California 94025, USA
4. Deutsches Elektronen-Synchrotron DESY, Notkestraße 85, 22603 Hamburg, Germany
5. PULSE Institute, Stanford University and SLAC National Accelerator Laboratory, 2575 Sand Hill Road, Menlo Park, California 94025, USA

Original publication

“The 3D-architecture of individual free silver nanoparticles captured by X-ray scattering”, *Nature Communications* 6, 6187 (2015). DOI: 10.1038/ncomms7187

References

1. G. Wulff, “Zur Frage der Geschwindigkeit des Wachstums und der Auflösung der Kristallflächen”, *Z. Kristallogr.* 34, 449 (1901).
2. D. Reinhard, B. Hall, D. Ugarte, and R. Monet, “Size-independent fcc-to-icosahedral structural transition in unsupported silver clusters: An electron diffraction study of clusters produced by inert-gas aggregation”, *Phys. Rev. B* 55, 7868 (1997).
3. M. Seibert et al., “Single mimivirus particles intercepted and imaged with an X-ray laser”, *Nature* 470, 78 (2011).
4. C. Bostedt et al., “Ultrafast X-ray scattering of xenon nanoparticles: Imaging transient states of matter”, *Phys. Rev. Lett.* 108, 093401 (2012).
5. F. Baletto, R. Ferrando, A. Fortunelli, F. Montalenti, and C. Mottet, “Crossover among structural motifs in transition and noble-metal clusters”, *J. Chem. Phys.* 116, 3856 (2002).
6. K. Sander, C. Peltz, C. Varin, S. Scheel, T. Brabec, and T. Fennel “Influence of wavelength and pulse duration on single-shot x-ray diffraction patterns from nonspherical nanoparticles”, *J. Phys. B: At. Mol. Opt. Phys.* 48, 204004 (2015).

Heavy metal at ultra-high static pressures.

Core-level-crossing transition revealed in osmium

Metallic osmium (Os) is one of the most exceptional elemental materials. At ambient pressure it has the highest known density and one of the highest cohesive energies and melting temperatures. It is almost as incompressible as diamond. As any other material, under extreme compression osmium was expected to change its crystal structure. However, using a device for generation of ultra-high static pressures and high-brilliance synchrotron X-rays, it was found that even at pressures twice higher than in the centre of the Earth osmium preserves its crystal structure, but undergoes electronic transitions, one of which may be associated with pressure-induced interactions between core electrons. This fundamental result has important implications for understanding physics and chemistry of highly compressed matter, for design of materials to be used at extreme conditions, and for modelling interiors of giant planets and stars.

High pressures are known to affect radically properties of chemical elements: metals like sodium may become transparent insulators, gases like oxygen solidify and become electrical conductors or even superconductors. Achieving higher and higher pressures opens new horizons for a deeper understanding of matter and the discovery of new physical and chemical phenomena at extreme conditions. The diamond anvil cell (DAC) technique for studying materials at extreme conditions was invented in the late 1950s. Hitherto the maximum static pressure generated at room temperature in a conventional DAC was reported to be about 400 GPa (4 million atmospheres) [1]. Recently our group developed a new technique of ultra-high static pressure generation in a

double-stage diamond anvil cell (ds-DAC) [2], which employs an additional pair of anvils, two semi-balls made of nanocrystalline diamond (NCD) (Fig. 1). NCD anvils possess enormous strength. They are synthesized at high pressure high temperature conditions from glassy carbon balls in large-volume presses [3]. Secondary anvils serve for further pressure amplification in a ds-DAC, up to 640 GPa in [2], compared to a conventional DAC. In this work, in experiments on osmium metal, we extended the static pressures achievable in ds-DACs up to above 750 GPa, the pressure more than twice higher than in the Earth's centre.

Under such conditions, pressure determination is based on the equation of state (EOS) of one or several standards mixed with the sample being studied. The absolute accuracy of the EOS measurements - which is particularly important when aiming to compare experiment against theory - cannot be higher than the accuracy of the static pressure scale. Shock-wave and ramp compression experiments achieve terapascal (TPa) pressures, but only at high temperatures. The EOSs obtained in experiments below 100 GPa, using different dynamic and static methods and for different standards, tend to agree to within 2–3 GPa, but discrepancies increase with pressure and frequently reach unacceptable levels of the order of tens of gigapascals at a pressure around 0.5 TPa. Much more accurate results are obtained when using standards with internally consistent EOSs, especially if the materials used as pressure markers have different or, even better, contrasting elastic properties, as e.g. gold, platinum, and tungsten. We conducted synchrotron X-ray diffraction experiments in conventional and ds-DACs on Au–Pt mixtures at pressures up to 500 GPa, and on Au–W and Pt–W mixtures up to approximately 200 GPa. With Au as the pressure marker, we fitted the pressure–volume data of Pt using the third-order Birch–Murnaghan and the Vinet EOSs. Both EOSs

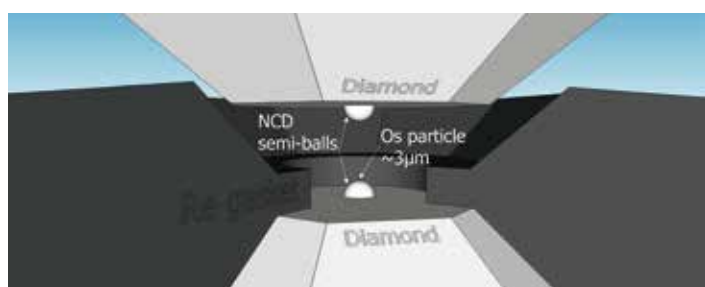


Figure 1

A schematic of the pressure chamber of the double-stage diamond anvil cell (ds-DAC) for ultra-high pressure generation. Semi-balls made of nanocrystalline diamond of extraordinary strength are attached to the culets of the opposed gem quality diamonds of the conventional DAC. A sample of osmium, shown as a small red dot on the top of the lower semi-ball, has a size of ca. 3 microns. It is compressed between the tips of the semi-balls, which are supported by a pressure-medium, solidified inert gases or paraffin, filling the pressure chamber of the primary DAC. Ultra-high pressure, 770 GPa in this work, is generated on the sample due to the two-stage exertion of a big force on a very small area. The diameter of the semi-balls is about 10 microns. The diameter of culets of the diamonds, to which the semi-balls are attached, is 250 microns.

(Figure courtesy of Elena Bykova.)

provide equally good fits, yielding parameters for Pt very close to those obtained from shock-wave data [4]. Pt and Au were used as pressure markers in independent powder X-ray diffraction experiments to study the EOS of tungsten. These results confirmed the necessity of EOS calibration well above 100 GPa for ultra-high-pressure studies and provided a self-consistent set of EOSs for Au, Pt, and W that we used in our experiments with Os.

X-ray diffraction at beamline P02.1 at PETRA III revealed that osmium maintains its hexagonal close-packed structure up to ca. 770 GPa, the highest pressures ever achieved (Fig. 2 a), but exhibits two anomalies in the compressional behaviour, the first at approximately 150 GPa and the second at 440 GPa (Fig. 2 b). At those pressures there was a sudden drop in the unit cell parameters ratio. As suggested by the state-of-the-art theoretical calculations, the first anomaly, at 150 GPa, is likely an electronic topological transition related to valence electrons in the outer shell of the atom. More interesting, and unexpected, was the anomaly at 440 GPa.

Generally, in solids, it is the valence electrons that give the material its properties and bond the atoms together. Changes in the structure come when these valence electrons are rearranged. Inner electrons that are closer and more tightly

bound to the atomic nucleus in the atom's core are not expected to affect the structure. Qualitatively new static pressure levels are needed to affect the core electrons of highly incompressible transition metals or covalently bonded materials. By compressing Os, one of the most incompressible metals, to over 770 GPa, we were able to access this regime and observe a new type of electronic transition, the core-level-crossing transition, that involves pressure-induced interactions between core electrons, and leads to observable changes of the material properties. Indeed, theoretical calculations led to the conclusion that the core electrons were pushed so close together that electrons of the 5p and 4f states started to interact, and the anomaly observed at 440 GPa may be a signature of the core-level-crossing electronic transition. This phenomenon has been never observed before in heavy elemental materials like osmium.

We believe that the ability to reach sufficiently high pressure levels to affect the core electrons of transition metals in static high-pressure experiments will open up opportunities in the search for new states of matter.

Contact: Natalia Dubrovinskaia,
natalia.dubrovinskaia@uni-bayreuth.de

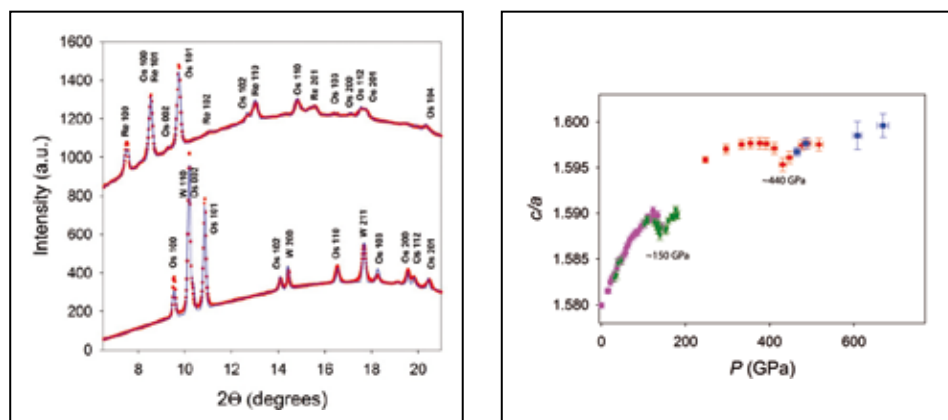


Figure 2

(a) The synchrotron X-ray diffraction patterns of Os at pressures of 774(10) GPa (top) and 517(10) GPa (bottom) give evidence that osmium has unprecedented structural stability and at such huge pressures maintains the same crystal structure as at ambient conditions. (b) Anomalies in the behaviour of the ratio of the lattice parameters detected upon compression revealed the signatures of the topological change of the Fermi surface for valence electrons (~150 GPa) and the core-level-crossing electronic transition (~440 GPa), as suggested by the state-of-the-art theoretical calculations.

Authors

L. Dubrovinsky¹, N. Dubrovinskaia², E. Bykova^{1,2}, M. Bykov², V. Prakapenka³, C. Prescher⁴, K. Glazyrin⁴, H.-P. Liermann⁴, M. Hanfland⁵, M. Ekholm^{6,7}, Q. Feng^{6,7}, L. V. Pourovskii^{8,9}, M. I. Katsnelson^{9,10}, J. M. Wills¹¹, and I. A. Abrikosov^{7,12}

1. Bavarian Research Institute of Experimental Geochemistry and Geophysics, University of Bayreuth, D-95440 Bayreuth, Germany
2. Laboratory of Crystallography, University of Bayreuth, D-95440 Bayreuth, Germany
3. Center for Advanced Radiation Sources, University of Chicago, Illinois 60437 Argonne, USA
4. Deutsches Elektronen-Synchrotron DESY, D-22603 Hamburg, Germany
5. European Synchrotron Radiation Facility, BP 220, Grenoble F-38043, France
6. Swedish e-Science Research Centre (SeRC), Linköping University, SE-58183 Linköping, Sweden
7. Department of Physics, Chemistry and Biology (IFM), Linköping University, SE-58183 Linköping, Sweden
8. Centre de Physique Theorique, CNRS, Ecole Polytechnique, 91128 Palaiseau, France
9. Radboud University, Institute for Molecules and Materials, Heyendaalseweg 135, 6525AJ Nijmegen, The Netherlands
10. Department of Theoretical Physics and Applied Mathematics, Ural Federal University, Mira street 19, Ekaterinburg, 620002, Russia

11. Theoretical Division, Los Alamos National Laboratory, Los Alamos, New Mexico 87545 USA
12. Materials Modeling and Development Laboratory, National University of Science and Technology 'MISIS', 119049 Moscow, Russia

Original publication

"The most incompressible metal osmium at static pressures above 750 gigapascals". *Nature* 525, 226–229 (2015). DOI:10.1038/nature14681

References

1. A.L. Ruoff, H. Xia, and Y. Vohra, "Miniaturization techniques for obtaining static pressures comparable to the center of the Earth: X-ray diffraction at 416 GPa". *Rev. Sci. Instr.* 61, 3830–3830 (1990).
2. L. Dubrovinsky, N. Dubrovinskaia, V. Prakapenka, A. Abakumov. "Implementation of micro-ball nanodiamond anvils for high-pressure studies above 6 Mbar". *Nature Commun.* 3:1163 doi: 10.1038/ncomms2160 (2012).
3. N.A.Solopova, N. Dubrovinskaia, L. Dubrovinsky. "Synthesis of nanocrystalline diamond from glassy carbon balls". *J. Cryst. Growth* 412, 54–59 (2015).
4. Yokoo, M. et al. "Ultra-high-pressure scales for gold and platinum at pressures up to 550 GPa". *Phys. Rev. B* 80, 104114 (2009).

New insight in materials synthesis.

Using X-rays to open the black box of nanoparticle formation

In order to tailor-make nanostructured materials for advanced applications in e.g. magnetism, it is crucial that we understand the mechanisms dictating particle nucleation and growth in material synthesis. Unfortunately, many of the synthesis methods used for inorganic nanoparticle production are very poorly understood. Here, we use high energy X-rays to follow the formation of iron oxide nanoparticles, allowing us to extract valuable information on mechanisms taking place in hydrothermal synthesis.

Magnetic nanoparticles are used in a broad range of applications from biomedicine to magnetic storage and thus play a crucial role in modern society [1]. In particular, iron oxide nanoparticles such as magnetite (Fe_3O_4) or maghemite ($\gamma\text{-Fe}_2\text{O}_3$) are used extensively. However, the magnetic properties of iron oxide particles are highly dependent on particle size and structure. To be able to tailor-make materials with well-defined properties for advanced applications, it is crucial that we gain full control of the particle characteristics as they form during synthesis [2]. To do so, we need clear insight in the formation mechanisms. We therefore set out to study the nucleation and growth mechanisms taking place in the hydrothermal synthesis of $\gamma\text{-Fe}_2\text{O}_3$ nanoparticles using high energy X-ray scattering.

To follow the formation of the nanoparticles, we need a characterization method that allows structural information to be extracted from both the amorphous precursor as well as the crystalline nanoparticles that form. Total Scattering, coupled with Pair Distribution Function analysis is here very well suited [3]. Whereas traditional scattering methods in crystallography only include Bragg diffraction in the analysis allowing crystalline structures to be studied, Total Scattering also takes diffuse scattering into account, meaning that structural information from amorphous and nanostructured

Figure 1

- A) Total Scattering data from the aqueous solution of ammonium iron citrate.
- B) Pair Distribution Function from the ammonium iron citrate solution. The black line shows the experimental PDF, the red line a modelled PDF, and the blue line the difference between the two.
- C) Structural model for the iron citrate complex used in the fit. The yellow polyhedra show octahedrally coordinated iron, the red spheres are oxygen, and the black spheres are carbon. Hydrogen atoms have been left out for clarity.

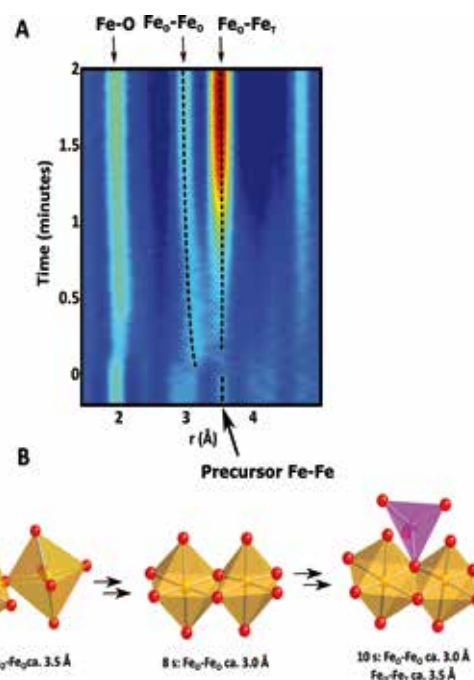
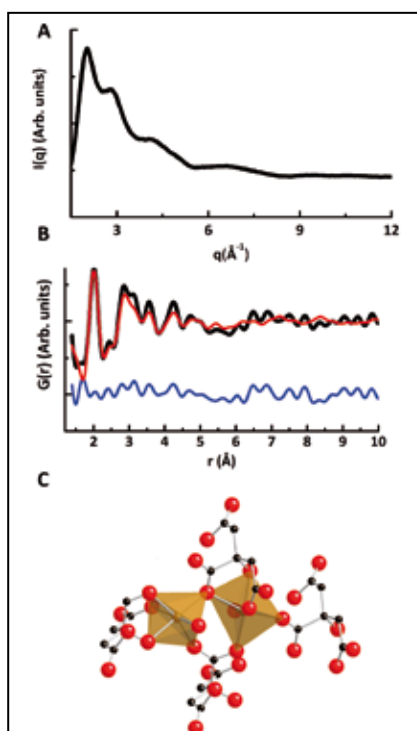


Figure 2

- A) Contour plot of the low r -range PDFs obtained at 320 °C and 4 M ammonium iron citrate. The dotted lines are guides to the eye showing the evolution of the Fe-Fe peaks. The intensity scale in the contour plot goes from blue through green and yellow to red. B) Structures observed in the low r -region of the initially observed PDFs at 0, 8 and 10 s. The yellow polyhedra show octahedrally coordinated iron, the purple polyhedron shows tetrahedrally coordinated iron, and the red spheres show oxygen.

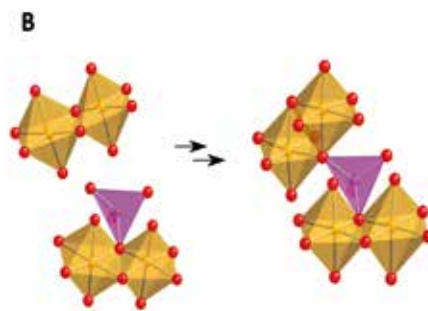
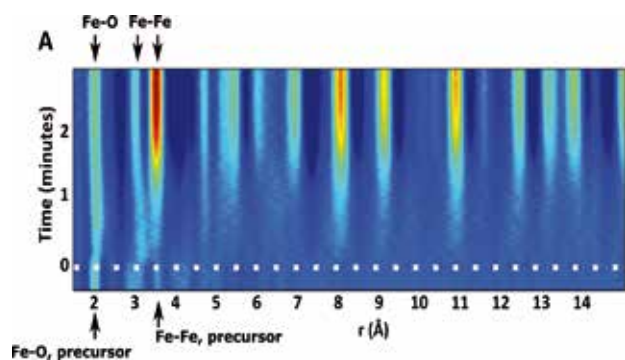


Figure 3

A) Time-resolved PDFs, plotted as a contour map. The intensity scale in the contour plots goes from blue through green and yellow to red. B) Cluster growth by condensation along tetrahedrally coordinated iron atoms.

compounds can be extracted. For this purpose, the Total Scattering data are Fourier transformed to obtain the Pair Distribution Function (PDF), which is a function in real space, simply representing a histogram of all interatomic distances in the sample. By structural modelling, the PDF can therefore be used to obtain information on atomic structure in samples with both short and long range order [4]. Our experiments were performed at the High Resolution Powder Diffraction beamline P02.1 at PETRA III using an energy of 60 keV.

The precursor for the maghemite nanoparticles is an aqueous solution of ammonium iron citrate [5]. Fig. 1a shows the total scattering signal from the precursor solution. The signal shows diffuse scattering features, which are difficult to interpret directly in terms of structural models. However, the Pair Distribution Function (Fig. 1b) has clear peaks representing the interatomic distances and by fitting the PDF with models from iron-citrate complexes, the data showed us that when dissolved in water, iron and citrate ions coordinate to form a polymer-like structure of corner-sharing $[\text{FeO}_6]$ octahedra, as shown in Fig. 1c.

As heating to 320 °C is initiated, the formation of the nanoparticles begins. Fig. 2a shows a contour plot of the low r region of the time resolved PDFs, allowing us to follow the development of local order in the synthesis. As soon as the temperature is raised at time = 0 s, the precursor structure decomposes, as is seen from the disappearance of PDF peaks from the iron citrate polymer. Very soon after, new PDF peaks begin appearing, showing the formation of an iron-oxide nanocluster, which eventually crystallizes to form maghemite nanoparticles.

The final maghemite particles take the spinel crystal structure where iron has both octahedral and tetrahedral coordination. This structure gives rise to clear peaks in the final PDFs obtained after 2 min, where the first peak at ca. 2.6 Å comes from Fe-O bonds, while the next peaks show the distances between edge-sharing octahedral iron sites ($\text{Fe}_\text{O}-\text{Fe}_\text{O}$) at 3.0 Å and corner-sharing octahedral and tetrahedral iron sites ($\text{Fe}_\text{O}-\text{Fe}_\text{T}$) at 3.5 Å. When considering the time-resolved PDFs obtained after the heating was initiated, it is clear that all three peaks appear very soon after the synthesis has begun. However, the $\text{Fe}_\text{O}-\text{Fe}_\text{T}$ peak appears slightly later than the Fe-O and $\text{Fe}_\text{O}-\text{Fe}_\text{O}$ peaks, and the data thus illustrate that the first, small clusters forming are built up by edge-sharing octahedra, with corner-sharing tetrahedrally coordinated iron soon appearing in the structures (Fig. 2b). As the synthesis continues, PDF peaks at higher r -values appear, showing that larger particles with some longer range order start forming. Simultaneously, the $\text{Fe}_\text{O}-\text{Fe}_\text{T}$ peak at 3.5 Å grows rapidly in intensity, as illustrated in Fig. 3a. By considering various mechanisms leading to particle formation, we found that the primary growth happens through cluster condensation along tetrahedral sites, as illustrated in Fig. 3b. The study therefore gave unprecedented insight into the nucleation and growth mechanisms of iron oxide nanoparticles, and open up for a deeper insight in materials synthesis in inorganic chemistry.

Contact: Bo Brummerstedt Iversen, bo@chem.au.dk,
Mogens Christensen, mch@chem.au.dk

Authors

Kirsten M. Ø. Jensen^{1,2}, Henrik L. Andersen¹, Christoffer Tyrsted¹, Espen D. Bøjesen¹, Ann-Christin Dippel³, Nina Lock¹, Simon J. L. Billinge^{2,4}, Bo B. Iversen¹, and Mogens Christensen¹

- Center for Materials Crystallography, Department of Chemistry and iNANO, Aarhus University, DK-8000 Aarhus C, Denmark
- Department of Applied Physics and Applied Mathematics, Columbia University, New York, New York 10027, United States
- Deutsches Elektronen-Synchrotron DESY, D-22607 Hamburg, Germany
- Condensed Matter Physics and Materials Science Department, Brookhaven National Laboratory, Upton, New York 11973, United States

Original publication

„Mechanisms for Iron Oxide Formation under Hydrothermal Conditions: An *in situ* Total Scattering Study”. *ACS Nano* 8, 10704-10714 (2014).

References

- Reddy, L. H., Arias, J. L., Nicolas, J. & Couvreur, P. “Magnetic Nanoparticles: Design and Characterization, Toxicity and Biocompatibility, Pharmaceutical and Biomedical Applications”. *Chem. Rev.* 112, 5818-5878, (2012).
- Jensen, K. M. Ø., Tyrsted, C., Bremholm, M. & Iversen, B. B. “*In Situ* Studies of Solvothermal Synthesis of Energy Materials”. *ChemSusChem* 7, 1594-1611, (2014).
- Billinge, S. J. L. & Levin, I. “The problem with determining atomic structure at the nanoscale”. *Science* 316, 561-565, (2007).
- Billinge, S. J. L. & Kanatzidis, M. G. “Beyond crystallography: the study of disorder, nanocrystallinity and crystallographically challenged materials with pair distribution functions”. *Chem. Commun.*, 749-760, (2004).
- Bremholm, M., Felicissimo, M. & Iversen, B. B. “Time-Resolved *In Situ* Synchrotron X-ray Study and Large-Scale Production of Magnetite Nanoparticles in Supercritical Water”. *Angew. Chem. Int. Ed.* 48, 4788-4791, (2009).

Visualising aging in Li ion battery electrodes.

XRF imaging of spinel materials with sub-micrometre resolution

The high-voltage $\text{LiNi}_{0.5}\text{Mn}_{1.5}\text{O}_4$ (LNMO) spinel is a promising material for high-energy battery applications, but faces problems of capacity fade. This is partly caused by transition metal (nickel and manganese) leaching that destroys the chemical and physical structure of the cathode material. We used fast micro-X-ray fluorescence spectroscopy to visualise the changes in elemental distribution from repeated cycling of $\text{LiNi}_{0.5}\text{Mn}_{1.5}\text{O}_4$ /carbon composite electrodes in LNMO/Li cells. Our results after scanning the sample at medium spatial resolution (500 nm) over a millimetre range show significant changes in morphology and elemental distribution, including formation of elemental hot-spots and material erosion, which became more pronounced at higher cycling rates.

The high-voltage $\text{LiNi}_{0.5}\text{Mn}_{1.5}\text{O}_4$ (LNMO) spinel is a promising material for high-energy battery applications because of its high operating potential of ~ 4.7 V versus Li^+/Li^0 . But this high potential also brings a number of problems. A significant challenge is that the conventional electrolyte is thermodynamically unstable at this high operating potential [1]. This can lead to oxidation of the electrolyte by the active material, producing passivating products which reduce battery cycle life and fade its capacity. Further, possibly as a consequence of these parasitic reactions with the electrolyte, transition metals can leach from the composite cathode. These elements dissolve in the electrolyte, leading to chemical and structural decay of the cathode material. Manganese containing phases are especially known to leach into the electrolyte at these high operating potentials [2-4]. The fate of the solvated ions is not clear at present, but a part of them deposits at the anode, further reducing cycle life and battery performance. The capacity fade effect is especially pronounced in LNMO/graphite full cells, because of the detrimental contribution of the deposited 3d metals on the anode impacting the solid-electrolyte-interphase (SEI) growth on its surface [2].

In the present study, we are especially interested in identifying the origin and correlation of structural and chemical damage and heterogeneities on the cathode. This is essential to improve the understanding of the aging mechanism and thus

electrode design and handling. As a first step towards characterisation of the effects on the mesoscale, we used fast micro-X-ray fluorescence spectroscopy (micro-XRF) scanning techniques with medium spatial resolution (500 nm) to visualise changes in elemental and charge distribution in LNMO composite electrodes cycled at different rates and at different states of charge. Charge distribution is imaged by mapping the Ni oxidation state through acquiring a stack of elemental maps straddling the Ni K-absorption edge. The results of this exploratory study showed significant effects on morphology and elemental distribution, including formation of elemental 'hot-spots' and material erosion areas hundreds of micrometres in size, becoming more pronounced at higher sweep rates. In nickel hot-spots, we observed hampered oxidation of nickel during charging.

One major aspect that allowed us to characterise these large sample areas (mm^2) with comparatively high resolution (500 nm) is the novel Maia fluorescence detector now installed at the Hard X-ray Micro/Nano-Probe beamline P06. Depending on the sample Maia detectors can scan faster than 1 ms per image pixel due to their large solid angle (1.2 sr), high count-rate capability (up to 20×10^6 photons/s), and by spreading photon acquisition over 384 individual detector pads [5]. At higher sweep rates C, the tendency towards morphological and chemical inhomogeneity increases, illustrated in Fig. 1,

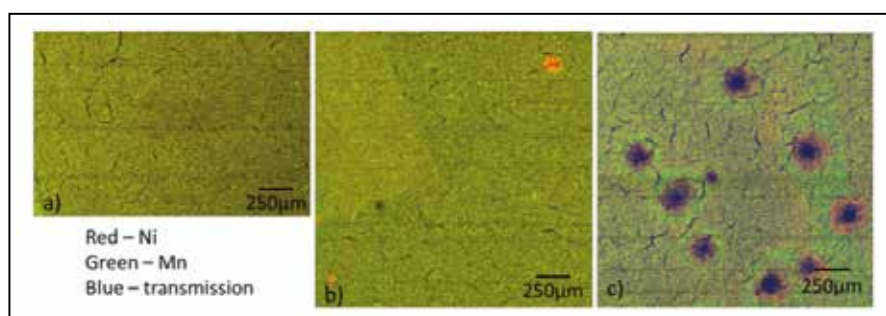


Figure 1

Elemental RGB images of electrodes cycled with different sweep rates (a) C/4 (slow), (b) C/2 (medium), and (c) 5C (fast) for approximately 25 cycles using micro-XRF. Green, Mn; red, Ni; and blue, transmission. Reprinted with permission from Boesenberg et al., *Chemistry of Materials* 27, 2525–2531 (2015). DOI: 10.1021/acs.chemmater.5b00119. Copyright 2015 American Chemical Society.

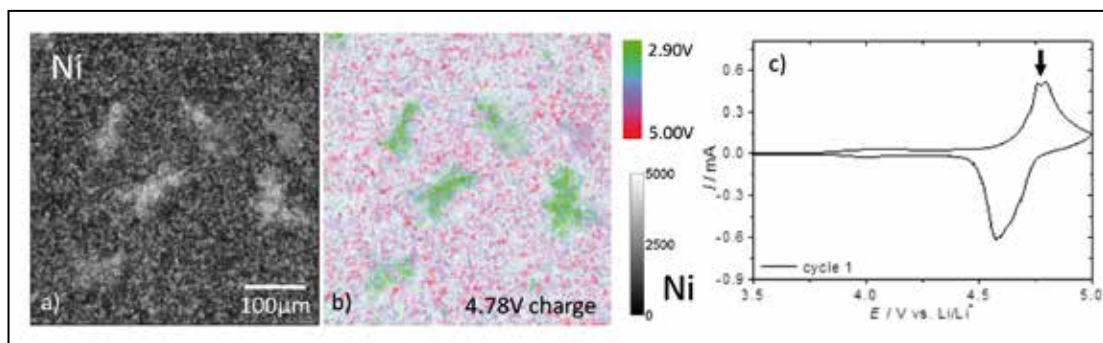


Figure 2

(a) Ni distribution map obtained by micro-XRF from a sample charged to 4.78 V, marked with an arrow in the cyclic voltammogram of the material in (c), and (b) the corresponding phase distribution map based on the state of charge. For this, a number of micro-XRF maps in the vicinity of the Ni K-absorption edge was collected, aligned in an image stack and then the state of charge (oxidation state) was determined by linear combination fitting of each pixel with references taken in the charged and discharged state. Reprinted with permission from Boesenberg et al., *Chemistry of Materials* 27, 2525–2531 (2015). DOI: 10.1021/acs.chemmater.5b00119 Copyright 2015 American Chemical Society.

where the cycling rate increases from Fig. 1a through 1c. The effect is strongest for the cell cycled at the highest rate, in Fig. 1c. Here we observed formation of craters or holes, where most of the active material is depleted. Interestingly, in the immediate vicinity of the holes, Ni is enriched, whereas in the wider area around the holes Ni is depleted and Mn is enriched. We therefore find not only dissolution and depletion of Mn and/or Ni but also redistribution of these metals. Furthermore, formation of cracks in the electrode was detected at all cycling rates, indicating mechanical stresses. Most likely, repeated lithium incorporation and release produces these cracks, but no direct correlation between the cracks and chemical inhomogeneities was observed.

For the sample in Fig. 2a at 4.78 V during charge (above the 4.7 V equilibrium voltage for the reaction) the distribution of Ni shows distinct hot-spots. A typical cycling curve with controlled voltage for this material is shown in Fig. 2c. The distribution of the oxidation state mirrors the distribution of the elemental nickel. As the nickel should oxidize during the charging process, the oxidation state represents the participation in the charge/discharge reaction of the battery cell. The hot-spots show little change in their oxidation state in comparison to the more homogeneous matrix (Fig. 2b). It was not possible to determine if the reduced participation in the oxidation reaction was caused by either sluggish kinetics resulting from the high Ni density and would occur at a higher over-potential or if it could also be an indication of a side reaction forming a stable species with Ni²⁺ oxidation state, for example NiF₂.

This work shows micro-XRF to be a powerful method to characterise correlations between chemical and structural inhomogeneities at the electrode level. We have investigated both elemental distribution as well as the distribution of the oxidation state as a measure of participation in the charge/discharge reaction. Severe structural and chemical defects

were identified with higher sweep rates in an exploratory study of LNMO composite electrodes. In zones surrounding these defects, the Ni/Mn ratio was altered. Mapping of the oxidation state of Ni at multiple degrees of charge/discharge revealed less oxidized regions in these Ni hot-spots.

Contact: *Ulrike Bösenberg, ulrike.boesenberg@desy.de*

Authors

Ulrike Bösenberg¹, Mareike Falk², Christopher G. Ryan³, Robin Kirkham³, Magnus Menzel⁴, Jürgen Janek², Michael Fröba⁴, Gerald Falkenberg¹, and Ursula E.A. Fittschen^{4,5}

1. Deutsches Elektronen-Synchrotron DESY, Notkestrasse 85, 22607 Hamburg, Germany
2. Justus-Liebig University Gießen, Institute of Physical Chemistry, Heinrich-Buff-Ring 58, 35392 Gießen, Germany
3. Commonwealth Scientific and Industrial Research Organisation CSIRO, Clayton, Victoria 3169, Australia
4. University of Hamburg, Institute of Inorganic and Applied Chemistry, Martin-Luther-King-Platz 6, 20146 Hamburg, Germany
5. Washington State University, Department of Chemistry, Post Office Box 644630, Pullman, Washington 99164-4630, United States

Original publication

“Correlation between Chemical and Morphological Heterogeneities in LiNi_{0.5}Mn_{1.5}O₄ Spinel Composite Electrodes for Lithium-Ion Batteries Determined by Micro-X-ray Fluorescence Analysis”, *Chemistry of Materials* 27, 2525–2531 (2015). DOI: 10.1021/acs.chemmater.5b00119

References

1. J. B. Goodenough, Y. Kim, “Challenges for Rechargeable Li Batteries”, *Chem. Mater.* 22, 587-603 (2010).
2. J.-H. Kim, N. P. W. Pieczonka, and L. Yang, “Challenges and Approaches for High Voltage Spinel Lithium-Ion Batteries”, *ChemPhysChem* 15, 1940-1954 (2014).
3. N. P. W. Pieczonka, Z. Liu, P. Lu, K. L. Olson, J. Moote, B. R. Powell, and J.-H. Kim, “Understanding Transition-Metal Dissolution Behavior in LiNi_{0.5}Mn_{1.5}O₄ High-Voltage Spinel for Lithium Ion Batteries”, *J. Phys. Chem. C* 117, 15947–15957 (2013).
4. W. Choi and A. Manthiram, “Comparison of Metal Ion Dissolution from Lithium Ion Battery Cathodes”, *J. Electrochem. Soc.* 153, A1760-A1764 (2006).
5. C. G. Ryan, R. Kirkham, R. M. Hough, G. Moorhead, D. P. Siddons, M. D. de Jonge, D. J. Paterson, G. De Geronimo, D. L. Howard, and J. S. S. Cleverley, “Elemental X-ray imaging using the Maia detector array: The benefits and challenges of large solid-angle”, *Nucl. Instruments Methods Phys. Res. Sect. A* 619, 37-43 (2010).

Fast strain mapping of nanowire LEDs using X-ray nanobeams.

Imaging strain in real devices

X-ray nanobeams are unique nondestructive probes that allow direct measurements of the nanoscale strain distribution and composition inside nanowire LEDs, which comprise a core-multi-shell heterostructure. Here, we made use of the observation that in the generic nanowire device configuration, which is found in high-speed transistors, solar cells, and light-emitting diodes, each wire exhibits very small degrees of random tilts and twists with respect to the substrate. Although the tilt and twist are very small, they give a new contrast mechanism between different wires. We image strain in complex nanowires made for nanoLED fabrication and compare experimental results to theoretical simulations, demonstrating that this fast imaging method is suitable for real nanostructured devices.

Novel devices based on self-assembled nanowires such as field-effect transistors, light emitting diodes (LEDs), and solar cells all have a number of generic, material-independent design features in common: the fundamental component consists of a nanowire core surrounded by a number of shells with varying composition and strain [1]. Changes of strain and composition in a sample can be considered as areas of different lattice constants, which are directly related to an X-ray scattering angle via Bragg's law. By mapping the positions of the Bragg reflections with the nano-focused X-ray beam we can map the distributions of the lattice constants across the sample on a nanometre scale [2,3].

Often, nanowires are slightly tilted with respect to each other. This is especially true for the core shell nanowires which exhibit spontaneous bending under strong axial stresses caused by the lattice mismatch between the core and the shell [4]. If each of the nanostructures on a sample is tilted slightly differently with respect to the substrate, the diffraction patterns will also be shifted, allowing us to separate out several wires illuminated in the same X-ray beam. In this way, different parts of the nanowires can be selected by scanning from one to another, and the homogeneity of the individual nanowires can be visualized.

The measurements were done on blue light (428 nm) emitting GaN/InGaN quantum well (QW) core shell nanowire structures, which were grown by the company glō AB [5]. The final nanostructures, as shown in Fig. 1a, consisted of an axially grown GaN core, a radially grown GaN core, a 5 nm thick InGaN QW with around 8 % In, and a GaN quantum barrier (QB). In order to focus on the individual nanowires, the sample was cleaved to create a sharp 60 degree corner with a few isolated nanowires at the tip (see Fig. 1c).

The experiment was conducted at the P06 Hard X-ray Micro/Nano-Probe beamline at PETRA III, at the nanoprobe end-

station as shown in Fig. 1c. The sample was brought into the focus of the $80 \times 100 \text{ nm}^2$ X-ray beam and was scanned in the beam while measuring the diffraction pattern with a CCD detector. The detector was positioned close enough that Bragg peaks from several different crystallographic plane families would be visible while still being able to resolve the details within individual Bragg peaks. A representative image is shown in Fig. 1e, where five of the strongest Bragg peaks are labelled.

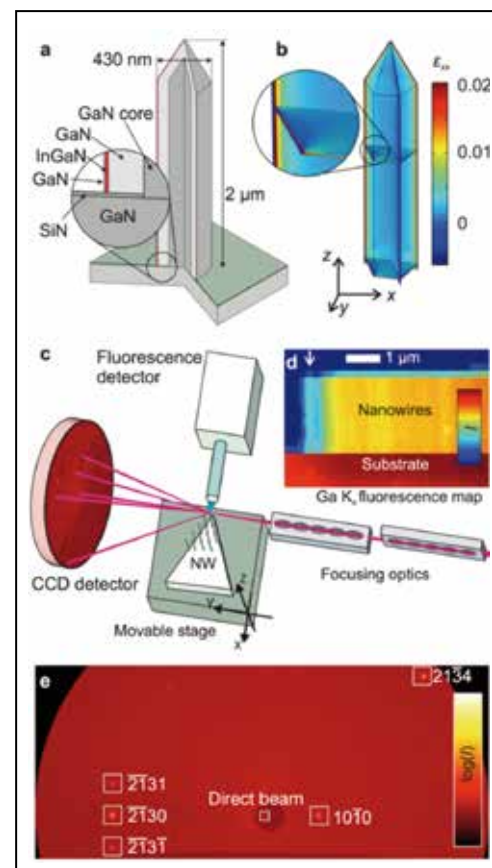
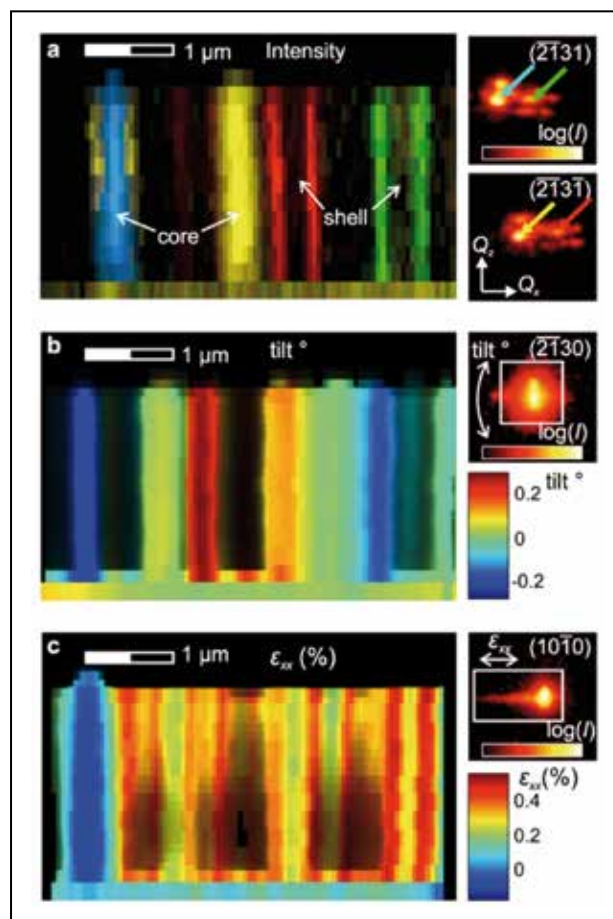


Figure 1

Experiment setup and measurement results. (a) Sketch of a nanowire (NW) showing the onion-like structure. (b) Finite element method simulation of strain distribution. (c) Nano-focused X-ray beam setup for diffraction mapping. (d) Gallium fluorescence map of the scan. A single nanowire at the edge of the forest is indicated with an arrow. (e) Part of the CCD image, where five Bragg peaks and the attenuated direct beam are visible.

Figure 2

- Intensity, tilt, and strain maps obtained from a single scan.
- (a) Diffraction map made using intensities of different regions of the Bragg peaks indicated with corresponding arrows. The colours indicate the corresponding region on the diffraction spot and the saturation of each colour is proportional to the intensity of the diffraction signal.
- (b) Map of the crystal tilt of the small forest of NWs. We can see that the NWs exhibit random tilting with respect to the substrate of around 0.2° .
- (c) In-plane strain map calculated from the peak positions. All three maps above show results of the same scan of the sample.



When an inhomogeneous crystalline material, such as a forest of nanowires (NWs), is illuminated with a nano-focused beam, the Bragg peaks at a given beam position consist of multiple smaller peaks, as shown in the right-hand side of Fig. 2a. The peaks are displaced slightly from each other because some of them come from different parts of the NWs; others are shifted due to the different tilt of the individual NWs. Having measured such Bragg peaks at each position on the sample, we can choose a region in reciprocal space, thus selecting a range of lattice constants and visualize its distribution across the sample. Such a map is shown in Fig. 2a, where four different colours represent regions of the measured intensities indicated with the corresponding arrows on the Bragg peaks. For example, the blue feature that corresponds to the GaN core of the nanowire comes from the strongest region of the $(\bar{2}131)$ peak shown with the blue arrow. On the other hand, the two green vertical stripes originate from a different position of the diffraction spot and show two sides of the InGaN quantum well of another nanowire.

The average strain and tilt in a small volume illuminated by the nano-focused beam can be found from the corresponding position of the Bragg peak on the detector. From Fig. 2b, we can see that individual nanowires exhibit uniform tilt with respect to the substrate within ± 0.2 degrees. Fig. 2c shows the in-plane strain map calculated from the lateral movement of the $(10\bar{1}0)$ Bragg peak with respect to the substrate peak. Here, due to different twisting (rotation around the substrate normal) of the NWs, the Bragg condition is satisfied for the core of the leftmost NW (blue), whereas the outer In-enriched layers are visible only in the remaining NWs to the right, hence the contrast.

Our study shows how scanning X-ray diffraction microscopy with a nano-focused beam can be used to map the strain and composition in heterogeneous nanowires and to separate different parts. Thanks to the high penetration power of X-rays, the individual nanowires can be picked separately from a small forest and imaged by relying on the structural differences. The study establishes opportunities for achieving significant statistics that are central to performing real materials science. Local inhomogeneities were observed in the InGaN/GaN NWs, with a tendency for the larger lattice constants to be at the top part. This can be assigned to the inhomogeneous In distribution in the shell.

Contact: Tomas Stankevic, Tomas.Stankevic@maxlab.lu.se

Authors

Tomas Stankevic¹, Emelie Hilner¹, Frank Seiboth², Rafal Ciechonski³, Giuliano Vescovi³, Olga Kryliouk⁴, Ulf Johansson⁵, Lars Samuelson⁵, Gerd Wellenreuther⁶, Gerald Falkenberg⁶, Robert Feidenhans'l¹, and Anders Mikkelsen⁵

- Niels Bohr Institute, University of Copenhagen, 2100 Copenhagen, Denmark
- Technische Universität Dresden, 01062 Dresden, Germany
- GloAB, 22370 Lund, Sweden
- Glo-USA, Inc., Sunnyvale, California 94089, United States
- Lund University, 22100 Lund, Sweden
- Deutsches Elektronen-Synchrotron DESY, 22607 Hamburg, Germany

Original publication

"Fast Strain Mapping of Nanowire Light-Emitting Diodes Using Nanofocused X-ray Beams", *ACS Nano* 9, 6978–6984 (2015). DOI: 10.1021/acs.nano.5b01291

References

- C. M. Lieber and Z. L. Wang, "Functional Nanowires", *MRS Bull.* 32, 99-108 (2011).
- M. Keplinger, B. Mandl, D. Kriegner, V. Holy, L. Samuelson, G. Bauer, K. Deppert, and J. Stangl, "X-ray Diffraction Strain Analysis of a Single Axial InAs_{1-x}P_x Nanowire Segment", *J. Synchrotron Radiat.* 22, 1-7 (2015).
- T. Stankevič, D. Dzhigayev, Z. Bi, M. Rose, J. Reinhardt, A. Mikkelsen, L. Samuelson, G. Falkenberg, I. A. Vartanyants, and R. Feidenhans'l, "Strain mapping in an InGaN/GaN nanowire using a nano-focused x-ray beam", *Appl. Phys. Lett.* 107, 103101 (2015).
- M. Keplinger, D. Kriegner, J. Stangl, T. Mårtensson, B. Mandl, E. Wintersberger, and G. Bauer, "Core shell nanowires: From the ensemble to single-wire characterization", *Nucl. Instrum. Methods Phys. Phys.* 268, 316-319 (2010).
- Company webpage: glo.se

Real-time imaging of grain dynamics.

Real-time grain rotation and lattice deformation observation with *in situ* X-ray nanodiffraction

A fundamental demand in material science is to observe or characterise the structures and dynamics of grains and grain boundaries in materials (for example, phase transitions, chemical reactions, crystal growth, grain rotation, dislocations, grain boundary migration). The current experimental methods, such as X-ray diffraction (XRD) and transmission electron microscopy (TEM), cannot achieve high spatial and temporal resolution at the same time. We present a new *in situ* X-ray nanodiffraction to measure high-resolution diffraction patterns from single silver bromide AgBr grains with up to 5 millisecond temporal resolution and for the first time we made an observation of grain rotation and lattice deformation induced by X-ray photons in the chemical reaction: $\text{Br}^- + h\nu \rightarrow \text{Br} + e^-$ and $e^- + \text{Ag}^+ \rightarrow \text{Ag}^0$. We expect the new method will have broad applications in materials science, physics, chemistry, and nanoscience.

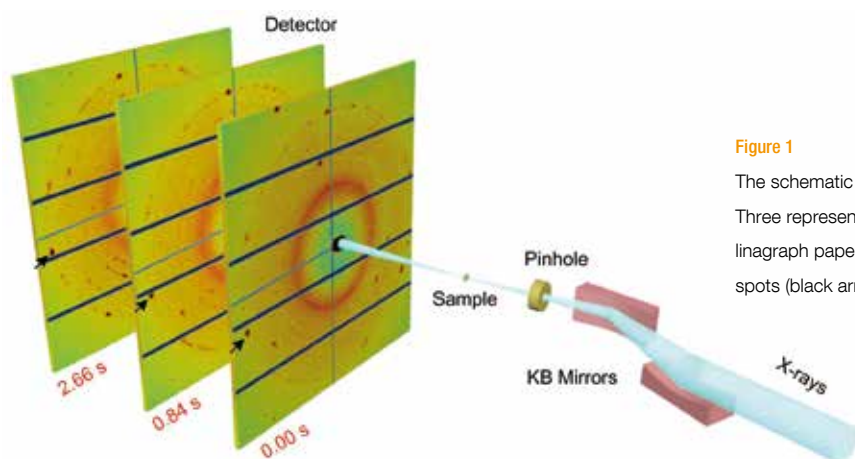


Figure 1

The schematic layout of an *in situ* X-ray nanodiffraction system.

Three representative diffraction patterns are measured from a Kodak linagraph paper at 0.00, 0.84 and 2.66 s, respectively, in which diffraction spots (black arrows) are rotating along the Debye-Scherrer rings.

X-ray diffraction (XRD), transmission electron microscopy (TEM), electron tomography, scanning electron microscopy (SEM), and optical microscopy, amongst others, are the current popular experimental methods to investigate many physical science phenomena, ranging from phase transitions, chemical reactions and crystal growth to grain boundary dynamics [1], but they all have their limitations and cannot have high spatial and temporal resolution at the same time. Utilizing Coherence Applications Beamline P10 at the PETRA III storage ring, we successfully performed first real-time measurements of grain rotation and lattice deformation during photoinduced chemical reactions with up to 5 ms temporal resolution.

The schematic layout of the *in situ* X-ray nanodiffraction instrument is shown in Fig. 1. Monochromatic X-rays are focused to a spot of $\sim 370 \text{ nm} \times 270 \text{ nm}$ by a Kirkpatrick-Baez (KB) mirror system. The sample is positioned at the focal spot with a flux of $\sim 6.74 \times 10^{11}$ photons/s and high-resolution diffraction patterns from the samples are collected by a PILATUS 1M or 6M detector. The readout time of PILATUS 1M allows us to measure high-resolution diffraction patterns with millisecond timescales. We studied three groups of samples in

an ambient environment at room temperature: Kodak direct print linagraph paper containing AgBr, gelatin and other materials; AgBr control samples consisting of either AgBr powder on Si_3N_4 membranes or AgBr/gelatin; and non-AgBr control samples consisting of TiO_2 /gelatin, CeO_2 /gelatin or Ag/gelatin.

Cubic AgBr grains with an average size of $\sim 700 \text{ nm}$ are distributed in a layer near the surface in the Kodak paper. The individual AgBr grain size is larger than the size of the X-ray nanofocus beam, so several large and high intensity diffraction spots are initially diffracted from single AgBr grains. With continuing X-ray exposure the AgBr grains are decomposed into smaller grains. Within this photolysis of the AgBr grains, large AgBr (200) and (220) spots gradually become smaller and the number of diffraction spots increase, while Ag (111) and (200) diffraction spots appear in the diffraction patterns because Ag nanograins start nucleating and growing, until Debye-Scherrer rings of AgBr (200), (220), Ag (111) and (200) start to appear after a few seconds. Furthermore we observed real-time grain rotation and lattice deformation during photoinduced chemical reactions with X-rays in the two groups of

AgBr samples, while we do not observe any motion of the diffraction spots in the controlled non-AgBr samples.

The evidence of the grain rotation is observed in all of the AgBr and Ag Debye-Scherrer rings. The AgBr (200) Debye-Scherrer ring is shown in Fig. 2a as an example. There are at least three types of grain-related features: Individual points, representing reciprocal lattice points momentarily intersecting the Ewald sphere; horizontal tracks, representing stationary diffraction spots and grains; curved tracks along the Debye-Scherrer ring. According to photographic theory [2], an absorbed X-ray photon can produce many photolytic Ag atoms, which can grow and agglomerate on the surface of and inside an AgBr grain. Due to inhomogeneous nucleation of Ag atom agglomeration inside the AgBr grain, stress is built up. With the growth of Ag nanograins, the resulting strain exceeds elastic deformation and the AgBr grain can fragment into smaller ones, which drives the grain rotation. By the release of the internal stress, the angular velocity of the major diffraction spot gradually slows down as a function of the exposure time and eventually becomes stable. In the experiments of this study, the angular velocity of the grain rotation is measured to be as fast as 3.25 rad/s which is significantly faster than that of previously reported grain rotation [1].

We also observed lattice deformation along with grain rotation during the X-ray exposure of the Kodak linagraph paper and controlled AgBr samples. Three types of Ag lattice deformation are observed in our experiments: the first is related to the fragmentation of AgBr grains; the second is irregular lattice deformation, i.e. diffraction spots are irregularly oscillated around the Ag Debye-Scherrer rings; the third type shows more significant lattice deformation, i.e. the tracks of diffraction spots form straight or curved lines across the Ag (111) and (200) Debye-Scherrer rings. Fig. 2b shows a diffraction spot initiating on the Ag (200) ring and moving in a straight line towards inside the Ag (111) ring, which corresponds to a lattice expansion of 0.424 Å. The diffraction spot then moves from inside the Ag (111) ring towards outside the Ag (200) ring, corresponding to a lattice contraction of 0.5 Å. The whole process of the photoinduced lattice deformation lasts 8.45 s and the magnitude of the lattice deformation is significantly larger than those previously reported by other authors [3,4]. The significant lattice deformation obtained from our experimental data is likely due to the crystal structure changes of the unstable Ag nanograins [5,6].

In conclusion, we anticipate that this technique will find broad applications across several disciplines, as both advanced synchrotron light sources and X-ray optics are currently under rapid development worldwide, the focal spot of the *in situ* X-ray nanodiffraction system can be further improved to the ~ 10 nm level, allowing the study of the sub-grain dynamics in materials.

Contact: Jianwei Miao, miao@physics.ucla.edu

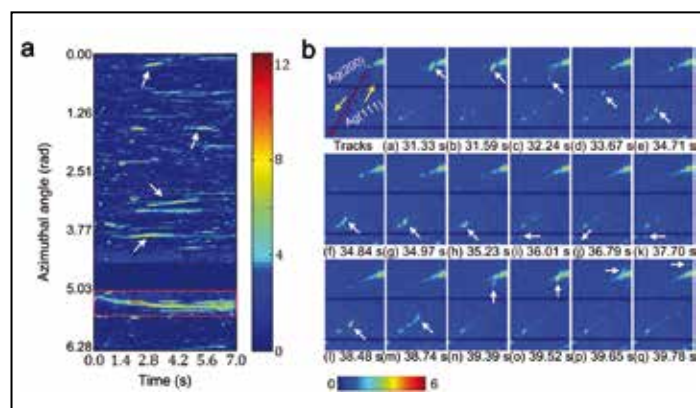


Figure 2

Real-time observation of grain rotation and lattice deformation in chemical reactions induced by X-ray photons.

a) Azimuthal plot of the diffraction intensity of the AgBr (200) Debye-Scherrer ring as a function of the exposure time (temporal resolution: 140 ms), measured from a Kodak linagraph paper.

b) A track image and 17 representative frames extracted from real-time measurements of a controlled AgBr/membrane sample (temporal resolution: 130 ms). The track image shows the trajectory of a diffraction spot between 31.33 and 39.78 s, where arrows show the motion of the diffraction spots.

Authors

Zhifeng Huang^{1§}, Matthias Bartels², Rui Xu¹, Markus Osterhoff², Sebastian Kalbfleisch², Michael Sprung³, Akihiro Suzuki⁵, Yukio Takahashi⁵, Thomas N. Blanton[†], Tim Salditt², and Jianwei Miao¹

1. Department of Physics & Astronomy and California NanoSystems Institute, University of California, Los Angeles, CA 90095, USA
 2. Institut für Röntgenphysik, Georg-August-Universität Göttingen, Friedrich-Hund-Platz 1, 37077 Göttingen, Germany
 3. Deutsches Elektronen-Synchrotron DESY, Notkestr. 85, 22607 Hamburg, Germany
 4. Kodak Technology Center, Eastman Kodak Company, Rochester, NY 14650-2106, USA
 5. Department of Precision Science and Technology, Graduate School of Engineering, Osaka University, 2-1 Yamada-oka, Suita, Osaka 565-0871, Japan
- § Present affiliation: Carl ZEISS X-ray Microscopy Inc., Pleasanton, CA 94588, USA
† Present affiliation: International Centre for Diffraction Data, Newtown Square, PA 19073, USA

Original publication

"Grain rotation and lattice deformation during photoinduced chemical reactions revealed by *in situ* X-ray nanodiffraction", *Nature Mater.* 14, 691–695 (2015). DOI: 10.1038/NMAT4311

References

1. L. Margulies, G. Winther, and H. F. Poulsen, "*In situ* measurement of grain rotation during deformation of polycrystals", *Science* 291, 2392–2394 (2001).
2. T. H. James, Ed., "*The Theory of the Photographic Process*", 4th edition (Macmillan Publishing Co., New York, 1977).
3. J. Diao, K. Gall, and M. L. Dunn, "Surface-stress-induced phase transformation in metal nanowires", *Nature Mater.* 2, 656–660 (2003).
4. M. L. Huberman, and M. Grimsditch, "Lattice expansions and contractions in metallic superlattices", *Phys. Rev. Lett.* 62, 1403–1406 (1989).
5. I. Shyjumon et al., "Structural deformation, melting point and lattice parameter studies of size selected silver clusters", *Eur. Phys. J. D* 37, 409–415 (2006).
6. T. C. R. Rocha, and D. Zanchet, "Structural defects and their role in the growth of Ag triangular nanoplates", *J. Phys. Chem. C* 111, 6989–6993 (2007).

Nature's tiny solar panels.

Native-like photosystem II rows reassembled inside an artificial crystal

Photosystem II (PSII) is a key enzyme in photosynthesis, catalysing the oxidation of water to oxygen.

Electron microscopy has shown that PSII forms solar panel-like concerted rows or arrays within its tightly packed native membrane. These assemblies have so far evaded study in molecular detail, as they readily dissociate when extracted for high-resolution X-ray crystallography. We have crystallised detergent-treated, purified core particles of PSII. Upon removal of detergent from the crystal, PSII particles rearrange into their original packing, creating a unique mimic of the native state. This allowed us to construct a high-resolution (2.44 Å) model of a native-like PSII superstructure.

Biological membranes are complex systems supporting elemental processes, such as energy conversion and nerve function. They combine a bilayer of lipid molecules and tightly packed, complex protein molecular machineries. Investigating structure and function of such complexes is as important as it is challenging. Electron or atomic force microscopy are used to image the membrane at nanometre resolution, while higher resolution structural models of isolated protein components commonly result from X-ray diffraction experiments using artificial crystals. This method allows the construction of (non-hydrogen) all-atom models but crucially requires highly purified samples and dissolution of the membrane by specialised detergents. These form a hemi-micelle ('belt') around the hydrophobic membrane-facing surface, rendering membrane proteins, such as PSII, soluble in aqueous solution. PSII was dissolved in the polyethylene glycol-type detergent $C_{12}E_8$. Extensive purification assured the removal of bulk membrane lipids and other protein constituents. An outline of the procedure – from membrane to structure – is shown in Fig. 1.

The total mass of the bound $C_{12}E_8$ was similar to the mass of PSII in the sample, thus it constrained crystal packing and formation of highly diffracting crystals. While upon crystallisation dark green crystals of rectangular shape appeared, only few direct protein-protein contacts were formed. The remaining contacts were mediated by the flexible detergent micelles, leading to poorly diffracting crystals. However, such micelles exist in equilibrium with free detergent molecules and dissociate when the detergent concentration is lowered below a critical concentration. We thus reduced detergent concentration far below this threshold. With this, crystals started to shrink by 15 % in size along their longest axis and diffracted to high resolution.

Diffraction data were collected at beamline P11 at PETRA III yielding a structure which could be refined to 2.44 Å resolution. Individual core particles of PSII could virtually not be distinguished from known structures [1]. But rather than isolated

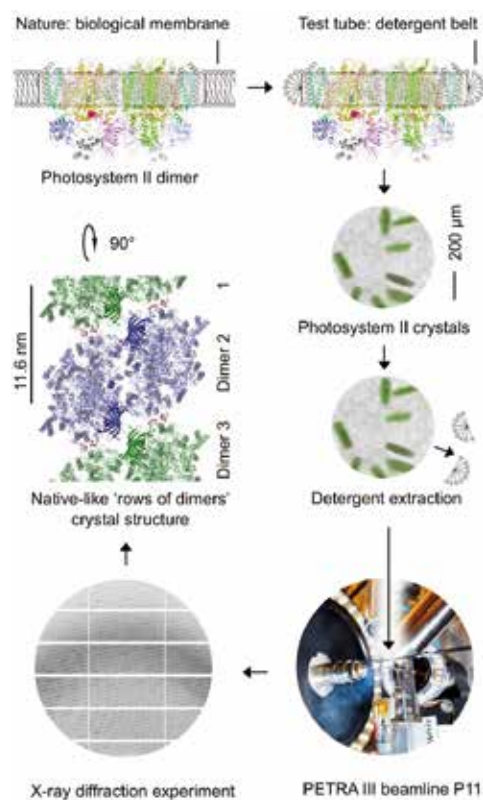


Figure 1

The experiment from membrane to structure (clockwise from top-left): the PSII protein complex is natively embedded in a lipid bilayer: the thylakoid membrane (view from the side, sunlight arriving from the top). Lipids were displaced by the $C_{12}E_8$ detergent, which forms a hemi-micelle ('belt') shielding the hydrophobic surfaces and allowing the isolation of the complex in an aqueous buffer system. Crystallisation of the protein by addition of polyethylene glycol and partial evaporation of solvent followed by removal of the detergent allowed PSII particles to snap back into a membrane-like arrangement (view from the top, sun-facing, rotated 90° to the above). Here, successive dimer particles (green/blue) are spaced at 11.6 nm and interconnected by two pairs of lipids (red) from the original membrane and a 'hand shake' of the central PsbO barrels. No detergent belt interrupts the rows. Diffraction data were collected from a single 200 µm crystal mounted at beamline P11 at PETRA III. The diffraction image represents 1 out of 1800 images used for structure determination.

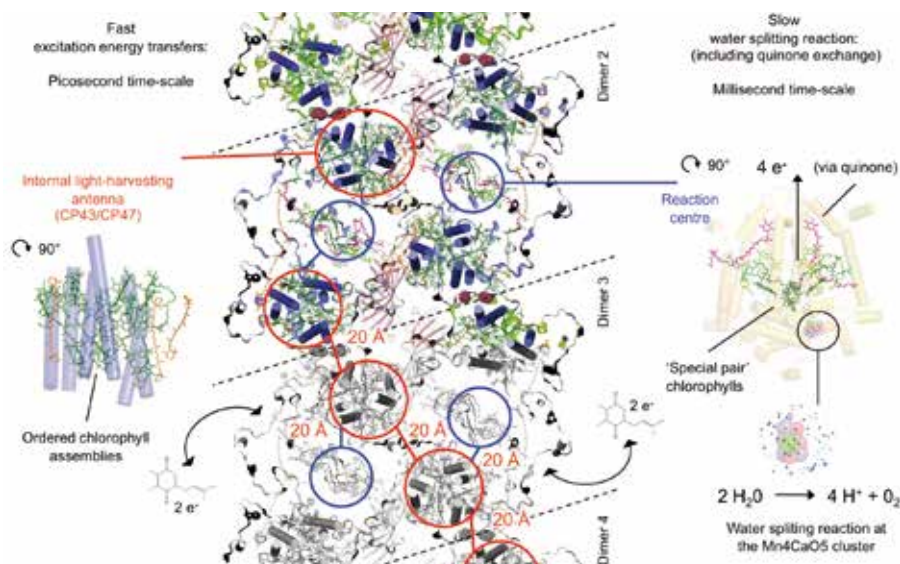


Figure 2

Native-like linear arrangement of four PSII core particles (dimers), schematic representation of the 200,000 non-hydrogen atom model. Each PSII dimer is a complex of 40 protein chains and 140 cofactors but it can be divided into two primary functional assemblies: Internal antenna subunits (red circles, detailed on the left) capture light and transfer excitation energy towards the reaction centres (blue circles, detailed on the right), where a Mn_4CaO_5 cluster catalyses the water-splitting reaction. The central model shows the extended structure, which tightly links antennae and reaction centres across the boundaries of individual PSII core particles.

core particles interspaced by (unobserved) amorphous detergent belts, a continuous ordered row of aligned PSII particles with 11.6 nm spacing (Figs. 1 and 2) was observed within the crystal. These rows were perfectly superimposable with electron micrographs of intact membranes [2,3], suggesting that the crystal mimics the native state in cyanobacteria (blue-green algae). In plants, alternative PSII / light-harvesting supercomplexes exist, which may shuffle within the membrane to adapt to light conditions [4].

In our model (see Fig. 2), PSII particles are aligned along their internal CP43/CP47 antennae, bringing their chlorophyll cofactors within 20 Å of one another – the same distance as between an antenna and its proximal reaction centre. Such distance allows excitation energy transfer between the antennae of successive PSII particles, which may be useful in reconciling the fast photon and slow chemical reactions: The PSII reaction centre converts two water molecules to molecular oxygen, four protons and four electrons, requiring four photons of light in the process. The reaction is far slower (millisecond time scale) than (photon) excitation energy transfer (picosecond time scale). Alignment of CP43/CP47 antennae might thus synchronise the arrival of photon energy at a reaction centre which requires that energy only at specific stages of the catalytic cycle. If a site cannot instantly make use of the

energy, it may rapidly be transferred to another reaction centre along the CP43/CP47 antenna relay, increasing the overall photon efficiency. The water splitting reaction itself is not hindered by the superstructure, as water, oxygen, and protons exchange via the luminal side (the far side as presented in Fig. 2), while electrons are delivered to plastoquinone which is exchanged via pockets perpendicular to the row axis.

The model presented, along with earlier electron micrographs, add to our understanding of biological membranes as spaces which are tightly packed with functional protein components – and possibly higher-order structure – rather than simply amorphous barriers. The experimental outcome is unique as a protein crystal is first formed without a native protein-protein contact and later snapped into just that native state by concerted rotation of PSII particles around at least two crystal axes. The strategy employed – control of the interplay of firstly detergent hemi-micelle around the protein and secondly the hydration state of the crystal – is a reoccurring scheme, which is crucial in obtaining well-diffracting crystals of membrane proteins in detergent space.

Contact: Martin Bommer, martin.bommer@hu-berlin.de
Anja Burkhardt, anja.burkhardt@desy.de
Athina Zouni, athina.zouni@hu-berlin.de

Authors

Julia Hellmich¹, Martin Bommer¹, Anja Burkhardt², Mohamed Ibrahim¹, Jan Kern^{3,4}, Alke Meents², Frank Müh⁵, Holger Dobbek¹, and Athina Zouni¹

1. Institut für Biologie, Humboldt-Universität zu Berlin, Unter den Linden 6, 10099 Berlin, Germany
2. Deutsches Elektronen-Synchrotron DESY, Notkestraße 85, 22607 Hamburg, Germany
3. Department of Physical Biosciences Division, Lawrence Berkeley National Laboratory, Berkeley, CA 94720, USA
4. LCLS SLAC National Accelerator Laboratory, Menlo Park, CA 94025, USA
5. Institut für Theoretische Physik, Johannes Kepler Universität Linz, Altenberger Straße 69, 4040 Linz, Austria

Original publication

"Native-like Photosystem II Superstructure at 2.44 Å Resolution through Detergent Extraction from the Protein Crystal", *Structure* 22, 1607–1615 (2014). DOI: 10.1016/j.str.2014.09.007

References

1. Y. Umena, K. Kawakami, J.-R. Shen, and N. Kamiya, "Crystal structure of oxygen-evolving photosystem II at a resolution of 1.9 Å", *Nature* 473, 55–60 (2011).
2. E. Mörschel and G. H. Schatz, "Correlation of photosystem-II complexes with exoplasmatic freeze-fracture particles of thylakoids of the cyanobacterium *Synechococcus sp.*", *Planta* 172, 145–154 (1987).
3. I. M. Folea, P. Zhang, E.-M. Aro, and E. J. Boekema, "Domain organization of photosystem II in membranes of the cyanobacterium *Synechocystis* PCC6803 investigated by electron microscopy", *FEBS Lett.* 582, 1749–1754 (2008).
4. R. Kourřil, E. Wientjes, J. B. Bultema, R. Croce, and E. J. Boekema, "High-light vs. low-light: effect of light acclimation on photosystem II composition and organization in *Arabidopsis thaliana*", *Biochim. Biophys. Acta.* 1827, 411–419 (2013).

Looking into the mirror.

Structural basis for the inhibition of protein activity by a Spiegelmer

In collaboration with NOXXON Pharma AG, Berlin, the first structure of a non-natural, mirror-image L-RNA aptamer (Spiegelmer) bound to its natural protein target was solved and analysed. The protein target, CCL2, is a small protein that is identified to be involved in a wide variety of diseases. To block the activity of the protein, the L-RNA aptamer (Spiegelmer) NOX-36 was generated and it already delivered promising phase IIa data from a study with diabetic nephropathy patients. The target and drug are today of high pharmacologically interest and is the first cross-chiral biomolecular complex of a non-natural L-oligonucleotide in complex with its natural protein target solved by X-ray crystallography, providing for the first time structural insights about an L-RNA aptamer and its molecular interactions.

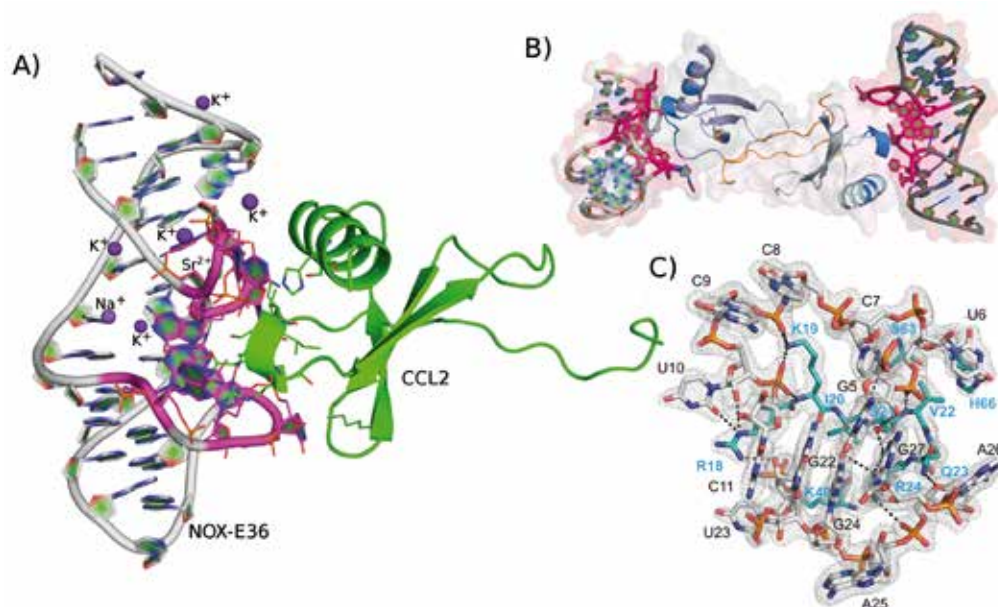


Figure 1

A) Refined model of the L-aptamer CCL2 complex, side chains of CCL2 and aptamer residues involved in complex formation are highlighted.

B) Biological assembly: two molecules of NOX-E36 are bound to a CCL2 homo-dimer. CCL2 residues involved in dimerization are highlighted in orange, those involved in aptamer binding in blue. The binding region of the aptamer is displayed in pink.

C) Detailed view of the interactions between the L-aptamer's binding pocket (nucleotides G5-C11 and G22-G27; grey) and the CCL2 epitope (amino acids 18-24, 49, 63, and 66; cyan). Only residues are depicted that are directly involved in binding via hydrogen bonds (shown as dashed lines).

The model is superimposed to the final 2mFo-DFc electron density map contoured at 1.0 σ .

Spiegelmers are chemically synthesized L-stereoisomer oligonucleotide aptamers, which are biologically very stable and immunologically passive due to their non-natural mirror-image configuration [1] and came in the focus of promising drug design investigations only a few years ago.

In order to identify a Spiegelmer, firstly aptamers are selected from oligonucleotide libraries to bind to the non-natural, mirror-image form of an intended target molecule (in case of our investigations the mirror-image or L-CCL2: D-CCL2) by an evolutionary screening technique called SELEX [1]. By chemical synthesis of the selected aptamer sequence from non-natural L-nucleotides, an exact mirror image of the aptamer is produced, the Spiegelmer, which consequently binds to the natural L-protein (in this case L-CCL2).

L-CCL2 itself is a member of the CC-chemokine family, a group of small secreted proteins that regulate leukocyte

migration in the human body [2]. CCL2 binds with high affinity almost exclusively to chemokine receptor 2 (CCR2), a G protein-coupled receptor (GPCR). Similar to other chemokines, CCL2 can form dimers and higher oligomers. Following a widely accepted model, receptor binding of CCL2 and chemokines in general takes place in a two-step process: the core domain of the chemokine binds to the N-terminus of the receptor followed by an interaction of the N-terminus of the chemokine with the helical bundle of the receptor [3]. Since in the case of CCL2 N-terminal residues are also involved in dimer formation, the second step leading to receptor activation very likely requires the monomeric form. Yet, dimerization and glucosaminoglycan (GAG)-binding are important for biological activity *in vivo* [4].

By attracting and activating immune cells, CCL2 plays a pivotal role in many inflammatory processes and has been shown to be involved in a wide variety of diseases with or without an obvious inflammatory aspect as, for example,

rheumatoid arthritis, multiple sclerosis, allergy and asthma, diabetic retinopathy, lupus nephritis, diabetic nephropathy and others [5]. Since no other drugs are available on the market, a human-CCL2-specific Spiegelmer, called NOX-E36 (emapticap pegol) was developed to block the activity of CCL2 and has already been tested successfully in a Phase IIa study in diabetic nephropathy patients [6].

Before our studies, no structural data of any L-RNA aptamers or L-RNA-protein complexes at high (i.e. atomic or near-atomic resolution) were available in the Protein Data Bank (PDB). In order to obtain structural information, we prepared the complex of the target protein CCL2 in the native conformation with the mirror-image L-RNA aptamer at physiological conditions. After complex formation, crystallization screening and tedious optimization of crystallization conditions, we could obtain crystals that gave rise to X-ray diffraction up to 2.2 Å at DORIS III (Consortiums beamline X13). However, molecular replacement phasing with the known structure of CCL2 as starting model did not provide positive results. To overcome this, a derivative of NOX-E36 harboring 2'selenomethyl-uridine in place of the native U31 was synthesized, a position known not to be important for target binding. New crystals were subjected to X-ray energies above the Se K-edge at PETRA III beamline P13 (EMBL Hamburg). The collected data allowed experimental phasing (SAD phasing, see Fig. 1) and subsequent model building and refinement of the structural model of the CCL2:NOX-E36 complex to 2.05 Å (see Fig. 2a).

An analysis of all contacts between symmetry-related molecules showed that the complex is a stable dimer of two CCL2·L-aptamer complexes, which are connected through interaction of two CCL2 molecules, mainly at the N-terminus of CCL2 (see Fig. 2b). Comparison with the known structures of CCL2 revealed that binding to the aptamer does not change the structure of the protein significantly, even in the residues that form hydrogen bonds with the L-RNA, with the exception of Lys19 (see Fig. 2c). Fig. 2a and 2c show that the Spiegelmer forms a pocket that binds tightly to a protruding patch of mostly basic and polar amino acids of CCL2. In this way, the aptamer binds directly to two of the five residues of

CCL2 involved in binding to CCR2 and to five of the six residues involved in GAG-binding. It can be assumed that blocking both receptor and GAG-binding regions contributes to the strong *in vivo* effects of the NOX-E36 L-aptamer.

We complemented our studies with Surface Plasmon Resonance measurements to assess the sequence specificity of aptamer binding and found that the conserved lysine 19 and arginine 24 are essential for the affinity of the aptamer to CCL2. In conclusion, the combination of binding and structural data provides a detailed understanding of the interactions between the L-aptamer drug and its target CCL2 and insight into the drug's mode of action. Moreover, we could describe the first high-resolution crystal structure of a non-natural, mirror-image L-RNA aptamer binding to a natural L-protein.

Contact: Christian Betzel, christian.betzel@uni-hamburg.de
Dominik Oberthür, dominik.oberthuer@desy.de
Sven Klussmann, sklussmann@noxxon.de

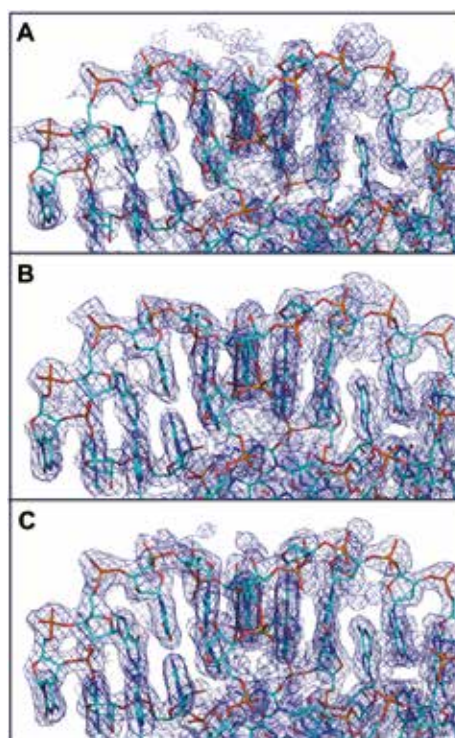


Figure 2
Experimental phasing: A) initial electron density map (all maps contoured at 1 σ), B) density modified map and C) final refined 2mFo-DFc-map, all displayed on top of a part of the final model.

Authors

Dominik Oberthür^{1,2#}, John Achenbach^{3#}, Azat Gabdulkhakov⁴, Klaus Buchner³, Christian Maasch³, Sven Falke¹, Dirk Rehders¹, Sven Klussmann³, and Christian Betzel¹

- Laboratory for Structural Biology of Infection and Inflammation, University of Hamburg, c/o DESY Building 22a, Notkestrasse 85, 22607 Hamburg, Germany
 - Center for Free-Electron Laser Science, Deutsches Elektronen-Synchrotron DESY, Notkestrasse 85, 22607 Hamburg, Germany
 - NOXXON Pharma AG, Max-Dohrn-Strasse 8-10, 10589 Berlin, Germany
 - Institute of Protein Research, RAS, Pushchino, Moscow Region 142290, Russian Federation
- # These authors contributed equally to this work

Original publication

"Crystal structure of a mirror-image L-RNA aptamer (Spiegelmer) in complex with the natural L-protein target CCL2", *Nature Communications* 6, 6923 (2015). DOI: 10.1038/ncomms7923

References

- A. Vater and S. Klussmann, "Turning mirror-image oligonucleotides into drugs: the evolution of Spiegelmer(R) therapeutics". *Drug discovery today* 20, 147-155 (2015).
- M. Baggiolini, B. Dewald and B. Moser, "Human chemokines: an update", *Annual review of immunology* 15, 675-705 (1997).
- X. Wang, J. S. Sharp, T. M. Handel, and J. H. Prestegard, "Chemokine oligomerization in cell signaling and migration", *Progress in molecular biology and translational science* 117, 531-578 (2013).
- A. E. Proudfoot et al., "Glycosaminoglycan binding and oligomerization are essential for the *in vivo* activity of certain chemokines", *Proc. Natl. Acad. Sci.* 100, 1885-1890 (2003).
- J. Dawson, W. Miltz, A. K. Mir, and C. Wiessner, "Targeting monocyte chemoattractant protein-1 signalling in disease", *Expert opinion on therapeutic targets* 7, 35-48 (2003).
- H. G. Haller, M. Baumann, and D. Eulberg, "CCL2 Inhibition with Emapticap Pegol (NOX-E36) in Type 2 Diabetic Patients with Albuminuria" in: 51st ERA-EDTA Congress (Amsterdam, 2014).

Insights into bi-specificity of A domains.

How an enzyme can selectively act on two structurally very different substrates

Non-ribosomal Peptide Synthetases (NRPSs) are modular enzyme complexes that produce many biologically active peptides as secondary metabolites. The substrate selection is carried out by an adenylation (A) domain, which recognizes and activates its cognate amino acid with high fidelity. Our work shows the structural basis for the unusual bi-specific nature of the A domain of an Anabaenopeptin synthetase (ApnA A₁) from a strain of cyanobacteria. Three active site residues were identified to have a crucial role in substrate recognition. Their substitution led to enzyme variants with altered specificity. Two of the variants were shown to activate a non-natural amino acid. A peptide product with non-natural amino acid incorporated into it could have new pharmacological properties or potential applications in labelling the peptide product in the host organism.

Many bacterial and fungal species employ large modular enzymes, called non-ribosomal peptide synthetases (NRPSs) in production of peptide secondary metabolites with antimicrobial activity. NRPSs consist of several modules that contain the necessary enzymatic units for recognition, activation and incorporation of the amino acid into the growing peptide chain [1]. The central unit in this system is the adenylation (A) domain, which selectively recognises and binds one of the 20 available amino acids. The creation of recombinant peptide synthetases with customised A domains could enable production of novel antimicrobial peptides.

Recently, Christiansen et al. (2011) discovered an unusual A domain from a cyanobacterial NRPS that is capable of activating arginine and tyrosine, two amino acids with very different chemical properties [2]. The peculiar bi-specificity of this A domain, called ApnA A₁, raised the question whether two separate binding pockets would be an explanation. To

address this question, structure studies were performed to gain insights into the molecular structure of ApnA A₁ from the cyanobacterial species *Planktothrix agardhii*. After extensive crystallization trials at the Sample Preparation and Characterization facility of EMBL Hamburg and subsequent data collection at the PETRA III beamlines, the crystal structure of the apo form of the enzyme was obtained. However, in the absence of the substrate only part of the protein was visible. The structure also lacked information about the substrate-binding site. Therefore further structural studies in the presence of the natural substrates of ApnA A₁ were needed.

The crystals of the apo-ApnA A₁ were soaked in solutions that contained the amino acid substrate (arginine or tyrosine) and ATP to obtain structures of the enzyme-substrate complex. Indeed, as a result from the X-ray diffraction experiments at PETRA III beamlines P13 and P14, the successful incorporation of both arginine and tyrosine in their activated form at the

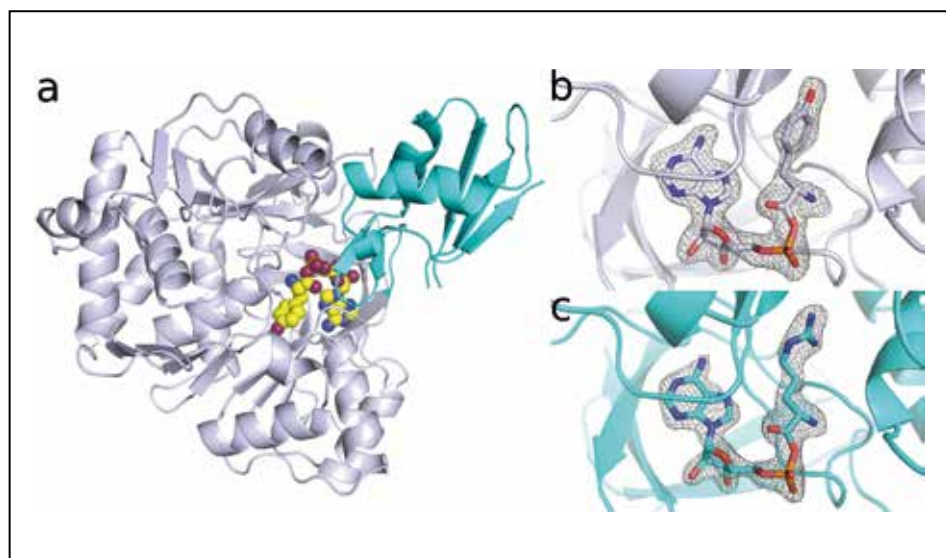


Figure 1

a) The crystal structure of ApnA A₁ in complex with the adenylylated tyrosine. The enzyme is shown as ribbon presentation in light grey and light blue while the bound substrate is shown as spheres with carbons, nitrogens and oxygens in yellow, blue and red, respectively. b – c) Close-ups of the adenylylated tyrosine and arginine within the binding pocket. The shown difference electron density (dark grey mesh representation) was calculated by omitting the ligands from the model. The map for the tyrosyl adenylylate intermediate (b) contoured at $0.12 \text{ e}\text{\AA}^{-3}$ ($\sigma = 2.0$) and for the arginyl adenylylate (c) at $0.14 \text{ e}\text{\AA}^{-3}$ ($\sigma = 3.0$). The adenylylated amino acids are represented as light grey (Tyr) and light blue (Arg) stick models. b,c) Reprinted with permission from the original publication. Copyright Wiley-VCH Verlag GmbH & Co. KGaA.

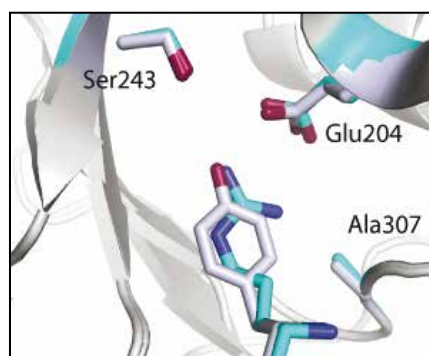


Figure 2

Overlay of the crystal structures with arginine (in blue) and tyrosine (in light grey) shows how arginine mimics the shape of tyrosine. Also the three crucial residues for substrate recognition are shown.

Reprinted with permission from the original publication.

Copyright Wiley-VCH Verlag GmbH & Co. KGaA.

binding pocket was confirmed (Fig. 1). The crystal structures of ApnA A₁ with the amino acids revealed that there was in fact only one common active site, which was able to adapt to both substrates. Furthermore, the arginine substrate was found to adopt a tyrosine-like conformation to fit better to the pocket (Fig. 2).

The structural information provided a starting point for mutational studies to pinpoint the residues responsible for the bi-specificity. A number of mutants were made and tested against the 20 canonical amino acids using a so-called hydroxylamine trapping assay [3]. As a result, three active site residues (Glu204, Ser243 and Ala307) were identified to play a key role in recognition of the substrate. Through systematic substitution of these residues, it was possible to switch the specificity of the enzyme and create enzyme variants that were mono-specific for arginine or tyrosine. Interestingly, to our knowledge an A domain with mono-specificity for tyrosine has not been encountered in nature.

The bi-specific nature of ApnA A₁ led to a hypothesis that the wild type enzyme or one of the variants could also utilise a non-natural amino acid 4-azidophenylalanine since this compound shares resemblance with both arginine and tyrosine. Indeed, two of the mutants accepted 4-azidophenylalanine as a substrate (Fig. 3). This opens up a possibility to incorporate a non-natural amino acid into the final peptide product and thus the creation of novel anabaenopeptins with interesting biological applications. For example a peptide with a non-natural amino acid could function as a traceable tag to map cellular pathways and processes that are important for the toxicity of cyanobacterial blooms.

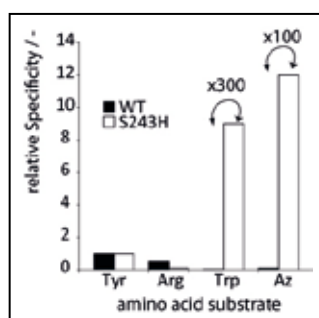
In conclusion, our work shed light on the unusual bi-specific nature of the A domain ApnA A₁ of Anabaenopeptin synthetase

from the cyanobacteria *Planktothrix agardhii*. Through structural studies of the enzyme in complex with its natural substrates, we were able to show how one binding pocket is sufficient to enable binding of both arginine and tyrosine. Furthermore, we identified three active site residues with particular importance for the substrate recognition using targeted mutagenesis. The mutation of these three residues enabled the creation of enzyme variants that were mono-specific for arginine or tyrosine. Two of the ApnA A₁ variants were also shown to activate a non-natural amino acid 4-azidophenylalanine (Az). This could allow engineering of recombinant Anabaenopeptin synthetases for the production of novel anabaenopeptins with the non-natural amino acid incorporated. These peptides could help to identify their potential binding partners in the original host organism and therefore elucidate the biological function of secondary metabolites in cyanobacteria.

Contact:

Andrea Rentmeister, a.rentmeister@uni-muenster.de

Figure 3
Specificity shift for different amino acids including the non-natural amino acid *p*-azidophenylalanine (Az) determined from kinetic data for the wildtype enzyme (WT) and the variant S243H.



Authors

Heidi Kaljunen^{1,2}, Stephan H. H. Schiefelbein³, Daniela Stummer^{3,4}, Sandra Kozak², Rob Meijers², Guntram Christiansen⁵, and Andrea Rentmeister^{3,4}

1. University of Helsinki, Department of Biosciences, Division of Biochemistry and Biotechnology, Viikinkaari 1, FI-00014, Finland
2. European Molecular Biology Laboratory (EMBL) Hamburg Outstation, c/o DESY, Notkestrasse 85, D-22603 Hamburg, Germany
3. University of Münster, Department of Chemistry, Institute of Biochemistry, Wilhelm-Klemm-Straße 2, D-48149 Münster, Germany
4. Cells-in-Motion Cluster of Excellence (EXC 1003-CIM), University of Münster, Germany
5. University of Innsbruck, Research Institute for Limnology, Mondseestr. 9, A-6310 Mondsee, Austria

Original publication

"Structural Elucidation of the Bispecificity of A Domains as a Basis for activating Non-natural amino acids", *Angew. Chem.* 127, 8957–8961 (2015), *Angew. Chem. International Edition* 54, 8833 - 8836 (2015). DOI:10.1002/anie.201503275

References

1. M. Strieker, A. Tanovic, M. A. Marahiel, "Nonribosomal peptide synthetases: structures and dynamics", *Curr. Opin. Struct. Biol.* 20, 234–240 (2010).
2. G. Christiansen, B. Philmus, T. Hemscheidt and R. Kurmayer, "Genetic Variation of Adenylation Domains of the Anabaenopeptin Synthesis Operon and Evolution of Substrate Promiscuity", *J. Bacteriol.* 193, 3822–3831 (2011).
3. N. Kadi and G. L. Challis, "Siderophore Biosynthesis: A Substrate Specificity Assay for Nonribosomal Peptide Synthetase-Independent Siderophore Synthetases Involving Trapping of Acyl-Adenylate Intermediates with Hydroxylamine", in: *Methods in Enzymology*, Vol. 458: Complex Enzymes in Microbial Natural Product Biosynthesis, Part A: Overview Articles and Peptides (Elsevier 2009).

Uncovering protein secrets using X-FEL pulses.

Three papers show how X-ray free-electron lasers can reveal the structure and function of proteins

The recently developed method of serial femtosecond crystallography provides a new route to determine the structures of macromolecules, avoiding previous restrictions set by the degradation of samples in the X-ray beam. Three recent papers by international collaborations involving DESY scientists highlight the rapid progress in this field and demonstrate its potential for determining the structures of large, delicate macromolecules as well as for examining how proteins move as they perform their work.

Serial femtosecond crystallography (SFX) uses intense ultrashort X-ray pulses from a free-electron laser to probe a stream of very small crystals, one after the other, and extract structural information about them. Since the first experiment of this kind, performed on protein crystals in 2009 [1], many experiments have followed in which biologically interesting and medically important macromolecules have been probed. These have included the first glimpses of photosynthesis in action [2] and the mechanism of inhibition of a protein from a parasitic organism [3]. By using ultrafast X-ray pulses of just tens of femtoseconds in duration, snapshot diffraction patterns can be obtained at X-ray doses far in excess of what can be tolerated in conventional measurements such as those carried out using synchrotron radiation. Although the crystal is vaporised by the interaction, a short enough pulse can be quicker than motion on the atomic scale. The enormous X-ray intensity means that crystals of a small fraction of a cubic micrometre can be used, which are often more easily obtained than large well-diffracting macroscopic ones. In general, the electron density maps obtained by SFX appear to be of higher quality than from data recorded in a conventional fashion, even for the same diffraction resolution, showing

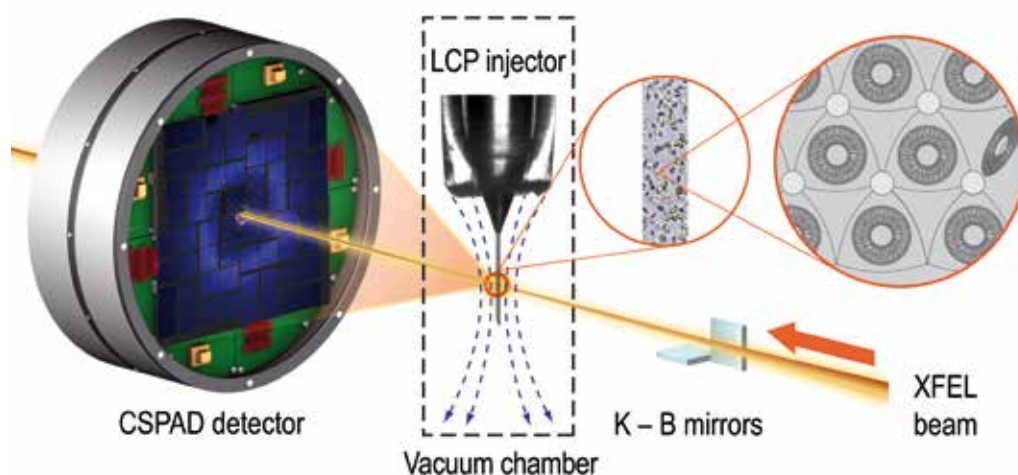
better definition of amino acid side chains and salt bridges for example. There is no need to cool samples to cryogenic temperatures, allowing measurements at ambient temperature, close to native conditions. This is especially important for time-resolved measurements, which are a natural fit to the methodology. The technique of serial crystallography has also been adapted, using much longer X-ray pulses, to the newest generation of intense synchrotron X-ray sources such as PETRA III [4].

A particularly successful application of SFX has been to G protein-coupled receptor (GPCR) crystals grown and delivered to the X-ray beam in a lipidic cubic phase matrix [5-6]. GPCRs are one of the most important classes of biological macromolecules for medicine and pharmacology, and are found embedded in the membranes of cells. Their role is to selectively transmit signals through the cell membrane from the outside to the intracellular lumen. They provide the molecular basis for the large variety of biological responses in all multicellular organisms. It therefore comes as no surprise that around a third of all prescription drugs operate in some way by binding to these molecules. However, GPCRs

Figure 1

Experimental setup for SFX data collection using an LCP injector. GPCR micro-crystals (first zoom level) dispersed in a liquid cubic phase medium (second zoom level) are injected as a continuous column with a diameter of 20 to 50 μm - stabilized by a co-axial gas flow (blue dash curved lines) - inside a vacuum chamber and intersected with 1.5- μm -diameter pulsed XFEL beam focused with Kirkpatrick-Baez (KB) mirrors.

Reproduced from W. Liu et al., Science 342, 1521–1524 (2013).



are also one of the most difficult classes of protein to study by X-ray crystallography. First, it is difficult to produce the large quantities of GPCR molecules required for crystallisation. Second, these integral membrane molecules lose their structural integrity if removed from the cell membrane. Third, GPCR molecules exhibit a high degree of structural heterogeneity, having many conformations between their “on” and “off” states, a characteristic which makes it difficult to assemble them in well-ordered crystal lattices.

The lipidic cubic phase (LCP) is a three-dimensional structure in which a lipid bilayer, itself very similar to a biological cell membrane, is curved into a repeating pattern. GPCR molecules can be comfortably accommodated in the bilayer and easily diffuse on the membrane to form crystals. For an SFX experiment, the crystals can be put into the path of the X-ray pulses while still contained within the LCP matrix using a special injection device (Fig. 1) that was developed by the group of John Spence at Arizona State University, a long-standing collaborator in this work. An advantage of this technique is that, due to the high viscosity of LCP and therefore its much lower flow rate, a smaller amount of protein is needed than with the aqueous liquid jet injector used for many other SFX experiments. Several GPCR structures have already been probed using SFX applied to crystals in LCP. Two are highlighted here: the angiotensin II type 1 receptor, and arrestin bound to human rhodopsin. The measurements were carried out at the Linac Coherent Light Source (LCLS) in the USA by large collaborative groups headed respectively by Vadim Cherezov of the University of Southern California and Eric Xu of the Van Andel Research Institute.

The angiotensin II type 1 receptor (AT₁R) is one of the GPCRs which control blood pressure and is one of the major targets for the treatment of hypertension. In this experiment, crystals of human AT₁R were used with an average size of $10 \times 2 \times 2 \mu\text{m}^3$, which is very small by normal GPCR standards. About 65 μl of LCP was injected into the LCLS X-ray beam over a period

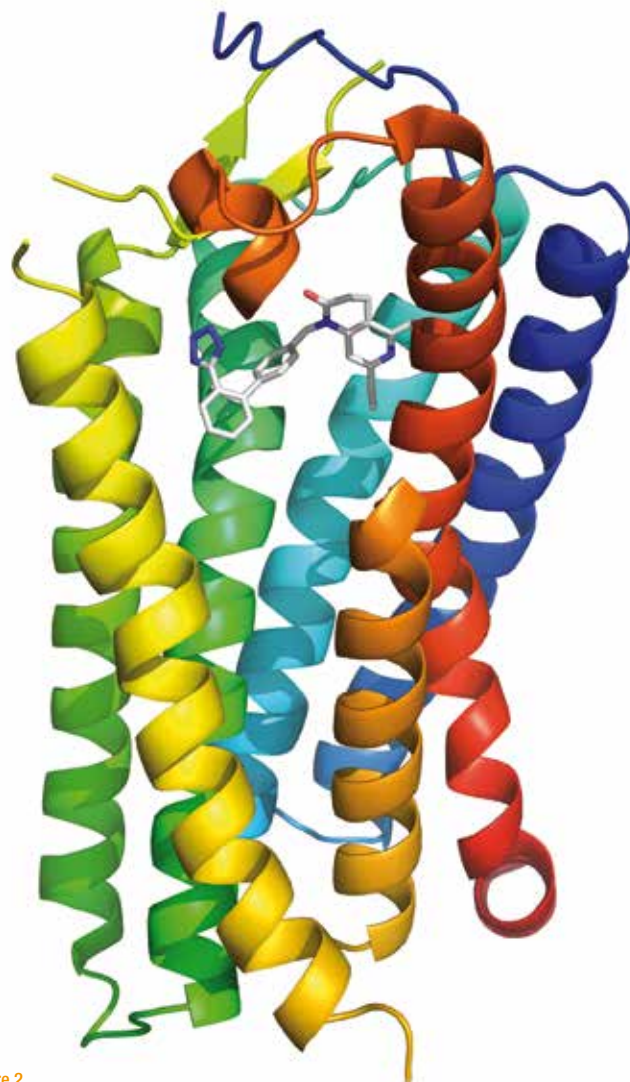


Figure 2
Cartoon representation of the AT₁ receptor showing ZD7155 (stick model) in the binding pocket.

of several hours, yielding 457,275 crystal diffraction patterns as identified by our open-source “hit finding” software Cheetah [7]. These frames were processed using CrystFEL, software developed at the Center for Free-Electron Laser Science (CFEL), DESY for handling data from serial crystallography experiments [8]. The resulting merged data set was further processed using conventional programs for macromolecular crystallography, yielding the structure of AT₁R at a resolution of 2.9 Å (Fig. 2).

The structure shows the classic pattern, common to all GPCRs, of seven alpha helices spanning the cell membrane, forming the main body of the receptor. The crystals used for this study also contained a chemical precursor (ZD7155) of the group of sartans which are very successfully used for the treatment of hypertension. The structure therefore allows us to see how ZD7155 interacts with the receptor, which is important information for understanding how it works and how newer drugs can be developed which are more effective.

Another application of the SFX technique combined with LCP was the solution of the biochemical “off switch” arrestin bound to rhodopsin. G-protein coupled receptors are so named because their immediate interaction partners inside a cell are G-proteins, which trigger downstream signalling of the receptor. The counterpart to G-proteins are arrestins. These show a high affinity to the activated receptor and sterically block their downstream signalling in order to allow a rapid regulation of the receptor’s activity. Rhodopsin is the light-sensitive protein responsible for vision through the naturally bound ligand retinal. Upon absorption of a single photon, the cis-trans isomerization of the retinal leads to a conformational change of the receptor, which subsequently allows binding of a G-protein through a cascade of events that triggers the electrochemical stimulation of a neuron and forms the molecular basis of vision. This fundamental physiological process needs to be tightly controlled in order to avoid “over-shooting” of the visual signal.

The conformational flexibility of the overall rhodopsin-arrestin complex made it very difficult indeed to grow large, well-ordered crystals from it. Experiments using synchrotron X-ray sources yielded data with a resolution of only about 8 Å. For the SFX experiment, 22,262 diffraction patterns were acquired and processed using Cheetah and CrystFEL, yielding data

with an anisotropic resolution limit of 3.8 Å in the crystal directions corresponding to the plane of the cell membrane, and 3.3 Å in the perpendicular direction.

The process of solving this structure was much more difficult than usual due to several crystal packing phenomena which complicate the handling of the data. The most obvious of these was the very long repeat distance along one of the crystal axes, which led to a very small spacing between spots in the diffraction patterns (Fig. 3a). Several further difficulties arose due to the nature of the packing of molecules within the crystal lattice. Nevertheless, the electron density map reveals how the arrestin molecule attaches to rhodopsin and causes it to reset.

As well as revealing the structures of important biomolecules, SFX holds the promise of seeing them in action by doing time-resolved experiments. The short durations of the X-ray pulses, which can be down to only a few femtoseconds, allow high time resolution while still delivering enough photons to record a diffraction snapshot from a crystal. Several biological systems, such as rhodopsin, start their activity in response to exposure to visible light. Therefore, by exposing the stream of crystals to a visible light “pump” pulse a short time before the X-ray pulse arrives, and then varying the time delay between

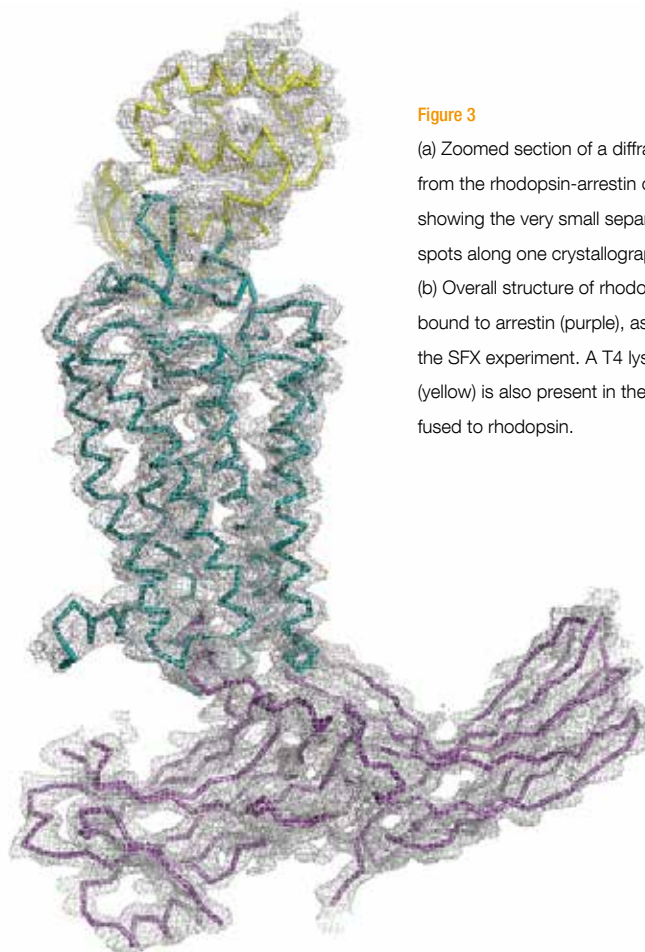
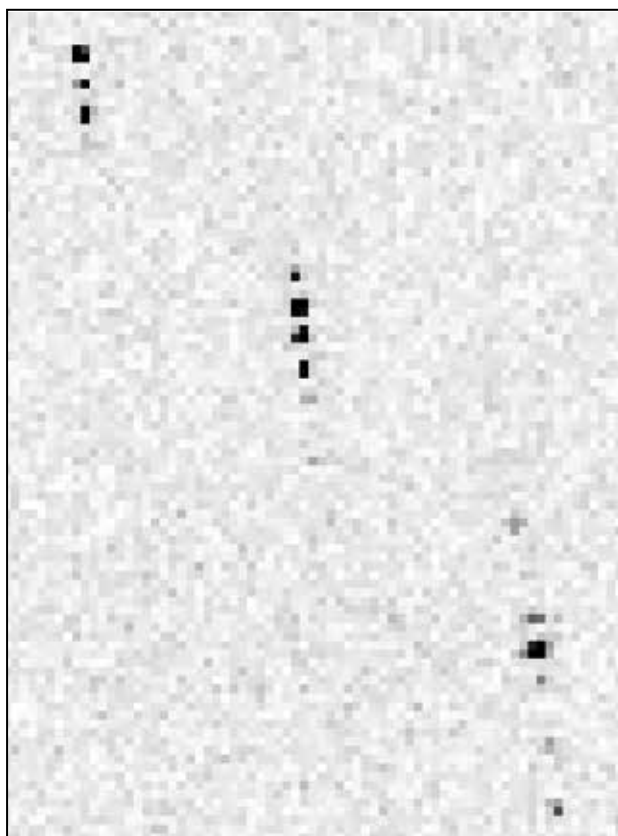


Figure 3

(a) Zoomed section of a diffraction pattern from the rhodopsin-arrestin complex, showing the very small separation between spots along one crystallographic direction. (b) Overall structure of rhodopsin (green) bound to arrestin (purple), as revealed by the SFX experiment. A T4 lysozyme molecule (yellow) is also present in the structure, fused to rhodopsin.

the light and X-ray pulses, the structure of a protein can be studied at different time points along the reaction. This technique of time-resolved SFX has been applied to several systems already, including one of the protein complexes involved with photosynthesis [2], and now at high resolution on the photoactive yellow protein (PYP) in collaborative experiments led by Marius Schmidt of the University of Wisconsin-Milwaukee.

Photoactive yellow protein is a small protein which enables certain types of bacteria to respond to light. This protein can easily be produced in large quantities and is highly water-soluble, which makes it a good choice for a proof of principle experiment of how SFX can yield time-resolved structural information more clearly than before. Time-resolved crystallography at synchrotron radiation facilities requires very large crystals to obtain measurable signal from single pulses. In such experiments the crystals are necessarily much larger than the penetration depth of the light used to photo-excite them, leading to a small fraction of molecules undergoing the reaction. In our SFX experiments the crystals were smaller than the optical extinction depth, allowing the pump light to homogeneously expose the crystal volume and initiate the reaction in a much larger fraction of the molecules. The difference electron density map, which shows which regions of the molecule have moved from their initial positions, shows clearer details compared to previous work using synchrotron sources (Fig. 4).

The pump-probe time delays used here were long, and so this experiment is primarily a proof of concept. However, future experiments will reduce the pump-probe delay to below 1 ps, which is only possible using the unique time structure of FEL X-ray pulses. In case of PYP a circular, reversible reaction has been studied. But the serial crystallography approach is equally applicable to irreversible reactions since the sample is freshly replenished on every X-ray shot. Such reactions were difficult if not impossible to investigate by time-resolved crystallography. Serial crystallography, therefore, will have a great potential for unravelling the kinetics and dynamics of protein reactions over a very wide range of timescales.

SFX gives us not only the ability to take pictures of some of the most interesting biochemical systems at resolutions approaching the atomic scale, but also to make movies of their activity. With many improvements being made in sample delivery, instrumentation and data processing, the pictures will soon get sharper in both space and time dimensions.

Contact: Thomas A. White, thomas.white@desy.de
Cornelius Gati, cornelius.gati@desy.de
Dominik Oberthür, dominik.oberthuer@desy.de
Henry Chapman, henry.chapman@desy.de

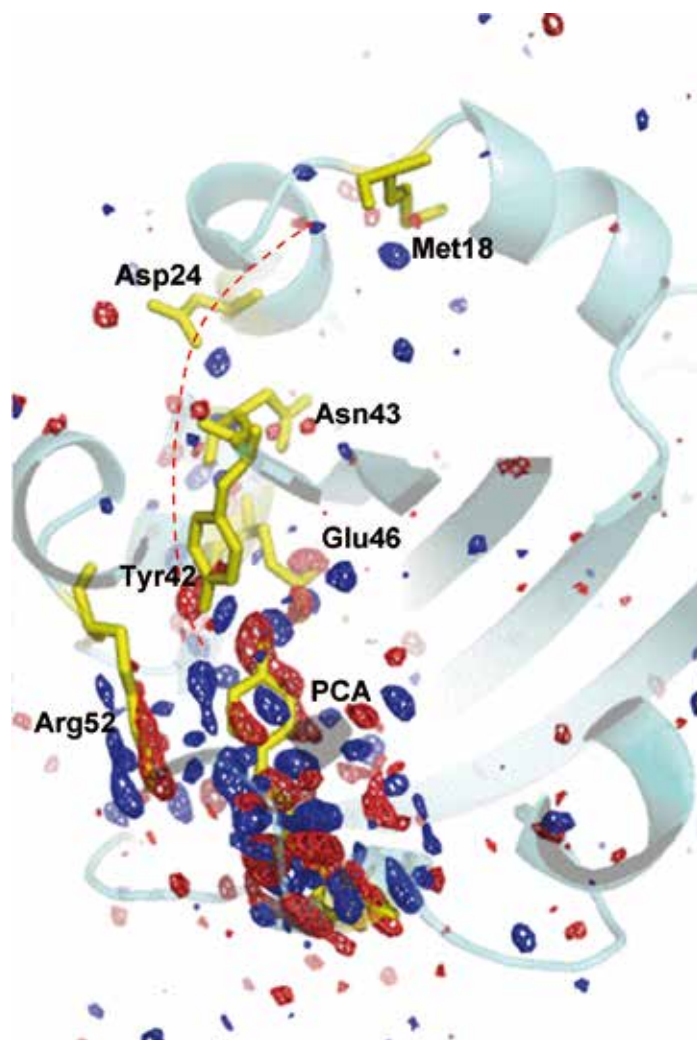


Figure 4

Difference electron density map from the time-resolved SFX experiment on photoactive yellow protein. Reproduced from J. Tenboer et al., *Science* 346, 1242–1246 (2014).

Original publications

1. H. Zhang et al., "Structure of the Angiotensin Receptor Revealed by Serial Femtosecond Crystallography", *Cell* 161, 833–844 (2015). DOI: 10.1016/j.cell.2015.04.011
2. Y. Kang et al., "Crystal structure of rhodopsin bound to arrestin by femtosecond X-ray laser", *Nature* 523, 561–567 (2015). DOI: 10.1038/nature14656
3. J. Tenboer et al., "Time-resolved serial crystallography captures high-resolution intermediates of photoactive yellow protein", *Science* 346, 1242–1246 (2014). DOI: 10.1126/science.1259357

References

1. H. N. Chapman et al., "Femtosecond X-ray protein nanocrystallography", *Nature* 470, 73–77 (2011).
2. C. Kupitz et al., "Serial time-resolved crystallography of photosystem II using a femtosecond X-ray laser", *Nature* 513, 261–265 (2014).
3. L. Redecke et al., "Natively inhibited typanosoma brucei cathepsin B structure determined by using an X-ray laser", *Science* 339, 227–230 (2013).
4. F. Stellato et al., "Room-temperature macromolecular serial crystallography using synchrotron radiation", *IUCrJ* 1, 204–212 (2014).
5. W. Liu et al., "Serial femtosecond crystallography of G protein-coupled receptors", *Science* 342, 1521–1524 (2013).
6. U. Weierstall et al., "Lipidic cubic phase injector facilitates membrane protein serial femtosecond crystallography", *Nature Communications* 5:3309 (2014).
7. A. Barty et al., "Cheetah: software for high-throughput reduction and analysis of serial femtosecond X-ray diffraction data", *J. Appl. Cryst.* 47, 1118–1131 (2014).
8. T. A. White et al., "CrystFEL: a software suite for snapshot serial crystallography", *J. Appl. Cryst.* 45, 335–341 (2012).

How to assess data misfits if experimental errors are unknown.

Correlation Map provides goodness-of-fit test for X-ray scattering and beyond

Assessing the dissimilarity of data sets is an important aspect of data interpretation. Data collected at the EMBL-P12 BioSAXS beam line at PETRA III was used to motivate and develop a new type of goodness-of-fit test to evaluate data-data and data-model discrepancies for small-angle X-ray scattering and other types of over-sampled 1D-spectra. The classical reduced χ^2 test widely used in physical sciences for over a century requires not only accurate estimation of scattering intensities, but also of experimental errors, which, if not correct, may render the test results invalid. Although the Correlation Map test uses only correlations between datasets, it maintains the statistical power of the reduced χ^2 test with correct errors to detect systematic differences, thus sidestepping the issue.

Small angle X-ray scattering (SAXS) is a well established technique that is used to obtain global structural parameters from an array of materials, encompassing both hard and soft matter. The EMBL-P12 beam line at PETRA III specifically focuses on SAXS from biological macromolecules to facilitate the understanding of the structure and dynamics of proteins, DNA, RNA, and exotic biological nanocomposites in solution [1]. The goal of BioSAXS is to measure exceptionally weak scattered X-ray intensities, $I(q)$, as a function of angle, 2θ , or momentum transfer q (where $q = 4\pi\sin\theta/\lambda$) and interpret these data in context of macromolecular shape. As in many other physical experiments, the analysis and modelling of BioSAXS data requires both the accurate recording of $I(q_k)$ at each point in q_k , $k = 1, \dots, K$, as well as their associated experimental errors, $\sigma(I(q_k))$. Specifically, to compare two or more datasets, or a data-model fit, the reduced χ^2 test [2] is usually employed:

$$\chi^2 = \frac{1}{K-1} \sum_{k=1}^K \left[\frac{I_{exp}(q_k) - I_{calc}(q_k)}{\sigma(I(q_k))} \right]^2$$

where the values of $\sigma(I(q_k))$ must obviously be correctly specified for the test to be valid. However, obtaining the correct error estimates may be just as difficult as obtaining the scattering intensities themselves, as the true values of $\sigma(I(q_k))$ are always unknown and have to be estimated from the experimental data.

Using a PILATUS 2M photon counting detector, we collected the statistics of thousands of SAXS data frames of pure water and showed that the behaviour $I(q)$ at each point in q – without considering $\sigma(I(q))$ – truly follows Poisson counting statistics that ultimately limit to normally distributed values. Further, when performing all pairwise comparisons of the water frames, the results show that the intensities $I(q)$ are not only normally distributed, but also uncorrelated, independent, and

joint-wise normally distributed, i.e. statistically independent. Consequently, it is possible to conceptualise an entire SAXS profile as simply being a simultaneously drawn random variable from a K -variate normal distribution $N(J, \Sigma)$, where J is the vector of the true, but unknown, intensities, Σ the variance-covariance matrix and K the number of data points in q :

$$J = \begin{pmatrix} \vdots \\ I(q_k) \\ \vdots \end{pmatrix}, \quad \Sigma = \begin{pmatrix} \ddots & & & & \\ & \sigma(q_k)^2 & \cdots & \sigma(q_k, q_l) & \\ & \vdots & \ddots & \vdots & \\ & \sigma(q_k, q_l) & \cdots & \sigma(q_l)^2 & \\ & & & & \ddots \end{pmatrix}$$

where the on-diagonal $\sigma(q_k)^2$ are the variances of the intensities, and $\sigma(q_k, q_l)$ the off-diagonal covariances. When estimating the variance-covariance matrix Σ from experimental data that do not exhibit systematic differences, all off-diagonal terms $\sigma(q_k, q_l)$ will be (close to) zero, or in the case of two frames only, a random pattern of values of +1 and -1 (Fig. 1a-c). In the case of systematic differences, consecutive areas, patches, of +1 or -1 correlation will emerge that are easily recognized in the image representation of this matrix (Fig. 1d-f).

Remarkably, when evaluating thousands pair-wise comparisons of two data frames, or a data-model fit, the probability of occurrence of the largest observed patch size of +1 or -1 follows the same distribution as that describing the longest head-or-tail runs of a plain coin-toss experiment [3]. From this, the probability (P -value) of observing a patch size similar to, or exceeding, the observed one corresponds to the area under the tail of the distribution. If the patch size occurs so that the P -value is less than a given significance threshold α (e.g., $\alpha = 0.01$) then statistically significant differences are present in the data or the model. The analysis of this Correlation

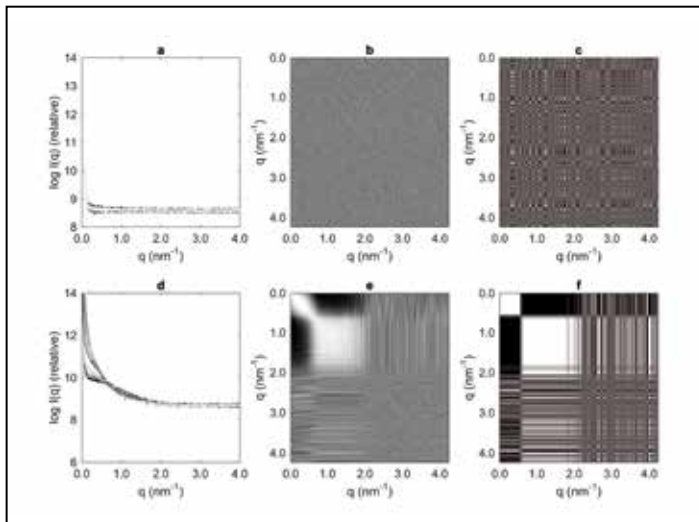


Figure 1

CorMap visualization. (a,d) One-dimensional SAXS data sets, each consisting of 20 data frames, obtained from aqueous buffer (a), lysozyme with accumulating radiation damage (unsubtracted data) (d). (b,e) CorMaps corresponding to the data sets at left, computed from all 20 frames. (c,f) Selected pairwise comparisons of two frames each. The corresponding probabilities of similarity (P value) of the two-frame comparisons are 0.3400 (c), and $<10^{-5}$ (f).

(Figure from Franke et al., Nature Methods 12, 419-422 (2015)).

Map (CorMap) therefore provides a quantitative estimate of the presence of systematic deviation based on the data only, without the requirement of knowledge of the associated errors.

The CorMap test may be directly employed to quantify systematic deviations in different scenarios e.g. for the detection

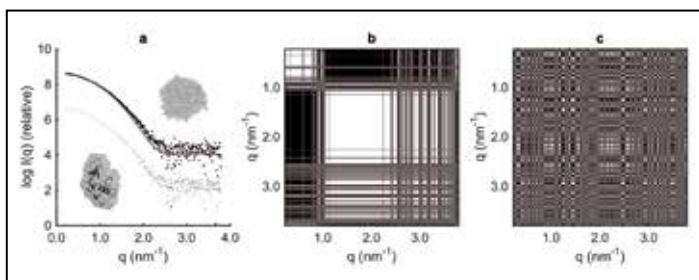


Figure 2

Figure 2 CorMap applications. (a) SAXS data model fits of a starting (misfitting) and final (fitting) bead model of lysozyme obtained during ab initio modelling using the program DAMMIF. (b, c) Corresponding CorMaps for the initial (b; $n = 449$, $C = 137$, $P < 10^{-6}$) and refined bead models (c; $n = 449$, $C = 10$, $P = 0.3532$). A spatial superposition of the final refined bead model and the lysozyme X-ray crystal structure is also displayed (black ribbons). (Figure from Franke et al., Nature Methods 12, 419-422 (2015)).

of radiation damage [4], incorrect data normalisation/scaling and of course, assessing model fits (Fig. 2). It has been found that the statistical power of the CorMap test is generally similar to that of a valid reduced χ^2 test, but unlike χ^2 , it does not depend on obtaining correct error estimates. Therefore CorMap is a powerful alternative that provides a valid statistical test to evaluate data-data or data-model discrepancies.

It is to note that the CorMap test has diverse applications, not only for SAXS, but also for other types of experiments that produce over-sampled 1D-spectra e.g. using scattering, reflectometry or spectroscopy. For example, we have shown that CorMap may be utilized to evaluate models for zero-applied-field muon spin rotation. The CorMap test has been integrated into the EMBL-P12 BioSAXS automated pipeline [5] for the near-real-time quality assessment of SAXS data and is freely available for academic use as part of the ATSAS software package [6].

Contact: Daniel Franke, franke@embl-hamburg.de,
Dmitri Svergun, svergun@embl-hamburg.de

Authors

Daniel Franke¹, Cy M. Jeffries¹, and Dmitri I. Svergun¹

¹ European Molecular Biology Laboratory, Hamburg Outstation, c/o DESY, Notkestraße 85, Hamburg 22607.

Original publication

“Correlation Map, a goodness-of-fit test for one-dimensional X-ray scattering spectra”, Nature Methods 12, 419-422 (2015). DOI: 10.1038/nmeth.3358

References

1. C. Blanchet, S. Spilotos, F. Schwemmer et al., “Versatile sample environments and automation for biological solution X-ray scattering experiments at the P12 beamline (PETRA-3, DESY)”, J. Appl. Cryst. 48, 431-443 (2015)

2. K. Pearson, “On the Criterion that a given System of Deviations from the Probable in the Case of a Correlated System of Variables is such that it can be reasonably supposed to have arisen from Random Sampling”, Philosophical Magazine Series 5, 157-175 (1900).
3. M. F. Schilling, “The longest run of heads”, College Math. J. 21, 196-207 (1990).
4. C. M. Jeffries, M. A. Graewert, D. I. Svergun, C. E. Blanchet, “Limiting radiation damage for high brilliance biological solution scattering: practical experience at the EMBL P12 beam line, PETRA III”, J. Sync. Rad. 22, 273-279 (2015).
5. D. Franke, A. G. Kikhney, D. I. Svergun, “Automated acquisition and analysis of small angle X-ray scattering data”, Nucl. Inst. Meth. A 689, 52-59, 2012.
6. M. V. Petoukhov, D. Franke, A. V. Shkumatov et al., “New developments in the ATSAS program package for small-angle scattering data analysis”, J. Appl. Cryst. 45, 342-350 (2012).

Towards miniaturized particle accelerators.

THz acceleration

We demonstrate the first linear acceleration of electrons with keV energy gain using optically-generated terahertz (THz) pulses. Increasing the operational frequency of accelerators into the THz band not only allows for greatly increased accelerating gradients due to relaxation of breakdown limits, but also realizes high acceleration gradients with less amount of pulse energy. With recent advances in the generation of THz pulses via optical rectification, increasing accelerating gradients by two orders of magnitude over conventional linear accelerators (LINACs) has become a possibility. These ultra-compact THz accelerators with extremely short electron bunches will strongly impact accelerator technologies used in free-electron lasers, ultra-fast electron diffraction, and medical therapy with X-rays and electron beams.

At radio frequencies (RF) where conventional accelerator-driven radiation sources are efficient, surface electric field gradients in accelerating cavities are limited by RF-induced plasma breakdown. The empirical studies on the breakdown threshold have shown that this effect becomes worse with increasing the operation frequency and decreasing the pulse length of the imposed fields on the accelerators [1]. In addition, low-frequency RF pulses provided by traditional sources are produced in a very narrow frequency spectrum (i.e. long pulse length). Practically, this results in a significant amount of average power that is deposited into the cavity if a high repetition rate is used.

The desire for high accelerating gradients inspired the use of presently available ultrafast near-IR terawatt and petawatt laser technology to achieve multi-GV/m gradients based on chirped-pulse amplification. However, due to the short wavelength, infrared optical acceleration suffers from difficulties

when used for the acceleration of electrons with significant charge per bunch. In order to prevent emittance growth and increased energy spread, the electron bunch needs to occupy a small fraction of the optical cycle. This becomes challenging when the bunch contains a large number of electrons. Another practical concern would be the timing precision between the optical cycle and the arrival of the electron bunch. Difficulties increase further when considering the available options for guiding the optical light in order to decrease the phase velocity to match the electron beam. Alternatively, laser-plasma wakefield accelerators have demonstrated GV/m accelerating electric fields with 100 TW - PW low repetition rate sources with percent-level energy spread and jitter for the electron bunch [2].

THz frequencies provide a promising trade-off between both optical and RF worlds. On one hand, the wavelength is long enough that we can fabricate waveguides with conventional machining techniques, provide accurate timing and

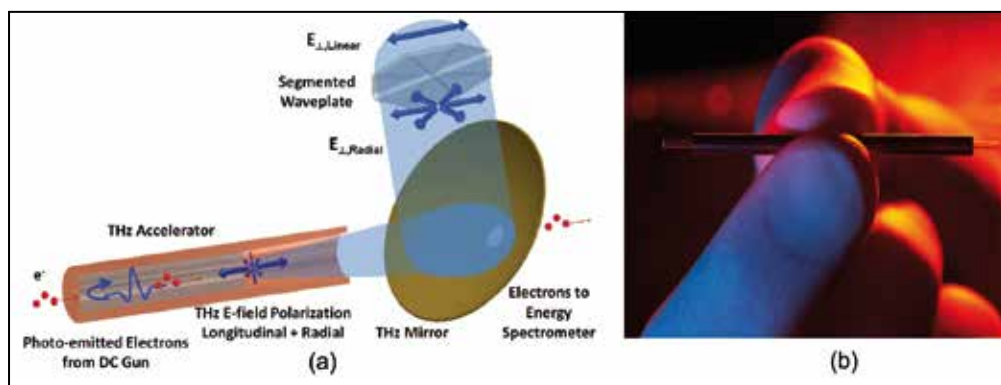


Figure 1

Terahertz-driven linear accelerator. (a) Schematic of the THz LINAC: A linearly polarized THz pulse (blue double arrow, top) is converted into a radially polarized pulse by a segmented waveplate before being focused into the THz waveguide depicted by the bronze cylinder. The THz pulse is reflected at the end of the waveguide (left) to co-propagate with the electron bunch which enters the waveguide through a pin-hole. The electron bunch is accelerated by the longitudinal electric field of the co-propagating THz pulse. The electron bunch exits the THz waveguide and passes through a hole in the focusing mirror (right) for the THz pulse. (b) Photograph of the compact mm-scale THz LINAC.

accommodate a significant amount of charge per bunch. Moreover, the frequency is high enough that the plasma breakdown threshold for the surface electric field increases into the multi-GV/m range. Additionally, using optical generation techniques we can have very short THz pulses (≤ 100 ps) which allows for a limited amount of pulsed heating and a limited amount of average power loading at high repetition rates [3].

We carried out the first experimental demonstration of linear electron acceleration using an optically-generated $10 \mu\text{J}$ single-cycle THz pulse centred at 0.45 THz. The THz pulse accelerates electrons in a circular waveguide consisting of a dielectric capillary with a metal outer boundary. The dielectric slows the group and phase velocity of the THz wave allowing it to capture and accelerate low energy electrons. A schematic view of the THz accelerator and a photograph of the LINAC are shown in Fig. 1(a). The THz waveguide supports a traveling $\text{TM}_{0,1}$ mode that is phase-matched to the velocity of the electron bunch produced by the DC photoinjector. Using 60 keV electrons an energy gain of 7 keV is observed for a 3 mm interaction length as shown in Fig. 1(b). The single-cycle THz pulse is produced via optical rectification of a 1.2 mJ, $1 \mu\text{m}$ laser pulse at a repetition rate of 1 kHz. The THz pulse, whose polarization is converted from linear to radial by a segmented waveplate, is coupled into the waveguide with 10 MV/m on-axis peak accelerating gradient. The 25 fC input electron bunch is produced with a 60 keV DC photo-emitting cathode excited by a 350 fs UV pulse. The achievable accelerating gradient in the THz structures demonstrated in this work is of the order of 1 GV/m with an IR pulse energy of 100 mJ when optimized for relativistic electron beams.

The performance of these structures improves with an increase in electron energy and gradient making them attractive for compact accelerator applications [4]. With upgrades to pump laser energy and technological improvements to THz sources, GV/m gradients are achievable in dielectric-loaded circular waveguides. The available THz pulse energy scales with IR pump energy, shown by a recently reported result of 0.4 mJ and $\sim 1\%$ IR-to-THz conversion efficiency [5]. Multiple

stages of THz acceleration can be used to achieve higher energy gain with additional IR pump lasers for subsequent stages. This proof-of-principle THz linear accelerator demonstrates the potential for an all-optical acceleration scheme that can be readily integrated into small-scale laboratories providing users with electron beams that will enable new experiments in ultra-fast electron diffraction and X-ray generation.

Contact: Franz Kärtner, franz.kaertner@cfel.de

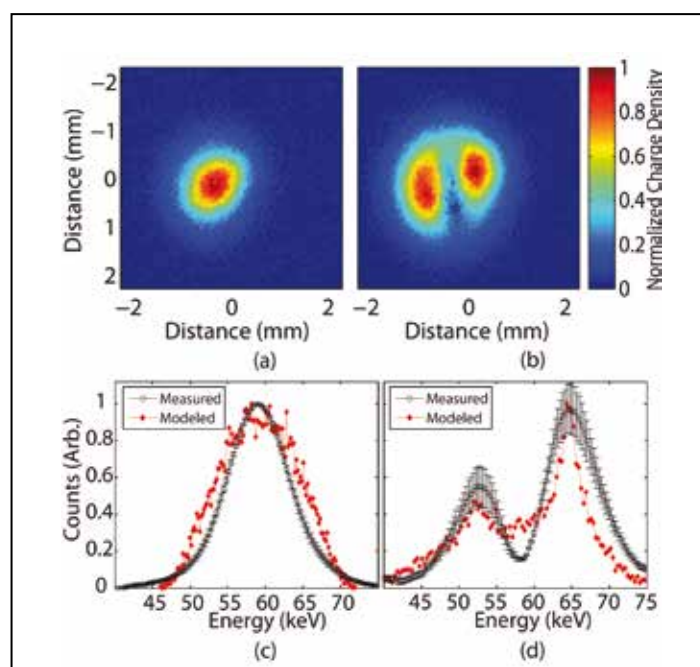


Figure 2

Demonstration of THz acceleration. (a) Image of the electron beam profile at a kinetic energy of $E = 59$ keV for THz off and (b) THz on. The bimodal distribution is due to the presence of accelerated and decelerated electrons which are separated spatially by a magnetic-dipole energy spectrometer. (c) Comparison between simulated (red) and measured (black) electron bunch profiles at 59 keV with 25 fC per bunch, $\sigma_x = 513 \mu\text{m}$ and $\Delta E/E = 1.25$ keV. After the pin-hole the transverse emittance is 25 nm-rad and the longitudinal emittance is 5.5 nmrad. (d) Comparison between simulated (red) and measured (black) electron bunch profile after acceleration with THz.

Authors

Emilio A. Nanni¹, Wenqian R. Huang¹, Kyung-Han Hong¹, Koustuban Ravi¹, Arya Fallahi^{4,5}, Gustavo Moriena², R. J. Dwayne Miller^{2,3,4}, and Franz X. Kärtner^{1,4,5,6}

1. Department of Electrical Engineering and Computer Science, Research Laboratory of Electronics, Massachusetts Institute of Technology, Cambridge, MA 02139, USA
2. Department of Chemistry, University of Toronto, Toronto, Canada
3. Max Planck Institute for the Structure and Dynamics of Matter, Hamburg, Germany
4. Center for Free-Electron Laser Science and The Hamburg Center for Ultrafast Imaging, Hamburg, Germany
5. Deutsches Elektronen-Synchrotron DESY, Ultrafast Optics and X-rays Division, Hamburg, Germany
6. Department of Physics, University of Hamburg, Hamburg, Germany

Original publication

"Terahertz-driven linear electron acceleration", *Nature Communications* 6, 8486 (2015); DOI: 10.1038/NCOMMS9486

References

1. V. Dolgashev, S. Tantawi, Y. Higashi, and B. Spataro, "Geometric dependence of radio-frequency breakdown in normal conducting accelerating structures", *Appl. Phys. Lett.* 97, 171501 (2010).
2. W. P. Leemans, B. Nagler, A. J. Gonsalves, Cs. Toth, K. Nakamura, C. G. R. Geddes, E. Esarey, C. B. Schroeder, and S. M. Hooker, "GeV electron beams from a centimetre-scale accelerator", *Nature Physics* 2, 696 (2006).
3. S.-W. Huang, G. Cirmi, J. Moses, K.-H. Hong, S. Bhardwaj, J. R. Birge, L.-J. Chen, E. Li, B. J. Eggleton, G. Cerullo, and F. X. Kärtner, "High-energy pulse synthesis with sub-cycle waveform control for strong-field physics", *Nature Photonics* 5 475 (2011).
4. L. J. Wong, A. Fallahi, and F. X. Kärtner, "Compact electron acceleration and bunch compression in THz waveguides", *Optics Express* 21, 9792 (2013).
5. J. Fülöp, Z. Ollmann, C. Lombosi, C. Skrobel, S. Klingebiel, L. Pálfalvi, F. Krausz, S. Karsch, and J. Hebling, "Efficient generation of THz pulses with 0.4 mJ energy", *Optics Express* 22 20155 (2014).

FLASH2 undulators.

Fast wavelength scans with variable gap undulators



Figure 1

The 30 meter long undulators with variable gap allow tuning the wavelength within minutes.

One of the main reasons for a second undulator line was the overbooking of the FLASH facility, which has been growing up to a factor 4 in 2012. This resulted in the project extending the facility by another undulator line in a separate tunnel with space six additional experimental stations in a new experimental hall. Important is that both users get pulse trains at a 10 Hz repetition rate with the flexibility in pulse number, pulse separation, pulse length varied independently for both undulator lines and, especially, that the wavelength can be chosen freely for both users.

After first lasing in August 2014, the setup procedures of FLASH2 have been improved steadily. Fast tunability, made possible with the variable gap undulators (see Fig. 1), was already demonstrated at the beginning of 2015, where a factor of two in wavelength was covered in 0.5 nm steps within 30 minutes. This possibility has been shown on

numerous occasions at several electron beam energies, while FLASH1 delivered beam to users.

After a 4 month shutdown starting in February of 2015, needed to finalize the installation of the photon diagnostics in the FLASH2 tunnel (shown in Fig. 2), FLASH2 has been running in parallel to FLASH1 user operation permanently. The wavelength range from 5 to 60 nm has been covered. The pulse energies achieved so far have been from a few micro joules up to levels exceeding 0.5 mJ, depending on undulator gap and electron beam energies.

A typical result of a wavelength scan is shown in Fig. 3. This scan demonstrates power levels exceeding 100 μ J over the complete range, where the minimum wavelength is similar to the one delivered simultaneously to FLASH1 users. In Fig. 3, no tuning was necessary from 14 to 16 nm.



Figure 2
Photon section in the tunnel during installation with the GMD Intensity monitor, the online spectrometer OPIS, apertures and the MCP intensity detector and the deflecting mirrors.

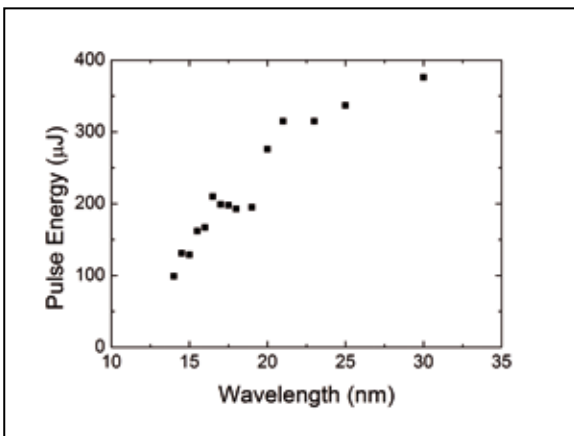


Figure 3
FLASH2 tunability. Results shown are for an electron beam energy of 0.7 GeV, corresponding to a radiation wavelength at FLASH1 of 13.5 nm. The electron charge was around 260 pC in this case.

As can be seen, the pulse energies levelled off between 17 and 19 nm. For wavelengths longer than 19 nm, correction of the incoming angle and position resulted in a further increase of pulse energy. This shows that an orbit feedback could recover the increase in pulse energies that is expected with increasing undulator field, corresponding to a closing of the undulator.

The radiation has been transported to the experimental hall, where the first beamlines are being installed. Transport to the experimental stations will follow in the beginning of 2016, after which the first experiments are planned in parallel to FLASH1 users.

Contact: *Bart Faatz* (bart.faatz@desy.de),
Markus Tischer (markus.tischer@desy.de)

The right time, in the right spots.

All-optical free-electron laser synchronisation enables time-resolved experiments limited only by the pulse duration

X-ray free-electron lasers like FLASH or the forthcoming European XFEL provide intense light pulses with a few tens of femtoseconds in duration in the ultraviolet or X-ray spectral range. With this short-wavelength light, it is possible to image single molecules and atoms, and to determine the structure of solid-state samples. To study dynamics in those specimens, time-resolved experiments are commonly carried out in a pump-probe geometry with the help of an optical laser, where the first pulse is used to initiate dynamics while the second pulse is used to probe the transient structure of the sample. Consequently, the level of synchronisation between the two pulses severely affects the achievable time resolution. Ideally, the synchronisation accuracy is better than the individual pulse durations – and this is addressed successfully at FLASH as reported here.

The level of synchronisation, or arrival time jitter, between the X-ray photon pulse generated by a linear accelerator (linac)-driven free-electron laser (FEL) and the optical pulse from an independent optical laser sets a first limit to the achievable time resolution in a pump-probe experiment. The second, fundamental limit is given by the individual durations of the X-ray and the optical pulses. In the past, so-called timing tools had been developed to determine the pulse lengths and relative arrival time of the pulse pairs, and time-sort the acquired experimental data a posteriori [1,2]. However, these tools typically require specific hardware and may not fit to the experimental geometry or it might not be possible to employ them at all. Moreover, this approach is intrinsically inefficient, if the temporal jitter is larger than the characteristic timescale of the studied dynamical process, i.e. for most relative delays no pump-probe signal is observed. Therefore, it is more desirable to provide synchronisation accuracy better than the pulse

duration a priori, which obviates the need for additional timing measurements in most experiments.

Furthermore, with better synchronisation of critical linac sub-components such as electron gun laser and accelerator cavities the FEL performance in terms of X-ray intensity and stability is improved. This is because the underlying self-amplified spontaneous emission (SASE) process of the FEL depends on the energy and momentum composition of the electron bunch, which is to a large extent affected by the stability of the accelerating fields as well as the timing stability of the laser-driven electron generation. Therefore, FEL user experiments critically depend on the accuracy of synchronisation of the different accelerator subsystems.

A few-femtosecond-level synchronisation of the complete accelerator facility requires a highly stable reference signal distribution beyond the capabilities of conventional radio frequency-based schemes. Thus, at FLASH and the European XFEL an all-optical synchronisation system is being developed and implemented, which augments the radio frequency infrastructure (see Fig. 1, and [3]). The system is based on a low-noise mode-locked optical master laser oscillator, where the timing information is provided by the precise repetition rate of the emitted femtosecond pulse train. It is distributed to the remote accelerator locations on optical fibres, which are actively length-stabilised to few tens of nanometres, resulting in an arrival time stability of the laser pulses of better than 1 fs rms at the end of the fibre.

There, the optical reference pulse train can be utilized for electron beam diagnostics as basis for the accelerator stabilisation. The relative arrival time of an electron bunch is determined by mixing its transient electric field with the optical reference. This information is included in the feedback system which regulates

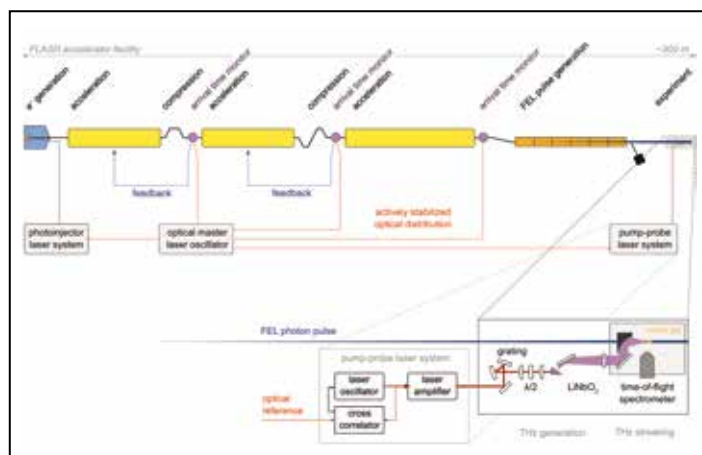
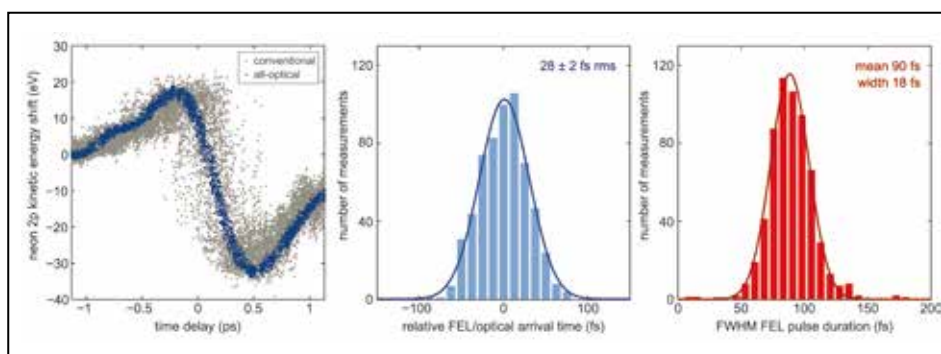


Figure 1
FLASH soft X-ray free-electron laser with its all-optical synchronisation system (upper half) and the experimental arrangement to evaluate the facility-wide performance.

Figure 2

Results from THz photoelectron spectroscopy. Left: Streaking map comparison between conventional, RF-based synchronization of the accelerator (grey) and the new, all-optical scheme (blue). Middle: Relative timing fluctuation between the FEL and the optical laser pulses. Right: Distribution of FEL pulse durations reconstructed simultaneously with the timing jitter.



the accelerating fields in the superconducting cavities to stabilise the electron bunch arrival time to a minimal value – which was 19 fs rms for the specific machine operation parameters in this study. Meanwhile, an even lower electron bunch arrival time jitter is routinely available at FLASH.

The optical reference pulse train can also be used to lock any external laser system to the master laser oscillator. In a balanced optical cross-correlator, where pulses of the external laser and the reference are mixed twice in a nonlinear crystal, the relative timing of these pulses is measured without any disambiguation of their temporal order or any influence of amplitude fluctuation. Employed at the pump-probe laser system at FLASH, this scheme resulted in 5 fs rms timing jitter between the reference and the system's oscillator – improving the performance by almost an order of magnitude compared to the traditional radio frequency-based scheme.

To evaluate the performance of the facility-wide all-optical synchronisation infrastructure single-shot terahertz (THz) photoelectron spectroscopy is utilized (see also [1]). In this experiment, sketched in the lower part of Fig. 1, the FEL photon pulse ionizes neon gas, generating a burst of photoelectrons that resemble the ionizing pulse's temporal shape. When a single-cycle THz pulse is overlapped, the detected kinetic energy distribution of photoelectrons is modified depending on the relative delay of the ionizing FEL pulse and the THz pulse. If the delay (phase) is set such that the overlap occurs at the “streaking ramp” of the THz vector potential, as shown in the left panel of Fig. 2, the relative arrival time between the THz pulse and the FEL pulse can be retrieved. As the THz pulse is generated by optical rectification from the pump-probe laser system this streaking measurement is equivalent to an arrival time measurement between the FEL and optical laser pulses.

The total timing jitter is finally found to be 28 fs rms, as shown in the middle panel of Fig. 2, as a measurement for the overall performance of the synchronisation system. Simultaneously, the temporal FEL pulse profile in this study can be reconstructed from the measured photoelectron spectra and an average pulse duration of 90 fs FWHM (full width at half maximum) was observed demonstrating that all-optical synchronisation schemes push the available temporal resolution for dynamic studies toward the limit given by the FEL pulse duration.

In summary, the interplay of all timing-critical components of FLASH and the all-optical synchronisation system was

evaluated, and results in a total timing jitter of 28 fs rms, which is significantly less than hundreds of femtoseconds of jitter observed in user experiments at FELs with conventional radio frequency synchronisation. On top of that, a more detailed analysis of the uncorrelated contributions to the total timing jitter suggests that the existing infrastructure should support sub-10 fs accuracy when shorter pulses are delivered at FLASH and the European XFEL. Finally, few-femtosecond synchronisation will be mandatory for the development of next-generation seeded free-electron lasers, where the FEL pulse properties can be tailored by an external laser.

Contact: Sebastian Schulz, sebastian.schulz@mpsd.mpg.de
Adrian L. Cavalieri, adrian.cavalieri@mpsd.mpg.de

Authors

Sebastian Schulz^{1,2,3}, Ivanka Grguraš^{2,4,5}, Christopher Behrens^{1,6}, Hubertus Bromberger², John T. Costello⁷, Marie Kristin Czwalinna¹, Matthias Felber¹, Matthias C. Hoffmann⁶, Markus Ilchen⁸, Haiyun Liu², Tommaso Mazza⁸, Michael Meyer⁸, Sven Pfeiffer¹, Paweł Prędki^{1,9}, Sven Schefer⁵, Christian Schmidt¹, Ulrike Wegner^{1,8}, Holger Schlarb¹, and Adrian L. Cavalieri^{2,3,4,5}

1. Deutsches Elektronen-Synchrotron DESY, Notkestraße 85, 22607 Hamburg, Germany
2. Max-Planck-Institut für Struktur und Dynamik der Materie, Luruper Chaussee 149, 22761 Hamburg, Germany
3. The Hamburg Centre for Ultrafast Imaging (CUI), Luruper Chaussee 149, 22761 Hamburg, Germany
4. Center for Free-Electron Laser Science (CFEL), Luruper Chaussee 149, 22761 Hamburg
5. University of Hamburg, Luruper Chaussee 149, 22761 Hamburg
6. SLAC National Accelerator Laboratory, 2575 Sand Hill Road, Menlo Park, California 94025, USA
7. School of Physical Sciences and National Center for Plasma Science and Technology (NCPST), Dublin City University, Glasnevin, Dublin 9, Ireland
8. European XFEL GmbH, Albert-Einstein-Ring 19, 22761 Hamburg, Germany
9. Department of Microelectronics and Computer Science, Lodz University of Technology, ul. Wólanska 221/223, 90-924 Łódź, Poland

Original publication

“Femtosecond all-optical synchronization of an X-ray free-electron laser”, *Nature Communications* 6, 5938 (2015). DOI: 10.1038/ncomms6938

References

1. I. Grguraš et al., “Ultrafast X-ray pulse characterization at free-electron lasers”, *Nature Photonics* 6, 852-857 (2012).
2. M. Harmand et al., “Achieving few-femtosecond time-sorting at hard X-ray free-electron lasers”, *Nature Photonics* 7, 215-218 (2013).
3. J. Kim et al., “Drift-free femtosecond timing synchronization of remote optical and microwave sources”, *Nature Photonics* 2, 733-736 (2008).

X-ray focusing down to below 10 nm.

Novel X-ray optics based on high numerical aperture multilayer Laue lenses

The short wavelength and the penetrating nature of X-rays make this radiation ideal for the microscopic investigation of complex materials. However, taking full advantage of these properties requires advances in the fabrication of optical elements with a nanometre precision, matching the image resolution we wish to achieve. New developments in nanotechnology are finally bringing this goal within reach. We report on first imaging experiments obtained with a multilayer-based volume zone plate that was fabricated in DESY's multilayer lab and tested at PETRA III. Using the method of ptychography a resolution of 8 nm on an image of a grating using 22 keV X-rays was achieved.

Multilayer Laue lenses (MLLs) are promising optical elements for focusing X-rays to nanometre spots. These diffraction based zone plates are based on depth-graded multilayers. The layers in such structures are deposited layer by layer with sub-nanometre precision using magnetron sputtering. The thickness of sputtered layers can be controlled considerably better than the positioning of zones in a lithography process. Large aspect ratios can be easily obtained by slicing the multilayer to the desired thickness. In addition to layer thickness precision, a high-quality lens requires a low film stress and interface roughness. Similar to standard zone plates, used to focus soft X-rays, the resolution of an MLL is determined by its smallest zone height. State-of-the-art multilayer technology achieves multilayers with a period thickness < 2 nm, which means that focusing to a spot of similar diameter should be possible.

The numerical aperture NA of a lens describes the range of angles over which the optic focuses X-rays of a certain wavelength λ . The achievable resolution, or focal spot size, is equal to λ/NA . To achieve significant efficiency in the hard X-ray regime, zone plates must have a much higher optical

thickness than zone plates for soft X-rays. For example, 20 keV X-rays require a 6 μm thick zone plate. Layer spacing follows the Fresnel zone-plate formula (Fig. 1a) but since MLLs are thick they also have to simultaneously obey Bragg's law. This means that each layer has to be properly tilted (Fig. 1b). If Bragg's condition is met at each point in the zone plate the efficiency of a MLL can be as high as theoretical efficiency ($> 60\%$).

We developed a novel and simple method to achieve the desired curvature of these layers. During the deposition, a straight mask is used to cover about half of the substrate [1] and the wedged layers form in the penumbra of this mask. The multilayer is then cut in the position of the desired gradient profile with a focused ion beam. Measurements of MLL's performance at P11 beamline (PETRA III synchrotron) demonstrated that the desired curvature was achieved thus obeying Fresnel zone plate and Bragg's law simultaneously [2]. This gave rise to a much higher NA of the optic and hence higher resolution than could possibly be achieved with an MLL fabricated from parallel layers.

The MLL used in our experiment was an off-axis section of the full ideal zone plate and therefore deflected the focused beam away from the direction of the incident and undiffracted (zeroth order) beam. In this way, only the focused beam illuminates the sample, and a high-resolution scanning microscope can be implemented measuring the X-rays transmitted through the sample as it is rastered through the focus. In addition, a full diffraction pattern at each point of the scan is recorded using a LAMBDA detector [3]. First, the conditions under which the MLL simultaneously matched the layer tilt curvature and the zone plate, had to be found. This was done by measuring far field diffraction to map the efficiency of the zone plate across its pupil. The experimental and simulated data at different energies and zone plate tilts are shown in Figure 2. Note that simulations were assuming

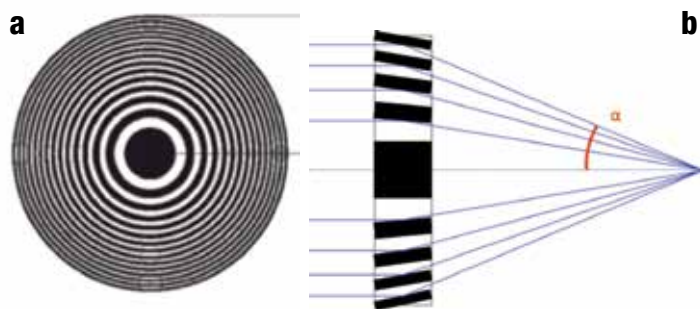


Figure 1
(a) A schematic view of a zone plate. It consists of layers that are getting smaller with increasing radius (Fresnel zone plate law) since smaller zone layers diffract X-rays to a larger angle. (b) A high aspect ratio zone plate (as seen from the side) also has to simultaneously obey Bragg's law, thus requiring that each layer is properly tilted.

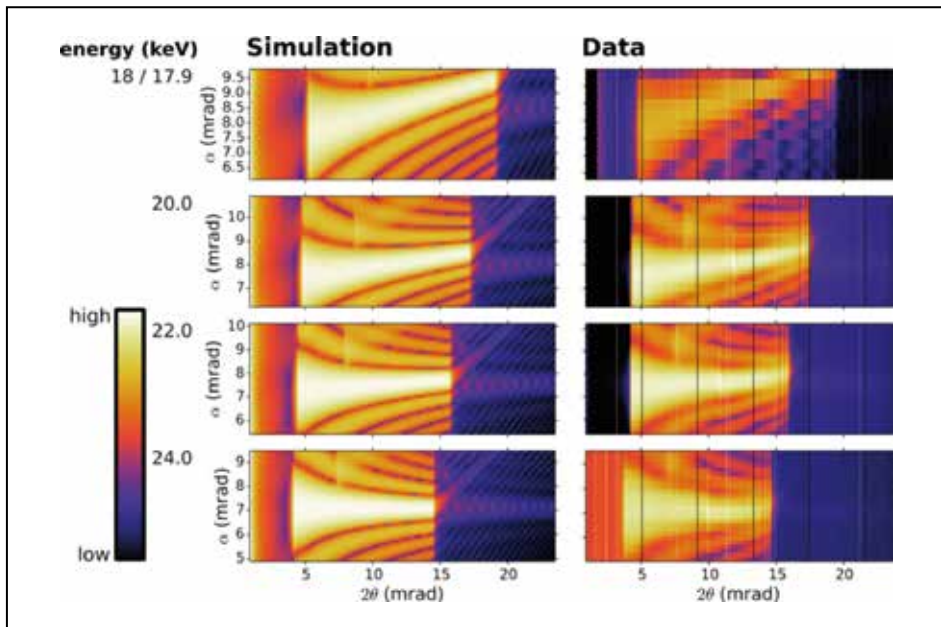


Figure 2

Simulated (left) and experimental (right) diffraction efficiency are plotted for four different energies. In both cases plots of the far-field 1D diffraction of the lens represented as scattering angle versus MLL tilt (α) are shown. Each scan is shown on a log scale. The same intensity scale is used in each plot where low diffraction efficiency is black and high is white. Simulated diffraction efficiencies are calculated for a perfect, wedged MLL while experimental data were collected from the wedged MLL tested at PETRA III.

a perfect MLL structure and calculated using the beam propagation method [4]. 2D plots of the zone plate diffraction efficiency as a function of diffraction angle 2θ and MLL tilt angle α for a given photon energy show a maximum efficiency at one particular lens angle, i.e. horizontal in the plot. For this particular MLL high diffraction efficiency was achieved for energies between 22 and 24 keV.

As a sample we used a sliced periodic multilayer, which is a grating with a known period. This object was placed close to the focus and scanned laterally. At each scan position, a far field diffraction pattern was measured. Since the object was a grating, this pattern is a shearing interferogram of the diverging wave from the focus, which is phase shifted as the grating is stepped through the scan. Using a ptychographic reconstruction, equivalent to interferometric phase determination [2] we determined that the RMS phase error across a major portion of the lens was only about 0.07 rad or 0.016 waves (Fig. 3). Since the X-ray wavelength was only 0.5 Å, this results in a wavefront error of 0.005 Å, representing the most perfect lens for electromagnetic radiation ever made.

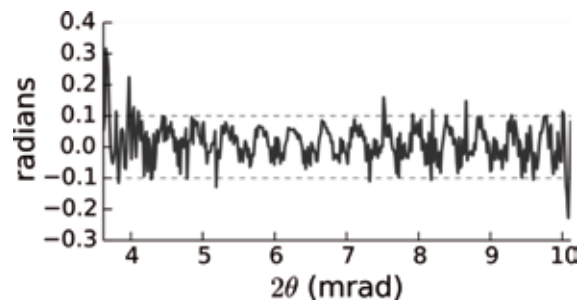


Figure 3

Line phase error of the retrieved pupil across a major portion of the lens. The plot shows a peak to valley variation of about -0.1 to 0.1 radian. This means the RMS phase error is only ~ 0.07 radian.

This technique is being developed further by implementing two dimensional focusing using a matched pair of two crossed MLLs.

Contact: Saša Bajt, sasa.bajt@desy.de

Authors

Andrew J. Morgan¹, Mauro Prasciolu², Andrzej Andrejczuk³, Jacek Krzywinski⁴, Alke Meents², David Pennicard², Heinz Graafsma², Anton Barty¹, Richard J. Bean¹, Miriam Barthelmeß¹, Dominik Oberthuer^{1,5}, Oleksandr Yefanov¹, Andrew Aquila⁶, Henry N. Chapman^{1,5,7}, and Saša Bajt²

- Center for Free-Electron Laser Science, DESY, Notkestrasse 85, 22607 Hamburg, Germany
- Deutsches Elektronen-Synchrotron DESY, Notkestrasse 85, 22607 Hamburg, Germany
- Faculty of Physics, University of Białystok, K. Ciołkowskiego 1L, 15-245, Białystok, Poland
- SLAC, 2575 Sand Hill Rd., Menlo Park, CA 94025, USA
- Dept. of Physics, University of Hamburg, Luruper Chaussee 149, 22607 Hamburg, Germany
- European XFEL GmbH, Albert Einstein Ring 19, 22761 Hamburg, Germany
- The Hamburg Centre for Ultrafast Imaging, Luruper Chaussee 149, 22607 Hamburg, Germany

Original publication

"High numerical aperture multilayer Laue lenses", *Sci. Rep.* 5:09892, DOI: 10.1038/srep09892

References

- M. Prasciolu, A. F. G. Leontowich, J. Krzywinski, A. Andrejczuk, H. N. Chapman, and S. Bajt, "Fabrication of wedged multilayer Laue lenses", *Opt. Mater. Express* 5, 748-755 (2015).
- S. Bajt, M. Prasciolu, A. J. Morgan, H. N. Chapman, J. Krzywinski, and A. Andrejczuk, "One Dimensional Focusing with High Numerical Aperture Multilayer Laue Lens", 12th International Conference on X-Ray Microscopy (XRM 2014), Melbourne, Australia, 26-31 October, 2014, Editors: Martin de Jonge and David Paterson (in press).
- D. Pennicard, S. Lange, S. Smoljanin, H. Hirsemann, H. Graafsma, M. Epple, M. Zuvic, M.-O. Lampert, T. Fritzsche, and M. Rothermund, "The LAMBDA photon-counting pixel detector", *Journal of Physics: Conference Series* 425 062010 (2013).
- A. Andrejczuk, J. Krzywinski, and S. Bajt, "Influence of imperfections in a wedged multilayer Laue lens for the focusing of X-rays investigated by beam propagation method", *Nucl. Instr. Meth. Phys. Res. B* 364, 60-64 (2015).

Simple and advanced X-ray 3D imaging.

Shining X-ray light on sandpaper

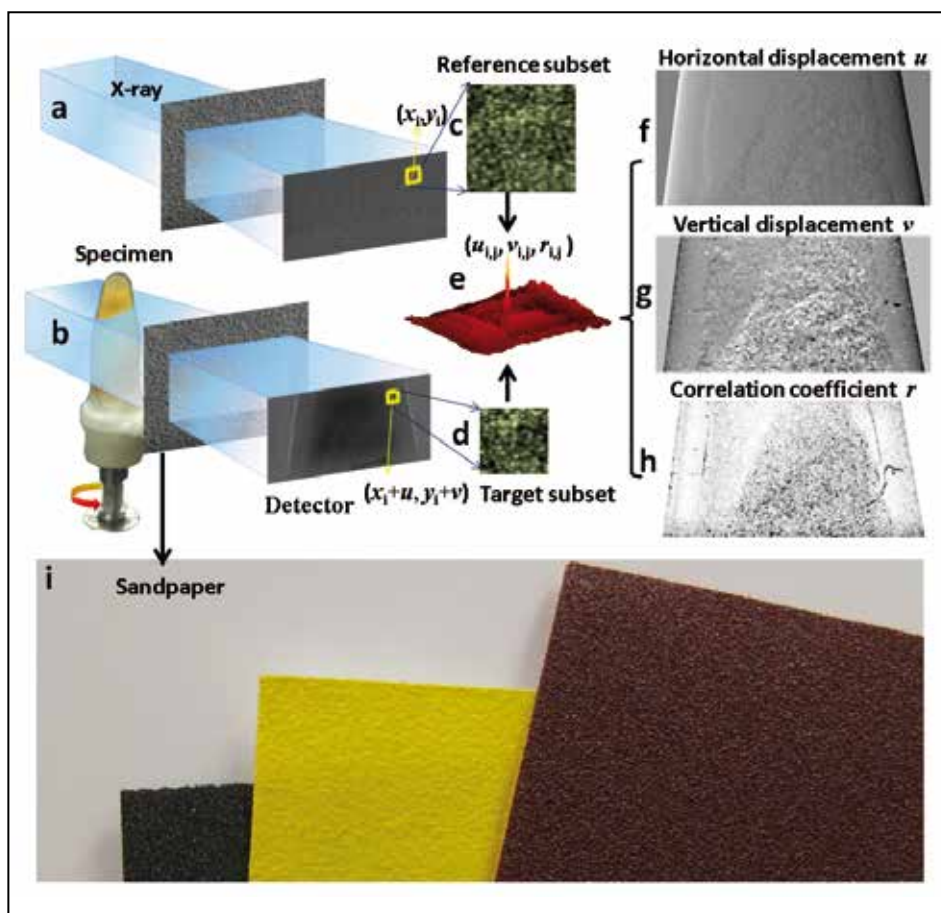
X-rays absorption contrast computed tomography (CT) imaging proves a powerful and invaluable tool for biomedical study and material science. Absorption contrast is however poor for samples with weak absorption. In contrast, phase sensitive imaging can allow significantly enhanced contrast with potential lower radiation dose. However, the extraction of such phase information is quite involved and a sophisticated experimental arrangement often is often required. We present a method for three-dimensional (3D) X-ray phase contrast CT by simply shining X-ray through a piece of sandpaper. The advanced X-ray imaging method allows study of materials in a hitherto unforeseen level.

X-rays have been used for imaging since their discovery in the late 19th century because X-rays can penetrate deep inside objects which are opaque to visible light. Conventional X-ray imaging, known as absorption imaging, takes advantage of the fact that a material has a distinctly different density to its surroundings. An image of a human skeleton is possible as the bones absorb the X-rays passing through the body far

more than the tissue around them. However, producing images of soft tissues is more complex, as there is the range of densities required to produce an imaging using the absorption method. Phase contrast imaging allows the imaging of structures of similar levels of transparency by highlighting small differences in the refractive indexes of the materials within the structure. Although a few X-ray phase contrast

Figure 1

Speckle image (a) without the specimen and (b) with the specimen and the phase object (sandpaper), (c) reference and (d) target subset speckle image, (e) example of correlation coefficient map for the subset, (f) horizontal and (g) vertical displacement and (h) correlation coefficient image, (i) and a photo of sandpaper. The acquisitions were obtained with the sample mounted on a vertical rotation axis. A set of 900 projections with orientation angles ranging from 0° to 180° were used. The phase shift induced by the sample is then derived from the two transverse phase gradients for each projection, and CT reconstructions were then performed using phase image sets. After reconstruction, compared to conventional absorption CT images, the 3D phase CT images show greatly enhanced contrast. As shown in Fig. 2, one can observe the fatty tissue and small features showing a high level of detail. This study shows that phase CT can be performed with a simple experimental setup, and it can be easily implemented since no special optics is involved. The sandpaper is cheap, robust and commercially available. Such a quick and simple technique will help people easily image more complex samples. These features make the technique an attractive candidate for material imaging such as in-vivo imaging of biological systems containing soft tissue.



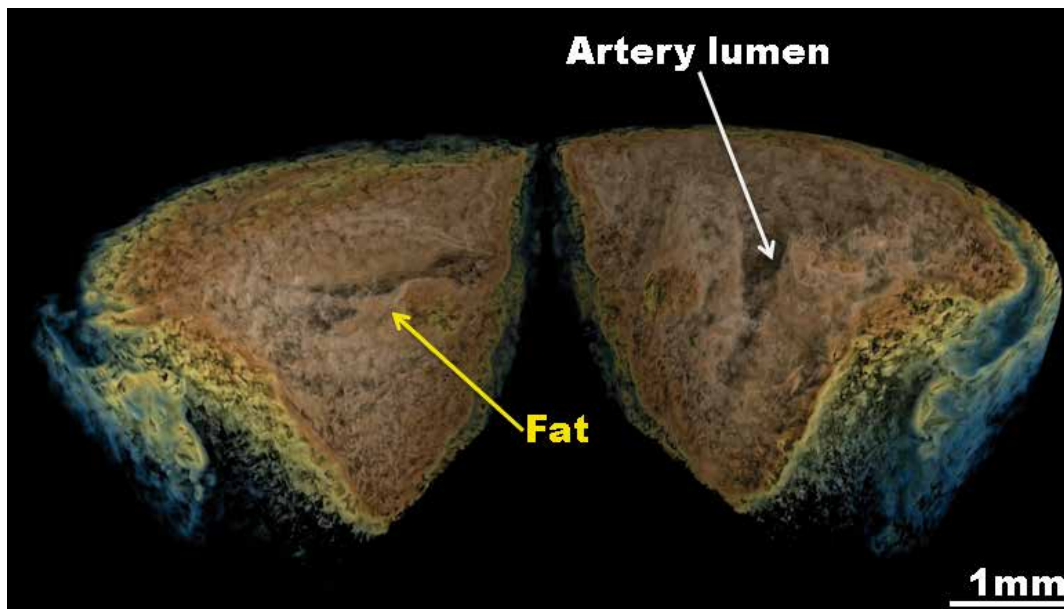


Figure 2

3D rendering of human artery: distinctive contrast can be observed between the artery lumen and fat.

imaging techniques have been developed in the past two decades, many of them are limited by either sophisticated experimental conditions or stringent beam properties. In contrast, an X-ray speckle tracking (XST) technique can produce two-dimensional (2D) phase contrast imaging using a simple experimental arrangement involving only the specimen, an X-ray imaging detector and a phase object containing random high spatial frequency structures [1,2]. Apart from the conventional X-ray radiography, X-ray Computed Tomography (CT) allows visualizing the internal structure of a sample. We presented extension of the XST method from 2D projection to give 3D volumetric phase information using simple materials, such as sandpaper. In addition, we also demonstrate that a dark-field image can be simultaneously generated from the correlation coefficient map by applying the cross-correlation algorithm between the speckle images with presence and absence of sample [3].

The experimental layout is shown in Fig. 1. In Fig. 1a, a partially coherent X-ray beam passes through the abrasive paper and a speckle pattern is produced on the detector caused by interference of the randomly scattered radiation. One image is firstly taken of the speckle and then a second image is taken with the specimen inserted (Fig. 1b). Fig. 1c and 1d show a small subset of the two speckle images. In order to track the changes to the speckle between the two images, a cross-correlation algorithm is employed. A correlation map can be generated for every subset of each reference-sample image pair. Fig. 1e shows the correlation map obtained from the reference subset (Fig. 1c) and target subset (Fig. 1d). The peak value r_{ij} and its position in the correlation map is calculated for each subset of each image. With u_{ij} and v_{ij} corresponding to the in-plane local displacement vector of the speckle pattern caused by refraction in the sample, two displacement maps (u , v) can be made as shown in Fig. 1f and 1g. The wavefront gradient

is calculated as the ratio of this rigid body translation to the distance between the sandpaper and detector. The corresponding correlation coefficient map (r) is shown in Fig. 1h. The correlation coefficient is related to the scattering from the sample and can be used to generate a dark-field image [4]. The X-ray dark-field imaging indicates the different scattering power of different parts of a sample and provides additional and complementary information even though they may have similar absorption contrast.

Contact: Hongchang Wang,
Hongchang.wang@diamond.ac.uk

Authors

Hongchang Wang¹, Sebastien Berujon^{1†}, Julia Herzen^{2††}, Robert Atwood¹, David Laundry¹, Alexander Hipp², and Kawal Sawhney¹

1. Diamond Light Source Ltd, Harwell Science and Innovation Campus, Didcot, OX11 0DE, UK

2. Institute of Materials Science, Helmholtz-Zentrum Geesthacht, Geesthacht, Germany

†Present address: European Synchrotron Radiation Facility, BP-220, F-38043 Grenoble, France

††Present address: Physics Department and Institute of Medical Engineering, Technische Universität München, Germany

Original publication

H. Wang, S. Berujon, J. Herzen, R. Atwood, D. Laundry, A. Hipp, and K. Sawhney, "X-ray phase contrast tomography by tracking near field speckle", *Sci. Rep.* 5, 8762 (2015). DOI: 10.1038/srep08762

References

1. S. Berujon, E. Ziegler, R. Cerbino, L. Peverini, "Two-Dimensional X-Ray Beam Phase Sensing", *Phys. Rev. Lett.* 108, 158102 (2012).
2. Morgan, K. S., Paganin, D. M., and Siu, K. K. W., "X-ray phase imaging with a paper analyzer", *Appl. Phys. Lett.* 100, 124102-124104 (2012).
3. Pan, B., Xie, H.-m., Xu, B.-q., and Dai, F.-l., "Performance of sub-pixel registration algorithms in digital image correlation", *Measurement Science and Technology* 17, 1615 (2006).
4. Wang, H., Kashyap, Y., and Sawhney, K., "Hard-X-Ray Directional Dark-Field Imaging Using the Speckle Scanning Technique", *Phys. Rev. Lett.* 114, 103901 (2015).

A new sample holder for thousands of micro-crystals.

Low background silicon microchip for serial crystallography

At low emittance synchrotron sources it has become possible to perform structure determinations from microcrystals which were previously considered too small for diffraction experiments. These experiments require new sample delivery methods. We have developed a novel sample holder from single crystalline silicon with micropores, which can carry thousands of crystals and significantly reduces the background scattering level. For loading, the suspended microcrystals are pipetted onto the chip and excess mother liquor is subsequently soaked off through the micropores. Crystals larger than the pore size are retained and arrange themselves according to the micropore pattern. Using our chip we were able to collect diffraction data with 1.5 Å resolution from protein microcrystals with sizes of 4 micrometres and smaller in one batch.

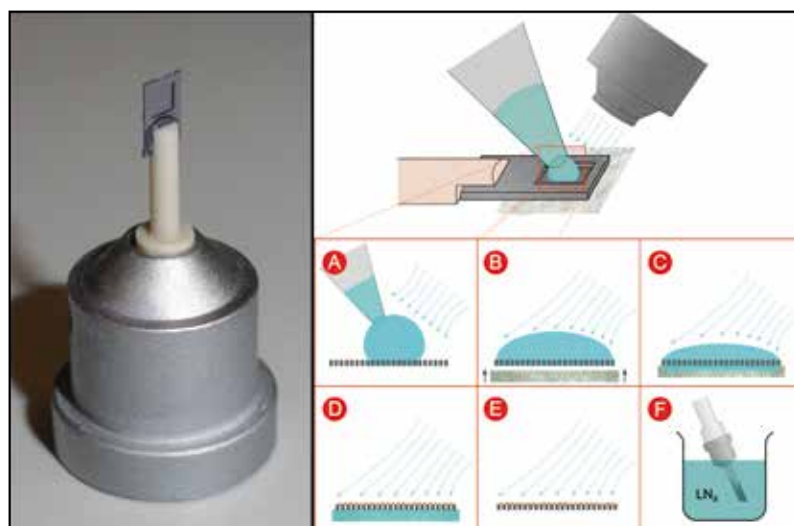


Figure 1

Micro-patterned silicon chip mounted on a standard magnetic cap compatible with data collection at macromolecular crystallography beamlines (left). The loading procedure is illustrated on the right: A droplet of crystal suspension is applied to the chip using a conventional micropipette (A). By attaching a small wedge of filter paper from the lower side (B) the mother liquor is removed (C, D) while the crystals remain in the pores of the chip (E). Dehydration of the crystals during loading is prevented by applying a stream of humidified air. After loading the chip can be flash-frozen by plunging it into liquid nitrogen for subsequent cryogenic data collection (F).

Macromolecular X-ray crystallography (MX) is very powerful method for structure determination from biological macromolecules such as proteins which can be performed both with X-ray laboratory sources and at synchrotron sources. Conventional MX typically requires crystals with sizes larger than 20 microns. For data collection a single crystal is mounted in a nylon loop and subsequently exposed to the X-ray beam. A strong limitation in MX is radiation damage, which causes a loss of diffracting power of the crystals as a function of dose. As a consequence the amount of structural information which can be collected from a given crystal of a certain volume is limited. Therefore, ideally, measurements are performed using large single crystals.

Unfortunately, in many cases only small crystals can be obtained from a certain protein and conventional MX tends to fail here. A recent approach to overcome the limitations of radiation damage in MX is the so called 'diffraction-before-destruction' approach which became recently possible at

X-ray free-electron lasers (XFEL's). Here diffraction patterns from hundreds to ten-thousands of microcrystals are collected by exposing each of them to a high intensity femtosecond X-ray pulse. In so called serial-femtosecond crystallography (SFX) the crystals diffract the incoming X-rays before they are destroyed by them [1,2]. SFX requires the measurement of thousands of crystals for a successful structure determination.

In order to deliver such large number of crystals to the X-ray beam in a reasonable time so called liquid jets have become the standard method for sample delivery at XFEL's. A drawback of this method is the large amount of sample which is required for a structure determination since only a very small fraction of the crystals is hit by the X-ray beam pulses.

Serial crystallography has recently also been successfully employed at synchrotron sources [3,4]. A more efficient sample delivery approach has been proposed by Zarrine-Afsar et al. [5]. They use micro-patterned solid substrates as a sample

holder where the crystals arrange themselves in a periodic array and can be automatically raster-scanned through the X-ray beam.

Following their approach we have developed a micro-patterned chip from single crystalline silicon which acts as a sample holder for thousands of crystals and can be used both at synchrotron sources and XFEL's (Fig. 1). The chip has a $1.5 \times 1.5 \text{ mm}^2$ membrane part with a thickness of about $10 \mu\text{m}$, which is surrounded by an outer frame. The membrane is composed of more than 20,000 holes with sizes of down to $1 \mu\text{m}$ and can be easily loaded with a $\sim 2 \mu\text{l}$ drop of crystal suspension by using a micro-pipette. By attaching a piece of filter paper at the lower side of the chip the mother liquor is soaked through the holes while the crystals are retained by the chip and align themselves according to the pore pattern. Dehydration of the crystals during loading is prevented by applying a stream of humidified air [6]. For measurements at cryogenic temperatures the chip is flash frozen by plunging it into liquid nitrogen after loading. Since the chip is made from single-crystalline silicon, its background contribution is limited to a few silicon Bragg reflections, which only occur at certain orientations and thus can be avoided. The efficient removal of the mother liquor further contributes to a very low background signal.

First serial crystallography experiments using our chip have been carried out on lysozyme and CPV18 microcrystals at beamline I24 at the Diamond Light Source synchrotron. The periodic arrangement of the CPV18 microcrystals on the chip after loading is shown in Fig. 2 (top). For data collection at cryogenic temperatures crystals were centred in the X-ray beam and a series of oscillation images were collected from every crystal. The resulting partial datasets were merged to a complete dataset which was used for structure refinement. Figure 2 (bottom) shows the resulting high-quality electron density maps of CPV18 providing a very high level of structural details.

In summary, our chip very is very well suited as a sample holder for crystallography experiments with micro- to medium-sized crystals. Due to the sieve-like structure all crystals which are larger than the pore diameter are retained by the chip and thus no precious microcrystals are wasted. The use of single

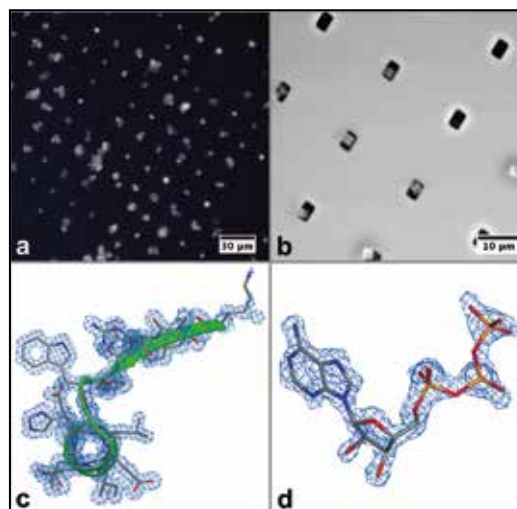


Figure 2

Images of CPV18 microcrystals with a size of up to $4 \mu\text{m}$ loaded onto the silicon chip as observed with differential interference contrast microscopy (a) and environmental scanning electron microscopy (b). The resulting high quality electron density ($2F_o - F_c$ contoured at 1σ) obtained by X-ray micro-diffraction provides a high level of structural details as shown for a portion of the CPV polypeptide chain (c) and a bound ATP (d).

crystalline silicon as substrate material and the effective removal of the mother liquor significantly reduces background scattering which finally results in better data quality than what can be obtained with standard mounting techniques. The periodic arrangement of the crystals on the chip by the pore pattern allows for fully automated data collection by raster scanning of the chip, thereby making most efficient use of the beamtime. The chip is not only applicable to diffraction experiments at cryogenic temperatures but also at room temperature when exposing it to a stream of humidified air.

In addition to experiments at synchrotron sources described here the chip is also very well suited for SFX experiments at XFEL's where a whole chip can be raster-scanned in a few minutes at data acquisition rates of up to 120 Hz.

Contact: Philip Roedig, philip.roedig@desy.de
Alke Meents, alke.meents@desy.de

Authors

Philip Roedig¹, Ismo Vartiainen², Ramona Duman³, Saravanan Panneerselvam¹, Nicolas Stübe¹, Olga Lorbeer¹, Martin Warmer¹, Geoff Sutton⁴, David Ian Stuart^{3,4}, Edgar Weckert¹, Christian David², Armin Wagner³, and Alke Meents¹

1. Deutsches Elektronen-Synchrotron DESY, 22607 Hamburg, Germany
2. Paul Scherrer Institut, Villigen PSI, 5232, Switzerland
3. Diamond Light Source Ltd., Diamond House, Harwell Science & Innovation Campus, Didcot, Oxfordshire, OX11 0DE, United Kingdom
4. Division of Structural Biology, Wellcome Trust Centre for Human Genetics, University of Oxford, Oxford, OX3 7BN, United Kingdom

Original publication

"A micro-patterned silicon chip as sample holder for macromolecular crystallography experiments with minimal background scattering", *Sci. Rep.* 5, 10451 (2015).
DOI: 10.1038/srep10451

Images taken from original publication. Original publication is licensed under a Creative Commons Attribution 4.0 International License (CC BY 4.0).

References

1. H. N. Chapman et al., "Femtosecond X-ray protein nanocrystallography", *Nature* 470, 73–77 (2011).
2. S. Boutet et al., "High-Resolution Protein Structure Determination by Serial Femtosecond Crystallography", *Science* 337, 362–364 (2012).
3. F. Stellato et al., "Room-temperature macromolecular serial crystallography using synchrotron radiation", *IUCrJ* 1, 204–12 (2014).
4. C. Gati et al., "Serial crystallography on in vivo grown microcrystals using synchrotron radiation", *IUCrJ* 1, 87–94 (2014).
5. A. Zarrine-Afsar et al., "Crystallography on a chip", *Acta Crystallogr. Sect. D Biol. Crystallogr.* 68, 321–323 (2012).
6. J. Sanchez-Weatherby et al., "Improving diffraction by humidity control: A novel device compatible with X-ray beamlines", *Acta Cryst. D* 65, 1237–1246 (2009).





Light Sources.

> FLASH

88

> PETRA III

92



Figure 1

The FLASH facility in September 2015. Both adjacent experimental halls “Kai Siegbahn” (FLASH2, centre left) and “Albert Einstein” (FLASH1, centre right) are attached via the office building to the newly constructed PETRA extension hall North (in the right corner). The filled area on top of the FLASH tunnels is slowly covering with vegetation.

FLASH has been in continuous operation in 2015, except for a three weeks interruption in May. The break was needed to add another thousand tons of sand above the FLASH2 electron beam dump and in the area between the two FLASH tunnels to ensure sufficient radiation shielding for operation with maximum beam power. In order to avoid interference with user operation and to leave some flexibility for realigning displaced beamline components, this final civil construction work of the FLASH II project had been shifted to the end of a long beamtime period, in which 4152 hours of beamtime were provided for user experiments between February 2014 and May 2015.

On 15 June, a new user period started as planned with 167 shifts (12-hours) scheduled for 20 experiments in five beamtime blocks until 21 December 2015. This 2nd period marked the transition to regular half-year periods and two

calls for proposals per year with deadlines 1 April and 1 October. In the first half of 2016, 183 shifts are scheduled for 19 projects while 366 shifts were requested in total by 34 submitted proposals. For the first time, four of the 19 approved projects will be performed on FLASH2. In the future, with FLASH1 and FLASH2 operating fully parallel, it will be possible to schedule the same number of experiments in half a year for which a year was needed before. Assuming a constant proposal rate, this would lead to a reduction of the overbooking from currently about a factor four down to a factor two. Certainly the start of European XFEL and SwissFEL in 2017 will add further dynamics.

Overall, FLASH operation was remarkably stable during the user periods in 2015. An example of a 24 hour period with nearly constant pulse energy of about 100 μJ after a scheduled set-up time of ~ 4 hours in the beginning is shown



Figure 3
The two cylindrical vacuum chambers house two plane mirrors which steer the FLASH2 photon beam into the FLASH experimental hall "Kai Siegbahn".

in Fig. 2. Beam availability was in the usual high range of 96 % and down-times could be compensated with contingency time, except for 2.5 days loss of beamtime in June. A lightning stroke severely damaged the personal interlock system.

In 2015, about one third of all experiments at FLASH were performed on beamline BL1 using the CAMP chamber. CAMP is a multi-purpose end station for electron and ion spectroscopy, pump-probe and imaging experiments, the latter taking advantage of two large-area, single-photon counting 1 Megapixel pnCCD detectors with a pixel size of $75 \times 75 \mu\text{m}^2$, which is now permanently installed. After a successful year of experience with user operation CAMP is in high demand for various projects, not only because of the unique detectors but also because the system is versatile and well equipped for a wide range of gas phase

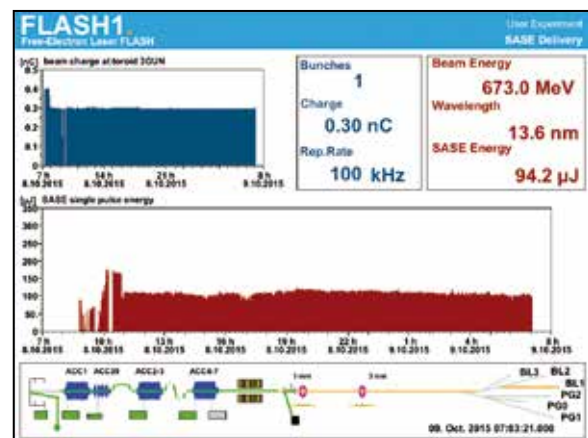


Figure 2
The FLASH1 status display shows the beam parameters (top panel), the FEL pulse energy in μJ for a 25 hour period on 8-9 October 2015 (middle) and a graphical representation of the beam path (bottom).



Figure 5
Installation of the first two beamlines in the FLASH experimental hall “Kai Siegbahn” (November 2015).

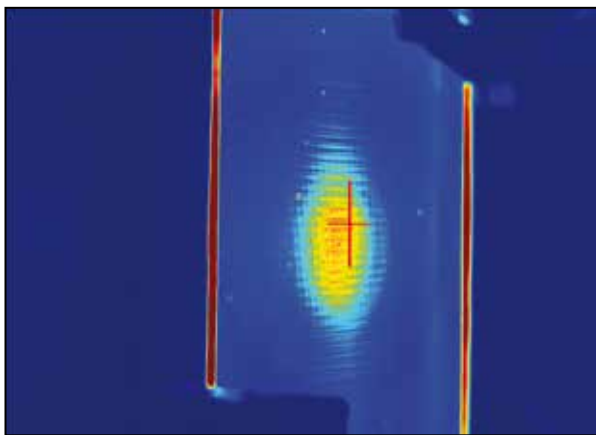


Figure 4
The first FLASH2 photon beam on a YAG screen in the experimental hall “Kai Siegbahn”. The interference pattern is produced by the mesh of an intensity monitor in the FLASH2 tunnel.

experiments. Last but not least, experiments using CAMP are very convenient and efficient for users because the system is permanently installed and serviced and supported by experienced facility staff. However, as frequent changes between very different CAMP configurations become inefficient and overload limited staff, it is considered to install an additional end station with a complementary configuration on another beamline in the future.

Two further permanent end stations will become available for user experiments in 2016: The Raman spectrometer on PG1 in the experimental hall “Albert Einstein” and the reaction microscope (REMI) on FL26 in the experimental hall “Kai Siegbahn”. The commissioning of the Raman spectrometer progressed very well in 2015 but was more laborious than expected; the first user experiment is planned in December 2015. REMI will be installed on FL26

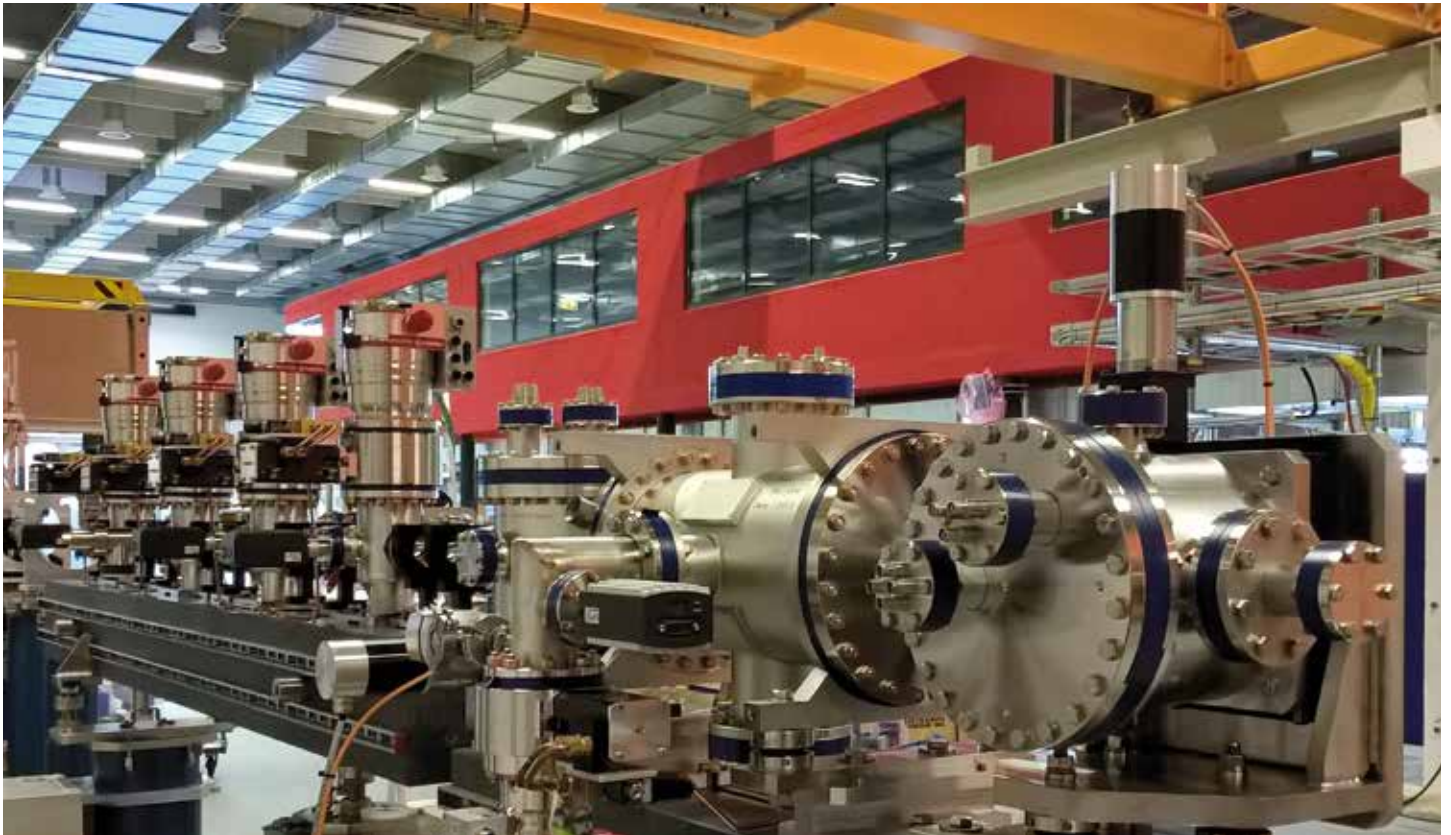


Figure 6
Photon diagnostics in the experimental hall "Kai Siegbahn".

early 2016 and first experiments should be possible by summer.

In parallel to the user operation of FLASH1, all the vacuum installations of the photon beam transport system in the FLASH2 tunnel were completed between December 2014 and April 2015, including the final photon diagnostics components and two plane mirrors.

The mirrors steer the FLASH2 beam into the experimental hall "Kai Siegbahn" at fixed position and angle, and also produce a parallel beam offset for shielding in the tunnel (Fig. 3). Since end of May FLASH2 has been running continuously in parallel to FLASH1 with its own commissioning and test programme which is, however, constrained by the machine parameters required for the user experiments on FLASH1. The latest achievements are reported in the

research highlight section of this report. The first FEL beam was already transported to the experimental hall in June (Fig. 4).

The installation of the first two beamlines, FL24 and FL26, as well as the photon diagnostics in the experimental hall "Kai Siegbahn" is still ongoing (Fig. 5 and Fig. 6). It is planned to finish this work early in the year 2016, including the set-up of the "Reaction Microscope" (REMI) as permanent end station on FL26, and to perform the first experiments in summer 2016. However, it will take till early 2017 until the Kirkpatrick– Baez (KB) focusing optics has been delivered and installed on FL24 and until the new optical burst-mode laser system will become available for two-colour pump-probe experiments with femtosecond-scale resolution.

Contact: Josef Feldhaus, josef.feldhaus@desy.de



Figure 1

Aerial view of the PETRA III experimental hall "Max von Laue" at DESY and the two new extension halls in the east (upper left corner) and north (lower right corner) in September 2015.

From January 2014 until April 2015 PETRA III was not operational for users to accommodate the PETRA III extension by raising two further experimental halls and preparing the installation of new beamlines. For this work the PETRA III storage ring had been partially demolished and reconstructed with new components. First beam was stored in mid of February 2015 and already at the end of March 2015 X-rays were available for the commissioning of the beamlines. The operation for users was successfully resumed on 27 April and continued without longer shutdown periods until 12 November, adding up to 2630 hours beam time for scheduled users. The average availability was 95 %. The call for proposals for the first half of 2016 (excluding EMBL beamlines) was very successful: 550 proposals were submitted. This number includes already 36 proposals for the new PETRA III extension beamlines P64 and P65. The new beamlines will offer first user beam in the early summer 2016.

On 12 November 2015 a shutdown period of PETRA III has started which will last until 7 April 2016 when the regular user run will be resumed. During this shutdown new frontend components will be installed. A call for proposals for beam times in the second half of 2016 is scheduled, the deadline is 1 March 2016. The new beamlines P64 and P65 will offer first user beam in the early summer 2016.

Storage ring tunnel

After rebuilt of the storage ring to accommodate the new PETRA III extensions beamlines P21-P25 and P61-P66 the

operation of PETRA III was restarted successfully with keeping the electron beam parameters fully within specifications. In 2015 roughly 60 % of the operation was dedicated to time resolved X-ray experiments with filling patterns of 40 or 60 electron bunches in the storage ring. Especially in the 40 bunch mode the highly charged electron bunches suffer from short life times of 1.3 h. The lost electrons can cause a local activation of machine components inside the PETRA III tunnel which end of the year has been observed at a few ring components indeed. In order to make sure that no further parts in the PETRA III ring tunnel will be activated during operation, in the future the share of 40 and 60 bunch filling patterns will be reduced to 50 % or less.

In the past, some experiments, in particular nuclear resonant scattering measurements, suffered from side bunches between the main bunches. Compared to the main bunch, the charge of these side bunches is five orders of magnitude smaller. Caused by intra beam scattering or during the top-up procedure they appear at well-defined time delays from the main bunch (e.g. at 8 ns offset). To strip off the side bunches a 'cleaning' procedure has been established at PETRA III. It can be executed on demand and removes side bunches pattern within a few seconds.

New concept for data transfer

Since 2013 all PETRA III beamlines P01-P14 are fully operational for users. During the year 2015 several experimental stations have been upgraded. Moreover the high data rates created

by fast detectors needed a new concept for the data transfer from the beamlines to the analysis facilities which had to be developed. A step towards a faster data management system was made by the SPEED project of DESY and IBM. It is based upon an upgraded hardware infrastructure – like the network to connect all fast detectors with one or more 10 GB links. In addition newly installed proxy nodes buffer the incoming data in parallel and transfer them to the storage nodes at an enhanced speed. This new system has been successfully installed and is in operation since April 2015. It works together with the new control software SARDANA which now runs at most of the DESY beamlines at PETRA III.

New detectors and optics

Two new fast detectors are available since at PETRA III beamlines: an EIGER 4M (*DECTRIS Ltd.*) detector for beamlines P10 and P06 as well as a LAMBDA 2M detector with a GaAs sensor (*X-Spectrum GmbH*) for beamline P02 (see Fig. 2). Both are capable to run at a 2 kHz frame rate and will make efficient use of the high ‘SPEED’ system.

Two beamlines have been equipped with new optical components. At the Extreme Conditions Beamline P02.2 an iridium coated double X-ray mirror has been installed. The mirrors pass the full undulator harmonics to the experiment and depending on the photon energy the gain in flux is about a factor of 100 as compared to the standard crystal monochromator. The high photon flux in combination with the above mentioned LAMBDA detector will be used for time resolved investigations of matter under extreme conditions with 0.5 millisecond time resolution. First commissioning data prove the potential of this new setup.

At the Helmholtz-Zentrum Geesthacht HZG imaging beamline P05 a multilayer monochromator was integrated in the beamline optics to achieve a gain in flux of roughly a factor of ten as compared to standard crystal monochromators. The advantage of multilayer monochromators is a ‘cleaner’ X-ray beam as well as a higher resolution compared to coated double mirrors. The setup is under commissioning and will be used to significantly enhance the throughput of micro- and nano-tomography.

Further large installations

To satisfy the requests of an increasing number of user experiments with biological samples a preparation laboratory



Figure 2
LAMBDA 2M GaAs detector (*X-Spectrum GmbH*) at the Extreme Conditions Beamline P02.2 at PETRA III.



Figure 3
Vertical X-vis Rheometer setup at the PETRA III beamline P10.

for biological materials has been installed in the PETRA III experimental hall ‘Max von Laue’. It complies with the biosafety level ‘BSL-2’. Accordingly, BSL-2 classified experiments are possible at most beamlines under corresponding safety regulations.

A vertical rheometer setup has been installed at the Coherence Applications Beamline P10. It combines X-ray with visible light enabling structural rheology on all length scales from molecules to macroscopic dimensions (see Fig. 3). Several experiments have already been conducted with great success.

In the frame of a BMBF project from University of Kiel, the new optical pump laser for investigations of the response of surface near molecules on light has become operational at the High Resolution Diffraction Beamline P08. First experiments have been conducted successfully.

At the Resonant Scattering and Diffraction Beamline P09 an X-ray magnetic dichroism (XMCD) setup has been installed and commissioned. The maximum magnetic field is 1.2 T and 0.8 T when using a cryostat. First successful experiments have been conducted.

In the next year it is planned to upgrade the optics of selected beamlines by introducing further stabilized monochromators, germanium crystals for better flux throughput and focussing elements to achieve smaller foci. This will further enhance the capabilities of PETRA III beamlines.

Contact: Oliver H. Seeck, oliver.seeck@desy.de,
Rainer Wanzenberg, rainer.wanzenberg@desy.de



Figure 4

Top: View of the PETRA III extension hall east and the CSSB building in the background. Left: View of the extension hall north. (December 2015).

PETRA III Extension

The construction of the two PETRA III extension halls, technical hall infrastructure and beamlines continued in 2015 in parallel to the re-commissioning of the rebuilt storage ring in the spring and the user operation of beamlines in the experimental hall “Max von Laue” until the scheduled shutdown in the middle of November. The major work concentrated on the second phase of the hall civil engineering consisting of the facade (Fig. 4), completed in the summer, and the completion of the interior which has been going on throughout the rest of the year.

For the technical building infrastructure priority was given to extension hall north to meet the time schedule for the planned start of commissioning of the two phase 1 canted undulator beamlines P64 and P65 in sector 3. They are both dedicated to X-ray absorption (XAFS) techniques. Unexpected issues of an external contracted company had led to serious delays in the installation of the cooling water supply. In order not to compromise the start-up of the new beamlines, considerable efforts have been made by DESY infrastructure groups to temporarily implement a separate local cooling water system.

The construction of the two beamlines proceeded in parallel, making use of scheduled service periods to install the undulators and to complete the electrical connections, media and interlock systems of the frontends inside the ring tunnel. Following the construction of the experimental and control

hutches, the installation of the optical beamline components (Fig. 5) and their media infrastructure including the computing network could be completed in time for the technical commissioning.

An important milestone for the startup of both XAFS beamlines, the mandatory technical review of the radiation safety interlock and the permission of operation issued by the state authorities, could be reached in the second week of September. First white beam in the optics hutch was seen shortly after and the commissioning of beamline P65 began on 23 September (Fig. 6).

Following the initial beamline alignment and monochromator tests, beam for test experiments at P65 was available middle of October, a pre-requisite for the first successful experiments of an external user group in the last days before the shutdown. In these *in situ* experiments, temperature dependent reduction processes on Pt/ceria/alumina catalysts were studied successfully by measuring Pt L_3 -edge XANES.



Figure 5

Installation of components in the optics hutch of the two XAFS beamlines P64 and P65 in sector 3 of the PETRA III extension hall north (August 2015).

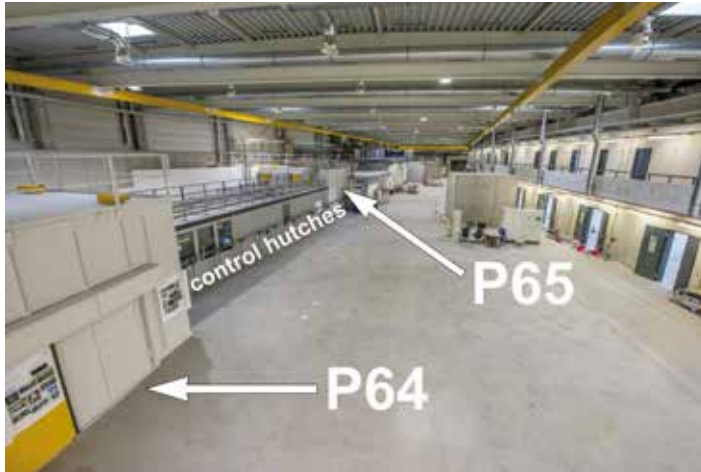


Figure 6
View into extension hall north showing the completed experimental hutches for beamlines P64-65.

The commissioning of beamline P64 could not be achieved in full extent as planned. During this phase it was noticed that changing the gap of the 2 meters long undulator induces a severe distortion of the electron beam orbit. A careful investigation revealed that magnetic fringe fields of the canting dipole magnets between the undulators interfere with the undulator frame and magnet structure causing this effect. A thorough quantitative analysis of different options to solve the problem has been performed by the DESY undulator group. A reconstruction of the dipole magnet coils combined with additional magnetic shielding seems to be a suitable solution. However, this substantial modification requires some effort and considerable time so that provisional measures will have to be taken to allow an operation of the beamline for experiments in 2016 - with somewhat limited capabilities. The temporary workaround uses gap controlled compensating fields from additional magnet coils which have already been tested to some extent. A monochromatic beam at the experiment was not available before the shutdown, beamline commissioning will resume after machine startup in March 2016. It is noted that the undulator used at P65 has a short magnet structure which is not affected by the dipole fringe fields. Beamlines P22-P24 in hall east will be operated with long undulators and hence also need modified canting dipole magnets.

In hall north, the damping wiggler beamline P61 will only be implemented as a phase 3 beamline. However, the "Large Volume Press" (LVP) instrument for the downstream section of the beamline has already been installed at its final position in September (Fig. 7). This custom-designed 6-ram LVP is funded by the German 'Federal Ministry of Education and Research' (BMBF) and implemented within the collaboration of the Bavarian Geo-Science Institute (BGI, University of Bayreuth) and DESY. Until the beamline will finally be completed, it is planned to use the LVP off-line for materials synthesis, which is of considerable interest for a sizeable user community as

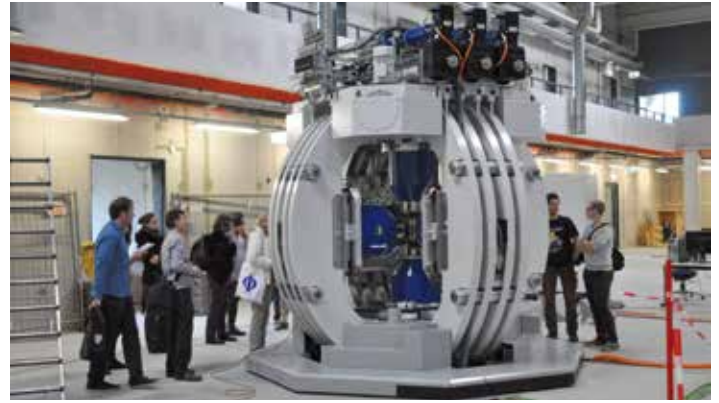


Figure 7
Large volume 6-ram press for beamline P61 installed in place (September 2015).



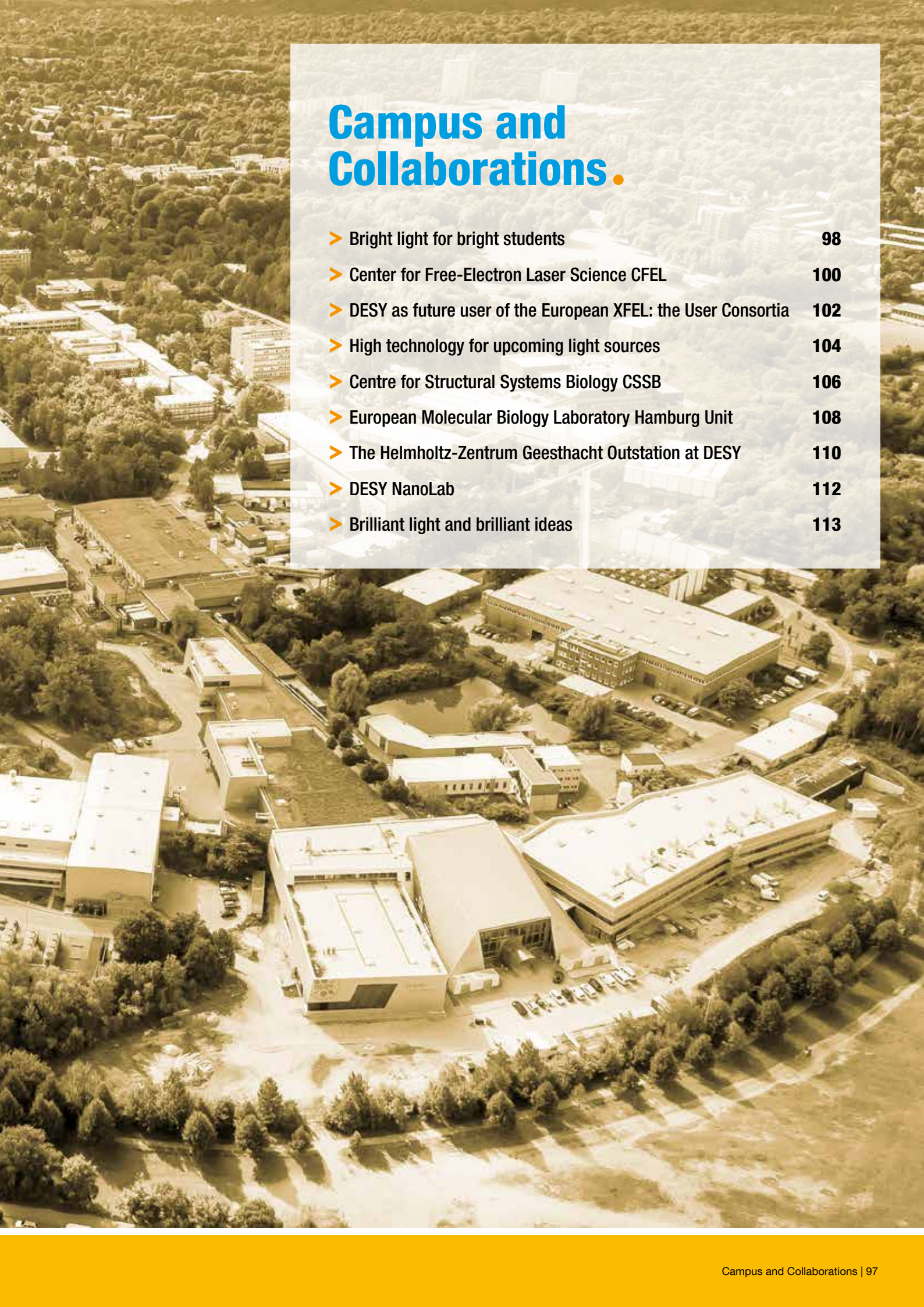
Figure 8
View into PETRA III extension hall east showing the completed experimental hutches for beamlines P21-24.

discussed during a dedicated workshop held at DESY in September.

In hall east, the front ends for undulator beamlines P22-P24 are being installed in the winter shutdown 2015/16. All experimental hutches have been set up (Fig. 8) and the installation of control hutches for P21 and P24 is ongoing. The call for tender for the 4 m long in-vacuum undulator of the Swedish high-energy X-ray materials science beamline P21 has been published in December 2015, contracts for the Laue-monochromator and the surface diffractometer have been signed. The detailed design of the rather complex beamline frontend has been completed and construction of components will start soon. The frontend installation is planned for the shutdown beginning in January 2017. New instrumentation for hard X-ray electron spectroscopy experiments at beamline P22 - built in collaboration with India - is being commissioned at beamline P09 in the experimental hall "Max von Laue". At P23, the German-Russian nano X-ray diffraction beamline, the new custom designed heavy load diffractometer has been installed in the experimental hutch. In 2016, the installation of all phase 2 beamlines in hall east will be pursued with high priority.

Contact: Wolfgang Drube, wolfgang.drube@desy.de





Campus and Collaborations.

- Bright light for bright students 98
- Center for Free-Electron Laser Science CFEL 100
- DESY as future user of the European XFEL: the User Consortia 102
- High technology for upcoming light sources 104
- Centre for Structural Systems Biology CSSB 106
- European Molecular Biology Laboratory Hamburg Unit 108
- The Helmholtz-Zentrum Geesthacht Outstation at DESY 110
- DESY NanoLab 112
- Brilliant light and brilliant ideas 113

Bright light for bright students.

DESY and Universities: a long-standing tradition



Figure 1

Lively discussions during the poster session of the “PIER graduate week”, October 2015.

A strong bond with Universities has been part of the DESY history from the very beginning. In photon science, this tradition traces back to the early days of synchrotron radiation, beginning at DORIS, the first storage ring at DESY to become a completely dedicated X-ray source, and is continuing with PETRA III and FLASH. A dedicated funding programme of the German ministry for research and education (BMBF) has enabled many German universities to contribute instrumentation and manpower to experimental stations over the years, thus playing a vital role in the development of the facilities and in their operation. Maybe even more importantly, the programme has fostered a close intertwining of scientists from both sides, in research as well as in education. Innumerable master and doctoral theses have been based on work performed at DESY.

With its oldest university partner, the University of Hamburg, DESY established PIER – Partnership for Innovation, Education and Research – as a new platform to foster their long-standing collaboration (Fig. 1, 2). With other Universities in northern Germany, Kiel and Göttingen are prominent examples, DESY is also developing common strategies to nourish scientific excellence and to closely cooperate in the education of scientists and professionals at high level.

University of Hamburg

One of the three focus research areas of the Physics Department of the University of Hamburg is photon science. Activities in this area centre mainly on big collaborative research projects such as the Federal Centre of Excellence “CUI – Hamburg Centre for Ultrafast Imaging”, the SFB 925 “Light induced dynamics and control of correlated quantum systems” (which has been successfully re-evaluated this year) and the BMBF priority program FSP 302 “Free-Electron Lasers”. Researchers from the University, DESY and other partner institutions on campus (e.g. EMBL, MPSD, European XFEL) collaborate on forefront research topics in photon science. Embedded into the collaborative research projects is a strong educational program which is also a central part in the PIER partnership between University and DESY. Consequently, graduate students in physics and nanoscience can choose among a large variety of courses devoted to photon science which are in many cases taught jointly by colleagues from DESY and the University. Even more important, students find a unique environment for their Bachelor, Master, or PhD thesis work on the University Campus in Bahrenfeld. Furthermore, university groups as well as their DESY counterparts offer students the possibility to join and participate in research projects already during their undergraduate studies.

Last year, the institutions on Campus have established a new joint weekly colloquium – the Hamburg Photon Science Colloquium. It brings eminent scientists from physics, chemistry, and life science with a common interest in Photon Science to Hamburg. This colloquium gives students the opportunity to interact with international leaders in the field and is a good example of how joint efforts are of benefit to all participants.

The presence of the Physics Department on Campus will grow further in the next years when the new Center for Hybrid Nanostructures (CHyN), which has seen the laying of the foundation stone this year, will be finished (Fig. 3). CHyN will be home to the groups of the Institute for Nanoscience and Solid State Physics (the former Institute for Applied Physics). In the long run, plans for the Physics Department foresee relocation of all teaching activities as well as of all research groups except the astronomical observatory to the Campus.

Christian-Albrecht University of Kiel

The Christian-Albrecht-University of Kiel (CAU) has been a long standing partner of DESY. After many years of successful cooperation, DESY and CAU signed an agreement establishing the “Ruprecht Haensel Laboratory” in 2011. It is named after the late Prof. Ruprecht Haensel, one of the pioneers of synchrotron radiation at DESY, ESRF founding director and former President of CAU. Scientists from CAU have set up and currently operate a number of instruments funded by the BMBF. These include a spin and momentum resolved photoemission experimental station, ASPHERE III (group K. Roßnagel/L. Kipp), an X-ray diffractometer for liquid interfaces LISA, equipped with an optical laser for pump-probe investigations, (group O. Magnussen/B. Murphy) and the joint CAU/Helmholtz-Zentrum Geesthacht Nanofocus Endstation of the P03 Beamline (group M. Müller/C. Krywka). These facilities are integrated in the PETRA III experimental portfolio. DESY and CAU are planning joint professorships in the near future to strengthen teaching in close proximity to the Kiel research focus Nano, Surface and Interface Science (KiNSIS).

Georg-August University of Göttingen

Recently, DESY and the Georg-August-University of Göttingen (GAU) established a joint professorship (S. Techert), which plays a bridging role between the two partners and enhances the cooperation in the field of structural dynamics in chemical



Figure 2

Students from the University of Hamburg together with DESY colleagues demonstrate soft X-ray fluorescence applications in materials science at the city-wide “Nacht des Wissens” on 7 November 2015 in the experimental hall “Max von Laue”.

systems. Special emphasis is given to the development of time-resolved x-ray diffraction methods.

At PETRA III, the University of Göttingen (group T. Salditt), also a long-term partner of DESY, has designed and realized the “Göttingen Instrument for Nano-Imaging with X-Rays” (GINI-X), dedicated to coherent nano-diffraction and imaging. Using a powerful combination of optical X-ray components, this instrument enables a beam focus down to 5 nm. Scientific efforts in these fields are also reflected in DESY related SFBs which have been granted to the Göttingen University by the DFG, including the SFB 755 “Nanoscale Photon Imaging”, SFB 1073 “Energy conversion on an atomic length scale” and the contribution to various Helmholtz Virtual Institutes.

The extremely fruitful cooperations with national and international universities will grow even stronger in the years to come, with DESY acting as partner but also as enabler of ambitious scientific endeavours.

Contact: Wilfried Wurth, University of Hamburg and DESY, wilfried.wurth@desy.de

Bridget Murphy, University of Kiel, murphy@physik.uni-kiel.de

Simone Techert, University of Göttingen and DESY, simone.techert@desy.de



Figure 3

A picture of the new Center for Hybrid Nanostructures (CHyN) construction site in December 2015.

Center for Free-Electron Laser Science CFEL.

Three institutions working successfully together within CFEL

In 2015, CFEL continued to grow despite the fact that the CFEL building is full with over 400 employees of which 85 % are scientists. Additionally, the planning of the new MPI building for the CFEL groups of the Max Planck Institute for the Structure and Dynamics (MPSD) has been started by the same architects that created the CFEL building. The construction start is scheduled for summer 2016 and the building will be placed next to the CFEL building between the Laser Physics Building, the Hamburg University workshop and PETRA III. Besides new lab, seminar and office space of about 5000 m², this new building will be rounded off with its own computer centre, a workshop, and a cafeteria.

On April 10th 2015 the Hamburg Photon Science Colloquium started its first semester with nine internationally renowned speakers in CFEL. The central idea is to form a well-recognized, very well attended common colloquia series with excellent speakers representing all Photon Science research fields and beyond. All colleagues from the University of Hamburg (UHH), the MPSD, DESY, European XFEL and Helmholtz-Zentrum Geesthacht (HZG) that are working in the area of Photon Science are jointly organizing this colloquium.

This year's edition of the biennial conference on femtochemistry FEMTO12 was hosted by CFEL, the Hamburg Center for Ultrafast Imaging (CUI), and DESY. The conference was organized and chaired by Jochen Küpper and took place



Figure 1
Nobel Laureate Ahmed Zewail received the "Tower of Light" from FEMTO12 chair Jochen Küpper (UHH & DESY-CFEL) for his public scientific "Leuchtturm" lecture on "Light and Enlightenment".

within the framework of UNESCO's International Year of Light. Highlights included the recording of molecular movies of chemistry in action, laser-controlled molecular dynamics, electron and energy transport for solar energy harvesting, and ultrafast processes in biochemical and biological systems.

On November 7th CFEL attracted almost 10000 visitors at the Night of Knowledge and DESY Open Doors Day 2015. With over 30 hands-on experiments on two floors and a 3 × 3 × 3 metre 3-D crystal lattice in front of the building for an acoustic demonstration of diffraction and interference (Fig. 2) CFEL was a major attraction on the campus.

CFEL Coherent Imaging Division leader Henry Chapman was awarded with the prestigious Gottfried Wilhelm Leibniz Prize from the German research foundation DFG. He received the 2.5-Million-Euro research prize for his pioneering work in the development of femtosecond crystallography. The technique allows obtaining the scattering image with X-ray lasers before destruction by the intensive light, thus creating the preconditions to investigate samples almost in their natural environment.

Two CFEL research group leaders received ERC starting grants. Melanie Schnell is supported with 1.499 Million Euro for her independent Max Planck research group "Structure and Dynamics of Cold and Controlled Molecules" at the MPSD. Her awarded "ASTROROT" project aims at combining broadband microwave spectroscopy and observation data from next generation telescope arrays, to investigate chemical processes in the universe. She also received the Akademie-Preis für Chemie 2015 by the Akademie der Wissenschaften zu Göttingen. Sebastian Loth is supported with 1.988 Million Euro for his Max Planck Research Group "Dynamics of Nanoelectronic Systems" at the MPSD and the Max Planck Institute for Solid State Research in Stuttgart. His awarded "dasQ" project plans to identify ways to utilize the quantum-mechanical effects which only occur in nanoelectronic systems for technological developments.

The CFEL junior research group of Andreas R. Maier from the UHH is part of the successful Horizon2020 project „EuPRAXIA“, which was awarded a total of 3 Million Euro and started November 2015. The EuPRAXIA consortium is coordinated by DESY and consists of 16 laboratories and universities from 5 EU member states and additional 18 international associated partners. Andreas Maier's group will work on a design study



Figure 2

3-D crystal lattice made from 125 35 cm diameter balls. The model demonstrates the effects of diffraction and interference acoustically by means of a loudspeaker which injects a 150 Hz sine tone onto the crystal. The audience was invited to find spots of constructive and destructive interference by wandering around the model. The idea came from Ben Whitaker in collaboration with Mike Nix of Leeds University and was realized by artists Lawrence Molloy and Dominic Hopkinson. The piece represents a synergistic interaction between art and science in a work that lures the audience to participate in a physical experiment to explore the art.

for an European Plasma Research Accelerator, with a special focus on plasma-driven Free-Electron Lasers.

The German-Russian collaboration VUVFAST is supported from German and Russian funding institutions with up to 2.1 Mio Euro for three years. The German part is led by Michael Rübhausen from the CFEL UHH-Advanced Study Group and the Institute for Nanostructure and Solid State Physics (INF) and Robert Blick from the INF. VUVFAST intends to develop and utilize ultrafast vacuum UV spectroscopy methods at PETRA III and at Siberia-2 in order to understand and improve the performance of modern condensed matter devices.

The collaborative research centre SFB 925 „Light induced dynamics and control of correlated quantum systems” was positively evaluated this year and will be funded by the Deutsche Forschungsgemeinschaft for another four year period. Several CFEL members (A. Cavalleri, M. Drescher, M. Eckstein, U. Fröhling, I. Gierz, R. Santra, O. Vendrell, W. Wurth) are PIs in the SFB.

Two CFEL-DESY groups were successful within the DFG priority program “Quantum Dynamics in Tailored Intense Fields” (QUTIF). Oliver Mücke and Franz Kärtner with “SOLids in Strong Terahertz and Infrared CE-phase stable waveforms” (SOLSTICE) and Jochen Küpper in collaboration with the Max Born Institute in Berlin with “Laser-Induced Electron Diffraction off strongly aligned and oriented molecules by tailored laser and DC electric fields” (LIED).

Robin Santra, the head of the CFEL-DESY Theory Division, was elected fellow of the American Physical Society (APS). He was awarded for his successful theoretical description of light-matter interactions. Dwayne Miller, MPSD director and head of the CFEL-MPSD Atomically Resolved Dynamics Division, was elected fellow of the Optical Society of America (OSA). He was awarded for his groundbreaking development of ultrabright femtosecond electron sources for probing atomic motions on

the primary timescales governing chemistry. Andrea Cavalleri, MPSD director and head of the CFEL-MPSD Condensed Matter Dynamics Division, was elected fellow of the Institute of Physics. He was awarded with the German-British Max Born Prize for his time-resolved measurements of photoinduced phase transitions in correlated electronic materials. He also received the Dannie-Heineman-Preis 2015 of the Minna-James-Heineman-Stiftung Hannover. Angel Rubio, MPSD director and head of the CFEL-MPSD Theory Division, was inducted as foreign associate of the U.S. National Academy of Sciences. He is awarded for his pioneering development of tractable first principles tools for calculating excited state properties of materials.

Former PhD student Cassi Hunt from CFEL-MPSD was awarded a Miller Research Fellowship 2015, which will allow her to pursue a three-year postdoctoral research stay in Berkeley. Antonia Karamatskou from the CFEL-DESY Theory Division was awarded a Louise Johnson Fellowship by CUI to perform theoretical research on the superconductivity of fullerides in the group Oriol Vendrell Romagosa. The second Louise Johnson Fellowship by CUI was awarded to Diana Monteiro who just received her PhD from the University of Leeds in the group of Arwen Pearson from CUI and CFEL. Diana will continue her work in Hamburg and will develop new methods for time-resolved biophysical studies. Cornelius Gati was awarded a postdoc fellowship through the Human Frontiers Science Program that funds research in the biological sciences. Directly after finishing his PhD in the Coherent Imaging Division he took up his award at the University of Oxford.

Four Humboldt Research Fellowship for Postdoctoral Researchers were awarded to the MPSD: Cristóbal Pérez and to Sérgio Domingos, both in Melanie Schnell’s group, James McIver in Andrea Cavalleri’s group and Xinxin Cheng in Dwayne Miller’s group.

Contact: Ralf Koehn, ralf.koehn@cfel.de

DESY as future user of the European XFEL: the User Consortia.

Strong partnerships for excellence

The European XFEL in Hamburg will offer worldwide unique opportunities for new scientific discoveries in research on complex matter using extremely brilliant light. DESY, besides being responsible for the construction and the operation of the European XFEL linear accelerator, prepares itself for a strong role as European XFEL user. The in-house research performed at the DESY Photon Science division, together with its long-standing experience in instrument and methods development at large photon sources, puts DESY in an ideal position for this role. Consequently, DESY is one of the most committed partners in the User Consortia at the European XFEL. User Consortia are groups of research institutions sharing a scientific goal and joining forces to realize advanced experimental capabilities at European XFEL, providing significant contributions – hardware, personnel – to the technical infrastructure. Up to now, seven consortia were accepted by the European XFEL Council after evaluation and are now being implemented. DESY is strongly engaged in five of them, being the lead institution of four and the second major partner in a fifth.

Together with the Helmholtz-Zentrum Dresden-Rossendorf (HZDR), DESY was able to attract substantial funding by the Helmholtz Association to establish three major instrumentation projects, the Helmholtz International Beamlines (HIB). Each of them is proposed as part of an international User Consortium for the European XFEL and led by DESY or HZDR. These User Consortia are:

SFX

Serial femtosecond crystallography and solution scattering at European XFEL, led by DESY. This consortium will contribute experimental instrumentation to the European XFEL for high-throughput structure determination of (nano)-crystalline biological macromolecular samples. The femtosecond pulses overcome radiation damage and

give the potential for measuring dynamics with high time resolution. The instrument utilises the spent beam from the Single Particles, Clusters, and Biomolecules (SPB) endstation, allowing two sets of experiments to be carried out simultaneously. Together, these stations form the innovative SPB/SFX beamline of European XFEL (Fig. 1). The SFX user consortium is comprised of members of the scientific communities in Germany, United Kingdom, Sweden, Slovakia, Switzerland, United States and Australia. Scientific coordinator: Henry Chapman, CFEL/DESY, henry.chapman@desy.de

HIBEF

Helmholtz International Beamline for Extreme Fields at the European XFEL, led by HZDR. This UC will establish high-power and ultra-intense lasers as well as high-field magnets and high-pressure cells at the High Energy Density (HED) endstation of the European XFEL. It will extend the scope of research that can be carried out at the HED instrument in a variety of science fields, including strong-field physics, relativistic laser plasmas, high-pressure planetary- and astrophysics, and magnetic phase transitions (Fig. 2). Scientific coordinator: Thomas Cowan, HZDR t.cowan@hzdr.de

hRIXS

Momentum-time resolved resonant inelastic X-ray scattering at the Heisenberg Limit at European XFEL, led by DESY in Cooperation with the University of Potsdam. This consortium will build a high resolution spectrometer complementing the capabilities of the Spectroscopy and Coherent Scattering (SCS) instrument in order to allow resonant inelastic X-ray scattering experiments at the transform limit in time and energy (Fig. 3). This proposal includes core partners from Germany, Switzerland, Finland, France, Sweden, Italy, and the UK as well as a broad international user's community. Scientific coordinator: Alexander Föhlisch,

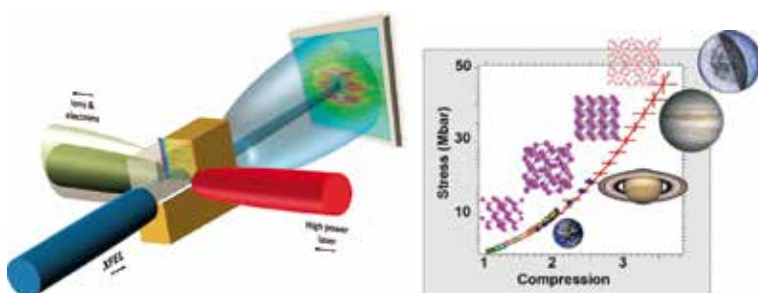


Figure 2

HIBEF Science. (Left) Ultra-intense laser-solid interactions probed by small angle X-ray scattering to reveal spatial modes of bulk plasma response driven by relativistic electron transport instabilities. [Phys Plasmas 21, 033110 (2014)]. (Right) Dynamic compression of carbon with High Energy lasers, indicating new high-pressure phases and complex unit cell structures, which are relevant to conditions inside of large planets and exoplanets. [Rev Mod Phys 84, 1607 (2012)].

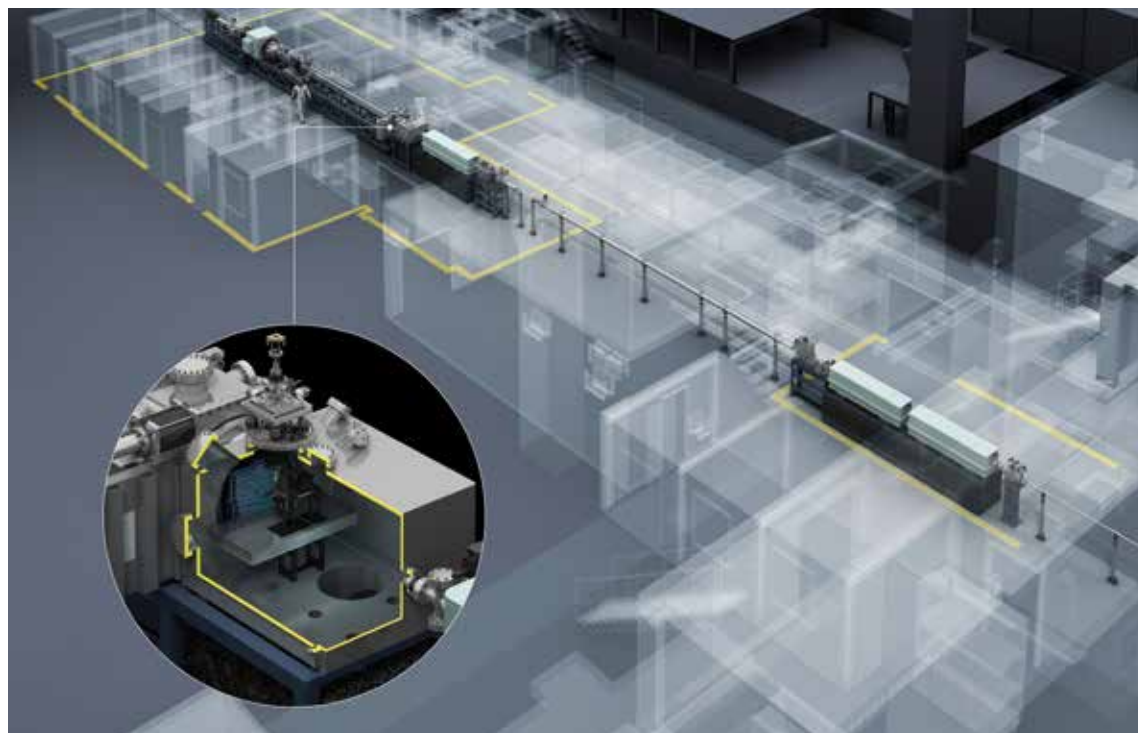


Figure 1

General view of the SPB/SFX beamline at European XFEL.

Helmholtz-Zentrum Berlin HZB and Univ. Potsdam,
alexander.foehlich@helmholtz-berlin.de

In addition to the above large instrumentation HIB projects Helmholtz International Beamlines, DESY leads two additional User Consortia:

DataXpress

A user consortium providing data analysis software and supporting hardware aiming at solving the data and reconstruction challenge for serial crystallography and single particle coherent diffraction experiments at the European XFEL. This proposal is led by DESY, and includes other partners from Germany, Sweden, and the USA. Scientific coordinator: Anton Barty, DESY, anton.barty@desy.de

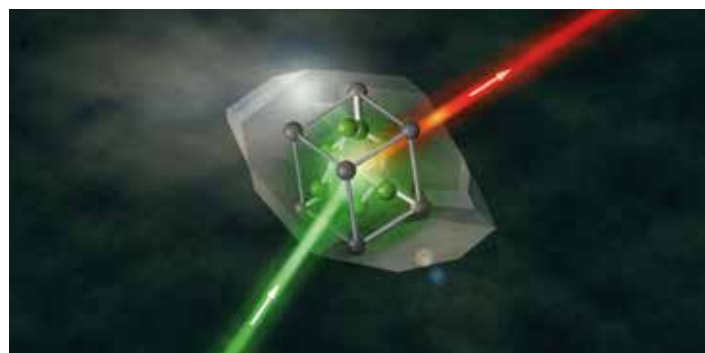


Figure 3

Excited state dynamics govern chemistry and transient materials properties. hRIXS will follow these dynamic pathways with time resolved soft X-ray resonant inelastic X-ray scattering and non-linear X-ray interactions (from: "Stimulated X-ray emission for materials science" Nature 501, 191–194 (2013)) with unprecedented precision. This unique selectivity will beat the complexity of dynamic pathways and trace the flow of excitations between selected atomic moieties.

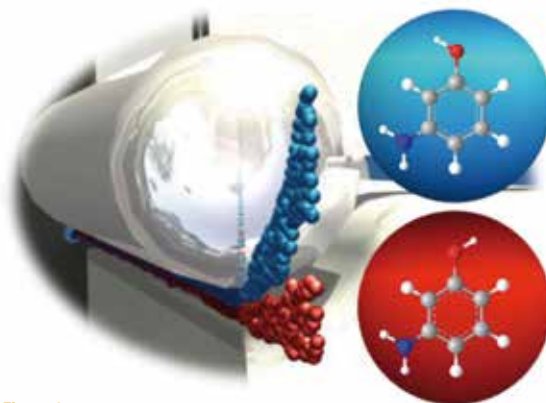


Figure 4

Structural isomers of complex molecules generally have different electric dipole moments for the same mass, which can be exploited to separate them using electric fields. The electric deflector disperses a molecular beam according to the dipole-moment-to-mass ratio, similar to a prism for light. This has been utilized in the production of samples of molecules all in one quantum state as well as the separation of cluster sizes and structural isomers, such as molecular conformers.

COMO

Controlled delivery of state-, size-, and isomer-selected samples of polar molecules and clusters for XFEL molecular-frame-imaging studies using soft and hard X-ray FEL radiation. The consortium will provide a molecular-beam-injector setup (Fig. 4) that can be attached to the European XFEL instruments, in particular Small Quantum Systems (SQS) and Single Particles, Clusters, and Biomolecules (SPB). This consortium is entirely run by DESY.

Scientific coordinator: Jochen Küpper, CFEL/DESY and Univ. Hamburg, jochen.kuepper@desy.de.

*Contact: Edgar Weckert, edgar.weckert@desy.de
Lucia Incoccia-Hermes, lucia.incoccia-hermes@desy.de*

High technology for upcoming light sources.

DESY develops new instrumentation for the European XFEL and beyond

Since 1994, DESY has been playing a key role in the development and scientific application of X-ray free electron lasers. The proof-of-principle experiments at the TESLA Test Facility (TTF) demonstrated the SASE (self-amplified spontaneous emission) FEL concept in the vacuum ultraviolet in the years 2000-2002 and initiated a number of X-ray FEL projects worldwide. TTF was extended to what is now FLASH, starting user operation in 2005, and DESY proposed and prepared the construction of the European XFEL. Early on, DESY started developing all the necessary technology including novel single shot photon diagnostics, femtosecond synchronisation and burst-mode pump-probe laser systems and initiated intense cooperation with national and international partners. It coordinated several European projects and also played a key role in forming the FELs OF EUROPE collaboration, in which all European FEL facilities and initiatives are now organised. Two prominent examples of new instrumentation developed by DESY are presented here.

The Adaptive Gain Integrating Pixel Detector (AGIPD) for the European X-ray Free-Electron Laser: Ultra-Fast and Adaptable

It was clear from the beginning that the European X-ray Free-Electron Laser (XFEL), with its extreme peak brilliance and unique time structure, needed conceptually new and tailor-made X-ray detectors. In 2007 AGIPD was one of the three projects selected, and now, 8 years later, this unique system is in the final development phase, with foreseen delivery of the first 1-million-pixel camera in the beginning of 2016, and a second identical camera foreseen for the end of 2016. Two of

the most difficult challenges were the large dynamic range of more than 10^4 and the extreme frame-rate of 4.5 MHz. In order to deal with the large dynamic range, the AGIPD consortium (DESY, PSI, Universities of Hamburg and Bonn) developed the adaptive gain concept, where every pixel automatically adapts its gain to the incoming signal strength. In this way every pixel can distinguish single photons from noise, with enough confidence so there are no false-positives in a 1 million-pixel image, as well as record more than 10^4 photons of 12 keV in a single pulse.

Since with current technology it is still impossible to readout a 1 million-pixel camera with a 4.5 MHz frame rate, the AGIPD consortium decided to store the images inside the pixels in an analogue memory, with random access and veto capabilities. Each image can be recorded in less than 150 nanoseconds, which is faster than the 220 nanoseconds (corresponding to a frame-rate of 4.5 MHz) required by the European XFEL, and fast enough for timing mode operations of various storage rings. The analogue memory is read out and digitized in the 99.4 millisecond gap between bunch trains of the European XFEL. In order to keep the pixel size at an acceptable level of 200 micrometre squared, the analogue memory had to be limited to 352 images per pixel.

Over the years various small-sized prototypes were designed, fabricated and tested, both in the laboratory and at various storage rings. From these tests it became clear that an ultra-fast imager with single photon sensitivity and large dynamic range is not only of interest to FELs, but will also find applications in time resolved storage ring experiments. These prototypes led in 2013 to the first version of the full sized readout chip, which was used to construct a full module with 512×128 pixels, depicted in Fig. 1a. 16 such modules will be used to construct the 1 million-pixel cameras, which consist of four independently movable quadrants.

Extensive testing of the system over the last 2 years, including single bunch imaging at 6.5 MHz at the APS, have revealed a number of small imperfections. These are corrected in a redesign of the readout ASIC, which will be submitted for manufacturing by the end of 2015. The improved ASICs can then be implemented into the system before first light of the European XFEL, which is expected by the end of 2016.

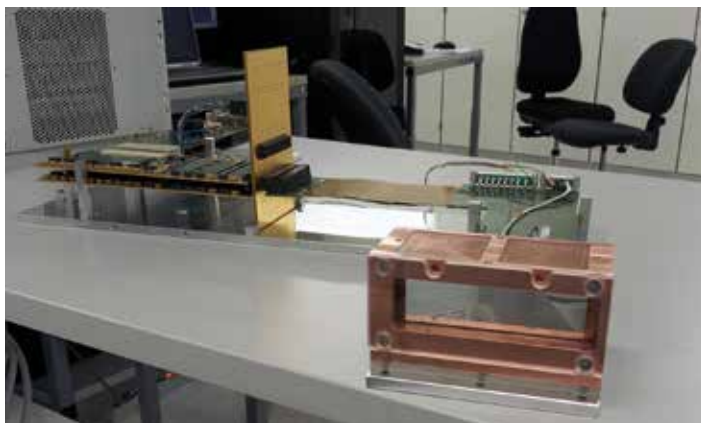


Figure 1
128 × 512 pixel module: module in the cooling block in front, electronics behind;
16 of such modules will form the 1 million-pixel camera.

Contact: *Heinz Graafsma, heinz.graafsma@desy.de*



Figure 2

X-ray gas-monitor detector XGM for European XFEL and SwissFEL. The chambers on the left and on the right represent the upgraded FLASH type gas monitor detectors (GMD) equipped with split Faraday cup electrodes for absolute photon intensity and beam position (horizontal and vertical) monitoring. The two chambers in the middle are huge area multipliers providing an extended dynamic range for beam position as well as pulse energy measurements.

Photon energy monitor for European XFEL and SwissFEL. Feel the hard X-rays

Currently, two new hard X-ray FEL facilities in Germany and Switzerland (European XFEL and SwissFEL) are under construction. Both facilities expect to have first light at the beginning of 2017. In order to make efficient use of these new light sources, precise knowledge of important photon beam parameters such as pulse energy is naturally essential. This requires the use of diagnostic tools which operate in parallel to the user experiment in a non-destructive way. Furthermore, due to the SASE (Self-Amplified Spontaneous Emission) specific shot-to-shot fluctuations, pulse-resolved diagnostics which measure each individual pulse are mandatory. Intensity monitors for X-ray FELs have to cover a large spectral range from the soft X-ray regime up to 24 keV as well as a very extended dynamic range from spontaneous emission to SASE in saturation. To accomplish these demanding requirements a state-of-the-art gas monitor detector (GMD) has been developed based on the FLASH GMD. The latter has been in continuous operation since 2005 [1] and moreover, a modified FLASH type GMD is also in use as a permanent device for the SXR (Soft X-ray Materials Science) instrument at LCLS [2, 3] since 2012.

When an FEL pulse passes through the ionization chamber of the GMD detector, the rare gas inside is ionized, and an electric field accelerates the ions upwards and the electrons downwards to be detected by Faraday cups. The absolute number of photons in each pulse can be deduced with an uncertainty of less than 10 % from the resulting electron and ion currents. Furthermore, the FEL pulse passes between two split electrode plates, allowing the pulse-resolved determination of the horizontal and vertical position of the beam. The gas in the ionization chamber has a very low pressure of between 10^{-2} – 10^{-4} Pa, and thus it is nearly transparent to the FEL pulse that proceeds unaltered to the experimental stations.

For the challenging hard X-ray regime, DESY developed an upgraded version of the GMD, the so-called XGM (Fig. 2, 3), which includes in addition huge area open electron multipliers (HAMP) developed in-house by the FLASH team. The latter

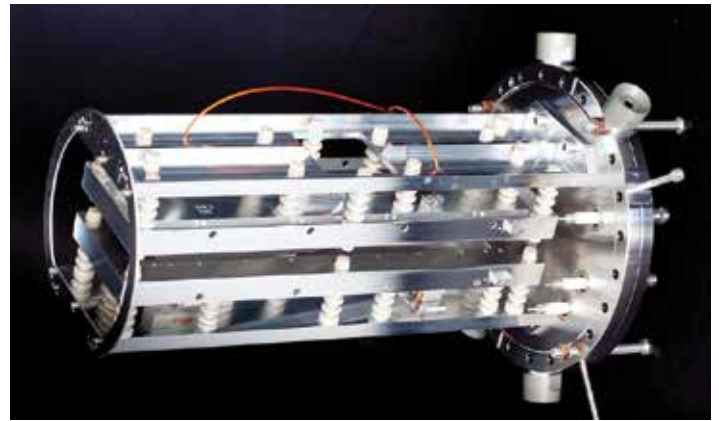


Figure 3

Inner parts of the upgraded version of the GMD with split Faraday cup electrodes. The beam passes from left to right on the centre flange axis.

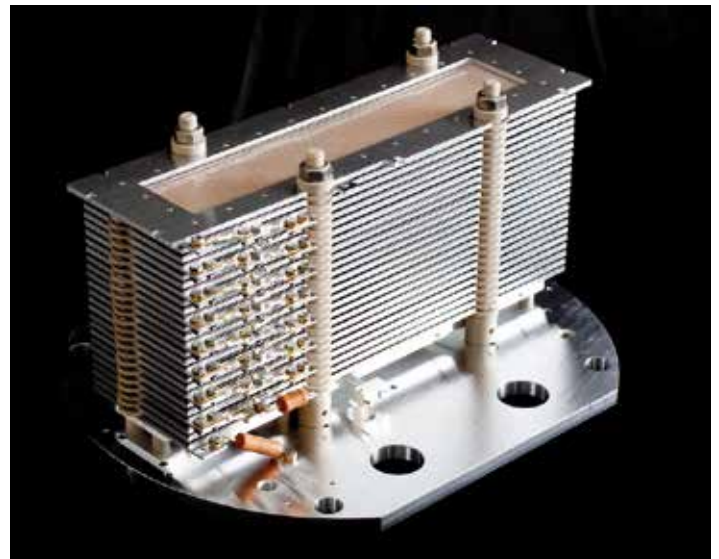


Figure 4

Huge area (20 cm × 5 cm) multiplier (HAMP) consisting of 24 CuBe meshes. The detector provides a gain of more than seven orders of magnitude. The FEL beam passes from left to right above the top mesh.

provides an extreme dynamic range of more than seven orders of magnitude (Fig. 4).

In total seven XGM devices have been assembled, tested, and finally calibrated in the extreme UV regime at the Metrology Light Source of the Physikalisch-Technische Bundesanstalt in Berlin during the last years. These devices are now ready to be permanently installed at the European XFEL and SwissFEL as an essential part of their photon diagnostics section enabling pulse-resolved intensity and photon beam position monitoring.

Contact: Kai Tiedtke, kay.tiedtke@desy.de,
Andrey Sorokin, andrey.sorokin@desy.de

References

1. K. Tiedtke et al., J. Appl. Phys. 103, 094511 (2008).
2. K. Tiedtke et al., Optics Express 22, 21214 (2014).
3. S. Moeller et al., J. Synchrotron Rad. 22, 606-611 (2015).

Centre for Structural Systems Biology CSSB.

Taking shape and gathering speed



Figure 1
CSSB building construction site
(30 October 2015, DESY Webcam)

Infectious diseases are a global threat and many have no available treatments. In addition, certain pathogens are becoming increasingly resistant to existing treatment options. The Centre for Structural Systems Biology (CSSB) builds a bridge between structure and systems biology. CSSB combines structural and molecular biological methods and imaging techniques with systems biology approaches to further our understanding of the molecular mechanisms of the infection processes. This knowledge will enable the development of better treatment methods against both bacterial and viral pathogens.

For structural biology research, the CSSB uses the world-leading, high brilliant X-ray light source, PETRA III, as well as the free-electron laser European XFEL which will be available for use in 2017. Advanced imaging technologies such as cryo-electron microscopy and “omics”* techniques available at CSSB will complement the existing structural biology analytical techniques. With this combination, pathogens will be studied over a range of different scales – zooming in to locate single atoms within a molecule, and likewise panning out to observe the dynamics of host-pathogen interactions happening in real time – creating a complete picture of the infection process.

In February 2015, Michael Kolbe accepted a joint appointment by the Helmholtz Centre for Infection Research (HZI) and the University of Hamburg (UHH) to become a W3 professor at the CSSB. The CSSB now has seven appointed group leaders. At present, CSSB’s research activities are still lacking a common building and therefore take place at various

partner sites. The research groups of Christian Löw (EMBL), Joerg Labahn (HZJ) and Martin Hällberg (CSSB Research Hotel) are already situated on the DESY research campus, near the future CSSB building. The groups of Tim Gilberger (BNITM, UHH) and Matthias Preller (MHH) are currently working at the sites of their home institutes. The research groups of Michael Kolbe (HZI), Thomas Marlovits (UKE) and Kay Grünewald (HPI, UHH, Oxford University) will remain at their previous home institutes until the CSSB building becomes operational.

The construction of the new CSSB building on the DESY Campus is proceeding rapidly. The four floor building will have over 3,000 square metres of laboratory space with room for up to six electron microscopes. The construction of the building’s shell was completed this summer and the building’s façade will be in place by the end of the year. The opening ceremony is expected to take place in early 2017.

A year of milestones

2015 was a year filled with important milestones for the CSSB. Many important steps were taken this year toward

*Note: The neologism omics informally refers to a field of study in biology ending in *-omics*, such as genomics, proteomics or metabolomics. Omics aims at the collective characterization and quantification of pools of biological molecules that translate into the structure, function, and dynamics of an organism or organisms.



Figure 2

CSSB topping-out ceremony
(from left to right):
Prof. Matthias Wilmanns,
Dr. Karl Eugen Huthmacher,
Kristin Alheit, Prof. Helmut Dosch,
Katharina Fegebank.

defining the CSSB's research initiatives and establishing the CSSB within the scientific and local community.

The CSSB milestones in 2015 included:

1st CSSB International Symposium

The 1st CSSB International Symposium, "Systems in Infection Biology – From Molecules to Organisms," took place at the Bernhard Nocht Institute for Tropical Medicine, Hamburg, from April 9-11, 2015. Approximately 130 participants attended the symposium with international speakers from the US, UK, Canada, Spain, Switzerland, Austria, and Israel. The symposium featured presentations from 25 invited speakers as well as additional talks selected from submitted abstracts. The symposium concluded with a panel discussion about the possible definition of "Structural Systems Biology". The outcome of the symposium had a major impact on subsequent discussions about the future CSSB Research Concept. The symposium was funded by and planned in cooperation with the Joachim Herz Stiftung.

CSSB Spring School

From 13-17 April, 17 PhD and post-doctoral students attended the first CSSB Spring School "Structural Systems Biology – From Molecules to Organisms" on the DESY Campus. The spring school was taught by CSSB group leaders and contained courses in sample preparation and analysis, advanced microscopy, single particle analysis, structure determination at atomic resolution and modelling of structure and dynamics of complexes. The spring school

was also funded by and planned in cooperation with the Joachim Herz Stiftung.

Public science event

On 7 September 2015 at 19:00, CSSB and the Academy of Sciences and Humanities in Hamburg hosted a moderated discussion for the general public with the title "Pathogens under super microscopes: a journey into invisible worlds". The panel discussion featured four renowned experts who not only discussed the threats infectious diseases such as Ebola and HIV pose to our health but also explained how scientists are working together to develop new methods and techniques for combating these infections.

Topping-out ceremony

On 9 September, CSSB celebrated its topping-out ceremony on the DESY Campus in Hamburg-Bahrenfeld. Hamburg's science senator, Katharina Fegebank, Dr. Karl Eugen Huthmacher from the German federal government, Schleswig-Holstein's scientific minister, Kristin Alheit and chairman of the DESY directorate Professor Helmut Dosch and other representatives of CSSB's nine partners joined Professor Matthias Wilmanns, CSSB scientific director, in celebrating this important milestone. Approximately 250 guests attended the ceremony and celebrations.

Contact: Ina Plettner, ina.plettner@desy.de
Matthias Wilmanns, matthias.wilmanns@embl-hamburg.de

European Molecular Biology Laboratory Hamburg Unit.

Research opportunities in structural biology

In 2015, the Hamburg Unit of the European Molecular Biology Laboratory (EMBL) moved into its fifth decade. We celebrated our 40th anniversary at the end of last year with an international symposium, looking at the unit's past and present activities, as well as considering future perspectives. The event also included a memorable reception by the Hamburg senate in the Hamburg town hall. At present, structural biology, the focus of the EMBL Hamburg Unit both in terms of research infrastructure provision and in-house research, is going through a dynamic transition process. Thanks to recent advances in instrumentation such as the most recent detector generation for applications in electron microscopy and emerging opportunities from X-ray free-electron laser facilities, it is now possible to study the molecular structures of large protein complexes – goals that were unthinkable until very recently. EMBL is preparing to meet these challenges by maintaining and further developing research infrastructures on DESY campus operated by EMBL, as well as engaging in forward-looking co-operations.

Research and services in structural biology

EMBL Hamburg's integrated life science facility at PETRA III encompassing laboratories for sample preparation and characterization, beamlines for structural biology, and data processing and evaluation, enables academic and industrial users access to a package of structural biology services and expertise. 2015 has seen several developments both in terms of instruments and methods.

The Sample Preparation and Characterization (SPC) facility

The SPC facility provides assistance to users of the biologically oriented beamlines at PETRA III by giving them access to a suite of biophysical methods to best characterize their samples, as well as protocols for sample optimization. An example of how the facility can support research groups without prior expertise in structural biology can be found in the highlights section of this report. Users of the Small Angle X-ray Scattering beamline can also book biophysical equipment to purify and characterize their sample using dynamic light scattering, circular dichroism, isothermal titration calorimetry and thermal shift assays. The high-throughput crystallization (HTX) facility doubled its production in 2015, preparing and imaging more than 1500 plates that can be remotely set up and monitored via the HTX website. A new service was provided this year to crystallize membrane proteins in the lipid cubic phase (LCP), using specialized crystallization screens. The first successful X-ray structure determination of an integral

membrane transporter protein was achieved in September, using a standard vapour diffusion/LCP setup by scientists of the EMBL Units in Hamburg and Grenoble.

Structural biology beamlines at PETRA III

At the PETRA III storage ring, EMBL Hamburg has designed, built and now runs three beamlines for applications in structural biology for the international user community: one beamline for Small Angle X-ray Scattering experiments and two for Macromolecular Crystallography.

Small Angle X-ray Scattering

The EMBL beamline P12 environment has been designed and optimized for scattering experiments on macromolecular solutions and includes several versatile options which cater for a variety of user needs and requirements. During 2015, a custom-designed miniature active beamstop was designed to ensure accurate data normalization and a multilayer monochromator (MLM) was installed in collaboration with the Helmholtz-Zentrum Geesthacht to significantly boost the intensity of the X-ray beam and enable rapid time-resolved SAXS experiments. The speed of the data collection was further enhanced to fully utilize the MLM capacity with the new rapid photon-counting EIGER 4M detector installed at the beamline within the framework of the Verbundforschungsprojekt PURE-SAXS (collaboration with the FH Lübeck).

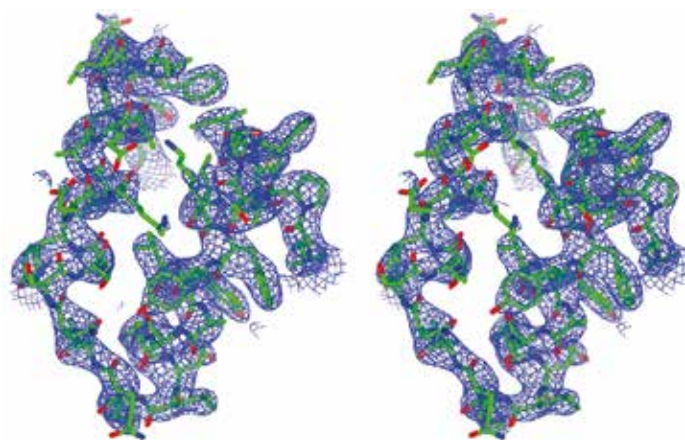


Figure 1

Stereo-views of 2Fo-Fc difference Fourier maps (1.5 σ cut-off), super imposed on the model of Cdc23 – a protein crucial for cell division – after the model refinement starting from the experimental phases (Cianci M., Groves M. R., Barford D., and Schneider, T. R. Data collection with a tailored X-ray beam size at 2.69 Å wavelength (4.6 keV): Sulphur SAD phasing of Cdc23Nterm. *Acta Crystallographica D*, in press).

Macromolecular crystallography

On beamline P13, the possibility to produce a beam of small size ($< 30 \mu\text{m}$) and high flux at low X-ray energy (3.8 – 6 keV) allows us to exploit the anomalous signal of naturally built-in sulphur atoms for crystallographic phasing even when only small crystals are available. In fact, when energies below 5 keV are used, it is advantageous to work with small crystals in order to reduce the absorption of diffracted X-rays within the sample. Several important crystal structures were solved employing the sulphur-SAD method on P13 this year (see Fig. 1).

Developments at P14 in 2015 included a transfocator – a device that allows the insertion of groups of Compound Refractive Lenses into the X-ray beam (Fig. 2). First data collection showed that time required for data collection could be reduced from 30 – 60 minutes under unfocussed conditions to less than two minutes. The collimated beam produced by the transfocator is exceptionally homogeneous and allows us to collect diffraction data of highest quality due to the even illumination of the crystals. Flexible combination of beam collimation by the transfocator and beam focussing by Kirkpatrick-Baez mirrors will provide the possibility to tailor the beam size precisely to the size of crystals under investigation. Crystal location by pre-rastering was added as a feature on P14 for crystals down to 10 – 20 μm in size.

A project with MAATEL (Grenoble, France) has also been initiated to deploy a CrystalDirect Harvester system as developed by our colleagues at EMBL-Grenoble (Marquez/Ciprian). Once in operation in 2016, this system will allow us to harvest crystals from crystallization plates with highly accurate robotics. Such a harvesting process has the advantage of being much more gentle for fragile crystals and of being remotely controllable.

External research user community engagement

Since 2011 EMBL Hamburg has coordinated the EU funded project BioStruct-X (www.biostruct-x.eu) that supports user access to established and key methods in structural biology.



Figure 2
Transfocator on P14 funded by a Swedish-German Röntgen-Ångström-Cluster grant.



Figure 3
Representatives from industry and BioStruct-X partners gathered for a three-day workshop on the DESY campus in July.

The project has been successful in creating a single gateway to European synchrotron infrastructures for structural biology applications. A workshop reaching out to users from industry was hosted by EMBL Hamburg, DESY and BioStruct-X in June (Fig. 3). The project will come to an end in 2016 and will be succeeded by iNEXT, coordinated by the University of Utrecht (www.inext-eu.org).

Method development

EMBL Hamburg groups have also made several contributions in terms of method development this year.

Correlation Map (CorMap) test: A statistical test that quickly and reliably discriminates between models that do and do not fit the experimental data. More details are presented in the highlights section of this report.

Small Angle Scattering Biological Databank (SASBDB): A curated repository of freely accessible and fully searchable SAS experimental data. Depositions include relevant experimental conditions, sample details, instrument characteristic and derived models (www.sasbdb.org).

New collaborations with scientists from Russia

EMBL is partner in two projects funded by the Federal Ministry of Education and Research (BMBF) and the Russian Ministry of Education and Science building upon collaborations between Russian and German institutes. SyncFELmed aims to advance combined synchrotron radiation and free-electron laser technologies in biomedical sciences (www.syncfelmed.org). Laseromix aims to develop methods to exploit the potential for measuring 3D structures and dynamics of single bioparticles using free-electron lasers by standardising protocols for sample preparation, provide novel sample delivery methods, and develop the first comprehensive software package to interpret the FEL data.

Contact: Matthias Wilmanns,
matthias.wilmanns@embl-hamburg.de

The Helmholtz-Zentrum Geesthacht Outstation at DESY.

GEMS - getting even more structure

Our PETRA III beamlines had a successful start after the long shutdown. Already in January, the annual German Engineering Materials Science Centre (GEMS) satellite workshop at the DESY Photon Science Users' Meeting demonstrated the major importance of *in situ* techniques in the field. Many user experiments profited from the GEMS expertise in complex sample environments, for example, the high-energy X-ray diffraction investigation of the "birth and death" of cutting tool coatings (see below in the section on HEMS/P07), nano-indentation and nanodiffraction of such hard coatings with highest spatial resolution, the study of phase transformations during laser-beam welding and *in situ* sintering of photonic glasses. The latter was only one of the many successful experiments of the GEMS central project within the Collaborative Research Centre SFB 986 ("Tailor-Made Multi-Scale Systems – M³"), coordinated by Technical University Hamburg-Harburg, TU HH) in 2015, demonstrating the important role that synchrotron-based techniques play in the SFB.

During an internal GEMS retreat in Kiel in June, we discussed how to further improve the effectiveness of the GEMS operation. We generated new project ideas and developed a mid-term strategy for the continuous development of our instrumentation at DESY.

The Grain Mapper at the High-Energy Materials Science beamline (HEMS, P07, jointly operated with DESY, highest in demand of all PETRA III beamlines) has finally gone into full user operation. With the acquisition of another fast two-dimensional XRD 1621 Perkin Elmer detector, both the main line P07 and the side station P07B can now simultaneously run with high frame rate detectors, thus enhancing the in-house research and educational capabilities. Within a Röntgen-Ångström-Cluster (RAC) project in cooperation with Linköping University (Sweden), a magnetron sputter and arc evaporation chamber was installed and operated in the X-ray beam at industrially relevant deposition rates. An example of this successful cooperation can be seen in the highlights section of this report, published in *Adv. Electron. Mater.* 1, 1400022 (2015). Within the same collaboration our industrial partner SECO Tools AB (Fagersta, Sweden) put a turning rig into operation for *in situ* characterisation of cutting tools at realistic cutting speeds.

Just before the PETRA III shutdown in November 2015, the X-ray optics of the imaging beamline (IBL, P05) was completed,

resulting in the first operation of the double multilayer monochromator. The tests demonstrated the significant increase of the photon flux at different photon energies which will have a real impact on scanning times for high-resolution microtomography. During the last cycles, a range of successful experiments with extended sample environments (e.g. oven and Mg corrosion) were performed at IBL. At the HEMS tomography station, a dedicated setup for grating-based microtomography was installed, tested, and operated as a user experiment. It was possible to establish a new phase-contrast method based on a single phase-shifting grating. This method was applied to the investigation of the water content in porous building materials in September 2015 (Fig. 1). The project is a cooperation of HZG with EMPA, Dübendorf, Switzerland, within the Helmholtz Virtual Institute for New X-ray analytic Methods in Materials Science (VI-NXMM) coordinated by the Karlsruhe Institute of Technology (KIT), Germany. The successful mid-term review of the VI-NXMM resulted in a fifth year of funding (until end of September 2016). Another main part of the VI is the production of X-ray optics for the nanotomography endstation of IBL where first tomograms have been acquired using new optical schemes. In another new RAC project, GEMS will collaborate with partners at HZG (Institute of Materials Research, Division "Metallic Biomaterials" as coordinator) and in Sweden on the application of synchrotron-based tomography techniques on

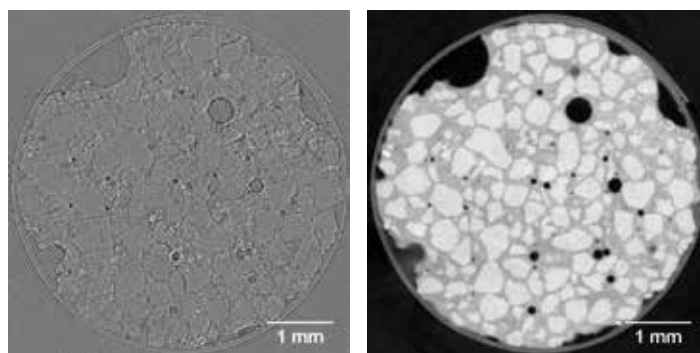


Figure 1

Tomographic scan of porous building material using 60 keV photon energy at P07. Several scans at different water content were performed. Reconstructed slices of the saturated mortar sample showing pure attenuation contrast (left) and grating based phase contrast (right) at the same sample height are shown. The increase in contrast of the new method allows for a more automatic segmentation to provide the information required for computational modelling of mesostructure. The images are courtesy of M. Griffa, F. Yang, R. Kaufmann: EMPA, Dübendorf, Switzerland.

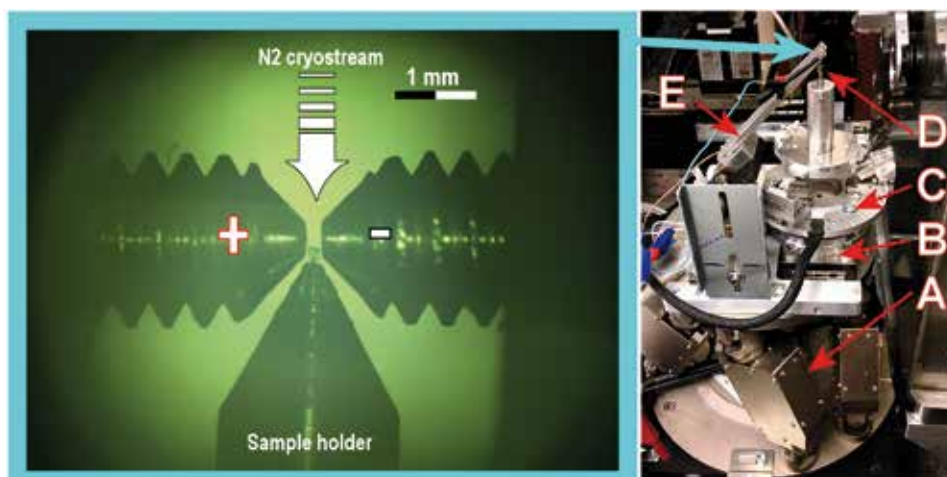


Figure 2

Left: Microscopic view of a wood sample (on holder tip) between the closely aligned electrodes of the E-field device. High electrical field strengths of up to 5 MV/m were applied *in-situ* during X-ray nanodiffraction. For protein crystal samples, a stream of nitrogen gas kept the samples at a temperature below -100°C. Right: Experimental setup installed at the P03 Nano-focus Endstation. Components from bottom to top: (A) hexapod for coarse alignment, (B) rotational positioner for sample rotation, (C) hexapod for precise alignment of sample in between electrodes, (D) sample on magnetic mount, (E) positioner for electrodes. The beam direction is right to left.

the development and characterisation of new Mg alloy bone implants.

At BioSAXS (PETRA III beamline P12, operated together with EMBL), further work on the installation of a high flux option (double multilayer monochromator) was carried out. Photon flux measurements in the optics hutch are in accordance with calculations. A fast detector (DECTRIS EIGER X 4M) was commissioned and is being integrated into a new protocol for fast time-resolved investigations. The accessible Q-range was increased by the implementation of a WAXS option via a modification of the detector tube. First measurements using a newly developed rheometer with a pressure option up to 300 bar were performed on synovial model liquids, showing the sensitivity of synovial liquids to hydrostatic pressure.

The Nanofocus Endstation, operated by HZG in co-operation with the University of Kiel, was the first P03 hutch to receive beam following the long shutdown of PETRA III. The beam size of 350 × 250 nm² was quickly restored and attained for the first time at 17 keV. Among the first experiments were studies on mineralized wood, metallic multilayers and nanoindentation *in situ* experiments on ceramics and glasses. Later in the year, more *in situ* experiments were performed, including an in-house study on the effect of high electric fields to biological samples (see Fig. 2), piezotronic measurements on single crystals, as well as an *operando* study of memory devices using nano-GISAXS. The strong focus of the Nanofocus Endstation on materials science-related research is evident

from all those successful studies. In collaboration with KIT and within the VI-NXMM mentioned above, high-efficiency polymer lenses were installed at P03 in order to directly demagnify the undulator source. The lenses were manufactured out of the photoresist SU8. Following a relatively short alignment procedure, a focal spot of 600 nm was achieved.

In order to expand the interactions with industrial scientists and to increase the use by industry, outreach activities took place. GEMS participated in the “Werkstoffwoche 2015” and continued its commitment to the Science Link Network. An article about successful measurements for Volkswagen AG in 2013 has been published in *LightweightDesign* 04/2015, 38-43. In addition, several measurements or feasibility studies have been performed with industry partners.

The life of GEMS in its provisional location will soon come to an end – to be continued at a new site: the planning of the GEMS wing of the Photon Science Building with new laboratories and office space has been finalised, construction work will start in spring 2016. Until then, there will be many opportunities for our users and collaborators to work on new and exciting projects in engineering materials science.

Contact: Martin Müller, martin.mueller@hzg.de
 Andreas Schreyer, andreas.schreyer@hzg.de

The DESY NanoLab provides experimental methods in the field of nanoscience, which are complementary to the techniques available at the DESY photon sources.

In 2015 the establishment of DESY NanoLab instrumentation continued in its temporary home in building 3. The high resolution scanning electron microscope (SEM) was fully commissioned (Fig. 1) and already upgraded by a high yield energy dispersive X-ray detector for spatially resolved chemical analysis.

The Pt marker deposition capabilities of the system were successfully tested. The patterning software allows image based writing of marker structures as demonstrated by the deposition of the DESY logo onto a Silicon wafer (see Fig. 2). Further on, the ultrahigh vacuum variable temperature scanning probe microscope was put into operation yielding promising first results. Its ultimate performance is currently limited by the non-optimized vibration conditions in building 3.



Figure 1

View inside the SEM chamber with sample manipulation stage (left), Pt precursor injection nozzle (top left) and imaging column (top).

With the uptake of the PETRA III user operation in May 2015 users were for the first time also welcomed in the DESY NanoLab for sample characterization before, during or after their beamtimes with methods complementary to the PETRA III beamlines. The user demands concentrated around scanning probe microscopy techniques, especially in combination with the Pt marker deposition capabilities of the SEM. In house research projects made often use of X-ray photo emission spectroscopy and the surface sensitive X-ray diffraction techniques, now fully implemented in the NanoLab X-ray laboratory. Also the performance of operando reaction experiments involving toxic and inflammable gases is now possible in the X-ray lab due to the installation of the respective gas safety environment. The access to the DESY NanoLab is possible for external users in two ways: either through a regular PETRA III or FLASH proposal (via DOOR), or through the submission of a proposal to the European user platform Nano Foundries Fine Analysis (NFFA Europe, www.nffa.eu), which provides combined access to the DESY NanoLab and short PETRA III beamtimes. Within this access programme, the DESY NanoLab is leading a work package dedicated to the development of a protocol for the reproducible transfer and positioning of nano-objects which represents a bottleneck for current X-ray nanofocus experiments.

The planning for the Photon Science building, which will be the new home of the DESY NanoLab, is finalized and the start of the construction work is scheduled for July 2016. The DESY NanoLab will be transferred to its new location early 2018. Future instrumentation will comprise a focussed ion beam facility for sample nano-structuring and a magnetic properties characterization laboratory.

Contact: *Andreas Stierle*, andreas.stierle@desy.de



Figure 2

DESY logo written onto a Si wafer by SEM deposition based Pt precursor cracking.

Brilliant light and brilliant ideas.

Transferring knowledge from the laboratory to society



Figure 1
Artist view of the
Innovation Centre on
the DESY Campus.

Over the past two years, four companies have been launched by DESY employees as spin-offs, all emerging from the Photon Science division. Additional projects also from other DESY divisions and at very different stages of development are currently supported by the DESY start-up office. In the coming years, DESY will build an Innovation Centre, funded by the City of Hamburg, to establish a start-up culture on the Campus. With this new centre, in close proximity to scientific expertise and infrastructure, an attractive environment for young enterprises related to DESY will be created. In addition, DESY drew in support from the Helmholtz Association to encourage spin-off projects. The so-called “Helmholtz Enterprise” initiative provides funding for the critical first phase of the company foundation, e.g. to cover the costs of external management support. DESY attracted “Helmholtz Enterprise” funding for four photon science spin-off groups.

The company “Class 5 Photonics GmbH”, a joint spin-off of DESY and GSI/Helmholtz Institute Jena, will build very flexible tuneable high performance femtosecond lasers generating short pulses at high rates. In recognition of the underlying concept, the young entrepreneurs received the Start-up Challenge award of the German Competence Networks for Optical Technologies OptecNet in 2014. In July 2014, the “X-Spectrum GmbH”, which enters the market with high-technology X-ray detectors, was founded by five members of the DESY photon science detector systems group (FS-DS), DESY being 10 % shareholder of the new enterprise. The scientists developed a fast X-ray camera with extremely high spatial resolution and high acquisition rates named “Large Area Medipix Based Detector Array (LAMBDA)”. It offers a very high dynamic range,

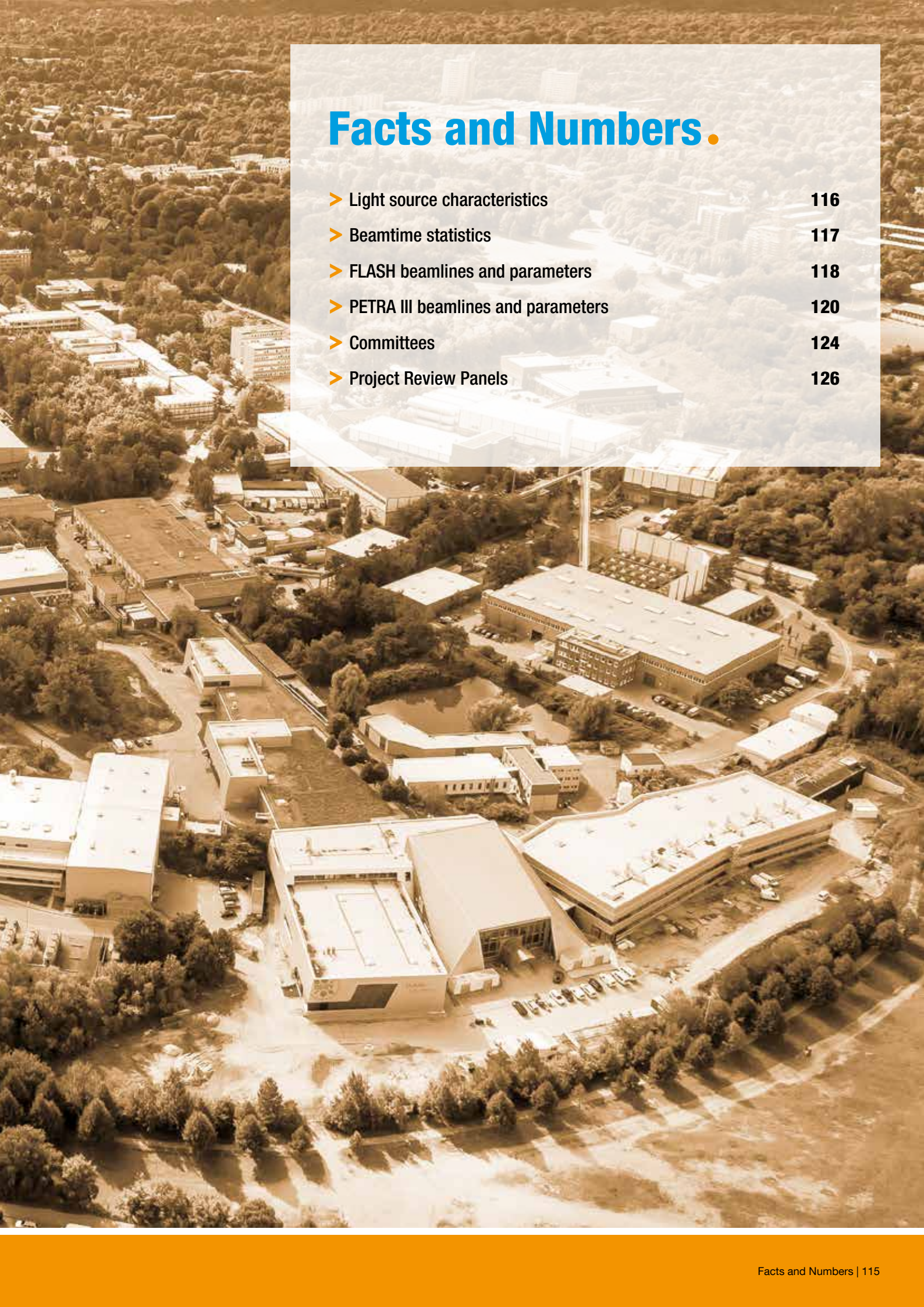
complemented with the possibility to take “colour” pictures by measuring the energy of the detected X-ray photons. With this innovative high-speed X-ray camera, the company won the Hamburg Innovation Award 2015 in the category “Start”. The “suna-precision GmbH” will provide nano-positioning systems for the scientific market and in particular for synchrotron radiation sources worldwide. Using DESY know-how and patents under licence, the company founders aim to combine various high-precision technologies to produce innovative devices that allow measurements to be made efficiently and with utmost precision in the nanometre range. These technologies surpass other products currently on the market due to a simple control system based on especially developed software and the ability of positioning with nanometre precision in vacuum.

In 2015, the “Cycle GmbH” started as a spin-off of the Ultrafast Optics and X-rays Group at DESY/CFEL and supplies innovative products that use ultrafast laser technology for scientific and industrial applications, such as synchronisation units with femtosecond precision. The company benefits from the Helmholtz Enterprise funds by turning an already patented ultrashort pulse laser (USP laser) into a market-ready product, to extend its range of products towards including laser sources. The USP laser is based on a novel idea for a fibre laser and produces a high-output beam of excellent quality in a particularly robust way.

Contact: Ilka Mahns (DESY start-up office),
ilka.mahns@desy.de



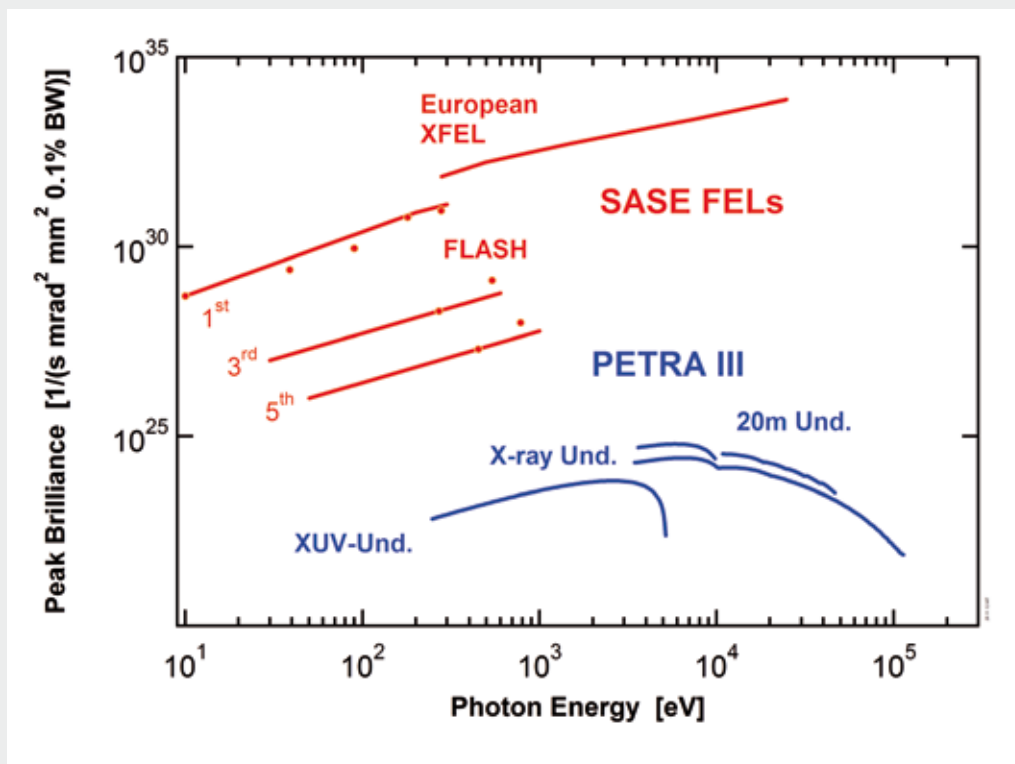
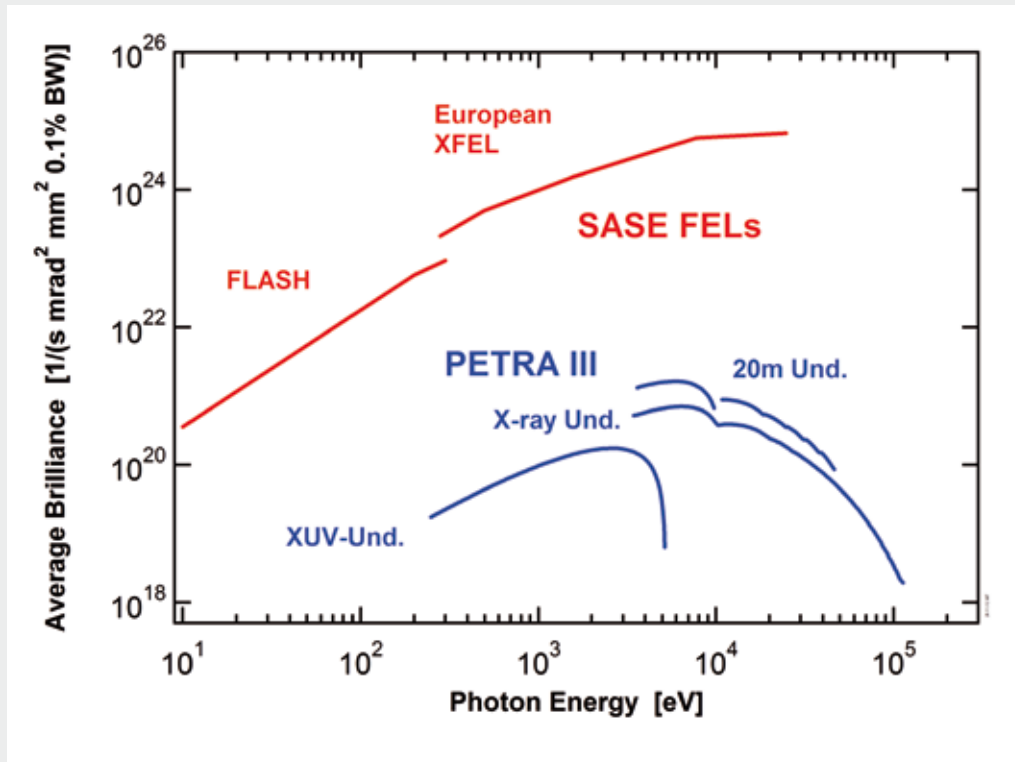




Facts and Numbers.

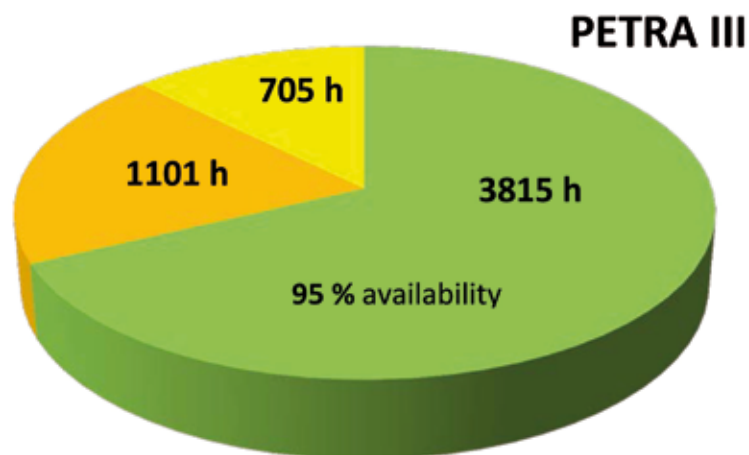
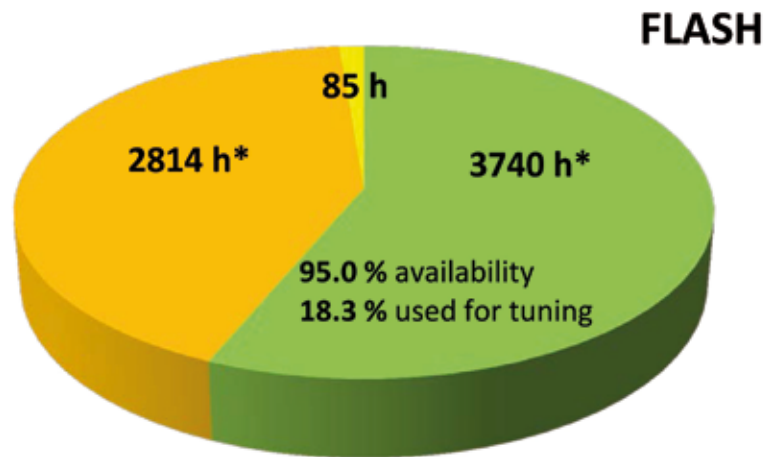
➤ Light source characteristics	116
➤ Beamtime statistics	117
➤ FLASH beamlines and parameters	118
➤ PETRA III beamlines and parameters	120
➤ Committees	124
➤ Project Review Panels	126

Light source characteristics.



Average and peak brilliance values for FLASH, PETRA III and European XFEL. Peak brilliance values are given for the optimum bunch charge at the respective photon energies. Dots represent experimentally measured values at FLASH.

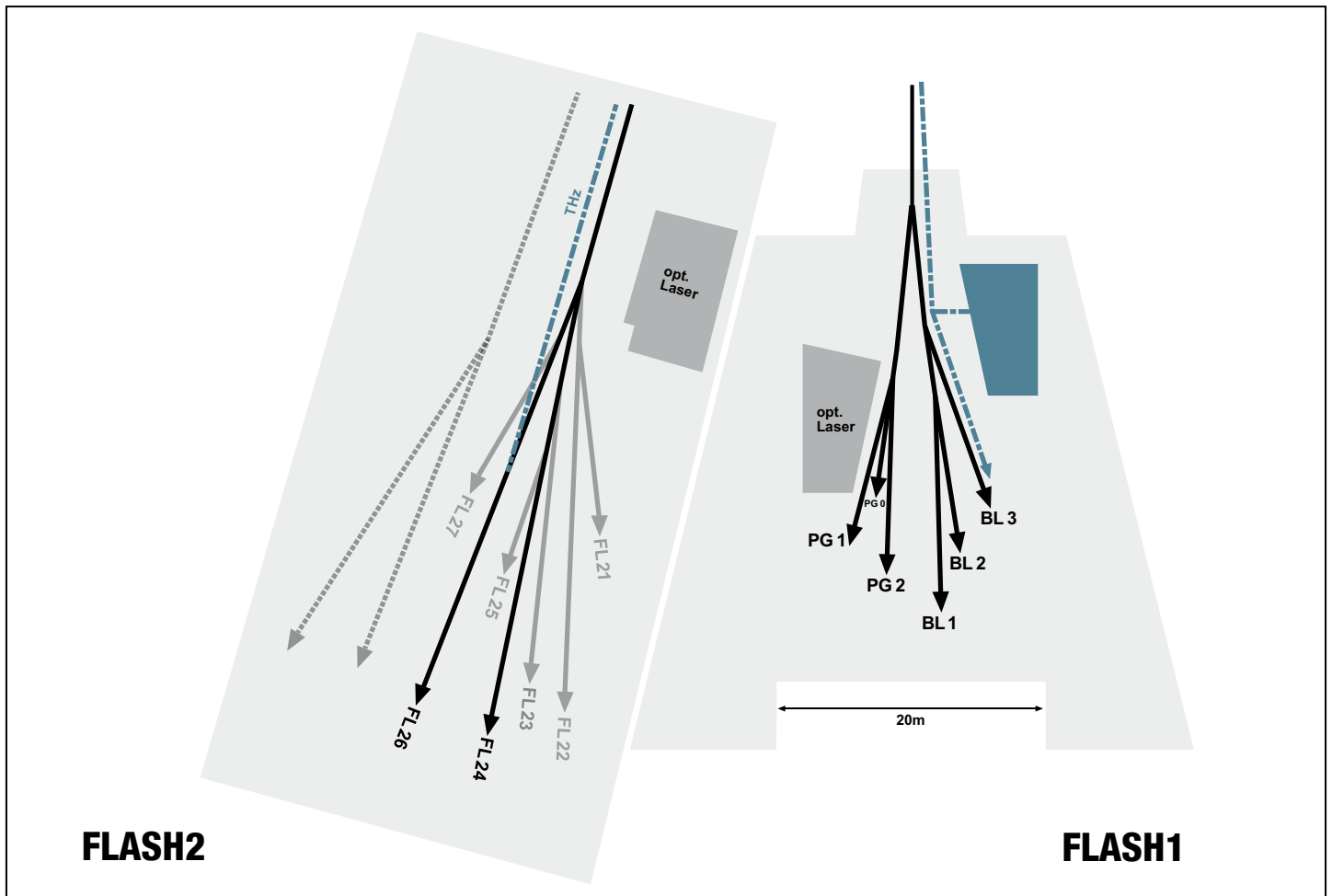
Beamtime statistics 2015.



■ User beamtime ■ Machine studies/test runs ■ Maintenance

Operation periods 2015

FLASH	01.01. - 02.11.2015 not included (*): - last machine study block in November: ca. 430 h - last user beamtime block in December: ca. 740 h - shutdown periods: ca. 950 h
PETRA III	27.04. - 12.11.2015 34 days machine studies and maintenance



Machine parameters FLASH

Electron energy (max.)	1.25 GeV
Length of the facility	315 m
Normalized emittance	1.5 mm mrad (rms)
Emittance	0.6 nm rad (rms)
Electron Bunch charge	0.05 – 1 nC
Peak current	1 – 2.5 kA
Electron Bunches per second (typ. and max.)	300 and 5000

FLASH lasing parameters

Photon energy (max.)	301 eV (fundamental)
Wavelength (min.)	4.12 nm (fundamental)
Photon Pulse duration (FWHM)	50 – 200 fs
Peak power	1 – 3 GW
Photon Pulse energy (average)	up to 500 μ J
Photons per bunch	$10^{11} - 10^{13}$
Average brilliance	$10^{17} - 10^{21}$ photons/sec/mm ² /mrad ² /0.1%
Peak brilliance	$10^{29} - 10^{31}$ photons/sec/mm ² /mrad ² /0.1%

FLASH1 beamlines

BL 1	non-monochromatic FEL photons Kirkpatrick-Baez (KB) focusing optics, FEL focal spot of $\sim 5 \mu\text{m} \times 7 \mu\text{m}$ (FWHM)	<i>TU Berlin*</i>
	split-and-delay unit for XUV pump - XUV probe experiments (in commissioning, up to ns delay)	<i>TU Berlin*</i>
	optional pump - probe experiments using FLASH1 optical laser system	
	permanent end station: multipurpose CAMP chamber with two pnCCD detectors, electron and ion spectrometers and collinear in-coupling optics for optical laser, optional supersonic gas jet (as sample)	
BL 2	non-monochromatic FEL photons focused to $\sim 20 \mu\text{m}$ /unfocussed beam size $\sim 5\text{-}10 \text{ mm}$ (FWHM, depending on wavelength)	
	XUV beam splitter with variable time delay (-3 ps to 15 ps) for photon diagnostics and XUV pump - XUV probe experiments	<i>Univ. Münster*</i>
	optional pump-probe experiments using FLASH1 optical laser system	
	about 3 x 4 m footprint for user-provided end station	
BL 3	non-monochromatic FEL photons, spectral range: $>4.5 \text{ nm}$ (carbon coated optics) focused to $\sim 20 \mu\text{m}$ /unfocussed beam size $\sim 5\text{-}10 \text{ mm}$ (FWHM, depending on wavelength)	
	optional pump - probe experiments using FLASH1 optical laser system	
	optional pump - probe experiments using THz radiation (unique to BL3):	
	- tunable: $10 - 230 \mu\text{m}$; up to $100 \mu\text{J/pulse}$; $\sim 10\%$ bandwidth	
	- broadband at $200 \mu\text{m}$, up to $10 \mu\text{J/pulse}$; $\sim 100\%$ bandwidth	
	- synchronized and phase stable to X-ray pulses (down to 5 fs)	
	- delivered to the experiment via vacuum beamline as:	
	(i) ultra-high vacuum ($\sim 10^{-8}$ mbar), shorter delay between THz and X-ray ($\sim 4 \text{ m}$ path difference), can accommodate up to 0.3 m wide setup	
	(ii) high vacuum ($\sim 10^{-6}$ mbar), longer delay between THz and X-ray ($\sim 7 \text{ m}$ path difference); can accommodate up to 2 m wide setup	
	about 3 x 4 m footprint for user-provided end station	
PG1	high resolution plane grating XUV monochromator (SX 700 type, $<10^{-4}$ bandwidth, carbon coated optics): - variable combination of photon flux and resolution (from high flux to high resolution) - controlled temporal-spectral properties at moderate resolution for pump - probe experiments - high photon flux with harmonic filtering	
	Kirkpatrick-Baez (KB) refocusing optics, FEL focal spot of $5 \mu\text{m}$ (vertically)	<i>Univ. Hamburg*</i>
	permanent end station: two-stage VUV-Raman spectrometer for high-resolution measurements close to Rayleigh line	<i>Univ. Hamburg*</i>
PG2	uses the same monochromator as PG1 $50 \mu\text{m}$ focus	
	XUV beamsplitter with variable time delay ($\pm 6 \text{ ps}$) for time resolved studies	<i>Univ. Hamburg*</i>
	optional pump - probe experiments using FLASH1 optical laser system	
	about 3 x 4 m platform for user-provided end station	

FLASH1 optical / NIR laser system for pump - probe experiments

10 Hz single pulse	a) compressed pulse transported over beamline 1.5 mJ , 60 fs synchronization to FEL better than 60 fs r.m.s. , corrected for drifts
	b) stretched pulse (chirped) transported over beamline pulse compressor must be included in experimental set-up 15 mJ , 200 ps uncompressed 10 mJ , 60 fs with external pulse compressor synchronization to FEL better than 60 fs r.m.s. , corrected for drifts
Burst-mode	up to 400 pulses / burst $20 \mu\text{J}$ per single pulse, 120 fs synchronization to FEL better than 60 fs r.m.s.

FLASH2 beamlines - under commissioning -

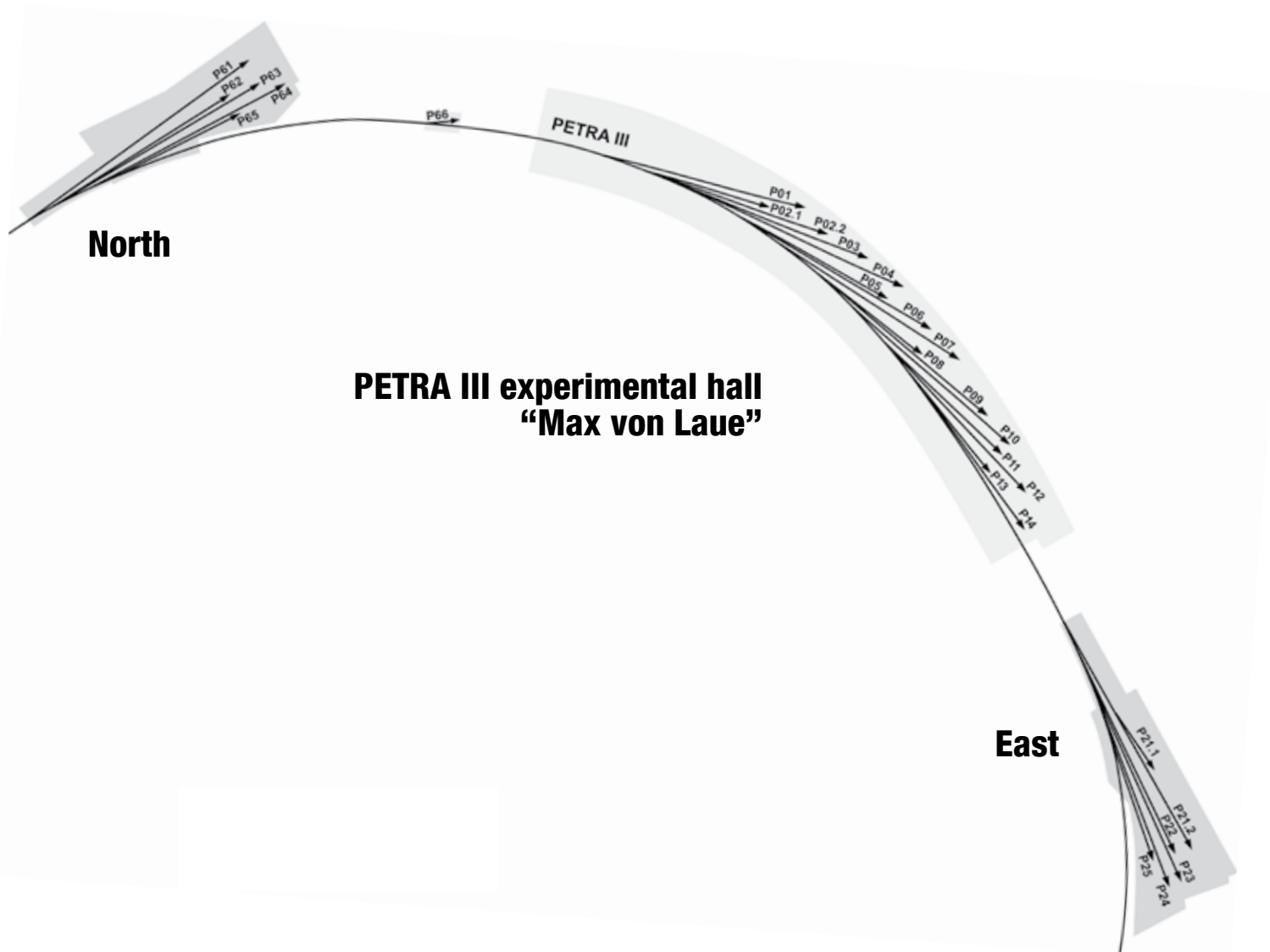
FL24	wavelength range: $4 - 16 \text{ nm}$ for the fundamental with 6σ acceptance, for harmonics down to 0.8 nm grazing incidence (1.8°) split-and-delay unit with $\pm 12 \text{ ps}$ time delay (to be installed 2017)	<i>Univ. Münster*</i>
FL26	wavelength range: $6 - 40 \text{ nm}$ with 6σ , up to 80 nm with 3σ acceptance	
	permanent end station: - split multilayer mirror & reaction microscope (REMI) for time-resolved spectroscopy - grazing incidence delay-line and refocusing optics for a second experiment in-line behind the REMI (under development)	<i>MPI-K Heidelberg</i>

All FLASH beamlines provide online photon diagnostics for intensity, wavelength, and beam position; fast shutter, aperture and filter sets.

*We would like to acknowledge all contributions to instrument development and operation provided within the framework of BMBF Verbundforschung.

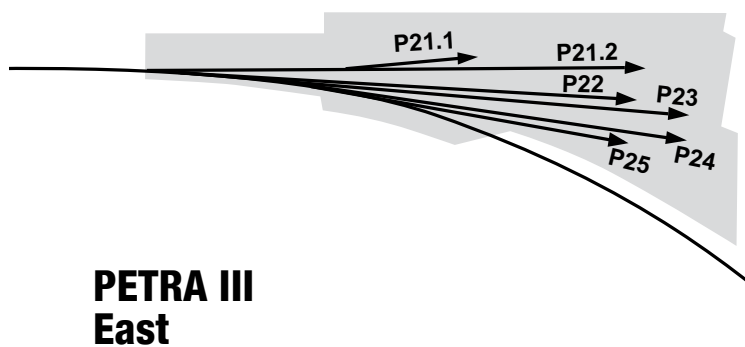
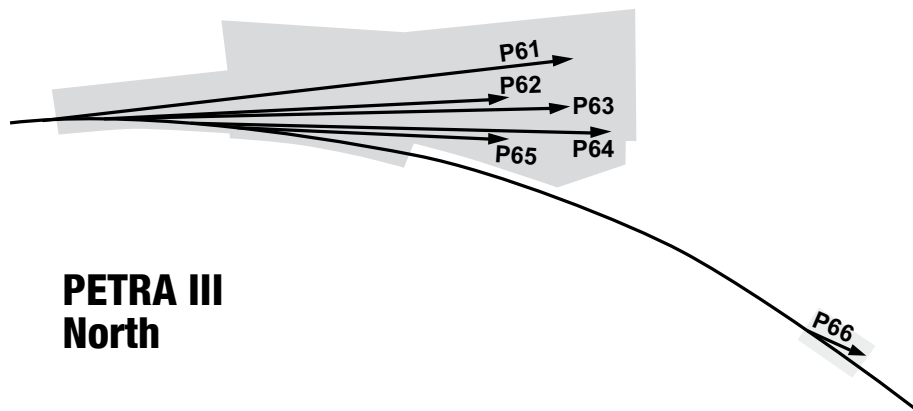
PETRA III.

Beamlines and parameters



Machine parameters PETRA III

Electron energy	6.08 GeV
Circumference of the storage ring	2304 m
Number of bunches	960, 480, 60, and 40
Bunch separation	8 ns, 16 ns, 128 ns, and 192 ns
Electron beam current	100 mA (top-up)
Horizontal positron beam emittance	1.2 nmrاد (rms)
Coupling factor	1.0%
Vertical electron beam emittance	0.01 nmrاد (rms)
Electron beam energy spread	0.1% (rms)
Horizontal x vertical beam size at 5 m undulator (high β section)	141 x 5.2 μm
Horizontal x vertical beam size at 5 m undulator (low β section)	36 x 5.7 μm



PETRA III beamlines

PETRA III experimental hall “Max von Laue”

Beamline and instruments	Operated by
P01 High resolution dynamics 10 (20) m U32 4.5 – 40 keV	DESY
Nuclear resonant scattering	DESY
Non-resonant IXS	DESY
X-ray Raman scattering	DESY
P02.1 Powder diffraction 2 m U23 60 keV	DESY
Standard & Time resolved powder diffraction	DESY
High resolution powder diffraction	DESY
P02.2 Extreme conditions 2 m U23 10 – 62 keV	DESY
Laser heated diamond anvil cells	DESY
General purpose high pressure	DESY
P03 Micro- and Nano-SAXS / WAXS 2 m U29 8 – 23 keV	DESY
Micro-small and wide angle scattering	DESY
Nano-beam scattering and diffraction	DESY
P04 Variable polarization soft X-rays 5 m UE65 200 – 3000 eV	DESY
UHV diffractometer	DESY
Photon-Ion spectrometer (PIPE)	DESY
Ultra-high resolution photoelectron spectroscopy (ASPHERE)	DESY
Soft X-ray absorption spectrometer	DESY
Nano focus apparatus for spatial and time resolving spectroscopy	DESY
P05 Micro- and nano-imaging 2 m U29 8 – 50 keV	HZG
Micro-tomography	HZG
Nano-tomography	HZG (in commissioning)
P06 Hard X-ray Micro/Nano-Probe 2 m U32 5 – 100 keV	DESY
Microprobe	DESY
Nanoprobe	DESY
P07 High energy X-ray materials science 2 m U29 (planned: 4 m U19) 50 – 200 keV	HZG
Multi-purpose triple-axis diffractometer	DESY
Heavy load diffractometer	HZG
Grain mapper	HZG
High energy tomography	HZG
P08 High resolution diffraction 2 m U29 5.4 – 29.4 keV	DESY
High resolution diffractometer	DESY
Liquid surface diffraction	DESY
P09 Resonant scattering and diffraction/HAXPES 2 m U32 2.7 – 50 keV	DESY
High precision psi-diffractometer	DESY
Heavy load diffractometer	DESY
Hard X-ray photoelectron spectroscopy	DESY
P10 Coherence 5 m U29 4 – 20 keV	DESY
X-ray photon correlation spectroscopy (4 – 20 keV)	DESY
Vertical rheometer (8.388 keV)	DESY
Coherent imaging (8 – 15 keV)	DESY
Multi-purpose diffractometer (8 – 20keV)	DESY
P11 Bio-imaging and diffraction 2 m U32 2.4 – 30 keV	DESY
Imaging of biological samples (2.4 – 10 keV)	DESY (in commissioning)
Macromolecular crystallography (5.5 – 30 keV)	DESY / MPG / HZI

Beamline and instruments		Operated by
P12	Bio SAXS 2 m U29 4 – 20 keV	EMBL / HZG
	Solution small-angle scattering	EMBL
P13	Macromolecular crystallography I 2 m U29 4 – 16 keV	EMBL
	Macromolecular crystallography	EMBL
P14	Macromolecular crystallography II 2 m U29 10 keV	EMBL
	Macromolecular crystallography	EMBL

PETRA III Extensions East and North

Beamline and instruments		Operated by
P21	Swedish high-energy materials science beamline 4 m IVU21 40 – 150 keV side branch: 2 m U29 50, 80, 100 keV	Swedish institution / DESY
	Diffraction and imaging Broad band diffraction	Swedish institution / DESY (operation planned 2017)
P22	X-ray spectroscopy 2 m U33 2.4 – 15 keV	DESY
	Hard X-ray photoelectron spectroscopy (relocated from P09)	DESY (operation planned 2017)
P23	Russian-German nano-diffraction beamline 2 m U32 5 – 35 keV	DESY
	Nano-XRD, in situ and complex environments	DESY (operation planned 2017)
	2 nd hutch instrument tbd	not yet funded
P24	Chemical crystallography 2 m U29 8, 15 – 45 keV	DESY
	Single crystal diffraction in complex sample environments	DESY (operation planned 2017)
	Small molecule crystallography	DESY (operation planned 2017)
P25	Education & testing	not yet funded
P61	High-energy materials science 40 m damping wiggler 50 – 200 keV / pink beam	DESY
	High-energy engineering materials science	HZG
	Extreme conditions in the large volume press	DESY (operation planned >2017)
P62	Small-angle X-ray scattering (tentative)	DESY (not yet funded)
P63	Instrument tbd	DESY (not yet funded)
P64	Time-resolved X-ray absorption 2 m U32 4 – 44 keV	DESY
	Time-resolved <i>in situ</i> XAFS, QEXAFS, bioXAFS	DESY (under commissioning, operation from Spring 2016)
P65	X-ray absorption Short U32 4 – 44 keV	DESY
	<i>Ex situ</i> and <i>in situ</i> XAFS of bulk samples	DESY (under commissioning, operation from Spring 2016)
P66	Superlumi Bending magnet 4 – 40 eV	DESY
	Time-resolved luminescence spectroscopy	DESY (operation planned >2017)

We would like to acknowledge all contributions to instrument development and operation provided within the framework of BMBF-Verbundforschung, the Röntgen-Ångström-Cluster (RAC), the Ioffe-Röntgen-Institute (IRI), and the Ruprecht-Haensel-Laboratory (University of Kiel).

Committees 2015.

Photon Science Committee PSC — advises the DESY Photon Science management

Markus Drescher (chair)

Melissa A. Denecke (vice chair)

Christian David

Stefan Eisebitt

Gwyndaf Evans

Maya Kiskinova

Henning Friis Poulsen

Harald Reichert

Anthony J. Ryan, OBE

Bernd Schmitt

Andrea Somogyi

Julian Stangl

Stefan Vogt

Martina Havenith-Newen

Simo Huotari

Thomas Pfeifer

Lucia Incoccia-Hermes (PSC secretary)

Universität Hamburg, DE

University of Manchester, UK

PSI, Villigen, CH

MBI and Technische Universität Berlin, DE

Diamond Light Source Ltd., Didcot, UK

Elettra-Sincrotrone Trieste, IT

DTU Fysik, Lyngby, DK

ESRF, Grenoble, FR

University of Sheffield, UK

PSI, Villigen, CH

Synchrotron SOLEIL, FR

Johannes Kepler Universität Linz, AT

APS ANL, Argonne, US

Ruhr-University Bochum, DE

University of Helsinki, FI

MPI for Nuclear Physics, Heidelberg, DE

DESY, Hamburg, DE



PSC Members (second half 2015) from the left:

1st row: Harald Reichert, Andrea Somogyi, Christian David,
Maya Kiskinova, Markus Drescher (chair).

2nd row: Gwyndaf Evans, Melissa A. Denecke (vice chair),
Simo Huotari.

3rd row: Henning Friis Poulsen, Stefan Vogt, Martina Havenith-Newen.

4th row: Thomas Pfeifer and Bernd Schmitt.

Absent here: Stefan Eisebitt, Anthony J. Ryan, Julian Stangl.

Laser Advisory Committee LAC — shared between DESY and the European XFEL

Uwe Morgner (Chair)	Universität Hannover, DE
Giulio Cerullo	Politecnico di Milano, IT
Mike Dunne	SLAC, Menlo Park, CA, US
Patrick Georges	CNRS, FR
Alfred Leitenstorfer	Universität Konstanz, DE
Robert W. Schoenlein	LBNL, Berkeley, US
William E. White	SLAC, Menlo Park, US
Andreas Galler (European XFEL LAC secretary)	European XFEL GmbH, Hamburg, DE
Oliver D. Mücke (DESY-CFEL LAC secretary)	DESY, Hamburg, DE

DESY Photon Science User Committee DPS-UC — represents the user community

Peter Müller-Buschbaum (Chair)	Technische Universität München, DE
Thomas Möller	Technische Universität Berlin, DE
Julian Stangl	Johannes Kepler Universität, Linz, AT
Gregor Witte	Ludwig-Maximilians-Universität München, DE
Joachim Wollschläger	Universität Osnabrück, DE

Komitee Forschung mit Synchrotronstrahlung KFS representative body of the German synchrotron radiation and FEL user community

Stefan Eisebitt (chair)	MBI and Technische Universität Berlin, DE
Bridget Murphy (vice chair)	Universität Kiel, DE
Ronald Frahm	Universität Wuppertal, DE
Jan-Dierk Grunwaldt	KIT Karlsruhe, DE
Christian Gutt	Universität Siegen, DE
Birgit Kanngießer	Technische Universität Berlin, DE
Lutz Kipp	Universität Kiel, DE
Tim Salditt	Universität Göttingen, DE
Hermann Schindelin	Universität Würzburg, DE
Andreas Schreyer	Helmholtz-Zentrum Geesthacht, DE
Peter Albers	AQura GmbH, DE

Project Review Panels 2015.

PRP1: VUV- and Soft X-Ray

Lucia Aballe	CELLS-ALBA Barcelona, ES
Stephan Fritzsche	Helmholtz Institut Jena, DE
Michael Meyer	European XFEL GmbH, Hamburg, DE
Luc Patthey	PSI, Villigen, CH
Jens Viefhaus (PRP Secretary)	DESY, Hamburg, DE

PRP2: X-Ray Spectroscopy

Ralph Claessen	Julius-Maximilians-Universität Würzburg, DE
Joerg Evers	MPI für Kernphysik, Heidelberg, DE
Raphael Hermann	FZ Jülich, DE
Håkan Rensmo	Uppsala University, SE
Sebastian Schoeder	Synchrotron SOLEIL, FR
Max Wilke	GFZ Potsdam, DE
Iztok Arcon	University of Nova Gorica, SL
Matthias Bauer	Universität Paderborn, DE
Greg Hughes	Dublin City University, IE
Maarten Nachtegaal	PSI, Villigen, CH
Wolfgang Drube (PRP secretary)	DESY, Hamburg, DE

PRP3: High Pressure and Extreme Conditions

Denis Andrault	Blaise Pascal University, Clermont-Ferrand, FR
Ulrich Schwarz	Ruprecht-Karls-Universität Heidelberg, DE
Sergio Speziale	GFZ, Potsdam, DE
Leonid Dubrovinsky	Bayerisches Geoinstitut, Bayreuth, DE
Diego Gatta	University of Milan, IT
Hanns-Peter Liermann (PRP Secretary)	DESY, Hamburg, DE

PRP4: Engineering Materials Science

Jens Gibmeier	Karlsruher Institut für Technologie KIT, DE
Jozef Keckes	Montanuniversität Leoben, AT
Svea Mayer	Montanuniversität Leoben, AT
Walter Reimers	Technische Universität Berlin, DE
Guillermo Requena	DLR and RTWH Aachen, DE
Gerold Schneider	Technische Universität Hamburg-Harburg, DE
Bernd Schönfeld	ETH Zürich, CH
Carsten Siemers	Technische Universität Braunschweig, DE
Axel Steuer	MAX IV Laboratory, Lund, SE
Martin Müller (PRP secretary)	HZG, Geesthacht, DE
Ulrich Lienert (DESY representative)	DESY, Hamburg, DE

PRP5: Soft Condensed Matter – Bulk

Uwe Klemradt	RWTH Aachen, DE
Yongfeng Men	Changchun Inst. of Applied Chemistry, CN
Michael Paulus	Technische Universität Dortmund, DE
Joachim Wagner	Universität Rostock, DE
Christian Gutt	Universität Siegen, DE
Thomas Hellweg	Universität Bielefeld, DE
Daniel Söderberg	KTH, Stockholm, SE
Rainer Gehrke (PRP secretary)	DESY, Hamburg, DE

PRP6: Soft Condensed Matter – Surfaces and Interfaces

Gerald Brezesinski	MPI Kolloid- u. Grenzflächenforsch., Potsdam, DE
Moshe Deutsch	Bar-Ilan University, Ramat Gan, IL
Tiberio A. Ezquerra	CSIC, Madrid, ES
Thomas Gutsmann	Leibniz-Zentrum Borstel, DE
Hyunjung Kim	Sogang University, Seoul, KR
Frank Schreiber	Universität Tübingen, DE
Oliver Seeck (PRP Secretary)	DESY, Hamburg, DE

PRP7: Imaging (full-field, scanning, coherent)

Oliver Bunk	PSI, Villigen, CH
Peter Cloetens	ESRF, Grenoble, FR
Koen Janssens	University of Antwerpen, BE
Hendrik Küpper	Universität Konstanz, DE
Stefan Vogt	APS ANL, Argonne, US
Julia Herzen	Technische Universität, München, DE
Stephan Peth	Universität Kassel, DE
Frank Witte	Charité - Universitätsmedizin Berlin, DE
Gerald Falkenberg (PRP secretary)	DESY, Hamburg, DE
Felix Beckmann (HZG representative)	HZG, Geesthacht, DE

PRP8: Methods and Instrumentation

Rolf Follath	PSI, Villigen, CH
Tim Salditt	Universität Göttingen, DE
Anatoly Snigirev	ESRF, Grenoble, FR
Horst Schulte-Schrepping (PRP secretary)	DESY, Hamburg, DE

PRP9: Hard Condensed Matter – Surface and Coherent Scattering

Peter Wochner	MPI, Stuttgart, DE
Johan Gustafson	University Lund, SE
Vaclav Holý	Masaryk University, Brno, CZ
Dieter Lott	HZG, Geesthacht, DE
Alexander Komarek	MPI CPFS, Dresden, DE
Bogdan Sepiol	Universität Wien, AT
Michael Sprung (Secretary)	DESY, Hamburg, DE

PRP10: Hard Condensed Matter – Bulk (diffraction and scattering)

Johan Chang	University of Zurich, CH
Robert Dinnebier	MPI für Festkörperforschung, Stuttgart, DE
Lars Ehm	Stony Brook University, Stony Brook, NY, US
Jochen Geck	IFW Dresden, DE
Hermann Gies	Ruhr-Universität Bochum, DE
Helen Walker	ISIS, Didcot, GB
Xiaodong Zou	Stockholm University, SE
Markus Huecker	BNL, Upton, US
Jörg Strempler (PRP secretary)	DESY, Hamburg, DE

PRP11: Soft X-Ray – FEL Experiments (FLASH)

Katharina Al-Shamery	Universität Oldenburg, DE
Michael Bonitz	Universität Kiel, DE
Christoph Bostedt	SLAC, Menlo Park, US
Chris Jacobsen	APS, Argonne, US
Steven Johnson	ETH Zürich, CH
Maya Kiskinova	Sincrotrone Trieste, IT
Jonathan Marangos	Imperial College London, GB
Ronald Redmer	Universität Rostock, DE
Robert W. Schoenlein	Lawrence Berkeley Nat. Laboratory, US
Bernd Sonntag	Universität Hamburg, DE
Urs Staub	PSI, Villigen, CH
Kiyoshi Ueda	Tohoku University, Sendai, JP
Marc Vrakking	MBI, Berlin, DE
Martin Weinelt	FU Berlin, DE
Gwyn P. Williams	Jefferson Laboratory, Newport News, VA, US
Stefan Karsch	LMU, München, DE
Josef Feldhaus (PRP secretary)	DESY, Hamburg, DE

PEC: EMBL Life Science beamlines P12-P14 / PRP12: Bio-crystallography at P11

Pau Bernadó	CBS/CNRS, Montpellier, FR
Kristina Djinovic-Carugo	Universität Wien, AT
Gwyndaf Evans	Diamond Light Source, Didcot, GB
Bob Fischetti	Argonne National Laboratory, US
Mariusz Jaskolski	University of Poznan, PL
Poul Nissen (Chair)	University of Aarhus, DK
Javier Pérez	Synchrotron SOLEIL, FR
Savvas Savvides	Ghent University, BE
Joel Sussman	Weizmann Institute of Sciences, Rehovot, IL
Bente Vestergaard	University of Copenhagen, DK
Christian Schroer (DESY observer)	DESY, Hamburg, DE

Photographs and Graphics:

David Ausserhofer/DFG

Lars Berg, Hamburg

Universität Hamburg

Gesine Born, Hamburg

CSSB

DESY

DFZ-Architekten GmbH

EMBL

European XFEL

Anne Gaertner/TUHH

Jonas L. Hansen, University of Aarhus

Axel Heimken

Rey Hori/European XFEL

Gisela Köhler, Hamburg

CFEL

HZG

Marta Mayer/DESY

Dirk Nölle/DESY

Frank Poppe/European XFEL

Reimo Schaaf, Hamburg

Rosemary Wilson/EMBL

Figures of the Research Highlights were reproduced by permission from authors or journals.

Acknowledgement

We would like to thank all the authors and all those who have contributed to the realisation of this Annual Report. ●

Imprint

Publishing and Contact:

Deutsches Elektronen-Synchrotron DESY
A Research Centre of the Helmholtz Association

Hamburg location:

Notkestr. 85, 22607 Hamburg, Germany
Tel.: +49 40 8998-0, Fax: +49 40 8998-3282
desyinfo@desy.de

Zeuthen location:

Platanenallee 6, 15738 Zeuthen, Germany
Tel.: +49 33762 7-70, Fax: +49 33762 7-7413
desyinfo.zeuthen@desy.de

Photon Science at DESY

Tel.: +49 40 8998-2304, Fax: +49 40 8998-4475
photon-science@desy.de
photon-science.desy.de

www.desy.de

ISBN 978-3-945931-00-4

Online version:

photon-science.desy.de/annual_report

Realization:

Tim Laarmann, Wiebke Laasch

Editing:

Lars Bocklage, Rainer Gehrke, Lucia Incoccia-Hermes,
Wiebke Laasch, Tim Laarmann, Wolfgang Morgenroth,
Elke Plönjes, Ralf Röhlsberger, Martin A. Schroer, Jens Viefhaus,
Hans-Christian Wille, Martin von Zimmermann

Layout: Sabine-Kuhls Dawideit, Büro für Grafik und Design,
Halstenbek

Printing: EHS Druck GmbH, Schenefeld

Copy deadline: December 2015

Reproduction including extracts is permitted subject
to crediting the source.



Deutsches Elektronen-Synchrotron A Research Centre of the Helmholtz Association

The Helmholtz Association is a community of 18 scientific-technical and biological-medical research centres. These centres have been commissioned with pursuing long-term research goals on behalf of the state and society. The Association strives to gain insights and knowledge so that it can help to preserve and improve the foundations of human life. It does this by

identifying and working on the grand challenges faced by society, science and industry. Helmholtz Centres perform top-class research in strategic programmes in six core fields: Energy, Earth and Environment, Health, Key Technologies, Structure of Matter, Aeronautics, Space and Transport.

www.helmholtz.de